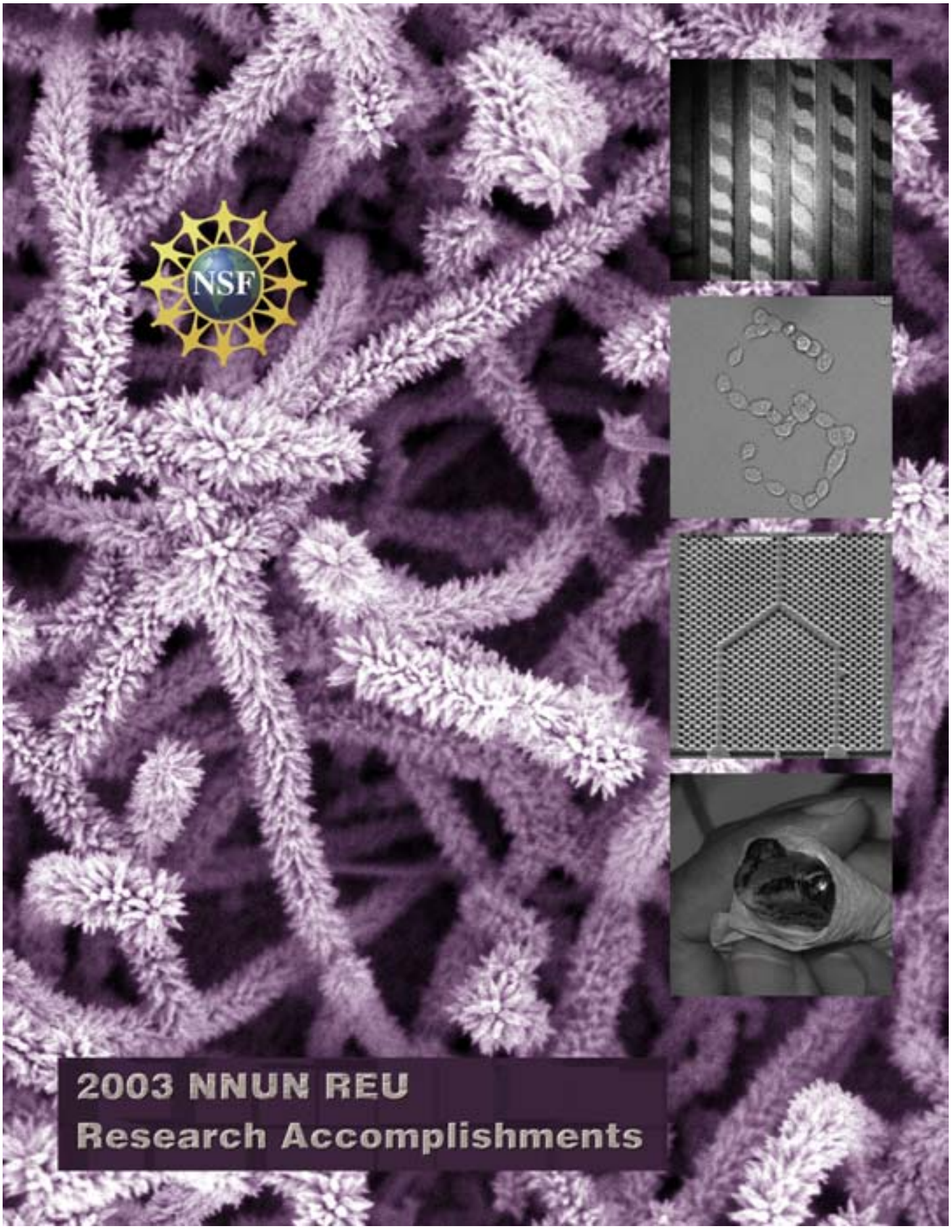

2003 NNUN REU
Research Accomplishments

The National Nanofabrication Users Network
Research Experience for Undergraduates Program

is made possible by the
National Science Foundation, Grant # EEC-9987915,
and the following partners and corporate sponsors.

Network Partners

• Cornell NanoScale Facility •
Prof. Sandip Tiwari, Director
Cornell University
CNF, 250 Duffield Hall
Ithaca, New York 14853-2000
Voice: (607) 255-2329
Fax: (607) 255-8601
http://www.cnf.cornell.edu/

• Materials Science Research Center for Excellence •
Prof. Gary Harris, Director
Howard University School of Engineering
2300 Sixth St, NW
Washington, D.C. 20059
Voice: (202) 806-6618
Fax: (202) 806-5367
http://www.msrce.howard.edu/~nanonet/NNUN.HTM

• Penn State Nanofabrication Facility •
Stephen J. Fonash, Director
Kunkle Chair Professor of Engineering Sciences
189 Materials Research Institute
The Pennsylvania State University
University Park, PA 16802
Voice: (814) 865-4931
Fax: (814) 865-3018
http://www.nanofab.psu.edu/

• Stanford Nanofabrication Facility •
Yoshio Nishi, Director
Stanford University
Center for Integrated Systems, Room 103
Stanford, CA 94305-4070
Voice: 650-723-9508
FAX: 650-725-0991
http://snf.stanford.edu/

• UCSB Nanofabrication Facility •
Prof. Mark Rodwell, Director
Department of Electrical and Computer Engineering
University of California, Santa Barbara
Santa Barbara, CA 93106-9560
Voice: (805) 893-8174
Fax: (805) 893-3262
http://www.nanotech.ucsb.edu/

Corporate Sponsors

Advanced Micro Devices
Agilent Technologies
AMP/Lytel Division
Analog Devices
Applied Materials
Canon, Incorporated
Hewlett-Packard Company
Hitachi, Ltd
Hughes Research Laboritories
IBM Corporation
Infineon Technologies
Intel Corporation
LG Electronics, Inc.
National Semiconductor Corporation
Panasonic USA
Philips
Renesas Technology
Robert Bosch Corp.
Taiwan Semiconductor Manufacturing Company
Texas Instruments, Incorporated
Toshiba America, Incorporated
Varian Semiconductor Equipment Associates

Cover Graphics

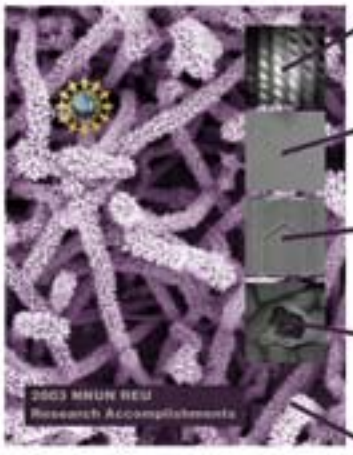

• SNF •
Evans
page 80

• PSNF •
Maness
page 64

• CNF •
McKnight
page 30

• MSRCE •
Cheng
page 46

• UCSB •
Reichman
page 112

The 2003 National Nanofabrication Users Network Research Experience for Undergraduates Program

Table of Contents

The proceeding photographs were taken by Ms. Melanie-Claire Mallison during the August 2003 NNUN REU Convocation at the University of California, Santa Barbara. In order, the photos are of:

Rachel Gabor, Harvey Mudd College, CNF intern
Aminata Kone, Clemson University, MSRCE intern
Daniel Gift, PSU, PSU intern
Grace Lee, UCSB, SNF intern
Rey Honrada, Allan Hancock College, UCSB intern

The 2003 National Nanofabrication Users Network Research Experience for Undergraduates Program

Introduction

The 2003 NNUN REU Interns at the August network-wide convocation, University of California, Santa Barbara, CA

Welcome to the 2003 Research Accomplishments for the National Nanofabrication Users Network Research Experience for Undergraduate Program.

Providing a focused experimental research experience in nanotechnology and its basic subjects in a 10 week period is a challenging task; this report demonstrates that with effort from staff, faculty, graduate students, and the participating students, not only can it be successfully achieved, but also it can lead to significant accomplishments by students who have just started on the path of technical education.

The NNUN partnership, through our complementary strengths, cross-fertilization, multi-site education, and use of each other's resources, provides exciting projects and the means to achieve them in a reasonable time. Each student in the NNUN REU: completes an independent research project selected for completion in 10 weeks, with strong technical support and faculty supervision; undergoes strong hands-on training and education (also available as streaming video at http://www.cnf.cornell.edu/nanocourses/nanocourse.html); and present their research efforts during convocations at individual sites and at one network-wide convocation, this year held at the University of California, Santa Barbara.

The focus on advanced research and knowledge, the strong mentoring and support, the strong exposure to a professional research environment, the strong expectations built into the research and presentations at convocations, the exposure to a wider variety of research conducted by peers and other users in diverse disciplines of science and engineering within the unifying facilities, and the strong scientific and social interactions across the network have been critical to the program's success. This year's participants also saw increased cross-site interactions through video-conferences and presentations, and hands-on experimentation.

I wish the participants the best wishes for future technical careers; NNUN hopes to see them build on this summer's experience. And my thanks to the staff, graduate student mentors, and faculty for their participation and involvement.

Sandip Tiwari, Director, NNUN

The 2003 NNUN REU Interns

Blast From the Past

NNUN REU Interns from Previous Years Check In

❖❖ ❖❖ ❖❖ ❖❖ ❖❖ ❖❖ ❖❖ ❖❖ ❖❖

Hi,

First of all, I want to thank you again for inviting me for the Summer 2002 NNUN internship at the UCSB Materials Science Lab. I can say today it is that internship which really focused my work here at UC Berkeley to getting prepared for Graduate School. In other words, before the summer of 2002, I was not clear on what I really wanted to do, and whether or not continuing my education to getting a PhD or at least a Masters would be what I should aim for immediately after graduation. After the internship, I was convinced that going to graduate school was my path because I honestly enjoyed the work I did at UCSB. In fact, it is during that summer that I understood what to do exactly to obtain my goal.

As for today, I currently take courses toward my Bachelors Degree and at the same time try to take courses focusing on the device structures and semiconductor device fundamentals. I'm doing my best to take courses in that field before I leave undergrad. I have also decided to take an extra semester to take indepth courses in that field, which I was introduced to at the Materials Science Lab at UCSB.

Finally, the internship also introduced me to UCSB the campus and its faculty, and convinced me that it should be one of the top schools on my list for graduate school.

Thank you!
Hani Aldhafari
2002 UCSB NNUN REU
hani_a@uclink.berkeley.edu

❖❖ ❖❖ ❖❖ ❖❖ ❖❖ ❖❖ ❖❖ ❖❖ ❖❖

Currently I'm attending University of California at San Diego. I have completed a Master of Science degree in Bioengineering in June 2003, and currently beginning experimental work for a Ph.D.

My research concentrates on mechanisms of cartilage growth and how content, synthesis, and assembly of cartilage matrix components affects mechanical properties of this tissue. Recent efforts in repairing cartilage defects have focused on fabrication cartilage constructs in vitro. However cartilage fabricated in this fashion has mechanical properties that are inferior to those of normal tissue. Thus, it is important to study cartilage growth in vitro in order to be able to induce a functional cartilage phenotype to generate clinically useful cartilage constructs.

My NNUN REU experience has definitely affected my choice to go to graduate school over a professional school. Even though my current position seems to be quite distant from nanotechnology, the skills I gained as an intern continue being useful in my graduate student career.

Anna Asanbaeva
2000 SNF NNUN REU
asanbaeva@ucsd.edu

❖❖ ❖❖ ❖❖ ❖❖ ❖❖ ❖❖ ❖❖ ❖❖ ❖❖

This summer I'm graduating with my Master's degree in Materials Science and Engineering at Ohio State University. Next month I'll be starting work on a Ph.D. at UCSB in the Biomolecular Science and Engineering Program.

My experience in the NNUN REU program had significant influence on my decision to join this program at UCSB. The seminars I attended that summer (2001), both of the professors at UCSB and the other NNUN interns exposed me to a lot of research areas of which I previously had no knowledge. It was that summer that I decided I wanted to pursue research which lies at the intersection of biology and more traditional engineering (esp. electrical (MEMs) and materials), and it was then that I learned of the Biomolecular Science and Engineering Program at UCSB.

Peace,
Lukmaan Bawazer
2001 UCSB NNUN REU
lbawazer@hotmail.com

❖❖ ❖❖ ❖❖ ❖❖ ❖❖ ❖❖ ❖❖ ❖❖ ❖❖

Hi,

I was in the program in the summer of 2001 at the Santa Barbara campus. I've just finished my first year of graduate school at Stanford University in the Department of Applied

Physics. I'm in the doctoral program. Having the NNUN on the CV certainly helped with my application.

I considered nanofab as a research path for a while, but I've now moved into biophysics and find it very rewarding. I may end up working on applications of nanofab to biology at some point. Hope this helps.

Austin Brown
2000 UCSB NNUN REU
shakespeare@poetic.com

❖❖ ❖❖ ❖❖ ❖❖ ❖❖ ❖❖ ❖❖ ❖❖ ❖❖

Hi, Melanie-Claire,

I am currently a first year graduate student in a MS/PhD track program at Columbia University in the department of applied phyiscs and applied mathematics. I would say that being in the NNUN REU program was a huge help. This semester I will work in the lab of Prof. Philip Kim who does very similar research to the type that I did in Prof. Hongie Dai lab in Stanford one summer ago.

Hope everything is going well in Cornell.

Rob Caldwell
2002 SNF NNUN REU
rvc2101@columbia.edu

❖❖ ❖❖ ❖❖ ❖❖ ❖❖ ❖❖ ❖❖ ❖❖ ❖❖

Hello,

Sorry for the long delay—I have been busy moving and was waiting for my new address to be finalized so I could give that to you at the same time.

I finished my BS in ECE at Cornell in May 2002. Currently I am a Ph.D. student at the University of Michigan, in the Electrical Engineering and Computer Science department. I am now beginning my second year.

I am a fellow of an NSF IGERT program at UM called "Molecularly Designed Electronic and Photonic Nanostructured Materials", which brings together students from chemistry, materials science, applied physics, and electrical engineering. My research interests are in BioMEMS. I just finished an internship over the summer, where I was at University of North Carolina-Chapel Hill with a stem-cell research lab to learn how nanotechnology can help biologists' research.

Hope this helps!

Sincerely,
Phil Choi
2001 CNF NNUN REU
philip.choi@umich.edu

❖❖ ❖❖ ❖❖ ❖❖ ❖❖ ❖❖ ❖❖ ❖❖ ❖❖

Dear Melanie-Claire,

Last summer I completed my internship at PSU under the supervisition of Dr. Pantano. Since then I have spent a semester abroad in Australia studying not only courses of my major but also one emphasizing Australian history. This was definitely one of the best eperiences of my life. I have learned so much during the five months spent abroad; not only schoolwise but about myself and life in general.

Currently, I am completing my Biomedical Engineering degree from Rensselaer Polytechnic Institute and am expected to graduate in May 2004. As of post-graduation plans, only time will tell.

Diane Colello
2002 PSU NNUN REU
coleld@rpi.edu

❖❖ ❖❖ ❖❖ ❖❖ ❖❖ ❖❖ ❖❖ ❖❖ ❖❖

Dear Melanie-Claire, Liu-Yen, and Krista;

Greetings from UC Santa Cruz! I hope you all are doing fine, enjoying the last days of summer (wait, I guess Cornell has already started Fall!). I find it slightly coincidental that I was intending to write you all a note to tell you how things have been going here in Santa Cruz, and then I received an email from Melanie-Claire asking for updates. I'm disappointed I couldn't make it to the convocation at UCSB this summer (I got your email about it, Krista). How did it go? It would have been nice to see SB again and spend time with everyone down there. Did anyone from last year attend the conference?

I wanted to let you all know that things are going quite well here and to tell you my experience in the NNUN REU program has positively influenced my school and career-related decisions over the past year. I gained a lot of skills and knowledge during the intern program. Some of these skills were immediately apparent; others I did not discover until months later. For instance, the multitude of PowerPoint presentations and practice talks helped me gain more confidence and comfort with public speaking, especially during required group presentations for various classes. I was also unfamiliar with PowerPoint until the internship, and now putting together a presentation is far less daunting. Other skills that were directly apparent to me included basic lab techniques and operations, successful note taking, and constructive time management. While these talents are quite useful, it is the less apparent, broad-based knowledge I gained that has helped me greatly in the past year.

After the summer NNUN program, I continued my education at UC Santa Cruz as a junior majoring in biochemistry. I had been toying with the idea of working in a research lab at UCSC, but after having such a positive experience in the NNUN program at UCSB (due mainly to my knowledgeable, flexible, and patient mentor), I knew I wanted to work in a lab. Many undergraduates, including myself, feel helpless and insecure when we consider the seemingly daunting task of finding and integrating ourselves into a successful research lab. Some of the challenges

include knowing what sort of research one is interested in, what type of group one works best with, and how to communicate this knowledge to a professor. A lot of these ideas seem very basic and obvious, but to an undergraduate, they are confusing and overwhelming, mostly because we have no experience to base our decisions and needs on. This is where the NNUN program really helped me. The selection of the professor and project was already arranged when I arrived at UCSB, easing my mind about having to search and select a research group myself. Subsequently, the time I spent working in the lab slowly introduced me to the particulars of lab administrative operations, inter-personnel and inter-lab relations, and other facets of research that cannot be taught in the lab courses most undergrads are required to take. The internship also eased the anxiety I felt that most undergrads share about approaching and talking with professors because I had almost daily interactions with them. The program made my assimilation into lab research straightforward and painless.

Back at UCSC, armed with constructive lab experience at UCSB, not only did I have a clearer sense of my research goals and feel secure approaching professors, but also, professors were appreciative of my skills and familiarity with lab research. I was able to gain a competitive internship in a large, productive lab that is quite popular among the undergrads because of the knowledgeable and amiable faculty, and because of the freedom granted to the undergrads in their research. Once I started working in the lab, it was quite easy to integrate myself into the lab, using my previous experience at UCSB as a model.

I have had a productive summer in the lab, and I am already starting on my own project, which I will continue through my senior year and will become my senior thesis. I am using daily several lab techniques that I learned at UCSB. Furthermore, I have been trying to decide for the last year whether I want to continue my education at a graduate school or go on to veterinarian school. After working at an animal clinic for two years and then experiencing lab research through the NNUN REU program and a UCSC lab, I just recently made the decision that I want to go to graduate school in biochemistry. I am grateful to NNUN for the exposure they gave me to other universities (I am certainly going to apply to Cornell's graduate studies). I am also considering eventually trying for a faculty position at a university after I receive my Ph.D.

Ultimately, the positive, instructive, and enlightening experiences I had as an intern in the NNUN program not only gave me valuable inter-personnel and lab-related skills, but also influenced my school and career-related decisions.

I want to thank all of you for your hard work and effort you have put into this program. I wish you all a good day and thanks again.

Sincerely,
Janelle Crane
2002 UCSB NNUN REU
xenalizoelle@hotmail.com (sort of)

❖❖ ❖❖ ❖❖ ❖❖ ❖❖ ❖❖ ❖❖ ❖❖ ❖❖

Hello, Ms. Mallison,

I apologize for the delay in my response to your email, but I do not check my Lehigh email very frequently anymore.

My time as an NNUN REU intern was invaluable in my ultimate decision to attend graduate school. Though I did my undergraduate in Chemical Engineering, in part, my experiences from last summer helped me to make the decision to attend graduate school in the biological sciences.

I am currently a first year Biology Graduate Student at the University of Delaware, where my background in engineering and my profound interest in biology is allowing me to further my education. Thanks to the REU program, I was able to see the interaction between biology and engineering, leading me to do my graduate work in the biological sciences.

I hope things went well for everyone this summer. I'm enjoying my first semester as a grad student. I would appreciate if you could send me a copy of the NNUN REU Accomplishments from this year.

Take Care,
Rose Deeter
2002 PSU NNUN REU
rdeeter@udel.edu

❖❖ ❖❖ ❖❖ ❖❖ ❖❖ ❖❖ ❖❖ ❖❖ ❖❖

Dear Ms. Mallison,

I graduated from Cornell this past May with a degree in Applied and Engineering Physics. I am going to stay at Cornell for one more year studying towards my Masters of Engineering degree. I plan to have a project that deals with nanotechnology or something similar.

My NNUN project has shaped my interests. I spent that summer creating a program that solved for the widths of liquid layers before, during, and after they came into contact. I found the coding work enjoyable actually. I took a class last semester called Computational Physics that deals with using computers and C/C++ to solve Physics problems. I really enjoyed the class also. I'm wrestling with the idea of doing some more coding work in this area actually. If I could apply it to Nano that would be even better.

So, that's what's on my plate for the next year. The NNUN was a great program and I recommended it to a few of my fellow U-grads. I'm glad I had the chance to participate in the program.

Peter Ercius
2001 UCSB NNUN REU
pae9@cornell.edu

❖❖ ❖❖ ❖❖ ❖❖ ❖❖ ❖❖ ❖❖ ❖❖ ❖❖

Ms. Mallison,

I just received the card a few days ago and thought it would be a good idea to send you a short biography on what I have done since the internship and what I'm doing now. So here goes.

After finishing my internship at UCSB in the summer of 2000, I went back to Georgia Tech to finish up my undergrad courses there. Following a semester abroad in the spring of 2002, I finally graduated with my Bachelor's degree in materials science and engineering. Before graduating from Georgia Tech, I had decided that I wanted to attend graduate school in materials science and get at least my Master's degree and possibly a Ph.D. I looked at several schools and ultimately decided to attend UC San Diego in the fall of 2002.

The summer before starting graduate school I returned to work at MicroCoating Technologies in Atlanta for my second consecutive summer internship there. I left Atlanta to move out to San Diego this past September and started work on my Master's degree. I passed my comprehensive examination and obtained my Master's degree this July.

Since then I have decided to stay and work on my Ph.D. here at UCSD, doing research on carbon nanotubes. Participating in the NNUN internship along with my other research experience helped me to see what the academic research lifestyle of a graduate student was like; helping me to make my decision to attend graduate school.

Andy Gapin
2000 UCSB NNUN REU
agapin@ucsd.edu

❖❖ ❖❖ ❖❖ ❖❖ ❖❖ ❖❖ ❖❖ ❖❖ ❖❖

Hi, MC, I will graduate this fall with a B.S. in chemical engineering and just started conducting angiogenesis and nerve repair research. My plans are to get married next June and attend medical school next fall. I just submitted my application and have my first interview tommorrow.

Hope all is going well with you!

Cara Govednik
2002 CNF NNUN REU
cgovednik@hotmail.com

❖❖ ❖❖ ❖❖ ❖❖ ❖❖ ❖❖ ❖❖ ❖❖ ❖❖

Hello, Melanie-Claire,

Here is a short biography of myself:

My name is Nathalie Guébels. I was an NNUN intern at UCSB during the summer of 2000. This was the summer after my sophomore year at UCSB. Being part of a research group gave me a lot of motivation to go to graduate school and work as a graduate researcher. I pursued this idea by entering the five-years' BS/MS program at UCSB.

The following summer I had an internship at Raytheon Infrared and worked as a graduate researcher the summer of 2002.

I just graduated in June 2003 with both my BS and my MS in Electrical Engineering and I am currently looking for a job in the surroundings of Santa Barbara, after having traveled for two months.

I definitely think that my experience at NNUN influenced my area of interest. The different fields that have inspired me the most are nanotechnology, electro-optics, instrumentation and bio-instrumentation.

Sincerely,
Nathalie Guébels
2000 UCSB NNUN REU
nguebe00@umail.ucsb.edu

❖❖ ❖❖ ❖❖ ❖❖ ❖❖ ❖❖ ❖❖ ❖❖ ❖❖

Hello! :)

Things are good with me. Next week I will be beginning my orientation for becoming a Graduate Student Instructor at the University of Michigan Chemistry Department. I am part of the 5 year doctoral program and will be doing research as well as teaching. I am currently working on some thin film deposition techniques and time-of-flight measurements of electron/hole mobilities. Afterwards, my goals, as I see them now but are subject to change, are to become a professor of chemistry at a liberal arts or small college or university.

Outside of career information, I was married just last weekend and am living with my new spouse in an apartment in Monroe, MI.

As for how the CNF NNUN REU program helped me get where I am, I was able to get a letter of recomendation from my PI which, I'm sure, helped to show the University of Michigan that I'm not just some smart guy going to school in Wisconsin, but that I have ambition and am talented enough to be a research chemist. At the end of my school year, I was recognized by faculty members of my research potential and was inducted into Sigma Xi. This achievement I definitely attribute to my work at Cornell last summer.

Well, I hope this is enough bio for you needs. My snail mail address is in my signature. I hope to hear from you soon.

Alex Hansen
2002 CNF NNUN REU
viochemistry@iwon.com

❖❖ ❖❖ ❖❖ ❖❖ ❖❖ ❖❖ ❖❖ ❖❖ ❖❖

My name is Jon Hong and I was an NNUN REU intern at Cornell during the summer of 2000. Currently, I am enrolled as an MS student at Boston University in Biomedical Engineering conducting research on the drug-

induced apoptosis of hair cells. The work I'm doing is relatively new, but our lab is part of the Hearing Research Center here at BU: http://www.bu.edu/hrc/index.html

My experience as an NNUN REU intern influenced me in a few ways. It got me interested in the area of micro/nanofabrication as applied to bioengineering. Specifically, the technology was applied in my senior design project and also influenced my course selection in the rest of my undergraduate studies and in my graduate career so far. A few years down the road, I would like to work in industry, in a biotech-related area or possibly biotechnology intellectual property. There may be a time when I continue graduate studies beyond the MS towards a Ph.D., but I have not decided when that will be.

Jon Hong
2000 CNF NNUN REU
jonbh@bu.edu

❖❖ ❖❖ ❖❖ ❖❖ ❖❖ ❖❖ ❖❖ ❖❖ ❖❖

Hi, it's great hearing from you!

I recently participated in a research program offered through Cornell's Center of Material Science. It was a vigorous, yet exciting ten week program. I worked with Prof. Archer in the Chemical and Biomedical Engineering Department. In the future, I plan to attend graduate school to specialize in either Chemical Engineer or Biomedical Engineering. Currently, I am a graduating senior with one year left till graduation.

Wish me luck! Thanks for the email.

Karrie D. Houston
2002 Howard NNUN REU
karriehouston@hotmail.com

❖❖ ❖❖ ❖❖ ❖❖ ❖❖ ❖❖ ❖❖ ❖❖ ❖❖

Hi, Melanie,

After participating in the NNUN REU program, I returned for my senior year at the University of Notre Dame, from which I graduated Magna Cum Laude in May, 2003.

Following graduation, I participated in the ONR's Naval Research Enterprise Intership Program at the Space and Naval Warfare Systems Center in San Diego, CA, working on advanced MEMS sensors. My experience at Stanford Nanofabrication Facility proved to be a valuable tool in my work for the Navy.

I'll be starting a MS/PhD program at Princeton University this fall, with an emphasis on semiconductor devices and physics, specifically in nanotechnology.

Scott Sheridan Howard
2002 SNF NNUN REU
showard@nd.edu

❖❖ ❖❖ ❖❖ ❖❖ ❖❖ ❖❖ ❖❖ ❖❖ ❖❖

After my experience as a REU Student at CNF, I continued my fourth year of Mechanical Engineering. I presented my REU research project in my school and received credit for it. From January 2003 till July 2003, I worked as a COOP student in the pharmaceutical company, Merck Sharp & Dohme in Barceloneta, Puerto Rico. As a COOP student, I worked full time for seven months next to a coach engineer. I was interviewed to get this job. The interviewers asked me about my research work at CNF and they were impressed by it. My experience in Cornell also helped me a lot in improving my English.

Currently, I'm in my fifth year of Mechanical Engineering and I plan to graduate in December 2004 (I didn't study for a semester since I was working). After I finish, I plan to work in the industry for 7 or 8 months and then continue graduate studies in the field of Bioengineering. My interest in Bioengineering awakened through the project I did in Cornell. I want to attend graduate school in the United States and then come back to Puerto Rico to work.

Gizaida Irizarry Rosado
2002 CNF NNUN REU
gizaida@hotmail.com

❖❖ ❖❖ ❖❖ ❖❖ ❖❖ ❖❖ ❖❖ ❖❖ ❖❖

Melanie,

How did the 2003 REU program go? I hope they didn't give you too hard of a time.

Upon my 2003 BSEE graduation, I began full-time employment in Motorola's Integrated Electronics Systems Sector at Deer Park, Illinois. Presently, I am finishing a bi-directional electrical to fiber optics communication module design. The 2002 NNUN REU program provided "real-life" experience in working on a project that didn't have a known solution. This experience has proven very useful in my present design project. My short term educational goal includes beginning a Masters degree in Electrical Engineering within the next few years due to my experiences at the NNUN REU program.

Michael Krause
2002 CNF NNUN REU
mpk171@yahoo.com

❖❖ ❖❖ ❖❖ ❖❖ ❖❖ ❖❖ ❖❖ ❖❖ ❖❖

Hi, Melanie:

I am currently entering my second year as a Bioengineering graduate student in the UC Berkeley/UCSF joint graduate group. My current research focus is on tissue engineering as related to the effect of peptide analogs of various proteins on cells in vitro. After I complete my Ph.D.,

I plan to take a research position in industry at a biotech company. My NNUN REU experience has left me with many fond memories and a lasting impression of UCSB. I believe the summer I spent in the NNUN program really solidified my decision to apply for graduate school, and gave me a real taste for what graduate research would be like. The NNUN program was an awesome experience for me, and I recommend it to any undergrad interested in summer research; it was well organized and the program was well developed; I especially thought the summer convocation was a very valuable experience.

Best Wishes,
Hayley Lam
2001 UCSB NNUN REU
hayley74@uclink4.berkeley.edu

❖❖ ❖❖ ❖❖ ❖❖ ❖❖ ❖❖ ❖❖ ❖❖ ❖❖

Hi, Melanie,

This is Chun-Cheng Thomas Lin. How are you doing? Recently, I have been working in Integrated Circuit Research Lab with my professor. We finished several funding proposals in June and submitted them for the benefit of our research lab in the coming years.

From the experience of the NNUN REU program, I am able to become a lab assistant for a fabrication class this coming fall. My internship at Cornell assured my eligibility for the position and convinced the professor I was well qualified. The lab training in the USC cleanroom was a breeze for me and I quickly adapted to the environment. The USC cleanroom is smaller than CNF and some of the machines are older. But, the equipment for fabrication processes are similar and the physics behind each tool is the same.

In the future, I plan to pursue a Ph.D. for my education. I am not sure where I would like to go, and I have not yet applied to any school. The field I would like to go into is Analog Circuit Design and VLSI. Though I personally will not be involved in fabrication, like becoming a process engineer, I will continue gaining knowledge related to fabrication processes in order to help me to design better circuits.

I thank all the CNF staff for giving me the experience last year. I am glad that you sent out this email so that we all can keep in touch with everyone. Thank you, Melanie. Please say hi for me to everyone there, if any of the staff still remembers me. Take care and keep in touch.

Best Regards,
Thomas Lin
2002 CNF NNUN REU
chunchel@usc.edu

❖❖ ❖❖ ❖❖ ❖❖ ❖❖ ❖❖ ❖❖ ❖❖ ❖❖

Hey, Melanie,

This is Brian Manuel from the summer of 2001. I am currently in my fifth year of study at North Carolina A&T State University finishing up my Mechanical Engineering major. As you may remember, I am in a dual degree program with Morehouse College. I've completed all my requirements to receive a BS in Applied Physics after I complete my term at NCA&T. Although I really enjoyed my time at NNUN, and learned a great deal, my path has not come across any more research experiences.

The summer after NNUN, I interned at a power company in Memphis, TN, mostly doing CAD work. Last summer, I interned at GE Aircraft Engines in Cincinnati, OH. I worked on the engine for the F16 millitary fighter performing analysis on engine parts as well as facilitaing changes in design to engine hardware. I did plan on doing research for this semester at NCA&T, however I have not found time yet.

Later Gater,
Brian Manuel
2001 CNF NNUN REU
brman70@hotmail.com

❖❖ ❖❖ ❖❖ ❖❖ ❖❖ ❖❖ ❖❖ ❖❖ ❖❖

I graduated in May from the University of Pennsylvania Materials Science Department. This summer I've been working at IBM for Don Eigler doing low temperature STM. In the fall I will be starting a Ph.D. program in the Materials Science Department at UCSB on an NSF Fellowship. I will be working for Evelyn Hu on electronic and optical materials. (I also plan on doing as much hiking, kayaking and surfing as I can in my spare time.)

The NNUN REU program helped me significantly in my graduate school decisions. I was able to spend time at one of the schools I was considering attending and learn more about the academic program as well as the research opportunities there. I was also able to meet and work with many graduate students and professors which helped reinforce my plans to attend graduate school. I am now attending graduate school at the school where I did my NNUN REU internship.

Kelly McGroddy
2002 UCSB NNUN REU
kellymcg@seas.upenn.edu

❖❖ ❖❖ ❖❖ ❖❖ ❖❖ ❖❖ ❖❖ ❖❖ ❖❖

Melanie,

Recently graduating from the University of Minnesota with a B.S. in Electrical Engineering, I have spent Summer '03 working in the area of molecular electronics at the

National Institute of Standards and Technology in Gaithersburg, MD. In the fall, I will be attending Harvard University in pursuit of a doctorate in Electrical Engineering.

The NNUN REU experience was pivotal in my decision to apply to and attend grad school. The opportunity to work with experts in my field and get a glimpse of life as a graduate student was just as formative as the chance to socialize and interact with a group of my undergraduate peers. My favorite aspect of the program was living in the house in Stanford and having discussions on every topic imaginable with my newfound friends who were all quite intelligent and witty. In fact, two people I met that summer made numbers three and four on my "Top 10 list of extraordinary people." Ahhh, good times.

Curtis Mead
2002 SNF NNUN REU
cmead@fas.harvard.edu

❖❖ ❖❖ ❖❖ ❖❖ ❖❖ ❖❖ ❖❖ ❖❖ ❖❖

Hi, Melanie-Claire!

Well this year has been a pretty exciting one for me:

I spent the past year studying abroad at University College London in the Electrical Engineering and Physics departments. Besides repeatedly going on holiday and taking a few exams, I also received the Barry M. Goldwater Scholarship for mathematics, science, and engineering. My participation in the NNUN REU was paramount to the success of my application for this award.

Currently, I'm returning to Southern Methodist University to complete a triple major in Electrical Engineering, Physics, and Mathematics. I hope to work in the university's new fabrication facilities for my Senior Design project.

Upon completion of my undergraduate studies, I plan to attend graduate school to study quantum devices in a physics or engineering department, ideally focusing on the emerging field of quantum computation for a Ph.D.

Hope this helps. How is the program going this year?

Thanks,
Michael Shearn
2002 SNF NNUN REU
mshearn@mail.smu.edu

❖❖ ❖❖ ❖❖ ❖❖ ❖❖ ❖❖ ❖❖ ❖❖ ❖❖

I am currently a graduate student in the School of Applied and Engineering Physics at Cornell University. Originally from Oklahoma, I received my bachelor's degree in Physics, Chemistry, and Math from Southern Nazarene University in Bethany, Oklahoma.

In the summer of 2000, I participated in the National Nanofabrication Users Network Research Experience for Undergraduates Program as an intern at the Cornell Nanofabrication Facility. During that summer, I worked under Professor George Malliaras, making organic thin film transistors through photolithography. That summer greatly contributed to my decision to pursue graduate study at Cornell University.

In short, it was obvious that Cornell was a leader in nanoscale technology and that George was one of the best professors on the planet!

Since returning to Cornell as a graduate student in the summer of 2002, my work has shifted from organic transistors to organic light emitting devices based on transition metal complexes.

Jason Slinker
2000 CNF NNUN REU
js395@cornell.edu

❖❖ ❖❖ ❖❖ ❖❖ ❖❖ ❖❖ ❖❖ ❖❖ ❖❖

Hey, Melanie,

Hope all is well up at Cornell. Things here a busy like normal, which is good though, keeps me out of trouble. :) Anyways, about what I have been up to.

After my REU summer, I came back to Penn State for another school year. Around December last year though, I received a internship for a start up company called BioElectroSpechere in Harrisburg. They were being funded by a couple different sources including the Department of Defense. The project that they were working on was a molecule detection system that would first be able to cut the time of finding a certain strain of DNA from 3 hrs to 3 mins. The same technology was also going to be able to be setup for the detection of Biological Weapons such as Anthrax. My list of jobs at the company was constantly changing.

The most related part to my NNUN experience was my work on the creation of the Microfluidic channels in silicon wafers and the setup of a small wafer process room. Most of the wafer work was done at the Penn State Nanofab though. Unfortunately after the USA went to war in the spring, the government pulled a lot of funding and one of our main grants was lost, requiring BioElectroSpechere to cut back and my position was one that was cut in may. So for most of this past summer I work with a friend making eye glasses at Lenscrafters, till August when I went to Hawaii and lived with my friend for most of August before having to come back to school for one last year.

And that is where I'm at now. Hope this gives you an idea of what I have been up too.

Take care and talk to you soon,
Jason Smeltz
2002 Howard NNUN REU
jes354@psu.edu

❖❖ ❖❖ ❖❖ ❖❖ ❖❖ ❖❖ ❖❖ ❖❖ ❖❖

Hi, Melanie-Claire:

Here's my update.

I participated in the 2001 NNUN REU program at the Stanford site. I have since received my bachelor's degree from Brown University in Materials Engineering (2002). I am currently a second-year graduate student at Northwestern University in the Department of Materials Science and Engineering. My research involves the self-assembly and liquid crystalline properties of fluorescent molecules for use in optoelectronic and solar cell devices.

To answer your question, the SNF REU definitely played a role in where I am today. I was able to get hands-on research experience and make a more educated decision about going to graduate school.

Hope this helps. Take Care.
Marina Sofos
2001 SNF NNUN REU
sofos@northwestern.edu

❖❖ ❖❖ ❖❖ ❖❖ ❖❖ ❖❖ ❖❖ ❖❖ ❖❖

Hi, Melanie,

How are you? I am doing alright. I finally decided to attend MIT. I like it here so far. Please keep in touch... :)

I attended NSF's REU program in summer 2002 under Professor Jim Plummer and Dr. Michael Deal, Department of Electrical Engineering, Stanford University, working on "Stress Effects on Crystallization of Amorphous Silicon Pillars". I completed my B.Sc. in Biochemical Engineering and minor in Mathematics at the University of Southern California (USC) in May 2003 with the highest honors, Summa Cum Laude. During graduation I received the "Outstanding Chemical Engineering Student Award" as the top student of my class.

I've been offered fellowships from Cornell (NBTC Fellowship), Stanford, UC Berkeley (University Fellowship), Caltech (University and Special Institute Fellowship), and MIT (Wm C & Margaret H Rousseau Fellowship) to pursue a Ph.D. in Chemical Engineering. As I said, I joined MIT for graduate studies. A fter completing my Ph.D., I want to stay in academia and continue research.

NSF's REU program has helped me in shaping my career path by exposing me to research, bringing me in close contact with the active scientific community and by enhancing my motivation for future research.

Sincerely yours,
Mahmooda Sultana
2002 SNF NNUN REU
msultanausc@yahoo.com

❖❖ ❖❖ ❖❖ ❖❖ ❖❖ ❖❖ ❖❖ ❖❖ ❖❖

Hi, Melanie,

Here it is:

After the REU at Howard, I went back to the University of Washington to finish up my BS in Electrical Engineering. I graduated last June then had some fun in California. Now, I'm looking for a job (hoping to get one that is research oriented) and this year I am spending time with family and friends, saving up for a Europe trip, and preparing for graduate school. I'm planning to get my masters in Engineering Physics (or Electrical Engineering). Thanks to the program, I'm certain that I'm headed this direction. I had a wonderful experience.

Thanks,
Veronica Valeriano
2002 Howard NNUN REU
vvaleria@u.washington.edu

❖❖ ❖❖ ❖❖ ❖❖ ❖❖ ❖❖ ❖❖ ❖❖ ❖❖

Hi, MCM,

I recently graduate from MIT with a triple major in Physics, Electrical Engineering, and Mathematics. This fall, I will begin graduate studies in Physics at Harvard University as a Hertz Fellow. My research interest remains the physics and chemistry of active nanostructured materials. The NNUN program was very helpful in solidifying this interest.

For more detail on my activities, I have appended a recent list of distinctions.

Distinctions:

2003 Malcolm Cotton Brown Award as top ranked MIT senior pursuing experimental physics

2003 Elected to Sigma Xi (scientific research), Sigma Pi Sigma (physics), and Phi Beta Kappa (arts and sciences) honor societies

2003 Runner-Up, Stanford Entrepreneur's Challenge

2003 Henry Ford II Scholar Award as top ranked senior in MIT School of Engineering

2003 Fannie and John Hertz Foundation Fellow

2003 One of 20 named to USA Today All-USA 1st Academic College Team

2002 Winner in Tiny Technologies Category, MIT $1K Entrepreneurship Competition

2002 Elected to Tau Beta Pi (engineering) and Eta Kappa Nu (electrical and computer engineering) honor societies

2002 First place nationally, Intel Undergraduate Research Award

2001 Barry M. Goldwater Scholar

Regards,
Alex Wissner-Gross
2001 PSU NNUN REU
alexwg@MIT.EDU

❖❖ ❖❖ ❖❖ ❖❖ ❖❖ ❖❖ ❖❖ ❖❖ ❖❖

Dear Melanie:

It is great hearing from you. I hope you have had a relaxing summer despite the transition to Duffield :) and its headaches.

This past summer I participated in a similar REU program at MIT. The program was sponsored by NSF and MIT's material processing center. My project was titled "Synthesis and Characterization of Fluorescent Silica Nanoparticles and Applications in Microfluidic Systems". My CNF summer research experience played an important role in helping me understand the fabrication steps involved in the project.

Now I am back at UMASS for my senior year, taking classes ,preparing for the GRE exam and dueling on graduate program choices. But Cornell and MIT are among my top choices.

I wish everyone a smooth transition to Duffield Hall.

All the best,
Sara Yazdi
2002 CNF NNUN REU
syazdi@ecs.umass.edu

❖❖ ❖❖ ❖❖ ❖❖ ❖❖ ❖❖ ❖❖ ❖❖ ❖❖

Hi, Melanie-Claire,

I graduated from Swarthmore College this past June with a B.S. in Engineering and a B.A. in Math. I'm headed into a Ph.D. program in electrical engineering this fall at MIT (we're moving me out tomorrow!). I got an NSF graduate fellowship, which sounds fancy for things like this.

I really enjoyed my NNUN REU experience - it definitely made me enthusiastic about going to graduate school. At the same time, it told me that the nanofab field was not really the one for me (but you probably don't want to put that in your report).

Thanks very much, and take care.
Laura Zager
2002 SNF NNUN REU
lzager@mit.edu

❖❖ ❖❖ ❖❖ ❖❖ ❖❖ ❖❖ ❖❖ ❖❖ ❖❖

2003 NNUN REU Program at

Cornell NanoScale Facility

Cornell University, Ithaca, NY

http://www.cnf.cornell.edu

CNF/NNUN REU Intern ..... Major & School Affiliation ..... Principal Investigator

First Row, From left to right:

Ms. Melanie-Claire Mallison ..... Cornell NanoScale Facility ..... CNF REU Program Coordinator
Mr. Michael Campolongo ..... Electrical & Computer Engr, Rowan University ..... George Malliaras
Ms. Maria Nguyen ..... Chemical Engineering, Cornell University ..... Christopher Ober
Mr. Ardavan Farjadpour ..... Nanoengineering, University of Toronto ..... Sandip Tiwari

Second Row:

Mr. Sterling Fillmore ..... Physics, Brigham Young University ..... Christopher Umbach
Mr. Alireza Masnadi-Shirazi ..... Electrical Engineering, University of Texas Arlington ..... James Engstrom
Mr. Justin Scott ..... Mechanical Engineering, UC Berkeley ..... Amit Lal
Mr. Michael Miranda ..... Electrical Engineering, University of Notre Dame ..... Edwin Kan
Mr. Andrew Newton ..... Bioengineering, Pre-Med, Kansas State University ..... Amit Lal

Third Row:

Ms. Rachel Gabor ..... Chemistry, Harvery Mudd College ..... Michael Spencer
Ms. Heather McKnight ..... Physics, Brigham Young University ..... Michal Lipson & Roberto Panepucci
Ms. Jill Fitzgerald ..... Chemical Engineering, Louisiana State University ..... Harold Craighead
Ms. Olabunmi Agboola ..... Molecular & Cellular Biology, University of Illinois at U-C ..... Antje Baeumner
Ms. Denise Budinger ..... Cornell NanoScale Facility ..... CNF Financial Manager

Laser Lysis of Liposomes in a Microfluidic Device

**Olabunmi Agboola, Molecular and Cellular Biology,
University of Illinois at Urbana-Champaign**

Dr. Antje Baeumner, Dept. of Biological & Environmental Engineering, Cornell University
John Conolly, Biological Engineering, Cornell University
bunmi4me@cs.com, ajb23@cornell.edu

Abstract:

The focus of this project is to study the lysis of liposomes using lasers. Laser lysis has been found to be highly successful with *E. coli* and other bacteria, yeast, and mammalian cells. The lysis principle is assumed to be due to the heating of intracellular water and interactions with the cell membrane. Liposomes are phospholipid membrane vesicles that are used as signal amplification systems in microbiosensors for the detection of RNA molecules. They entrap electrochemically or optically active molecules that are detected upon lysis of the liposomes. Currently, liposomes are lysed using a detergent—beta-octyl glucopyranoside (OG). Laser lysis will be compared to the detergent lysis in order to determine its efficiency. It will be analyzed using a spectrophotometer, and fluorometer.

In order to laser lyse the liposomes, a liposomal solution will be passed through a microchannel made from polydimethyl siloxane (PDMS) and exposed to a laser mounted perpendicular to the channel. Experimental conditions involve varying the flow rates and laser wavelengths, which would optimize the parameters for laser lysing.

Introduction:

Most studies conducted on RNA, DNA, HIV, and etc., use cell lysing techniques to retrieve the information of interest. This has lead to the discovery of genetic diseases' base-sequence, the discovery of vaccines, and analysis of new diseases.

The current method of lysing cells have many disadvantages, such as; portability, intense labor and time requirements, and damage to the molecule of interest. Detergents, and other cell-membrane degrading chemicals have been used in cell lysis, but cause another necessary step of "neutralizing" the nucleic acids and proteins to prevent the degradation of the desired molecule. Mostly bacterial cells, such as, *E. coli*. have been used as an entrapment cell for these molecules. However liposomes are synthetic phospholipid bilayer membranes, which can also entrap these molecules into its walls.

Liposomes have a long history in the study of biological membranes. According to Collaborative Laboratories, Inc., liposomes have been evaluated as delivery systems for drugs, vitamins, cosmetic materials, and liposomes can be custom designed for almost any need by varying the lipid content, size, surface charge and method of preparation [1]. Liposomes enable water soluble and water insoluble materials to be used together without the use of surfactants or other emulsifiers; which *E. coli* cells can not. Liposomes have many advantages over bacterial cells, such as; the prevention of oxidation, stabilization, and controlled hydration. The system of laser lysing in a microfluidic device has been used, using *E. coli* cells. Therefore to improve this system, liposomes were chosen as the entrapment marker for lysis.

In this experiment, experimental conditions will be varying the flow rates 1μL/min, 2μL/min, and 5μL/min, and varying laser wavelength with 980 nm and 1480 nm lasers. The varying flow rates correlate directly to varying exposure times, and the varying wavelengths correlate to different water absorption coefficients, i.e. the water absorption coefficient is about 50 times higher at 1480 nm which should result in a more effective liposome lysis.

Procedure:

The template for the microfluidic device was fabricated at the Cornell NanoScale Facility, and consisted of a wafer with 80 nm depth channels and a perpendicular trench. First, PDMS was produced by mixing 20 mL of elastomer base and 2 mL of the reagent. Next, 10 mL of PDMS was poured onto the

wafer and into a small Petri dish. Both samples were then baked at 60ºC for 1 hour. The PDMS pieces were peeled from the template and Petri dish resulting in a piece with channels and a blank piece. The device was created by cutting the two pieces, punching a hole on the opposite respective sides, and attaching them together. A laser was then placed in the perpendicular trench while a flow rate pumping system was attached to the channels. Finally, after flowing the liposomes and exposing them with the laser, the device was washed with PBS and sucrose, and the liposomal solution was placed in an Eppendorf tube for analysis.

Results and Conclusions:

The lysis of liposomes using 980 nm and 1480 nm lasers with 100 mW power setting in a microfluidic device was investigated. Therefore, polydimethyl-siloxane (PDMS) devices were made from silicon templates as described in Mohit Dhawan's thesis on page 3 [2]. The devices were used immediately after fabrication. In order to determine the liposome lysis efficiency, a negative and positive control was established. The negative control consisted of 5 µL of liposomes diluted 1:200 in PBS plus sucrose (osmolarity 0.1 M) and subsequently analyzed in the spectrophotometer at 200-1100 nm. The positive controls consisted of 5 µL of liposomes, 100 µL of 300 M OG detergent, and 895 µL of PBS. Each experiment was done 6-7 times to ensure accuracy, then analyzed in the spectrophotometer at 200-1100 nm, and a fluorometer (excites-565 and emits 586). After retrieving data, the numbers were averaged and compared to the negative and positive control for a percentage. (See Figure 1 and 2.)

Thus, the best condition to lyse liposome is with a 1480 nm laser and at 1 µL/min. This leads to about 70% liposomal lysis. 100% lysis was unable to be reached. However this method can still prove to be useful, because some of the molecules of interest are still exposed.

Acknowledgments:

I would like to thank the CNF staff, the NNUN, the NSF, my P.I. Dr. Antje Baeumner, my mentor Mr. John Conolly, Mr. Mohit Dhawan, and all of those who have advised, helped and supported me throughout my project.

References:

[1] Collaborative Laboratories, "Liposomes: Controlled-Delivery Systems," http://www.collabo.com/liposome.htm, 7/16, 2003.

[2] M. Dhawan, "Laser Induced Cell Lysing System", Ph.D. dissertation, Cornell University, Department of Biological & Environmental Engineering, (Ithaca), (2003).

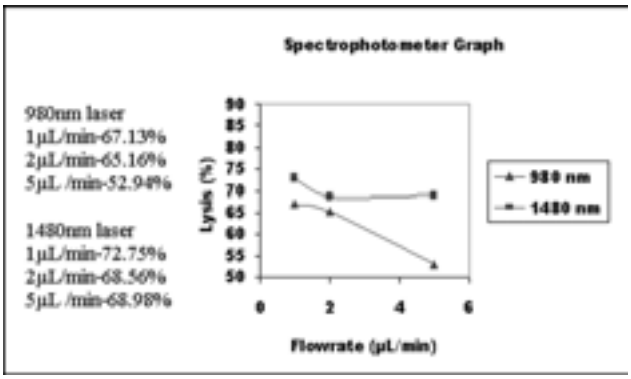

Figure 1

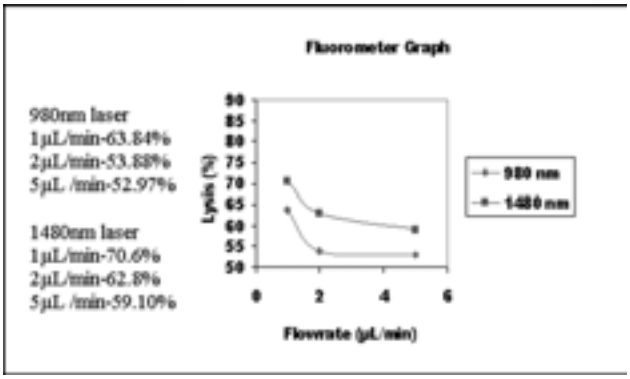

Figure 2

Interdigitated Microelectrode Arrays for Organic Light Emitting Diodes

Michael Campolongo, Computer and Electrical Engineering, Rowan University

George Malliaras, Materials Science and Engineering, Cornell University

Jason Slinker, Applied and Engineering Physics, Cornell University

camp3203@students.rowan.edu, george@ccmr.cornell.edu

Abstract:

The objective of this project was to investigate the processes that occur during the operation of transition metal-complex-based organic light emitting diodes (OLEDs). Therefore, devices were developed with a planar architecture consisting of arrays of interdigitated electrodes to facilitate electrical and optical characterization. Once fabricated, the devices were to be used to study the fundamental processes that take place in the organic semiconductor material, such as charge injection, transport, and electron-hole recombination. It was demonstrated that the devices are functional in a nitrogen glove box environment, and their quantum efficiencies are comparable to those of sandwich-structured devices.

Introduction:

Electroluminescence in organic materials was first discovered in the 1960s. It was found that anthracene single crystals are capable of light emission when provided with the appropriate electrodes and voltage bias. The high operating voltage and short life, however, rendered such devices inadequate for practical purposes [1]. As a result, early OLED technology became merely an academic interest. In 1990, electroluminescence was discovered in the conjugated polymer polyphenylenevinilene (PPV) [2]. Devices utilizing PPV demonstrated much greater performance in comparison to OLEDs of the previous decades. Since the early 1990s, much attention has been given to OLED technology, namely for use in flat panel displays and its potential influence on solid state lighting applications [3].

Light emitting devices based on transition metal complexes have been studied extensively [4], but primarily in a layered, sandwich-structure configuration. These devices are beneficial for ease of processing, but impede investigation of the organic layer, which is the area of interest in investigating the operational mechanism of such devices. Devices in a planar configuration have proven more advantageous for this purpose, and have already been used to determine the emissive profile [5]. For this reason, it is interesting to develop planar structures.

The device geometry allows for devices to interface with an integrating sphere for optical characterization. A single device contains six 1 x 0.5 mm active regions, each consisting of 125 pairs of 2 μm wide electrodes (Figure 1). The contact pads at the ends of the central channel are grounded, while the other six contact pads are used for voltage biasing. Gold was selected as the material for the ohmic contacts due to its low work function. This is adequate since the focus of the project was to investigate the processes inside the organic material, rather than to optimize the electrode contacts.

Procedure:

The devices were fabricated at the Cornell NanoScale Science & Technology Facility (CNF) using

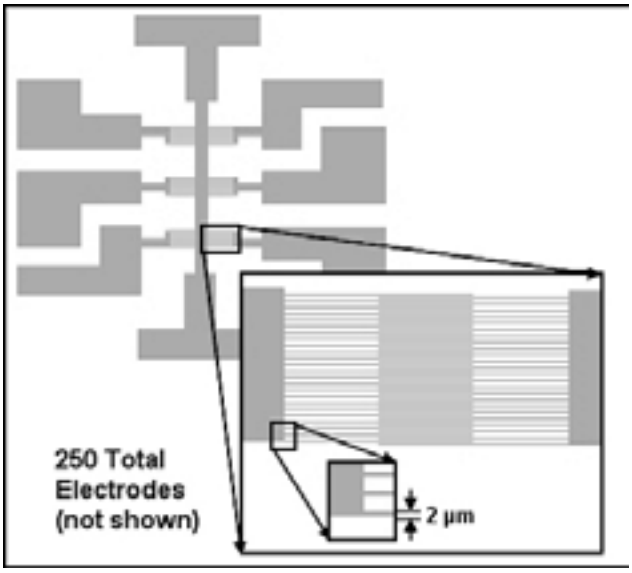

Figure 1: Pictorial representation of active region.

standard photolithographic techniques and metal deposition, and were patterned on 1 x 1 inch quartz substrates (Figure 2). In preparation for exposure, the substrates were vapor primed with HMDS for 34 minutes in the Yield Engineering Systems LP-III Vacuum Oven. They were then spin-coated with Shipley SC1827 photoresist at a speed of 4000 rpm for 30 seconds, and baked at 115ºC for 3 minutes.

The GCA 6300 5X g-line Stepper was used to expose the devices in order to precisely define the 2 µm features. However, the field size of the stepper was only large enough to expose the active region. As a solution to this problem, each device underwent two exposures. The active regions were first exposed by the stepper while the contact pads were exposed using the HTG System 3HR Contact/Proximity Aligner.

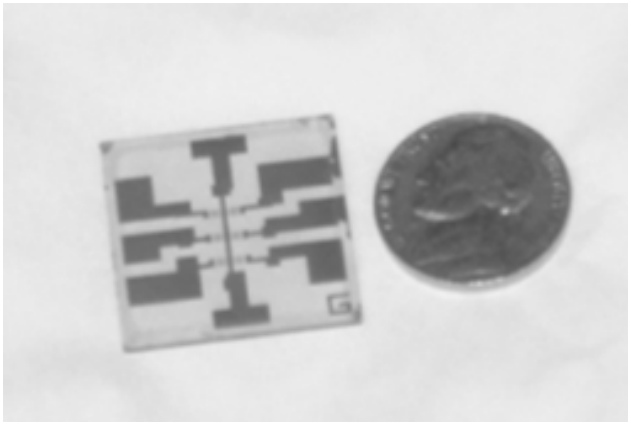

Figure 2: Planar devices on a 1 x 1 inch quartz substrate.

After development in MF-321, the devices were placed in the PlasmaTherm 72 Reactive Ion Etching System to perform a 30 nm resist etch. Next, using the CVC SC4500 E-gun Evaporation System, a 10Å adhesion layer of chromium was deposited onto each substrate, followed by a 400Å layer of gold. The devices were then placed in the Veeco Microetch Ion Milling System and etched for 5 seconds with a rotating chuck set at 10º. Finally, they were vapor primed once again, spin -coated with the transition metal complex solution, and baked at 80ºC overnight.

Results and Conclusions:

The devices were fabricated with a tris(4,4'-di-tert-butyl-2,2'-dipyridyl) ruthenium (II) hexafluoro-phosphate active layer for characterization. The devices successfully interfaced with the integrating sphere and displayed stable operation in a nitrogen glove box environment. The device current and radiance for 10 V and 20 V operations are shown in Figure 3. From this data, the turn on time was estimated to be 10 minutes. The external quantum efficiency ranged from 0.3 to 1%, which is comparable to that of the sandwich-structure configuration.

Further studies will be conducted on these devices to investigate charge injection, transport, and recombination within the organic material.

Acknowledgements:

I wish to thank the CNF, the NNUN REU program, and the NSF for making this experience possible. I would also like to express my thanks to Jason Slinker, Man Hoi Wong, and the Malliaras Research Group for their assistance and support.

References:

[1] Z.D. Popovic, H. Aziz, "Reliability and Degradation of Small Molecule-Based Organic Light Emitting Devices (OLEDs)," IEEE Journal on Selected Topics in Quantum Electronics, Vol. 8, No. 2, pp. 362-371, March/April 2002.

[2] J.C. Scott, G.G. Malliaras, "The Chemistry, Physics, and Engineering of Organic Light-Emitting Diodes," Conjugated Polymers, New York: WILEY-VCH, Ch. 13, 1999.

[3] A.R. Duggal, "OLED Design for Solid State Lighting Applications," Lasers and Electro-Optics Society, 2002. LEOS 2002. The 15th Annual Meeting of the IEEE, Vol. 1, pp. 247-248, November 2002.

[4] J. Slinker, D. Bernards, P. Houston, H. Abruña, S. Bernhard, G.G. Malliaras, "Solid-State Electroluminescent Devices Based on Transition Metal Complexes", accepted by Chemical Communications

[5] G. Kalyuzhny, M. Buda, J. McNeill, P. Barbara, A.J. Bard, J. Am. Chem. Soc., Vol. 125, pp. 6272-6283, May 2003.

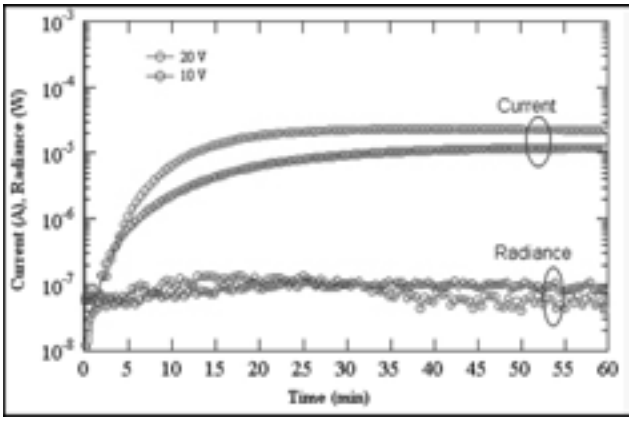

Figure 3: Current and radiance measurements obtained for two different biasing conditions.

Optimizing Shallow Trench Isolation for SOI CMOS Transistors

Ardavan Farjadpour, Nanoengineering, University of Toronto
Sandip Tiwari, Electrical & Computer Engineering, Cornell University
Uygar Evren Avci, AEP, Arvind Kumar, ECE, Cornell University
ardavan.farjadpour@utoronto.ca, st222@cornell.edu

Abstract:

The unavoidable effects of electrical interference that influence proper device behavior are a growing concern as electronic devices shrink to nanometer dimensions and device densities increase within silicon dies. In this regard, a reliable method is required to allow for precise device isolation while also not placing constraints on device density and functionality.

Shallow trench isolation (STI) is a standard process used in nanofabrication to isolate the active areas of semiconductor devices, and consists of digging trenches in the silicon wafers and filling them with a dielectric oxide material. In order to optimize the STI process for SOI CMOS transistors having feature sizes in the tens of nanometers, certain experimental parameters relating to the formation of the trenches must be carefully chosen. The most important of these parameters involves the nitride layer thickness in the oxide-nitride-oxide (ONO) layer, growing conditions of the various layers, as well as the type of dielectric oxide placed in the trenches. The ability to achieve planar post-polished surfaces that are also defect free is vital to normal device operation.

The focus of this project is the optimized fabrication and characterization of uniform, nanosize trenches to enable further size reduction of semiconductor electronic devices.

Procedure:

In order to dig trenches within the silicon substrate, it is not possible to simply use photoresist as an etch mask mainly due to the fact that the chlorine gas used to etch the silicon will burn the resist. Consequently, an oxide-nitride-oxide (ONO) layer was used as an etch mask. The first dry oxide layer, later acting as a sacrificial layer during the chemical mechanical planarization (CMP) process, was grown using a clean high-temperature metal oxide semiconductor (MOS) furnace at an ambient temperature of 900˚C. A target thickness of 20 nm resulted in a 30 minute growth time. A standard nitride layer of four varying thicknesses – experimental parameters in the optimization process – was then deposited on top of the original dry oxide layer using a low pressure chemical vapor deposition (LPCVD) process involving the MOS furnace at a temperature of 800˚C. The nitride layer functions as a stop layer during the CMP procedure.

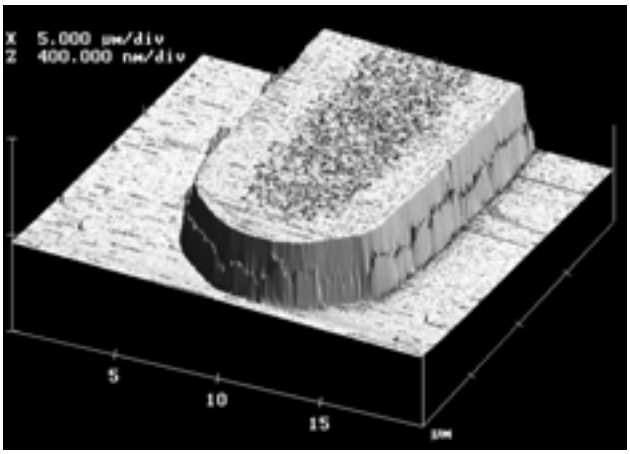

Figure 1: A well defined ONO stack atop a silicon substrate.

Subsequently, a 3rd and final oxide layer measuring 50 nm consistently was deposited using plasma enhanced chemical vapor deposition (PECVD). This final oxide layer was used to protect the nitride layer during the silicon trench etch procedure as the nitride layer thickness is a key experimental quantity.

Using standard optical lithography techniques, 1.3 µm resist features were created to define the trench boundaries. An important aim of this experiment was to determine the limits of the sizes of the trenches that could be formed and also their minimum distance apart which the mask design incorporated. With the resist pattern defined, the underlying ONO stack was then etched using a reactive ion etch (RIE) procedure using CHF_3 and O_2 gas which involved a intentional slight overetch into the silicon substrate. The resist layer

was removed using oxygen plasma etch and a subsequent wafer clean using nanostrip so as to prepare the wafers for silicon etch. Figure 1 shows that the ONO stack etch mask features were relatively well defined, an important condition for creating high precision trenches.

Next, silicon trenches of a height of 140 nm were formed via silicon RIE involving chlorine gas. During this procedure, the top most oxide layer was also partially etched but nonetheless acted to protect the nitride layer lying beneath. The deep trench formed through the combination of the silicon and ONO trenches was filled with a dielectric material—either TEOS or undoped n1.46 oxide—using a PECVD mechanism at a temperature of 400˚C that also incorporated a slight overfill (see Figure 2). CMP was used to planarize the surface of the filled trenches, a technique that consists of a mechanical arm applying pressure to the surface of the silicon substrates in the presence of a slurry mixture to facilitate the uniform removal and planarization of the top surface. The slurry involved in the CMP was a KOH based SS12 slurry used in conjunction with an IC1400 SS12 polishing pad.

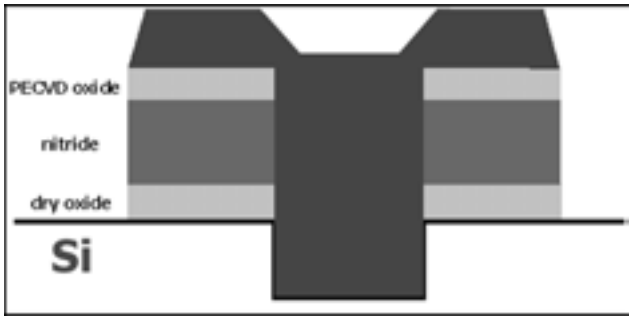

Figure 2: A schematic of the silicon trench filled with a dielectric oxide material.

Finally, the remaining nitride and oxide layers were removed via a hot phosphoric acid etch at a temperature of 170˚C, leaving essentially the original silicon surface with filled trenches on the substrate.

The experimental work consisted of digging trenches in four inch p-doped silicon wafers while carefully observing key variables. The wafer distribution consisted of five wafers with nitride layer thickness of 115 nm, five with 150 nm, five with 220 nm and lastly, three with 50 nm. Half of the wafers used HF TEOS as the dielectric trench fill while the other half used undoped n1.46 oxide.

Results & Conclusions:

Accurate, well defined and reproducible trenches of high quality were created with a variety of shapes and sizes. The trench surfaces were quite planar (refer to Figure 3)—despite slight dishing—and the boundaries were distinct (see Figure 4). There is an inherent difficulty in knowing precisely the degree of gap-fill within the trench but this may be discerned through electrical measurements. Wafers incorporating nitride layer thicknesses of 220 nm deposited at 800˚C produced the most accurate trenches mainly because they withstood the irregularities of the CMP process best. The choice of dielectric did not have a major effect on trench formation.

Acknowledgments:

I am greatly indebted to my mentors Uygar Evren Avci and Arvind Kumar for their patience and guidance. Much thanks to Dr. Sandip Tiwari and the rest of his group for their assistance. Lastly, thank you to Ms. Mallison, the CNF staff and NSF for making the experience possible.

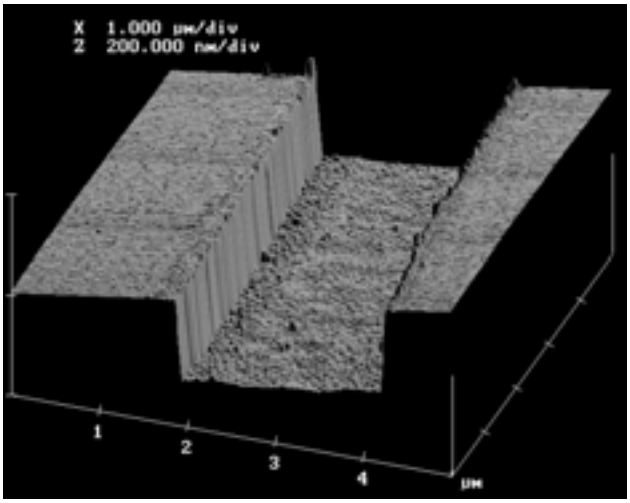

Figure 3, above: Two final filled trenches protruding from the surface of the silicon substrate.

Figure 4, below: Final SEM image of a trench.

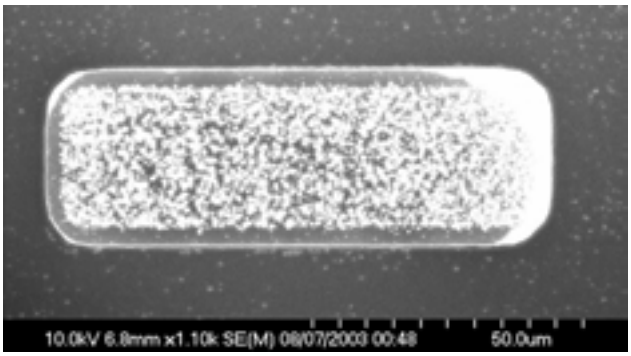

Two-Dimensional Nanobumps Using Ion Sputtering

Sterling D. Fillmore, Physics, Brigham Young University

Dr. Christopher Umbach, Dept. of Materials Science and Engineering, Cornell University

sdf6@email.byu.edu, umbach@ccmr.cornell.edu

Abstract:

Corrugations with wavelengths of 30 to 65 nm and amplitudes of 2 to 4 nm are created on the surface of a boroaluminosilicate glass through bombardment with Ar^+ ions in a conventional ion mill. The Ar^+ ions range in energy from 0.5 to 0.9 keV. The wavevector, wavelength, and amplitude of the corrugations are dependent upon the angle of incidence. By ion bombarding a surface at both high and low angles of incidence, we have studied the effects of superimposing corrugations that run perpendicular to one another. The corrugations were characterized by atomic force microscopy (AFM).

Introduction:

One-dimensional corrugations can be etched on amorphous, crystalline, and metal surfaces by ion bombardment. The creation of these periodic surface structures is driven by two factors. First, more energy is imparted to the sample by an ion that strikes the sample at a point of negative curvature (see point A, Figure 1) than an ion that strikes at a point of positive curvature (see point A´, Figure 1). The difference in impact energy causes the areas of negative curvature or pits to erode faster than the areas of positive curvature or peaks. If this were the only driving factor, then the surface structure would consist of pits that become deeper and deeper with ion bombardment. This first factor competes with the viscous flow of the material. As the pits deepen, the surface relaxes. Material flows from the peaks to the pits to minimize the chemical potential energy of the surface. With bombardment, these two driving factors come to equilibrium with an allowed surface curvature. This equilibrium curvature defines the periodicity of the subsequent corrugations.

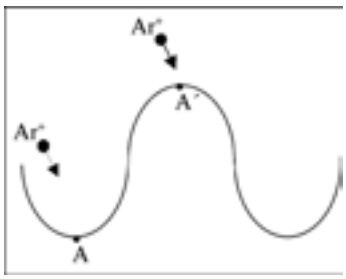

Figure 1: Ions that strike areas of negative curvature (A) impart a greater amount of energy than ions that strike at areas of positive curvature (A´).

The ion incidence angle determines the wavevector of the corrugations. From normal incidence to a critical angle of 75º off normal, the wavevector of the corrugations is parallel to the projection of the ion beam velocity on the sample. At the critical angle of 75º off normal and greater the wavevector of the corrugations changes by 90º. In the latter range, the corrugation wavevector is perpendicular to the projection of the ion beam velocity on the sample. This change in wavevector is shown in Figure 2. Figure 2A is an AFM image of an unmilled sample. The arrows on Figures 2B and 2C show the projection of the ion beam on the sample. The sample of Figure 2B was milled at 45º off the normal, and Figure 2C was milled at 80º off the normal.

One-dimensional periodic surface structures have been observed since 1962. Two-dimensional, overlaying corrugations have not been reported until now. Here, the 90º change in corrugation wavevectors with different incidence angles is used to create superimposed, perpendicular corrugations.

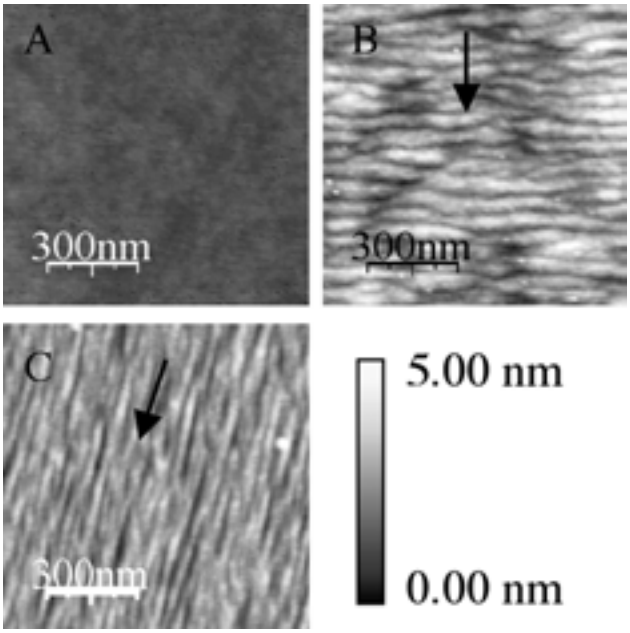

Figure 2: AFM images of (A) unmilled samples, (B) sample milled at 45º from normal, (C) sample milled at 80º from normal. The overlaid arrow shows ion beam velocity projection on sample.

Procedure:

Corning Code 1737, boroaluminosilicate glass pieces were washed with acetone and isopropyl alcohol, and blown with dry nitrogen. After washing, the samples were placed in a Veeco Ion Mill and milled with an incoming ion angle of 45º off the incident, at 650 V and 80 mA for 20 minutes. This created corrugations with a wavevector that ran parallel to the projection of the incoming ions.

A second set of perpendicular corrugations were etched on top of the first by changing the incoming ion angle to 80º from the incident. The second milling parameters were 900 V and 80 mA. The milling times of the different samples were; 5 seconds, 15 seconds, 1 minute, 2.5 minutes, and 10 minutes.

The samples were removed from the ion mill and washed with deionized water, acetone, and isopropyl alcohol, and blown dry with nitrogen. This washing seemed to remove surface charges and facilitated AFM imaging.

Results and Conclusions:

The etched samples were imaged using a Digital Instrument Dimension 3100 AFM. Figure 3 shows AFM images at different times while etching the second set of perpendicular corrugations. Figure 3A shows the original corrugations with a wavevector parallel to the beam's projection before the second etching. Figure 3B was etched a second time at 80º off the normal for 5 seconds; similarly 3C was etched for 15 seconds, 3D was etched for 1 minute, 3E was etched for 2.5 minutes, and 3F was etched for 10 minutes. The broad arrow overlaid on each image shows the projection of the ion beam on the sample. Image 3B shows that after only 5 seconds the original parallel corrugations have begun to erode.

Image 3D is of particular importance. It shows that two perpendicular corrugations have been superimposed on the sample surface. After 2.5 minutes of 80º etching (see Figure 3E) the perpendicular corrugations begin to dominate the original corrugations. After 10 minutes (see Figure 3F) the perpendicular corrugations completely dominate.

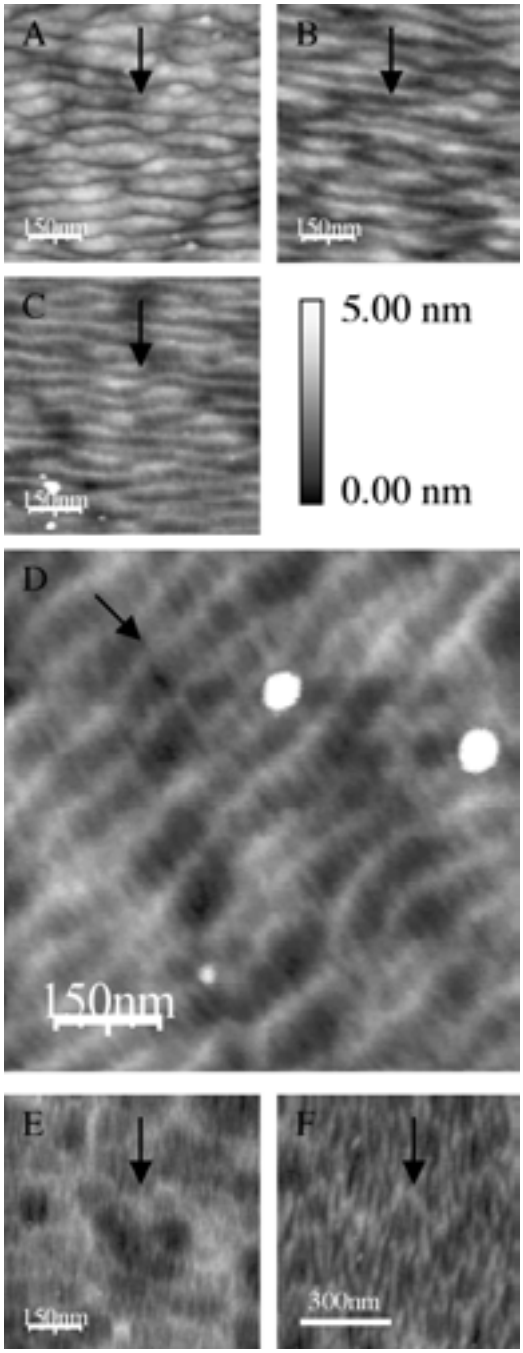

Figure 3: AFM images of (A) original corrugations etched at 45º, (B) original corrugations with second 80º etching for 5 seconds, (C) 15 seconds, (D) 1 minute, (E) 2.5 minutes, (F) 10 minutes. The overlaid arrow shows ion beam velocity projection on sample.

Acknowledgements:

I thank Dr. Christopher Umbach of the Cornell Center for Materials Research for his guidance in this project. I also thank the staff at CNF for their support and the NSF for funding this research.

References:

[1] M. Navez, C. Sella, D. Chaperot, Comptes Rendus, J. de Phys. 254, 240 (1962).

[2] C. Umbach, R. Headrick, K. Chang. Phys. Rev. Lett., 87, 24, 246104 (2001).

[3] R. Bradley, J. Harper, J. Vac. Sci. Technol., A 6, 2390 (1987).

[4] T. Mayer, E. Chason, A. Howard, J. Appl. Phys., 76, 3, 1633 (1994).

Microfluidic Device for Pharmaceutical Research

Jill Fitzgerald, Chemical Engineering, Louisiana State University

Harold Craighead, Applied and Engineering Physics, Cornell University

Gus Lott, Molecular Biology and Genetics, Cornell University

jfitzg3@lsu.edu, hgc1@cornell.edu

Abstract:

Current pharmaceutical research involves large robotics spread over numerous labs. We have developed a small, integrated tool to perform most of the operations that are necessary for pharmaceutical drug screening.

Our multiplexed, multi-layered microfluidic device cultures cells, compartmentalizes the drugs to be tested, applies the test drugs to the cells, and images the transient and steady state response of the cells. The device is relatively inexpensive and fits on a single microscope slide. The device is fabricated using soft lithography in polydimethlysiloxane (PDMS) [1], a technique available to most researchers at universities around the world. Process integration is accomplished by pneumatic valves and pumps [2].

Introduction:

Microfluidic tools are becoming popular because they provide an improved system to perform typical laboratory procedures. Some of the advantages they have include reduced size, reduced reagents and wastes, and improved data analysis. The devices also allow for a higher degree of experimental control and process integration [1].

The material used to make these convenient microfluidic devices has a part in the effectiveness of them. The Whitesides group of Harvard University have found soft lithography in PDMS yields integrated systems with many properties ideally suited to biological applications. PDMS is easily integrated with outside components because it conforms to most materials. The polymer is also stable at 40°C to 90°C, transparent in the visible/UV regions, nontoxic to proteins and cells, and gas-permeable [1].

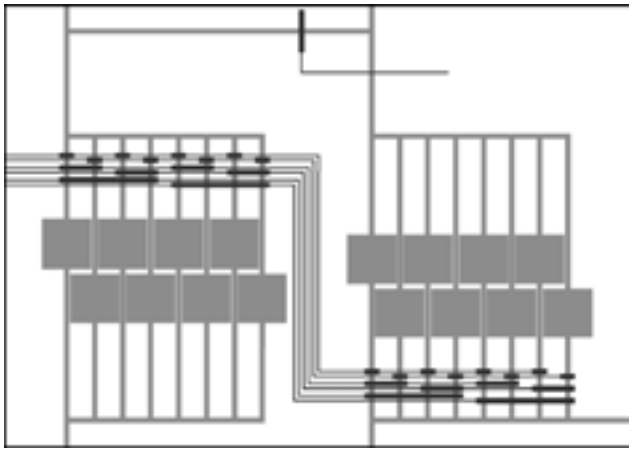

Figure 1: Our two layer device design.

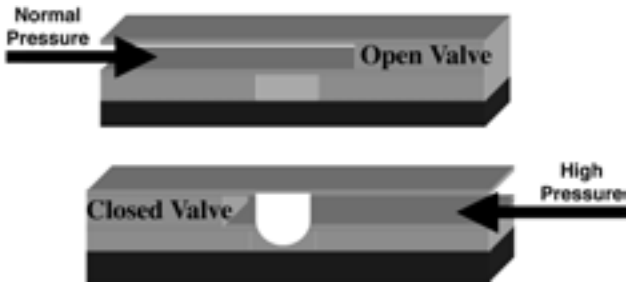

Figure 2: An example of the pneumatic valves used in our device.

Both reversible and irreversible sealing are possible as well. The PDMS channels can be irreversibly sealed to PDMS, glass, silicon, polystyrene, polyethylene, or silicon nitride by exposing the surface of the polymer and the surface of the substrate to an air or oxygen-plasma instead of using high temperatures, pressures, and high voltages like when sealing channels that are made in glass, silicon, or thermoplastics [1]. Two slabs of PDMS can be irreversibly sealed by adding an excess of the monomer to one slab and an excess of the curing agent to the other [1].

Reversible sealing is also simpler than in glass, silicon, and hard plastics because it makes reversible van der Waals contact to smooth surfaces; therefore, PDMS devices are detachable [1].

Device Design:

Our two layer device consists of a fluid channel layer and a pneumatic valving layer as seen in Figure 1. In the fluidics layer there are two sets of eight 500 x 500 x 30 μm wells with 100 μm width channels connecting them. The spacing between the wells and channels is 20 μm. One set of these wells is designed for cell culture while the other set is intended to be used to compartmentalize drugs prior to screening. Valved channels connect the two sets of wells so that drugs can be applied to the cultured cells. The

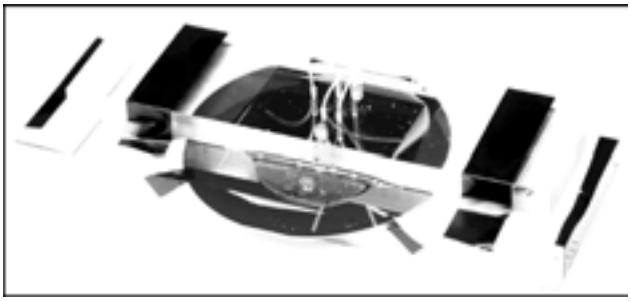

Figure 3: Silicon tubing interconnecting set-up.

pneumatics layer—the top layer—forms the valving system, which allows for any particular well to be addressed.

The valving system used was modeled after the system developed by the Quake group at California Institute of Technology. Their system includes the use of crossed-channel architecture. In our tool, pressure is applied to the upper channel and deflects the thin membrane down so that it closes the lower channel as seen in Figure 2 [2].

Fabrication:

Reactive Ion Etch by the Unaxis SLR 770 ICP Deep Silicon Etcher was used to make silicon masters containing 30 μm inverse features. The fluids and pneumatics layers were made in PDMS using a simple molding technique. PDMS is a two component polymer, and different ratios of the monomer and curing agent were used for each layer. The fluids layer was made softer and thinner so that it could be deformed by the applied pressure. The surface on the silicon master had to be surface treated so that the PDMS would resist adhesion to the master. The PDMS was poured on the mold in fluid form and cured in an oven to harden it. Once cured, the PDMS was manually peeled from the master. The final device was sealed to a glass substrate by plasma treating both the PDMS and substrate.

Interconnecting:

Silicone tubing was used to interconnect the device to the outside world. The process involved curing the silicone tubing directly into the PDMS by using a Plexiglas jig in order to create a continuous silicone interface. The jig had drilled holes in it that aligned to the interconnect pads on the master. The tubing was threaded through the holes, and the jig was visually aligned to the interconnect pads. Microscope slides were placed between the base and the jig in order to define thickness layer. The jig also had two extra holes drilled in it so that the PDMS could be injected on top of the master. The entire set up, as seen in Figure 3, was held together using electric tape while curing.

Results and Discussion:

Our device currently includes only eight wells, but the device is easily scaleable by the fact that 2n wells can be addressed with n valves.

Using a syringe pump, fluid was pumped into the fluids layer. As seen in Figure 4, the fluid did flow into the wells, and good isolation between wells was obtained. Pressure was also applied to the pneumatics layer by using a syringe pump, but the valves failed to actuate. Some tears in the layer may have caused the channels to collapse.

Future Goals:

Future work includes controlling fluid flow using valves and pumps, determining the pressure failure point for the interconnects, determining drug and cell interaction with PDMS, and developing a computer interface to control the system.

Acknowledgements:

I would like to thank all that made this project possible. Thanks to the Craighead Research Group, especially Professor Harold Craighead, Gus Lott, and Grant Meyer. Thanks to Frederick Maxfield of Cornell Medical School. Thanks to the CNF and all of its staff. Special thanks to the National Nanofabrication Users Network and the National Science Foundation.

References:

[1] Ng, J. M. K., I. Gitlin, A. D. Stroock, and G. M. Whitesides, "Components for integrated poly(dimethylsiloxane) microfluidic systems", Electrophoresis, Vol. 23, pp. 3461-3473, 2002.

[2] Unger, M. A., H. Chou, T. Thorsen, A. Scherer, and S. Quake, "Monolithic Microfabricated Valves and Pumps by Multilayer Soft Lithography", Science, Vol. 288, pp. 113- 116, 2000.

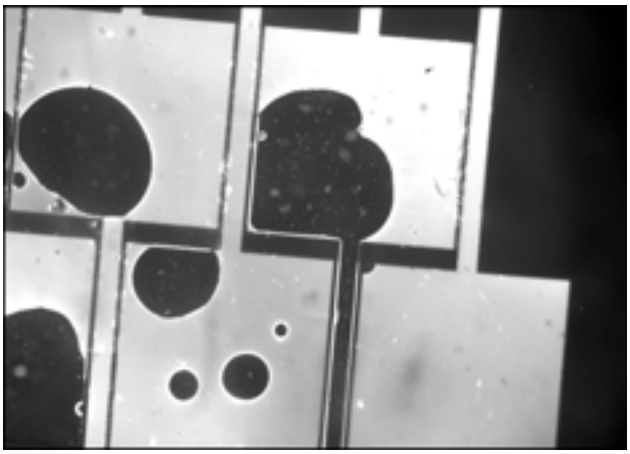

Figure 4: Fluid flowing through the channels.

Fabrication of Biomolecular Sieves with Novel Geometry

Rachel Gabor, Chemistry, Harvey Mudd College

Dr. Michael Spencer, Electrical & Computer Engineering, Cornell University

Lori Lepak, Chemistry, Cornell University

rgabor@odin.ac.hmc.edu, spencer@ece.cornell.edu

Abstract:

Two different devices were fabricated for the purpose of filtering mixtures of proteins with a size range of 1-20 nm. The first device consisted of arrays of 2, 4, 6, or 8 μm holes in a nitride layer over a through-etched window in a silicon wafer. Collagen monomers, rigid rods 300 nm long by 2 nm in diameter, were spun over the nitride layer. The monomers deposit on the surface in a 'hairball' geometry, leaving holes on the nanometer scale which can then filter a solution.

Another device was fabricated by etching holes through the silicon wafer from the backside, and through an oxide layer on the topside. These holes are skewed and joined by a thin layer of aluminum laterally. Aluminum (Al) can be evaporated reliably to thicknesses of 5-10 nm, and when etched away will leave channels of that height (though they may measure tens of μm laterally). These channels are then small enough to filter a solution containing biomolecules. Electrical gates were added to these channels to also separate the molecules based on charge.

Introduction:

The ability to separate biomolecules, such as proteins, by size would be very useful for biological applications such as separating DNA from hemoglobin for a blood test. A DNA strand has a diameter of about 2.0 nm and globular hemoglobin has a diameter of about 5.5 nm. Since proteins often have large variances in size, these sieves can separate them by taking advantage of these differences. Standard lithography techniques have a size limit of about 20 nm, too large to separate proteins in a size range of 5-15 nm. However, it is possible to accurately deposit materials on a wafer with a thickness within that size range. This lateral layer can be removed with a wet etch to produce a nanometer-sized constriction.

Two types of these devices were fabricated. The first, called the fabricated wafer, has nanoconstricted channels made using the previously described deposition technique. These devices are of a microscopic size which means they could be integrated into other chip-based devices, such as DNA analyzers. This summer they were also fabricated with integrated electrical gates, which could be used to separate the molecules by charge in addition to size. Their microscopic size also allows a very small sample volume to be used in the separation.

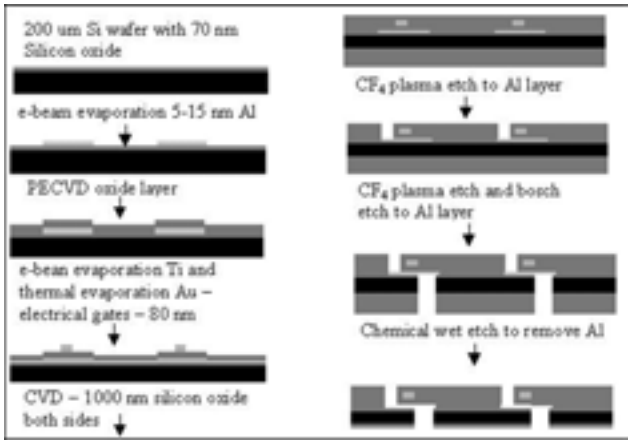

Figure 1: Fabrication process of fabricated wafers.

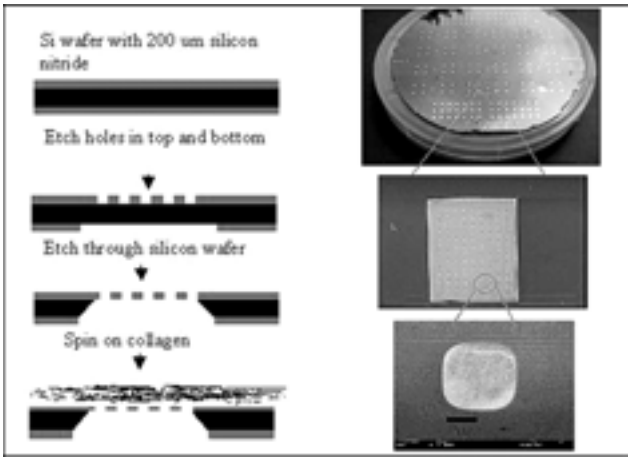

Figure 2: Fabrication process of collagen wafers and finished product (photo and TEM image).

The other type of device, known as the collagen wafer, was fabricated by spinning a layer of collagen over holes in a silicon wafer. The long, fibrous protein forms a sponge-like lattice over the surface, with holes in the 2-20 nm range. This can also separate proteins by size with the added bonus of being made of biological materials so they could be placed in the body.

Procedure:

The fabrication process for the fabricated wafers can be seen in Figure 1. The process for the collagen wafers can be seen in Figure 2.

Results:

During the CNF REU program, we were able to complete and fine-tune the fabrication process for both devices and begin flow testing on each device. Figure 3 shows an SEM of a cross section of a fabricated wafer channel. The hole in the upper right is the top hole etching down to the Al. The hole in the lower left is the bottom hole etching up to the Al. The "footing" at the top is a result of over-etching. In this particular wafer, the top hole was not etched long enough and the hole did not quite reach the Al. Further etching yielded a complete channel. Also seen in the SEM, as a bright horizontal band is the gold electrode, verifying that it is present in the system. The figure also includes a top view of a single device. The larger hole is the bottom hole, the smaller is the top hole and the band running through is the gold electrode. We successfully evaporated materials and made constrictions as small as 7 nm, beating the previous best of 20 nm.

The collagen wafers were also successfully built, with little alteration of the previous method.

The next step was to flow test these devices. NBTC REU intern Diego Rey designed PDMS reservoirs to use for flow-testing the devices. These reservoirs are small enough to only require a very small sample volume. As shown in figure 4, two types of reservoirs needed to be created, because while the fabricated wafers would require fluid to be pushed through, the collagen wafers would be unable to handle the strain and require laminar flow. The program ended before much flow testing could be done, so the results are as yet inconclusive. Also, while the electrical gates were successfully integrated, they have not yet been tested.

Further Work:

With future research in this project, we hope to find ways to make the constrictions even smaller. Also, more flow-testing needs to be done so that the flow process can be better understood. Finally, the electrical gates need to be tested to see if the integration was successful, and other possible integrations need to be tested.

Conclusion:

Two types of molecular sieves were developed for use in separating biomolecules by size. The first had nanoconstricted channels which were fabricated by taking advantage of the ability to laterally deposit layers of material to a small, accurate thickness on a wafer and later etch these layers away using chemicals. The second had nano-channels within a collagen sponge sitting on top of a silicon wafer. PDMS channels were designed for use with these devices, and the first one was integrated with electrical gates, and has the potential to be integrated into other devices.

Acknowledgements:

Dr. Michael Spencer, Lori Lepak, Diego Rey, the Spencer Group, CNF, NBTC, and NSF.

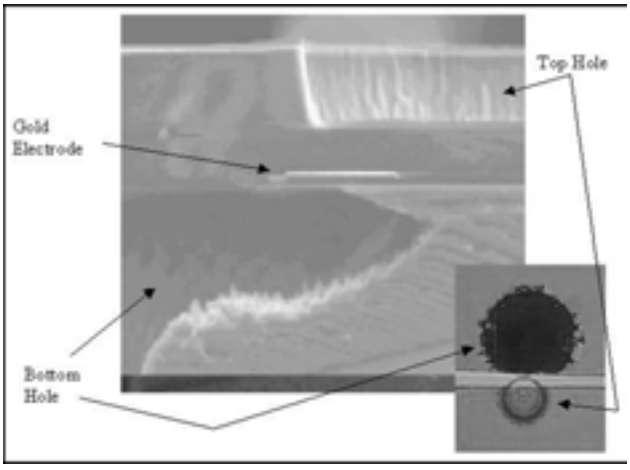

Figure 3, above: SEM and microscope image of fabricated wafers.

Figure 4, below: Flow patterns for both types of devices.

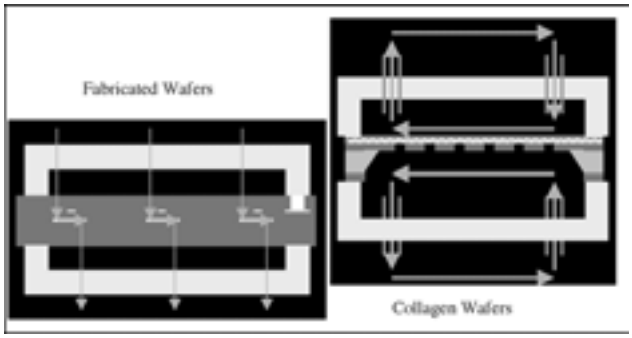

Chemistry-on-a-Chip: Multiphase Microfluidic Devices

Alireza Masnadi-Shirazi, Electrical Engineering, University of Texas at Arlington

Dr. James Engstrom, Chemical and Biomolecular Engineering, Cornell University

Mr. Abhishek Dube, Chemical and Biomolecular Engineering, Cornell University

ali_masnadi@hotmail.com, jre@cheme.cornell.edu, ad252@cornell.edu

Abstract:

This project focuses on the design and fabrication of a novel microfluidic system capable of handling any chemical and physical operation requiring a gas/liquid interface, such as heat exchanging, stripping, absorbing and mixing. Using microfluidic devices to perform these operations increases the efficiency due to the large surface area to volume ratio.

The project consisted of three major steps. (1) Fabrication of a liquid-phase Si wafer with microfluidic channels on the front side and small perforations ranging from 10 to 40 μm in diameter on the back side, such that these perforations connect the back side of the wafer to the channels etched on the front side of the wafer. (2) Fabrication of a gas-phase Si wafer with microfluidic channels etched on the front side. (3) Bonding the liquid-phase wafer to the gas-phase wafer such that the perforations on the back side of the liquid phase channel align completely with the channels on the gas phase wafer. Thus we have parallel gas/liquid channels connected by perforations that facilitate the formation of a gas/liquid interface. At the end, a pyrex wafer will be bonded to the top side of the liquid phase channel so the dynamics of the operations can be seen and characterized from above.

Introduction:

The goal of this project was to design and fabricate a multiphase microfluidic device that can handle any chemical or physical reaction which requires a gas/liquid interface. Since we wanted to have the gas and liquid streams in direct contact, a design involving a perforated membrane between the gas and liquid streams was suggested. Figure 1 illustrates a cross section of our proposed design.

As can be seen in Figure 1, gas and liquid flow continuously along parallel paths, and the perforations between these two channels allow the gas and liquid to react with each other. Two wafers would be needed, one to fabricate the gas channels and one to fabricate the liquid channels. Both wafers would undergo similar processing steps to form the channels, but the liquid-phase wafer would require additional steps to form the perforated membrane.

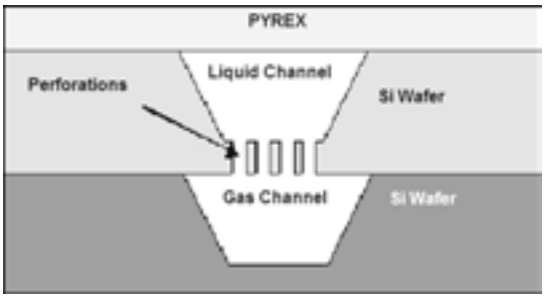

Figure 1: Cross section of a microfluidic device for gas/liquid interface.

Process:

The masks that were needed for the fabrication of the liquid and gas phase wafers had already been made by the Engstrom Research group. The wafers used were <100>-oriented Si, double sided polished, with 150 nm of LPCVD nitride. We first started with the liquid-phase wafer.

After performing standard photolithography steps on the front side of the liquid-phase wafer, the PT72 plasma etcher was used to etch the exposed nitride, which acted as a mask for the KOH etch. Then we used KOH etching to etch the liquid channels. At first we etched 300 μm deep channels on 550 μm thick wafers. Then for characterization and optimization, we etched shallower channels (150-200 μm deep) on 375 μm thick wafers. At this point, PECVD oxide was deposited on both front and back side of the liquid-phase wafers. The oxide on the back side wafer acts as a template for the Bosch etch and the oxide on the front side (patterned side) acts as a helium gas stop

when etching completely through the wafer during the Bosch process. Front to back side alignment was done to align the arrays of perforations along the length of the channels. Bosch etching was used to etch through the wafer and form the perforated membrane. The wafers were then dipped in HF to strip the remaining nitride and oxide layers.

The process for fabricating the gas-phase wafer was nearly identical to the fabrication of the front side of our liquid-phase wafers to form the channels. Thus, the processing steps for the KOH etch on the gas-phase wafers were done in batch parallel with the liquid-phase wafers. KOH etching is very aggressive and can find weaknesses or "pinholes" in the nitride mask and penetrate to the Si below. This results in a Si surface too rough for direct bonding of the liquid and gas wafers. Thus, a chrome-gold eutectic bonding method, which is more forgiving on the level of surface roughness, was used. Gold was deposited on the patterned side of gas-phase wafers, with a thin layer of chrome between the Si and gold to act as an adhesion layer.

Results and Conclusion:

The final structure of the liquid and gas phase wafers can be seen in Figures 2, 3 and 4. Figure 2 and 3 are optical microscope images of the liquid channels looking from above. The perforations can be seen along the length of the channel. Figure 2 shows the largest feature perforations and Figure 3 shows the smallest feature perforations. An SEM of the perforations from the back side of our liquid-side wafer can be seen in Figure 4. Due to the time constraints, we were unable to bond the wafers and characterize this multiphase microfluidic device; however more work is currently being done.

Acknowledgements:

I would like to thank Professor James Engstrom and Abhishek Dube for all their help. I would also like to thank Stephen Cypes for his guidelines and the CNF staff that made this program possible.

References:

[1] K.F.Jensen, "Microchemical Systems: Status, Challenges, and Opportunities", AlChE Journal, Vol. 45, No.10 (Oct. 1999), 2051-2054.

[2] S. Cypes, "MEng. Report", Cornell University, Dept. of Chemical and Biomolecular Engineering (2002).

[3] W. Ehrfeld,V. Hessel, H. Lowe, "Microreactors", Wiley-VCH, 2000.

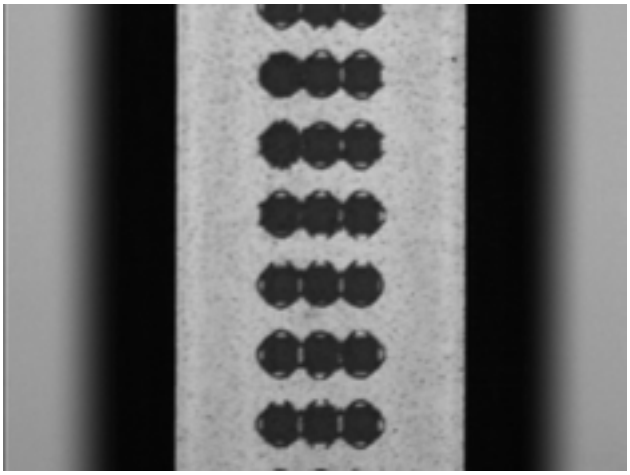

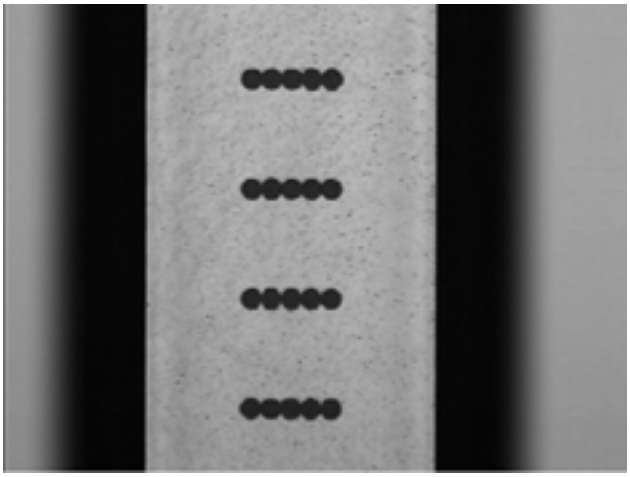

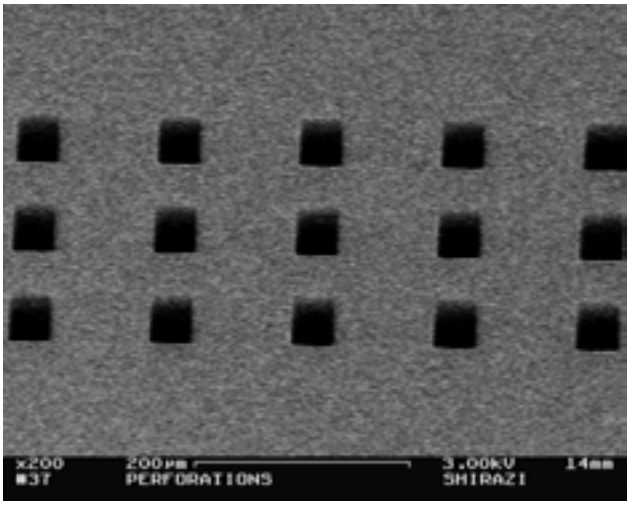

Figure 2, top: Looking from above a liquid channel with large feature perforations.

Figure 3, middle: Looking from above a liquid channel with small feature perforations

Figure 4, bottom: SEM image of perforations.

Embossing Polymer Waveguides for Integrated Optical Devices

Heather McKnight, Physics, Brigham Young University

Michal Lipson and Roberto Panepucci, Electrical & Computer Engineering, Cornell University

Bradley Schmidt, Electrical & Computer Engineering, Cornell University

hjm23@email.byu.edu, ml292@cornell.edu, panepucci@fiu.edu

Abstract:

Polymers are currently being investigated for many optical applications as a result of their ruggedness, low cost, flexibility and optimal light propagation. Embossing is an easy, low cost method to produced sub-micron devices by pressing a master with a negative image of the final structure into a polymer substrate under conditions of high temperature and pressure.

The focus of this project was to produce a reproducible method to nanoimprint, or emboss waveguides in polymers spun onto silicon substrates.

Conventional lithography and electron beam processes were used to produce masters in silicon and silicon oxide. These were embossed using polymethyl-methacrylate (PMMA), Teflon®, and a cyclo-olefin polymer in both positive and negative relief to produce channels and ridges for light propagation. The results were analyzed using scanning electron microscopes (SEM) and an atomic force microscope (AFM). Surface texture and the quality of pattern transfer were observed to be highly dependent on the materials used, and the temperature of embossing [1]. Submicron test structures, waveguides, and ring resonators were embossed successfully, and the method is being investigated to produce photonic crystals and other integrated optics for biosensing, display technologies, and optical switching.

Introduction:

Embossing is a convenient and reproducible method to fabricate optical devices because it is a method that can be performed with few requirements for equipment, on easily produced silicon substrates coated in polymers. High quality pattern transfer can be obtained quickly and can produce devices sufficiently smooth and uniform that light propagation should be possible. Waveguiding on-chip is a need for the small scale optics that will be emerging in the future with optical switching, and ring resonator devices for biosensing and display technologies.

Embossing was performed with masters fabricated with standard silicon semiconductor processes. The masters can be reused many times as a result of their durability and the anti-stiction coating. The polymers used were chosen for their widespread availability, low optical absorption in the visible wavelength range, and indices of refraction that were of the desired contrast for total internal reflection. The parameters tested were the temperature, time, and force of embossing, and the preparation of the polymer substrate.

Procedure:

Masters for embossing were created using conventional lithography and electron beam lithography techniques. A basic waveguide pattern was exposed onto photoresist on silicon. It was developed and etched using standard etching

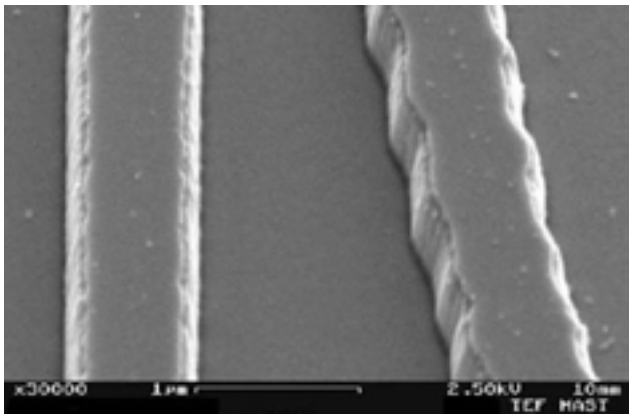

Figure 1: Silicon master detail of waveguide and ring structure.

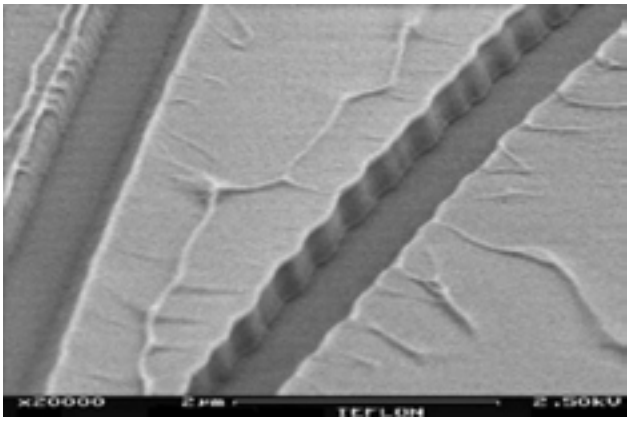

Figure 2: Embossed waveguide and ring structure in Teflon®.

procedures to the desired waveguide dimensions. Using image reversal, both positive relief (ridges) and negative relief (trenches) were created.

The Leica/Cambridge EBMF and Leica VB6: Vectorbeam System were also used to create the electron beam patterns directly on silicon. These masters were coated in a chemical vapor deposition process with a non-stick chemical called F6: Trichloro(1H2H2H-perflurooctyl)silane at Cornell's Nanobiotechnology Center.

The polymer substrates to be embossed were created by spinning various polymers onto Si wafers and onto Si wafers with a 4.5 μm layer of SiO, to act as additional lower index cladding. PMMA and Zeonor, the cyclo olefin polymer, (Zeonor 1020R, Zeon Chemicals L.P., Louisville, KY) were used as the high index core polymers. They have indices of refraction of 1.49 and 1.53 respectively. A Teflon® fluoropolymer (Teflon® AF 601S1-100-6, DuPont, Wilmington, DE) with an index of 1.29 was embossed as the low index cladding. A Fortin CRC Prepreg Mini Test Press was used for the embossing. Cleaved 1 inch^2 chips of the polymer substrate and master dies were embossed at forces ranging from 800-1100N. Temperatures between 180ºC and 260ºC were used depending on the glass transition temperature of the polymers.

Results and Conclusions:

Embossing of the PMMA and Zeonor was first conducted in the attempt to characterize and optimize the process. The results were inconclusive as the polymer adhered to the master and decomposed at higher temperatures. The Teflon® embossed better and had less stiction problems. It was discovered to be more successful to emboss trenches rather than ridges as a result of the polymer flow characteristics. Therefore, the embossing of trenches in the low index cladding material (Teflon®) was optimal. Accurate pattern transfer can be seen by comparing the silicon master in Figure 1 with the embossed structure in Figure 2. Sidewall roughness features on the master on the submicron scale transferred to the embossed waveguide with ease. Once the F6 anti-stiction process was discovered, numerous embossings could be conducted with the same master without the need for cleaning between embossing. Many structures were embossed to determine the size limits of the embossing. Large ring resonator structures are shown in Figure 3, and 40 nm photonic crystals holes in Figure 4.

From this study, we can conclude that embossing waveguides in various polymers in entirely feasible. Features on the order of 40 nm transferred from silicon masters to Teflon® accurately. Large rings could also be embossed, showing that there is little surface variation of the structures and sufficient continuity of form to produce waveguides and other optical devices that would be the same depth throughout the entire structure. Surface treatment of the master with the non-stick chemical was essential to reusability of the master and reproducibility of the embossed structure. Research is currently being conducted on filling the embossed trenches with a higher index polymer to test the optical properties of the waveguides.

Acknowledgements:

I would like to thank Dr. Roberto Panepucci primarily for his tireless support of my project. Thanks are also due to Dr. Michal Lipson, Bradley Schmidt and Amy Turner of the Cornell Nanophotonics group and to Dr. Mandy Esch of the Cornell NanoScale Facility.

References:

[1] M. Esch, S. Kapur, G. Irizarry, and V. Genova, Influence of master fabrication techniques on the characteristics of embossed microfluidic channels, Lab Chip, 2003, 3, 121-127.

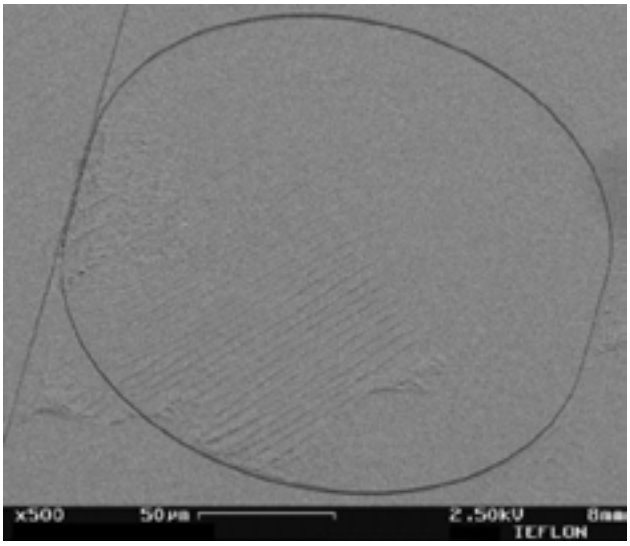

Figure 3, above: Entire embossed ring in Teflon®.
Figure 4, below: Photonic crystal pattern embossed in Teflon®.

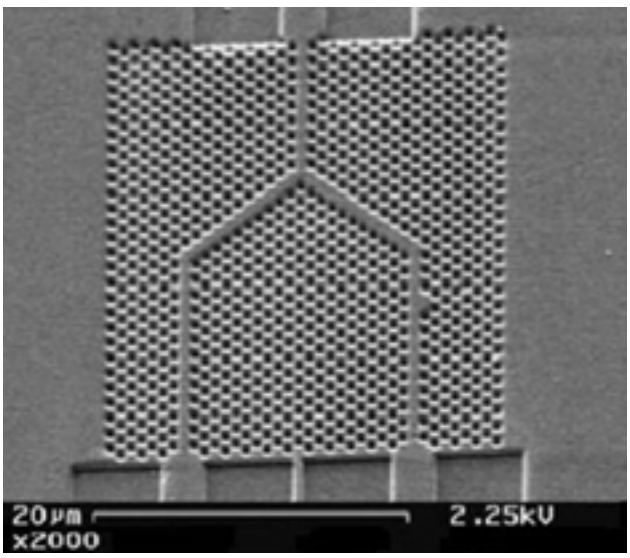

Novel Gate Stack Process for MOS-Based Structures

Michael Miranda, Electrical Engineering, University of Notre Dame

Dr. Edwin Kan, Electrical and Computer Engineering, Cornell University

Jami Meteer, Electrical and Computer Engineering, Cornell University

mmiranda@nd.edu, kan@ece.cornell.edu

Abstract:

Asymmetric charge injection has been achieved in metal oxide silicon (MOS) capacitor structures through the introduction of metal nanocrystals embedded in another metal with a different work function. The MOS capacitors are used in a tunneling diode configuration. From CV measurements, we can characterize the effective insulator thickness (the tunneling barrier) and work functions. IV measurements show that the nanocrystal triple interface (metal-metal-insulator) achieves higher current injection than the control samples without nanocrystals, by a factor of approximately two orders of magnitude.

The proposed mechanism for increased injection is potential barrier-lowering by fringing fields derived from the high sheet charge density at the metal-metal interface. The lower effective barrier height allows significant injection at voltages as low as 3 V which is 10^2 to 10^3 times higher than at -3 V. This can be explained by the exponential increase in Fowler-Nordheim (F-N) tunneling with decreased barrier height.

The increased injection can be even larger if the nanocrystal distribution is designed to minimize current crowding effect. This property of asymmetric injection coupled with the large energy barrier of SiO_2 can potentially be used to create a large population of electrons confined in Si, one component necessary for developing optoelectronic applications in Si systems. The charge injection properties of this device are also applicable in the design of low-voltage floating-gate CMOS structures.

Introduction:

The use of floating-gate CMOS devices for non-volatile memory is well-established [1]. For continued scalability, there is a need for lower operating voltages, faster write and access times, and higher reliability. Some of these concerns can be addressed through the introduction of nanocrystals to the structure of CMOS floating-gate structures.

To reduce the operating voltages, nanocrystals can be placed at the interface with the oxide layer. In this project, the crystals were grown on the silicon side of the oxide. The crystals subsequently formed a triple interface where the oxide, crystal, and silicon meet. Through proper work function engineering, an electric field (due to work function differences) can be created between the silicon substrate and the nanocrystals. This structure creates a fringing field at the edge of the interface (Figure 1). It is believed that this fringing field extends into the SiO_2 reducing the potential barrier that impedes current flow. This allows F-N tunneling to occur at lower forward bias voltages through the lower effective barrier. No significant change is present in the reverse bias condition since the fringing field does not penetrate to the other side of the oxide barrier.

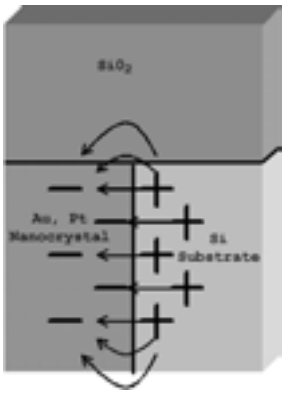

Figure 1: Triple interface with fringing fields.

The following research explores the effects of the nanocrystal introduction to the oxide- silicon interface of the MOS capacitor in an effort to create an asymmetrical charge injection structure.

Procedure:

100 mm silicon wafers were doped using two ion implants of phosphorous. The first implant was at 100 keV and the second at 25 keV, both with a 7° off-set from a 1-0-0 orientation. This was to create a degenerate doping level of approximately 8 x 10^{19} cm^{-3} at the surface. A 1.2 nm layer of gold or platinum was evaporated onto the doped wafers, leaving out a control. The gold and platinum nanocrystals were formed through self-assembly on the silicon surface. Plasma enhanced chemical vapor deposition (PECVD) was used to deposit an oxide layer of ~50 nm on top of the nanocrystals. One set, consisting of both nanocrystal types and a control, had a 200 nm chromium cap layer deposited. A second set used a sputtering technique to deposit a tungsten cap metal. Standard photolithographic methods were used to pattern the top pads of the capacitors.

To test the structures for asymmetric injection properties, current vs. voltage (I-V) and capacitance vs. voltage (C-V) curves were taken. I-V curves allow for the observation of

asymmetry in charge injection, while C-V curves give information allowing the oxide thickness and work functions to be determined. For both measurements, voltage sweeps were made in the positive and negative direction. This helps check for trapping states and supports repeatability.

All measurements were taken at a probe station and analyzed and processed using Matlab. The I-V measurements were taken with a HP4145 and the C-V measurements with a Keithley 590.

Results and Conclusions:

The data showed that asymmetric injection occurred in the platinum nanocrystal structure with the chromium cap metal. At 5 V there was a current three orders of magnitude greater than that at -5 V. The onset of asymmetric injection occurred at approximately 2.2 volts (Figure 2). Similarly, the structures with the tungsten cap metals showed asymmetric injection properties. A platinum nanocrystal device showed approximately two orders of magnitude increase in current from negative to positive 5 V, as did a gold nanocrystal device (Figure 3). Figure 3 also allows comparison with the tungsten control device showing the charge injection in the control being approximately two orders of magnitude below both of the nanocrystal triple interface structures. Increasing the voltage sweep range, Figure 4, shows that the charge injection is independent of starting voltage magnitude.

From the measurements taken, it can be concluded that due to the introduction of nanocrystals, asymmetric charge injection was achieved. High temperature characterization is needed to confirm that injection is due to FN tunneling.

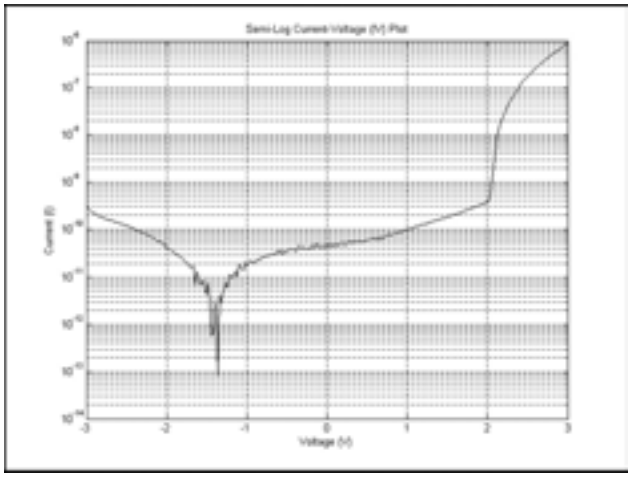

Figure 2: Platinum nanocrystals with chromium cap metal.

Acknowledgments:

This project was under the direction of principal investigator Dr. Edwin Kan of Cornell University. All work was performed at the Cornell NanoScale Facility with the aid of the facility's staff. Funding was provided by the National Science Foundation REU program through the National Nanofabrication Users Network. Thank you to Ms. Melanie-Claire Mallison, and a special thanks to my mentor Jami Meteer for all her help, guidance, and advice.

References:

[1] Campell, S.A. The Science and Engineering of Microelectronic Fabrication. NY, Oxford University Press; 1996.

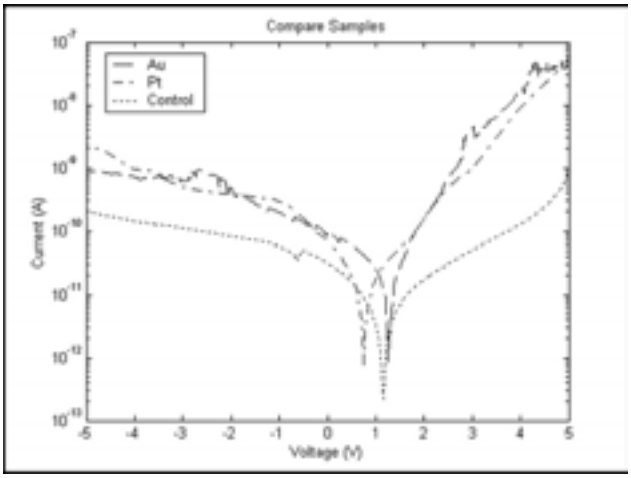

Figure 3, above: Tungsten cap metal.

Figure 4, below: Platinum nanocrystals with tungsten cap metal.

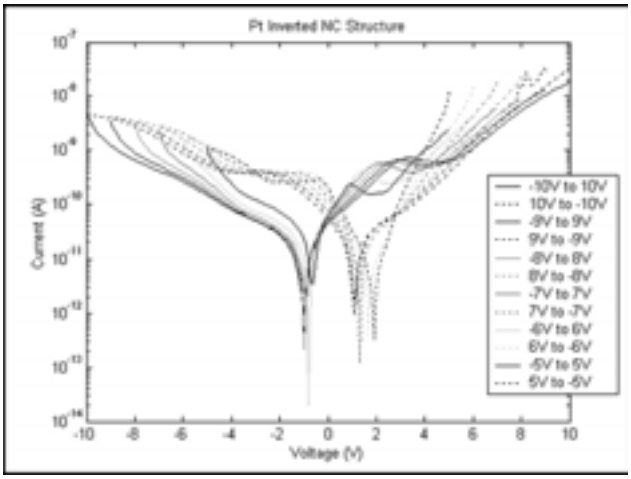

Ultrasonically Driven Microneedle Arrays

Andrew M. Newton, Bioengineering, Kansas State University

Professor Amit Lal, Electrical and Computer Engineering, Cornell University

Xi Chen, Electrical and Computer Engineering, Cornell University

newton@ksu.edu, al274@cornell.edu, xc35@cornell.edu

Abstract:

New advances in nanofabrication have enabled silicon MEMS production of minimally invasive, potentially painless microneedles that can be used in biomedical, chemical and fluid delivery applications. Microneedles can be powerful tools in transdermal drug delivery, blood or interstitial fluid sampling and the chemical analysis of small quantities of organic matter.

Here we have fabricated microneedle arrays using deep reactive ion etching (DRIE) and have tested the force required for skin penetration by using similarly permeable silicon rubber and vegetable skin simulates. This paper presents the fabrication process and preliminary experiments with silicon microneedles bonded to piezoelectric actuators.

Introduction:

The development of more effective and complex drugs has enforced the need to create innovative approaches to transdermal drug delivery, blood or interstitial fluid sampling and chemical analysis. This demand has increased the interest in the MEMS fabrication of microneedles. Microneedles are generally fabricated in two-dimensional arrays as either in-plane needles or out-of-plane needles and can be created as solid needles for increased permeability, or hollow needles with channels for direct fluid delivery.

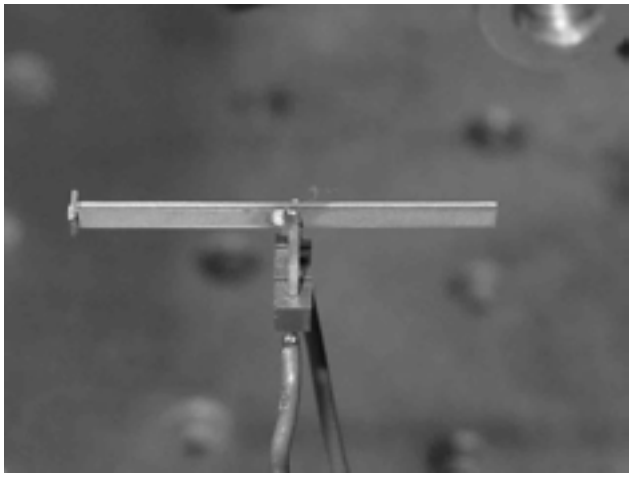

Figure 1. Test device: microneedle array attached to PZT.

Human skin is comprised of three layers; stratum corneum, viable epidermis and dermis. The 10-20 μm outer layer of skin, the stratum corneum, is primarily composed of dead cells and is responsible for the extraordinary barrier properties of skin. The viable epidermis, lies below at a depth of 50-100 μm and contains living cells and a limited number of nerve cells. Blood vessels and the majority of nerve cells lie within the deepest layer of skin, the dermis.

The attraction of fabricating microneedles is creating silicon-based biocompatible devices that can penetrate the upper layer of human skin without penetrating the deeper layers of skin that contain sensitive nerve endings and capillary blood vessels.

Justification of Ultrasound in Reducing Penetration Force:

Although fabrication of microneedles is relatively new and its applications are very attractive, researchers have discovered that there are major challenges concerning the penetration of microneedles into human skin. If the microneedles are not sharp enough, or their spatial density is too high, the skin will deflect the penetration attempt and create a flexed bending which the microneedles cannot penetrate. Conversely, if the microneedles are too long, the upper portion of the microneedle may not have enough flexural rigidity and could break off before penetration or under the skin.

By driving the microneedle arrays ultrasonically, we propose we can alleviate many present problems and can provide a more effective and efficient means to use microneedles in the penetration of human skin. Ultrasonic effects reduce surface deformation of skin at penetration via inertial stiffening and, after

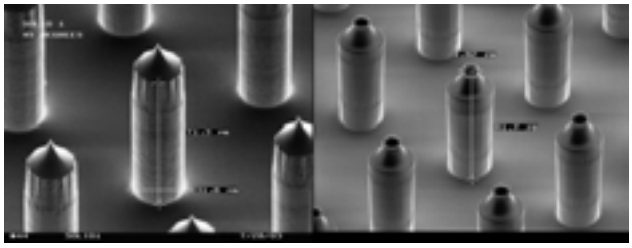

Figure 2. SEM photo of solid needles and hollow needles.

penetration, potentially provide a fluid lubricating layer for smoother insertion.

Fabrication of Microneedles:

Deep reactive ion etching (DRIE) processes on the PlasmaTherm 770 and UNAXIS 770 were used to fabricate two unique microneedle arrays, symmetric tips and asymmetric tips. Chromium masks were used to pattern the L-Edit designed arrays, and the regions protected by the metal mask remained to form the microneedles. Each procedure used {100}-oriented, p-type, 475-575 μm thick, 1-20 Ω-cm silicon wafers. All microneedle fabrication required a thermal oxidation with an expected thickness of 2 μm to be deposited and patterned on both the front and backside. Shipley 1827 photoresist was used during the lithography process and a 6:1 Buffered Oxide Etch (BOE) was used for surface compatibility and to remove remaining oxide for both microneedle arrays.

Symmetric tip wafers required silicon nitride to be patterned on the front side before an isotropic silicon etch for a depth of ~20 μm was performed using the UNAXIS 770. Asymmetric tip wafers utilized a thick photoresist patterning on the front side before a ~20 μm depth isotropic silicon etch. Frontside and/or backside DRIE processes were performed before removing photoresist with the Branson Barrel Etcher or nanostrip for both microneedle array processes.

Results and Discussion:

The primary result of this research was that by using ultrasonic actuation achieved with piezoelectric PZT actuators, we were able to reduce the penetration force significantly. At ultrasonic frequencies, the material being penetrated is effectively hardened permitting penetration to happen with less surface deformation which is important for the microneedles during penetration of the soft human skin.

The microneedle array dies and piezoelectric PZT plates were cut by laser machining. The microneedle array was glued onto the end of a PZT bar and driven at the half wavelength longitudinal mode of the PZT. The samples were mounted on a load cell to record the force applied and the microneedles with PZT were mounted on a micromanipulator for movement. This study is in contrast to previous microneedle works which have not engineered penetration dynamics.

From this study, we concluded that ultrasound can be used to facilitate reliable and predictable microneedle insertion, and has potential applications in automated microneedle insertion and body fluid sampling devices.

Acknowledgements:

Special thanks to Professor Amit Lal and Xi Chen, for their hard work, resources, guidance and assistance in this project, also the CNF staff for their support and expertise, and to Melanie-Claire Mallison for her dedication and commitment to this program.

References:

[1] Henry, S., McAllister, D.V., Allen, M.G. and Prausnitz, M.R., 1998, "Microfabricated Microneedles: A Novel Approach to Transdermal Drug Delivery," Journal of Pharmaceutical Sciences, vol.87, no.8, pp.922-925.

[2] Lin, L. and Pisano, A.P., 1999, "Silicon-Processed Microneedles," Trans. IEEE Journal of Microelectromechanical Systems, vol.8, no.1, pp.78-84.

[3] Prausnitz, M.R., McAllister, D.V., Kaushik, S., Patel, P.N., Mayberry, J.L., and Allen, M.G., 1999, "Microfabricated Microneedles for Transdermal Drug Delivery", Georgia Institute of Technology.

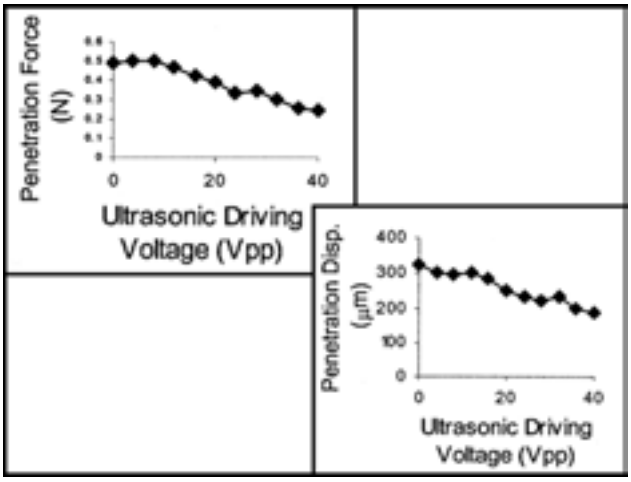

Figure 3, left. Displacement at penetration vs. ultrasonic driving voltage for solid symmetric microneedles (10x10 array).

Figure 4, right. Penetration force vs. ultrasonic driving force tests for solid symmetric microneedles (10x10 array).

Using SuperCritical CO_2 as an Environmental Benign Processing Solvent in Nanolithography

Maria Dung Nguyen, Chemical Engineering, Cornell University

Christopher K. Ober, Materials Science & Engineering, Cornell University
Nelson Felix, Victor Pham, Chemical Engineering, Cornell University
dn45@cornell.edu, cober@ccmr.cornell.edu

Abstract:

This study aimed to manipulate temperature and pressure parameters of supercritical CO_2 to produce 200 nm positive-tone nanostructures from a negative-tone photoresist consisting of a random copolymer, tetrahydropyran methacrylate-r-1H, 1H-perfluoroctyl methacrylate (THPMA-F7-MA) with photoacid generators (PAG). Electron beam and 248 nm lithography were used to imprint nanostructures onto the photoresist-coated wafer. An adapted version of the Diffused Enhanced Silylated Resist (DESIRE) process was implemented to produce positive-tone from negative-tone features in order to comply with industrial lithographic standards.

SEM and AFM images showed fair resolution of 300 nm structures after $scCO_2$ development (Figure 1). Patterns below 200 nm were distorted. Image distortions indicate acid diffusion and polymer swelling in negative-tone developments, and possible polymer cross-linking in positive-tone developments.

Introduction:

Supercritical CO_2 has emerged as the leading substitute for traditional aqueous and organic photolithographic solvents. $ScCO_2$ is environmentally benign and a non-ozone depleting agent, unlike traditional solvents. It is an ideal candidate for photoresist removal due to its lack of surface tension. A few of the processing benefits of $scCO_2$ include control of the solvation power through slight changes in temperature and pressure to dissolve appropriate solutes [1, 2].

The focus of this study is to produce good resolution positive-tone features using $scCO_2$. Because THPMA-F7-MA is a negative-tone photoresist, it must be converted to positive-tone. Two steps are added to the DESIRE process: silylation and flood exposure after e-beam exposure. These two steps involve the solubility switch of the exposed and unexposed areas of the photoresist required for image reversal. To achieve quality positive-tone features, this study, in part, also aims to improve these process conditions as well as the processing conditions of the $scCO_2$.

The characterization of the images is done using the Scanning Electron Microscope (SEM) and the Atomic Force Microscope (AFM).

Experimental:

A solution containing a 5% ratio of PAG/THPMA-F7-MA is mixed for approximately 24 hours. The photoresist solution is spin-coated onto a silicon wafer at 3500 rpm. A post-bake is applied at 110°C for 60 sec. The resist-coated wafer is then exposed using e-beam patterning. A post-exposure bake is applied to the wafer at 60°C for 60-90 sec. A negative-tone image can be developed by inserting the sample into a sealed container where there is a chamber which controls pressurizing and depressurizing of CO_2. A positive-tone image is produced by silylation and a flood exposure before development.

After e-beam patterning, the sample is placed under a glass container on a hot plate at about 60-65°C. A silylation agent, TMDS, is held in a cylinder glass container connected with a tube to a nitrogen gas tank [3]. The nitrogen gas passes through a tube submerged into the TMDS, bubbles the silylating agent, and becomes saturated with the TMDS vapors [3]. The N_2/TMDS gas flows over the sample and exits through a valve opening. Silylation occurs for 60-90 mins. After silylation, the sample is flood exposed for 30-60 sec under a HTG contact aligner followed by the development in the $scCO_2$ chamber. SEM and AFM images are taken after development for characterization.

Results:

The solubility switch chemistry is important. The original photoresist is soluble in $scCO_2$. During e-beam exposure, the PAG is activated in the exposed areas, releasing hydronium ions that replace the pyranol group ($scCO_2$ soluble) of the copolymer with a hydroxyl group ($scCO_2$ insoluble). The unexposed areas remain $scCO_2$ soluble. After development, the unexposed areas dissolve in $scCO_2$ and the exposed areas remain on the wafer. This is a negative-tone development. During silylation, the hydroxyl group is replaced with a silicon-rich group ($scCO_2$ soluble). A flood exposure step completes the solubility switch by activating the PAG in the unexposed regions. Processing produces a positive-tone development. The completeness of these two steps also determines feature resolution since this plays an integral part in image reversal.

In negative-tone developments, it has been discovered that acid diffusion and polymer swelling are responsible for the distortions. Pattern features were not aligned with the e-beam patterning. Inappropriate photoresist removal made corners and edges "rounded". Acid diffusion occurs mostly during the time between e-beam exposure and silylation. After e-beam exposure, the PAG in the exposed areas are activated and react with the polymer. If the sample is not silylated within 1-2 hours, unreacted PAG diffuses into the surrounding photoresist, causing these areas to become insoluble. After development, these areas that should remain dissolve, causing pattern distortions.

Polymer swelling in negative-tone developments is the result of the plasticization effect. During pressurization, the glass transition of the polymer decreases. The polymers are able to slip and slide under and over each other. During depressurizing, the glass transition of THMPA-F7-MA increases and the polymers lose their flexibility, freezing in place. After complete depressurization, the images appear "swollen". This plasticization effect suggests that THPMA-F7-MA may not be a suitable photoresist for this particular nanolithographic process.

The pattern distortions in positive-tone developments are not yet explained. Pattern distortions indicate possible polymer cross-linking; other possible causes are presently unknown.

Conclusions:

Acid diffusion, the plasticization effect, and possibly polymer-cross-linking are primarily responsible for the pattern distortions. However, the processing conditions of $scCO_2$ have yet to be determined. A temperature of 35°C and a pressure between 2500-3000 psi appear to yield decent resolution. In future studies, optimizing pattern feature resolution will depend upon the improvement of the process conditions of $scCO_2$ as well as the conditions before development.

Acknowledgments:

I would like to thank Ms. Melanie-Claire Mallison, Mr. Alex Pechenik, Mr. Garry Bordonaro, Mr. Nelson Felix, Mr. Victor Pham, and the CNF staff.

References:

[1] McHugh, Mark A.; Garach-Domech, Alberto, Park, Il-Hyun; Li, Dan; Barbu, Eugen; Graham, Paul; Tsibouklis, John. Macromolecules vol. 35, 2002, 6479-6482.

[2] DeSimone, J.M.; Guan, Z.G.; Elsbernd, C.S. Science vol. 257, 1992, 945-947.

[3] Pham, Victor Q.; Nguyen, Peter T.; Weibel, Gina L.; Ferris, Robert J.; Ober, Christopher K. Positive-tone resist for supercritical CO2 processing. Polymer Preprints (American Chemical Society, Division of Polymer Chemistry) (2002), 43(2), 885-886.

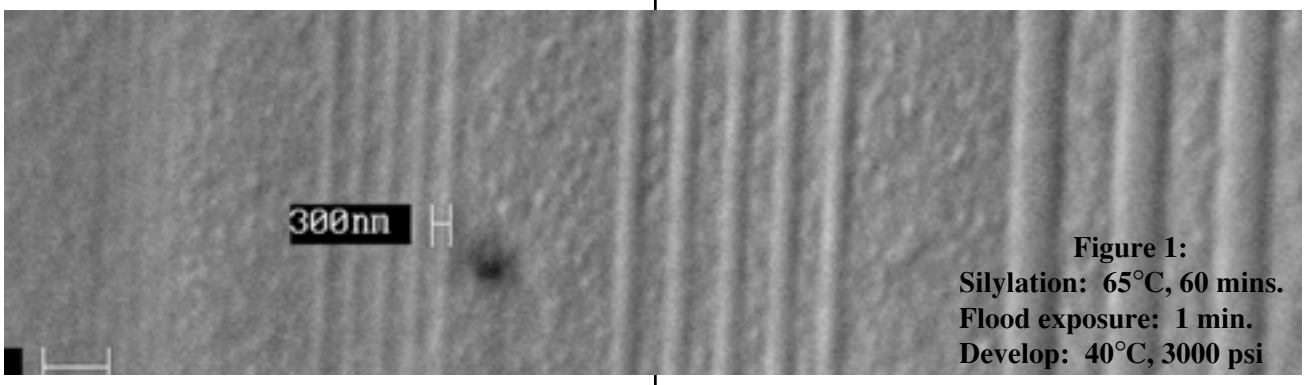

Figure 1:
Silylation: 65°C, 60 mins.
Flood exposure: 1 min.
Develop: 40°C, 3000 psi

A Novel Method of Creating Nanoscale Interconnects by Radioactive Decay

Justin A. Scott, Mechanical Engr. and Materials Science, UC Berkeley

Professor Amit Lal, Electrical and Computer Engineering, Cornell University
Serhan Ardanuc, Electrical and Computer Engineering, Cornell University
tj_scott@uclink.berkeley.edu, al274@cornell.edu

Abstract:

There are numerous applications of nuclear power that can benefit from levels of radioactivity no greater than what is found in a standard smoke detector. One proof of this functionality is a proposed method to form nanoscale interconnects. Our hypothesis suggests that paths of high conductivity are produced along nuclear tracks due to the damaging properties of radioactive decay. Ultimately, various blocks of materials will be aligned along damage paths to form interconnects. In order to prove these tracks are detectable, capacitors of various sizes and materials are created. The Atomic Force Microscope (AFM) is used to determine surface roughness and a probe station is utilized to reveal initial conductivity. Samples are then subjected to a radioactive source. Conductivity is subsequently re-characterized and initial results indicate a change in conductivity as a result of radiation exposure. Results are preliminary, but this method could potentially increase the success of three-dimensional devices.

Introduction:

While the discovery of nuclear power catalyzed a large number of projects that worked to harness it as a power source, more recently the focus has shifted to safety and limitation of doses. In contrast to this trend, there are a handful of projects in recent years that have worked to show the functionality of radioactivity. Nanotechnology is one field that has been working to demonstrate the benefits of nuclear power with doses that rival the level of radioactivity in a standard smoke detector. One example is the self-reciprocating cantilever beam powered by a radioactive source of 1 mCi of Ni-63[1].

One characteristic of radiation that has been exploited in devices such as the CR-39 track detector is the effect of damage [2]. Emitted radioactive particles leave damage paths that have been extensively researched. A similar concept is employed in the creation of nanowire clusters. This process utilizes lithography and exploits the damaging properties of heavy ion irradiation to form nanowires [3]. Like nuclear damage, heavy ion irradiation creates dislocations that are characteristic of areas with higher conductivity.

Combining ideas from existing research with heavy ion irradiation and nuclear damage, we hypothesize that it is possible to create conductive tracks that can be aligned to form interconnects. We believe it is possible to induce conductive tracks by radioactive decay and also increase this ability to transfer electrons by annealing. Controlled heating of the doped material will allow for enhanced diffusivity of free electrons to damage paths. The potential exists to create networks of communication that approach the complexity of neural networks in the human brain.

Method:

Capacitors are used to quantitatively demonstrate the existence of conductivity tracks for dielectric materials. The most effective process flow is seen in Figure 1. It consists of first depositing a 0.7 μm thick layer of silicon nitride (SiN). A 0.8 μm thick layer of polysilicon is then placed on top. Following this step, a pattern is transferred using photolithography and wet etching. Doped Phosphosilicate Glass (PSG), approximately 200 nm thick, is then deposited on the

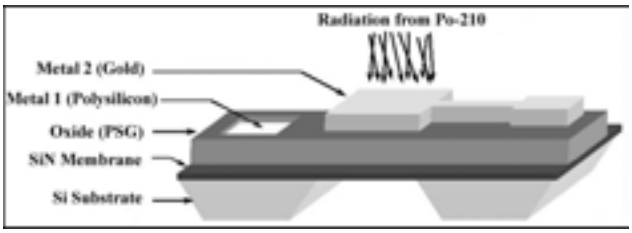

Figure 1: Diagram of capacitor.

first metal layer using a Plasma-Enhanced Chemical Vapor Deposition (PECVD) process. Some areas of the oxide layer are then etched away to clear bond pads for later conductivity measurements. Lastly, gold is evaporated on top of the PSG and patterned using a lift-off process.

Following our fabrication, initial conductivity tests of test dies are taken with an I-V Probe Station before and after annealing the dies at 250°C for two hours. AFM is subsequently used to reveal surface roughness. Dies are then exposed to a radioactive source of Po-210 for five minutes by placing capacitors top-side down on the source. Conductivity is re-characterized after exposure as well as after another annealing process at 400°C for four hours.

Results and Discussion:

Initial results indicate that there is a change in conductivity as a consequence of radiation exposure. In three of five devices tested, conductivity increased. The most pronounced increase could be noted in device 6 of die 4 where conductivity increased to 1.14 x 10^{-9}A from 2.3 x 10^{-11}A at 5 V (see Figure 2). Unfortunately, annealing almost exclusively reduced conductivity, contrary to what was expected. One possible explanation is that leakage current incorrectly represented the value of conductivity before the annealing process.

In addition, there were still two devices that experienced a decrease in conductivity after bombardment. To account for this, one possibility is that the devices were not exposed to the radiation source. Due to the inexact methods in measuring exposure, it was difficult to determine when devices were subjected to radiation. This could also explain the small discrepancy between conductivity, as noted in device 3 of die 3 (see Figure 3).

Conclusion:

After establishing an effective process flow, radiation bombardment was found to affect conductivity of fabricated devices. Work still needs to be completed with larger sample sizes in order to ensure conclusive results regarding conductivity. AFM and Scanning Tunneling Microscope (STM) scans also need to be completed in order to pictorially demonstrate conductivity path existence. Eventually, topographic images taken with the AFM will be subtracted from the STM to produce images of only the areas with higher conductivity.

Acknowledgements:

I would like to acknowledge Professor Amit Lal, Serhan Ardanuc, and the CNF staff for their support as well as the NSF and NNUN for their generous funding.

References:

[1] Li, H., Lal, A., Blanchard, J., Henderson, D., "Self-Reciprocating Radioisotope-Powered Cantilever," Journal of Applied Physics, vol. 92, no. 2, 1122-1127.

[2] Rao Y.V., Hagan M.P., Blue J., "Detection of 10-MeV protons, 70-MeV ^{3}He ions and 52-MeV ^{4}He ions in CR-39 Track Detector," Nuclear Tracks & Radiation Measurements, vol.6, no.2-3, 119-24.

[3] Lindeberg, M., Hjort, K., "Interconnected Nanowire Clusters in Polyimide for Flexible Circuits and Magnetic Sensing Applications," Sensors and Actuators A, 105 (2003), 150-161.

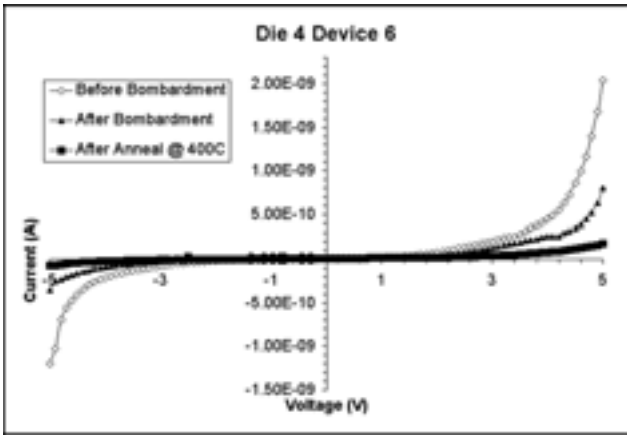

Figure 2, above: I-V characteristic of Die 4 Device 6.

Figure 3, below: I-V characteristic of Die 3 Device 3.

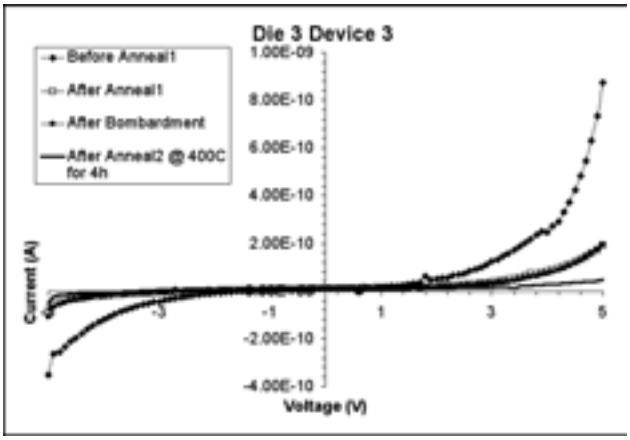

2003 NNUN REU Program at
Materials Science Research Center of Excellence
Howard University, Washington, DC
http://www.msrce.howard.edu

MSRCE/NNUN REU Intern ..... Major & School Affiliation ..... Principal Investigator

From left to right:

Dr. Juan White ..... MSRCE, Howard University ..... NNUN REU Principal Investigator
Ms. Aminata Kone ..... Chemical Engineering, Clemson University ..... Maoqi He & Gary Harris
Mr. Edgar Allen Cabrera ..... Biological Engineering, Cornell University ..... Kimberly Jones
Ms. Stephanie Cheng ..... Biology, Cornell University ..... Gary Harris
Mr. James Boedicker ..... Chemical Engineering, MIT ..... James Griffin
Mr. Moussa Souare ..... Electrical Engineering, University of Akron .. Clayton Bates, Gary Harris, Juan White
Mr. William Quinones ..... Mechanical Engineering, UCSB ..... Crawford Taylor
Dr. James Griffin ..... MSRCE, Howard University ..... MSRCE REU Program Coordinator & PI

The Effects of Thermal Annealing on InGaAsN and GaAsN

James Boedicker, Chemical Engineering, Massachusetts Institute of Technology

Dr. Gary Harris, Materials Science Research Center of Excellence, Howard University

Mr. James Griffin, MSRCE, Howard University

jqb@mit.edu, jagriffin@howard.edu

Abstract:

InGaAsN and GaAsN epilayers were grown on samples of GaAs using molecular beam epitaxy (MBE) with indium (In) and nitrogen (N) concentrations of less than 1%. Though nearly perfect samples of GaAs can be grown using MBE, the inclusion of N into the GaAs crystal causes lattice defects. Therefore, it has been suggested that thermal annealing of samples should improve material properties such as charge carrier mobility. This work has shown that electronic properties of GaAsN epilayers with ~1% nitrogen concentrations can improve after thermal annealing at 1023°K for 30 seconds.

Introduction:

Bandgap engineering is an area of research that has attracted much attention lately. In bandgap engineering, the bandgap of semiconductors are selected by controlling the molecular composition of the material. It has been found that the nitrogen composition in GaAsN and InGaAsN has unusual effects on the bandgap of the material (see Figure 1). By varying the nitrogen composition in these semiconductors, engineers can select the bandgaps of materials used in optoelectronic and photovoltaic devices.

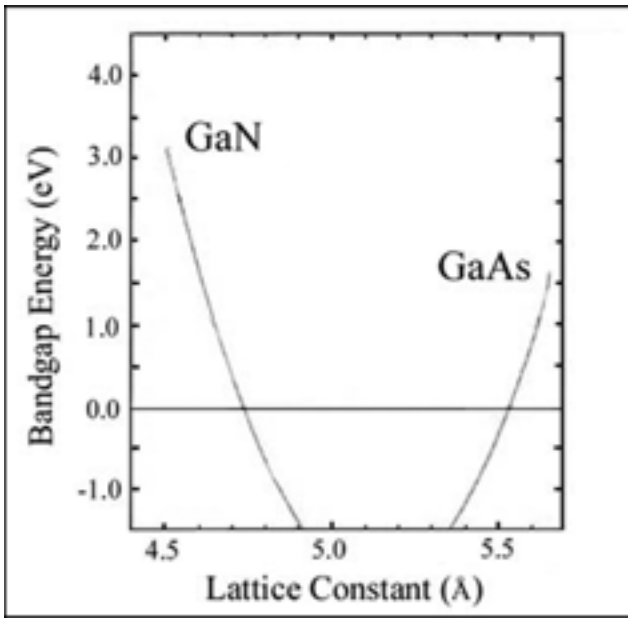

Figure 1: Adding a small amount of nitrogen to GaAs lowers the bandgap.

Incorporating nitrogen into semiconductors can often lead to the degradation of electrical properties. Epilayers of GaAsN and InGaAsN grown using molecular beam epitaxy (MBE) are more disordered than epilayers that do not contain nitrogen. This is the result of nitrogen causing crystal defects during the growth. Some crystal defects can be corrected by thermal annealing. This project will show of effects of thermal annealing on the carrier mobility in InGaAsN and GaAsN.

Procedure:

GaAsN and InGaAsN epilayers were grown onto base samples of GaAs using MBE. Ga, As, and In were evaporated from commercially obtained solid sources. A beam of monatomic nitrogen was made by creating a nitrogen plasma. Diatomic nitrogen gas was irradiated with high frequency radio waves, resulting in monatomic nitrogen. Since the nitrogen flux from the plasma source remained constant, the mole fraction of nitrogen in the growing epilayer was controlled by varying the evaporation rates of the semimetals. The dopants used during the growth were silicon (Si) for n-type layers and beryllium (Be) for p-type layers. After growing 1 μm of GaAs on the base sample, nitrogen containing epilayers were grown to thicknesses of approximately 1 μm. Nitrogen compositions varied between 0.07% and 0.94%. Dopant concentrations varied between 10^{16} and 10^{18} cm^{-3}.

Some of the samples were annealed after the growth. The annealing process took place in a rapid thermal annealer (RTA). Cleaned samples were sandwiched between pieces of GaAs and placed in the RTA. The annealing took place under an atmosphere of nitrogen and argon for 30 seconds at 1023°K. Temperature ramp rates were approximately 30ºK/s.

In order to perform the necessary electrical measurements, ohmic contacts had to first be applied to the sample surface. The samples and contacts were cleaned by rinsing with organic solvents and then etched with a 50% HCl solution for 60 seconds. Contacts of tin (Sn) were used for n-type samples and contacts of an In:Zn [3:1] blend were used for p-type samples. The contacts were alloyed onto the sample surface by heating to 723ºK under a hydrogen atmosphere for 60 seconds.

After contacts were attached, Hall measurements were taken. The Hall measurement apparatus used was a homemade device. It consisted of a sample holder with copper contacts, an electromagnet, and a multimeter. Measurements were taken in magnetic fields of 0.15 Tesla at room temperature.

Results and Conclusions:

From the Hall Effect measurement, the carrier mobility could be calculated. It was found that the epilayers had carrier mobilities between 100 and 800 cm^2/Vs. Annealing the samples did not have a large effect on the carrier mobilities of the majority of the samples.

Increases in mobility after annealing were only seen in GaAsN samples with nitrogen concentrations of 0.94%. Samples with lower nitrogen concentrations did not show a change in mobility after annealing, nor did the InGaAsN samples. One sample of InGaAsN with a nitrogen concentration of 0.94% even showed a drastic decrease in mobility upon annealing, but it is assumed that this is an experimental anomaly. (See Figure 2 for an overview of the results.)

These results agree with our predictions that the annealing would correct some of the crystal defects caused by nitrogen incorporation into the crystal. Epilayers with very low nitrogen percentages (< 0.2%) saw no mobility increases upon annealing; however, some of the epilayers with higher nitrogen concentrations had 20% increases in mobility after annealing. More nitrogen in the crystal should cause a greater number of defects. It is not clear why annealing did not increase the mobility in the InGaAsN samples. Increases may have been seen had more than 6 samples been tested.

Overall these results were unexpected. Previous work done at Howard University has shown consistent 20-30% carrier mobility increases after similar annealing procedures. This effect was seen in both GaAsN and InGaAsN samples. Further work should try to clear up the apparent disagreement in the studies.

Acknowledgements:

I would like to thank the following for their help and support this summer: Mr. James Griffin, Dr. Gary Harris, Dr. Clayton Bates, Dr. Juan White, the MSRCE staff and students, and the National Science Foundation.

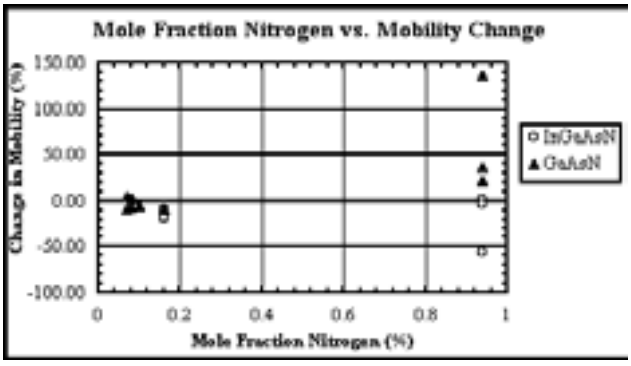

Figure 2: Carrier mobility increases after annealing InGaAsN epilayers with ~1% nitrogen content.

Characterization of Ion-Implanted Nanofiltration Membranes

Edgar Allen Cabrera, Biological & Environmental Engineering, Cornell University

Dr. Kimberly Jones, Civil Engineering, Howard University

eac28@cornell.edu, kljones@howard.edu

Abstract:

Besides operating pressures, a key contrast between reverse osmosis (RO) membranes and nanofiltration (NF) membranes is the difference in ion rejection. RO membranes highly reject divalent ions and effectively reject monovalent ions. NF membranes effectively reject divalent ions but poorly reject monovalent ions. Because of lower operating pressures, it would be advantageous to increase the NF membrane's rejection of monovalent ions without decreasing the pore sizes.

It has been determined in previous studies that electrostatic interactions have an important role in the rejection of charged species and contaminants. By increasing the magnitude of the net electric charge of the membrane, we can tailor the NF membranes to more effectively reject monovalent ions. This was done by using ion implantation to embed highly electronegative F-ions on the surface of NF-90 membranes at doses of $1x10^{10}$ atoms/cm^2 and $5x10^{10}$ atoms/cm^2. Flux experiments were then performed to compare these membranes with each other. AFM and contact angle measurements were also done on modified and unmodified membranes in order to determine the effect of ion implantation on the morphology and hydrophobicity of the membrane surfaces.

Introduction:

Nanofiltration membranes and reverse osmosis membranes are two types of membranes used in water filtration. RO membranes are used to desalt brackish water, but NF membranes have pores that are slightly larger. NF membranes can effectively reject divalent ions, but they reject monovalent ions poorly. Because they can function at lower pressures than RO membranes, NF membranes can be used at lower cost. Therefore, if there is a way to alter NF membranes to make them more effective at rejecting monovalent ions while still maintaining reasonable operating pressures, then nanofiltration can replace reverse osmosis as a more cost-effective method for removing ionic species from water.

One way to alter a membrane to get this result is by increasing the surface charge of the membrane. Previous studies have shown that electrostatic interactions play a crucial role in the rejection of charged species. The hypothesis of this research is that implantation of a highly electronegative ion (F^-) will increase the negative charge of the membrane surface, and would also help reduce fouling by keeping charged particles away from the membrane's surface by electrostatic repulsion.

The goal of this study is to characterize the effects of ion implantation on the monovalent ion rejection, surface morphology, and hydrophobicity of the membrane by comparing unmodified NF-90 membranes with membranes ion-implanted with F^- concentrations of $1x10^{10}$ atoms/cm^2 and $5x10^{10}$ atoms/cm^2.

Procedure:

Three experiments were designed to observe changes in monovalent ion rejection, surface morphology, and hydrophobicity of the membranes. Ion rejection is indirectly proportional to the salt flux through the membrane. By driving a salt water feed through a membrane and measuring the water flux through the membrane as well as the salt concentration of the permeate, salt flux can be calculated from the equation $J_s = J_w \times c_p$ where J_w is the water flux across the membrane and c_p is permeate salt concentration. Note that on diffusive mechanisms, salt flux is not actually dependent on water flux. Decreasing J_w does not decrease J_s; it simply increases c_p. Rejection experiments were conducted in a stirred cell apparatus. Ion concentrations in the permeate and feed streams were measured with an ion chromatograph. NaCl was the monovalent salt used in the experiments.

In order to examine the membrane's surface morphology, we used an atomic force microscope

(Topometrix TMX2010) in non-contact mode.

Hydrophobicity was observed using a goniometer (Advanced Surface Technology, Inc. VCA 2500), which measures contact angles.

Ion Rejection:

Figure 1 is a chart on the sodium and chloride fluxes through the membranes. For both ions, the highest flux is associated with the unmodified membrane. This is followed by the slightly modified membrane while the highly modified membrane allowed the least salt flux. From this data we can conclude that ion implantation decreases the salt flux which indicates a better rejection of the monovalent ions.

Morphology:

One possible reason that flux decreases may be a decrease in pore size. If we can use AFM to image a sample of the surface and view the pores, we may be able to determine if this is the cause. After multiple attempts, however, the relatively large (20 nm) tip of the probe was unable to discern any of the membrane's approximately 1 nm pores. Furthermore, there were no distinguishable differences in the morphology of the membranes.

Although we could not find any recurring differences between the membranes, we were able to notice a significant difference in the imaging settings. The unmodified membrane consistently required settings of setpoint 35% and amplitude of greater than 0.2V in order for the probe to detect the surface. In contrast, the ion-implanted membranes needed a setpoint of 50% and amplitude of around 0.15V. Ion implantation seemed to cause electrostatic interactions between the sample and the probe. This implies that AFM may later be used to characterize the electrostatic properties of an ion-implanted membrane.

Hydrophobicity:

After five trials, the average contact angles were calculated to be 58.0, 59.1, and 58.7 degrees for the unmodified, $1x10^{10}$, and $5x10^{10}$ membranes respectively. Since there are no significant differences and because there is no trend in the data, we conclude ion implantation has no significant effect on membrane hydrophobicity.

References:

[1] Bowen, W.R. et al. "Characterisation of nanofiltration membranes for predictive purposes: use of salts, uncharged solutes and AFM". Jrl. of Membrane Sci. 126 (1997) 91-105.

[2] Chaufer, B. et al. "Retention of ions in nanofiltration at various ionic strength". Desalination v. 104 (1996) 37.

[3] Grundke, K. et al. "Liquid-fluid contact angle measurements on hydrophilic cellulosic materials". Colloids and Surfaces A: Physicochemical and Engr Aspects 116 (1996) 79-91.

[4] Jagannadh, S.N., and Muralidhara, H.S. "Electrokinetic methods to control membrane fouling". Ind.Eng.Chem.Res., v.35, 1996, 1133.

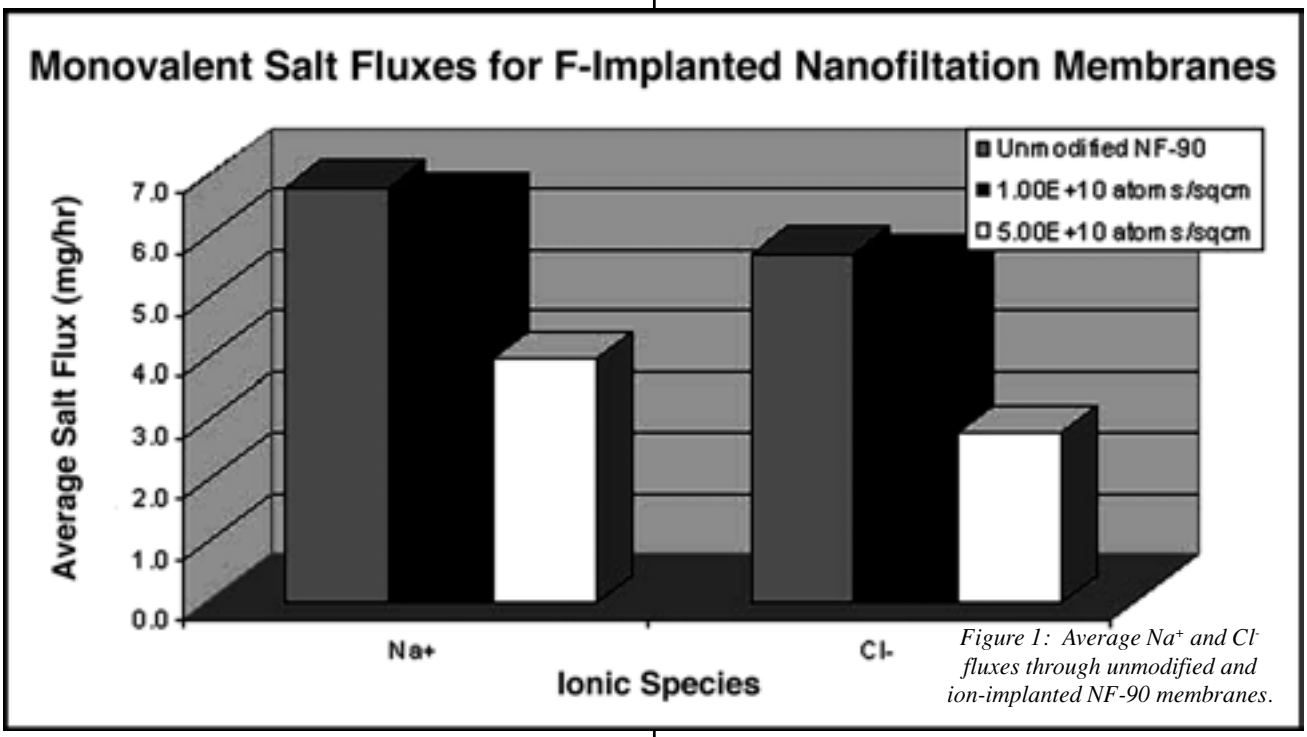

Figure 1: Average Na^+ and Cl^- fluxes through unmodified and ion-implanted NF-90 membranes.

GaAlAs/GaAs Heterojunction Prosthetic Retina

Stephanie Cheng, Biology, Cornell University

Dr. Gary Harris, Materials Science Research Center of Excellence, Howard University

Mr. James Griffin, Mr. Crawford Taylor, MSRCE, Howard University

Dr. Winston Anderson, Biology, Howard University

sic4@cornell.edu, gharris@msrce.howard.edu

Abstract:

Several diseases that deteriorate the retina have created a need for prosthetic retinas in the medical community. Most notably, age macular degeneration (AMD) and retinitis pigmentosa (RP) have affected many people worldwide and continue to be a serious problem. Several technologies are being explored, among them artificial electrical stimulation of the optic nerve through the use of solar cells. In the past, silicon solar cells have been made, but because the spectral response of silicon is better suited for the infrared, other materials need to be explored. One such material, gallium aluminum arsenide (GaAlAs), provides a much closer spectral response to that of the human eye than silicon does. Thus, this project focuses on the development and testing of GaAlAs/GaAs solar cells for prosthetic retinas.

GaAlAs/GaAs solar cells were fabricated using photolithography and then implanted into frog eyes for preliminary studies. One of the main concerns was the biocompatibility of the cells, and to address this, preliminary tests of the effects on GaAs inside of frog eyes were performed and found to be incompatible.

Introduction:

The human eye is a product of evolutionary genius. As with the rest of the human body, the eye works based on a series of signals that is sent to the brain. The retina is responsible for converting the light the eye receives into an electrochemical signal, which is sent to the occipital lobe of the brain for interpretation. The photoreceptors contained in the retina synapse with the bipolar cells, which in turn synapse with the ganglion cells. The ganglion cells then carry the electrochemical signal to the brain.

Several diseases have been known to deteriorate parts of the retina causing the gradual loss of vision that eventually leads to blindness. Retinitis pigmentosa (RP) is a family of inherited diseases and is a result of a gene mutation that causes the death of the photoreceptors. Symptoms include night blindness and tunnel vision followed by a loss of central vision. This disease affects 1.5 million people worldwide. Age macular degeneration (AMD) causes deterioration of the macula, a tiny area of the retina that allows for clear central vision. This is the leading cause of functional blindness in Americans over 65.

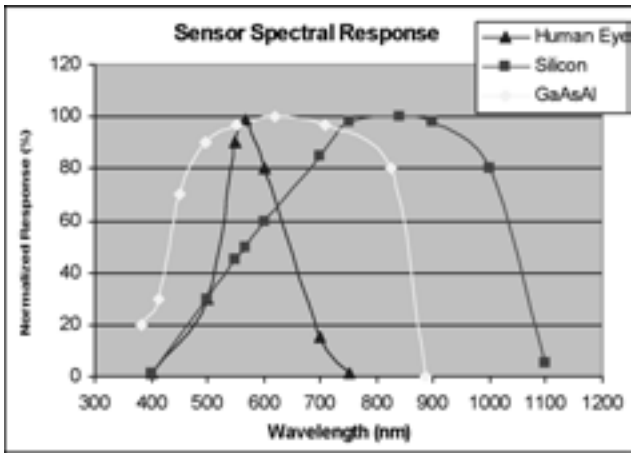

Figure 1: Spectral response of various materials.

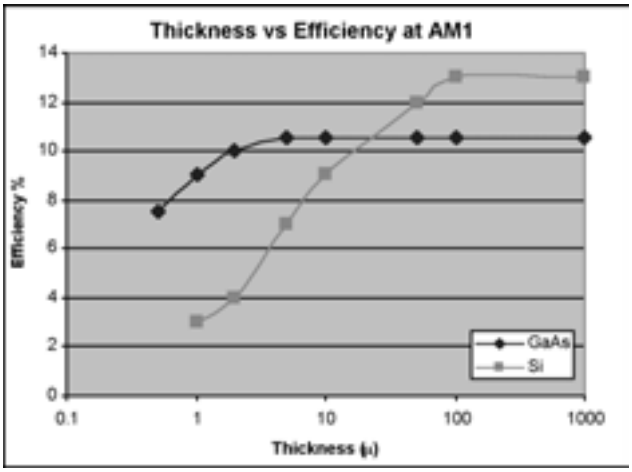

Figure 2: Thickness vs. efficiency of GaAs and silicon.

Currently there are no effective treatments for these diseases and others like them. Electrical stimulation appears to have some promise. Optobionics, a team based in Chicago, has implanted silicon solar cells into ten human subjects (http://www.optobionics.com/artificialretina.htm). The cells were inserted into the periphery of the retina so as to leave the central retina open in the event of newer technology. These subjects are currently still being monitored.

Though Si has its advantages, gallium aluminum arsenide appears to be even more advantageous. Due to a greater open circuit voltage, GaAlAs/GaAs heterojunction solar cells have a higher efficiency than Si solar cells. GaAlAs is also advantageous because Si's spectral response peaks in the infrared region whereas the response of GaAlAs closely resembles that of the human eye (Figure 1). Perhaps the most important difference between Si and GaAlAs/GaAs solar cells is the thickness versus efficiency of the cell. The prosthetic retina is implanted into the sub retinal pocket located in the back of the eye. This pocket is approximately 25 μm thick and Si layers are inefficient at this thickness (< 1%). GaAlAs/GaAs cells are much more efficient at this thickness than Si cells because of their sharp absorption (Figure 2).

Experimental:

Fabrication began with a sample that was cleaned and then spun with photoresist at 5000 rpm for 30 seconds. The sample was then allowed to pre-bake for 20 minutes at 100°C. A mask was then applied and developed. Then, 2000Å of material was etched off the surface of the material using two solutions. A 50:1:1 solution of H_20: H_2O_2: NH_4OH was used to etch for 2 minutes and then a 25:1 solution of H_2O: buffered HF was used for 5 minutes.

Once the mesa was created, a second pattern was applied. After development, 200Å Cr followed by 2000Å Au were evaporated onto the sample. After cooling, liftoff was done using acetone. A 200Å Ge, 200Å Ni, 2000Å Au backside contact was then evaporated onto the sample. The sample was alloyed at 450°C for 1 minute in H_2. The final layer was a 25Å Cr and 50Å Au transparent layer on the surface of the sample. The final product is depicted in Figure 3.

Biocompatibility was then tested using a common tree frog Rana pipiens. A silicon chip was placed in one eye and a GaAs chip was placed in the other eye. After 96 hours, both chips were removed.

Results and Discussion:

As shown in Figure 4, GaAs was not very biocompatible with the eye of a frog, and therefore probably is not compatible with the human eye. Further studies will need to be done. Suggested ideas include adding a protective coating on the chip, which will prevent corrosion of the GaAlAs by the enzymes in the eye.

Further experiments of efficiency and effectiveness of the cell can also be tested using Rana pipiens once again. In order to measure the solar cell's output power once implanted in the frog's eye, a flash of UV light into the frog's eye will damage the retina, and then power measurements with an electro-retinogram can be obtained for the cell.

References:

[1] Hovel, Harold J. Semiconductors and Semimetals vol. 11 Solar Cells. Academic Press, New York. p. 35, 102.
[2] Mims, Forest M. Engineer's Mini-Notebook. Radio Shack, USA. P.19.
[3] Ophthalmology Vol.110, #2, February 2003, 383-391.
[4] www.macula.org
[5] http://www.optobionics.com/

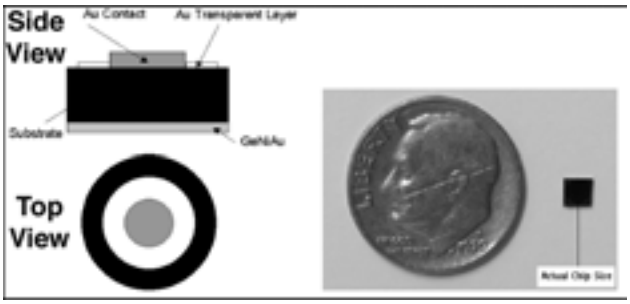

Figure 3, above: Side and top view of the product with size comparison.

Figure 4, below: Silicon and GaAlAs chip removed from the eye of a tree frog after 96 hours.

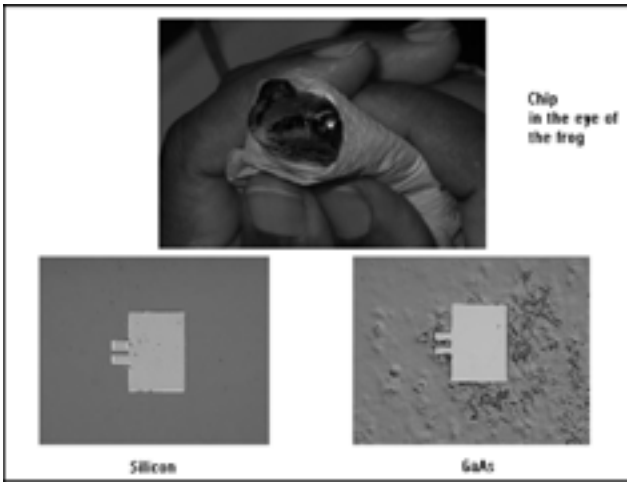

Catalytic Growth of GaN and other Nitride Nanowires for Electronic and Photonic Applications

Aminata Kone, Chemical Engineering, Clemson University

Dr. Maoqi He, Materials Science Research Center of Excellence, Howard University

Dr. Gary Harris, MSRCE, Howard University

akone@clemson.edu, mqhe@msrce.howard.edu, gharris@msrce.howard.edu

Abstract:

Gallium nitride nanowires have applications for UV light sources, high temperature nano devices, diodes, and others scientific tools. GaN nanowires can be grown by a direct reaction of ammonia with pure gallium at a temperature between 850°C and 900°C. Under these conditions the nanowires were mixed with a matrix of GaN platelets which makes their separation difficult. To prevent the formation of this matrix, a catalyst technique using NiO or Ni film has been investigated. Either catalyst should allow for the control of the location and size of the wires. In the case of NiO particles, SEM micrographs indicates that GaN nanowires with diameters between 11.1 and 21 nm were grown with a typical length of 1-5 μm. In the case of the Ni catalyst, the length and diameter of the nanowires were not determined.

Introduction:

A gallium nitride (GaN) nanowire is a semi-conductor obtained by the reaction of ammonia with pure gallium. GaN's physical and chemical properties, such as a bandgap of about 3.4 eV at room temperature and a large thermal conductivity (1.3 W/cm°C), make it suitable for emission of blue light or UV light and the fabrication of many other nanodevices [1]. Due to the advantages of GaN nanowires and the rapid development of nanotechnology, researchers are attracted to this technology. Catalysts were found to be helpful in the growth of GaN nanowires because they allow for the control of the size and the location of the wires. Catalysts also prevent the formation of matrixes when growing the wires from the catalyst particles. In the absence of a catalyst, the size of the wires are controlled roughly by the ammonia flow rate and furnace temperature, and their locations are random [1, 2]. Since catalysts can play a crucial role in the growth of GaN nanowires, NiO particles and Ni film were used as catalysts in this work.

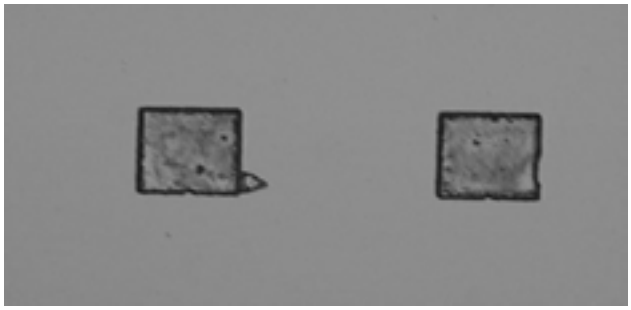

Figure 1: Second Method, wires grown on Ni film.

Experimental Procedures:

First method [3]: Drop a 0.01M $Ni(NO_3)2$ ethanol solution on two hot silicon substrates (~100°C). After the substrates dry, heat them at a temperature of 900°C at a pressure of 50 torr by flowing argon gas at 30 sccm. After 2 hrs, small particles of nickel oxide (NiO) were observed on the silicon substrate. In a boron nitride (BN) boat, about 1.5 gms of pure gallium were placed, one silicon substrate was mounted horizontally, and another one was mounted vertically. The boat was then placed in the center of the oven's quartz tube. The boat was heated for about 20 min at a temperature of

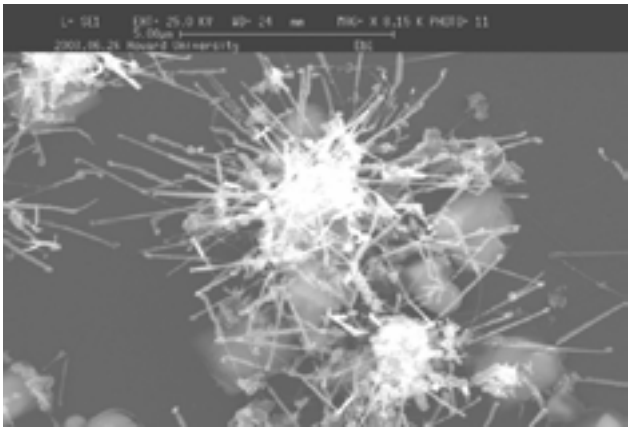

Figure 2: SEM of wires grown on Si substrate with catalysts NiO.

1000°C, a pressure of 10 torr, and an ammonia flow rate of approximately 10 sccm. At the end of the reaction, optical microscopy, scanning electron microscopy (SEM) and energy dispersive spectroscopy (EDS) were used to measure the results.

Second method: Ni film was used as a catalyst in this experiment. On a silicon substrate, a lithography technique was used to deposit a 0.2 mm x 0.2 mm x 50 nm Ni film (Figure 1). The substrate and 3 gms of pure gallium were placed in a boron nitride boat and heated at a temperature of 1000°C, at a pressure of 20 torr, and a flow rate of ammonia of 10 sccm. After 25 min, optical microscopy, SEM and EDS were used to measure the results.

Results:

In the first method, which used NiO particles as catalysts, SEM micrographs revealed small wires of diameter between 11.1 and 21 nm. Several wires grew from the big catalyst particles, but only single wires grew from the small particles. The length of the wires were between 1 and 5 μm, with a ball of Ga, N and NiO present at the nanowire tip (Figure 2).

Parameters such as temperature, time, and carrier gas were changed to determine their effect on the NiO particle reaction. When all the initial conditions remained unchanged except for the temperature of the reaction, which was changed from 1000°C to 920°C, almost no wires were found on the Si plates. Next, when all the parameters remained unchanged except for the time of the reaction, which was changed from 20 to 5 min, very few short wires were seen on the plates. When the experiment lasted 40 min, all the wires disappeared and gave place to big poly and amorphous crystals. Finally when all reaction conditions remained unchanged except for the carrier gas–argon was replaced by nitrogen–big whiskers were found on the silicon substrate.

In the second method, the SEM (Figure 3) revealed that short wires with diameters of ~50 nm grew mostly from the Ni film. EDS (Figure 4) shows that the composition of the nanowires in both methods was GaN.

Conclusion:

In these experiments, NiO particles and Ni films were used as catalysts to control the size and location of the nanowires and to prevent the formation of growth platelet matrixes. When the NiO particles were used as catalysts, the number and length of the wires ere proportional to the temperature and time of the reaction. However if the reaction lasted too long, for instance 40 min, the formation of the wires did not occur. The argon gas also played a crucial role in this experiment because it aided in the nucleation of the wires. To improve the production of nanowires in the future, the NiO particles and the Ni film should be nanosize instead of microsize so that only one wire can grow from each particle instead of many wires from the same particle.

Acknowledgments:

I would like to thank Ms. Melanie-Claire Mallison and all the MSRCE staff at Howard University, especially my mentor Dr. He and my advisor Dr. Harris.

References:

[1] Maoqi He, et al, Appl. Phys. Lett. 77, 3731 (2000).
[2] Y. Wu and P. Yang, J. Am. Chem. Soc. 123, 3165 (2001).
[3] Xialong Chen, et al, Adv. Mater., 12, 1423 (2002).

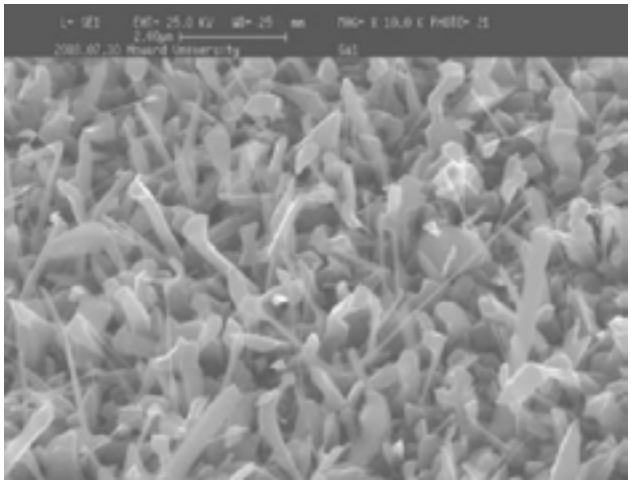

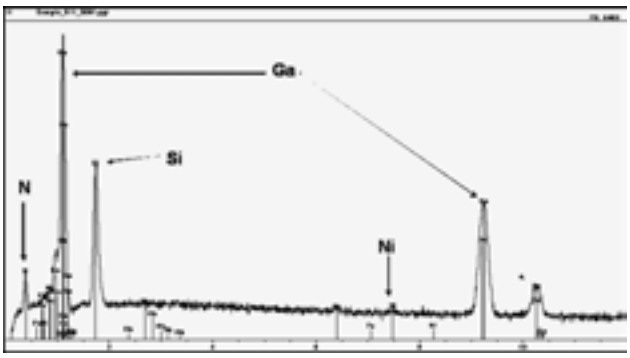

Figure 3, left: SEM of wires grown on Ni film.

Figure 4, above: EDS image of the GaN wires, some with Ni tips.

Fabrication of Silicon Carbide Atomic Force Microscopy Probes

William J. Quinones, Mechanical Engineering, UC Santa Barbara

Mr. Crawford Taylor, Materials Research Center of Excellence, Howard University

WillQuinones@aol.com, crawford@msrce.howard.edu

Abstract:

Atomic force microscopy (AFM) provides three-dimensional surface topography at nanometer lateral and sub-angstrom vertical resolution on insulators and conductors. The objectives of this project are to research the operational aspects of AFM, design and fabricate AFM probes out of silicon carbide (SiC), and compare results obtained with the SiC probes to those obtained using a standard Si probe. The favorable electrical and mechanical properties of SiC are addressed, along with the advantages of using SiC for AFM probes.

An outline of the fabrication steps is given.

Atomic Force Microscopy:

In AFM, a tip is attached to a spring in the form of a cantilever. As the tip moves over the surface, the cantilever bends back and forth in the vertical (z) direction because of atomic forces between the two. A laser beam is directed onto the cantilever and as the cantilever bends, the movement of the reflected beam is detected by a photo diode. A feedback circuit integrates this signal and applies a feedback voltage to the z-piezo (PZT) to exactly balance the cantilever bending. Since the probe force is proportional to the cantilever bending (Hooke's law), this is constant. The image of the surface is built up as a series of scan lines, each displaced in the (y) direction from the previous one. Each individual line is a plot of the voltage applied to the z-piezo as a function of the voltage applied to the x-piezo.

The three modes of operation are contact, noncontact, and tapping. In contact mode, the tip is scanned across the surface, and is deflected as it moves over the surface. In noncontact mode, a stiff cantilever is oscillated in the attractive regime, meaning that the tip is close to the sample, but not touching it. The forces between the tip and sample are on the order of picoNewtons (pN). In tapping mode, an oscillating probe extends into the repulsive regime, so the tip intermittently touches the surface. The advantage of tapping the surface is improved lateral resolution on soft samples. Lateral forces such as drag, common in contact mode, are virtually eliminated.

Silicon Carbide:

AFM tips and cantilevers are typically microfabricated from Si or Si_3N_4. Typical tip radiuses are in the range of 1-10 nm. For this project, the goal is to fabricate the probes out of SiC.

SiC crystallizes in many different polytypes, which

Property	3C-SiC (6H-SiC)	GaAs	Si	Diamond
Melting Point (°C)	Sublimes at 1825	1238	1415	Phase Change
Max. Operating Temp. (°C)	873 (1240)	460	300	1100
Thermal Conductivity (W/cm °C)	4.9	0.5	1.5	20
Thermal Expansion Coeff. (*10E-6 °C⁻¹)	3.8 (4.2)	6.9	2.6	
Young's Modulus (GPa)	448	75	190	1035
Physical Stability	Excellent	Fair	Good	Fair
Energy Gap (eV)	2.2 (2.9)	1.42	1.12	5.5
Electron Mobility (cm²/V s)	1000 (500)	8500	1350	2200
Hole Mobility (cm²/V s)	40 (50)	400	600	1600
Sat. Electron Drift Vel. (*10E7 cm/s)	2.5 (2)	2	1	2.7
Breakdown Voltage (*10E7 cm/s)	3 (4-6)	0.4	0.3	10
Dielectric Constant	9.7	13.2	11.9	5.5
Lattice constant (Å)	4.36	5.65	5.43	

Figure 1: Material properties of common semiconductor materials at 300K.

differ from one another only in the stacking sequence of a double layer. Each double layer consists of two planes of close-packed Si and C atoms (one Si atom lying directly over one C atom), and each successive double layer is stacked over the previous one in a close-packed arrangement. The two most common SiC polytypes are the 3C-SiC and 6H-SiC. The 3C polytype, also known as beta-SiC (or ß-SiC), is the only polytype with a cubic structure. 3C-SiC crystallizes in a ZnS-type structure and thus can be deposited on Si.

Silicon carbide (SiC) is well known for its mechanical hardness, chemical inertness, high thermal conductivity, and electrical stability at temperatures well above 300°C, making it an excellent candidate for high temperature and/or corrosive probing applications. In comparison to diamond, attractive features of SiC are that it can be doped both p- and n-type, and it allows a natural oxide to be grown on its surface. Figure 1 compares some of the material properties for single crystal SiC, Si, GaAs, and diamond.

Design:

Our design was based on dimensions of existing probes on the market. Figures 2 and 3 show the initial design and an existing commercial probe, respectively. Figure 4 suggests a fabrication scheme for the SiC probes based on some fairly common photolithographic and etching techniques. The geometry of the approach requires that the Si be in the (111) orientation.

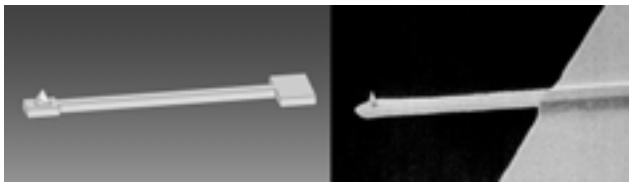

Figure 2, above left: SolidWorks model of cantilever and tip.

Figure 3, above right: SEM image of Silicon cantilever and tip.

Procedure:

To transfer the necessary patterns for the design, a mask was created. SiC growth was done epitaxially in a closed flow system. Propane combines with silane (3 silane : 1 propane) in the carrier gas hydrogen. 3C-SiC films were grown on Si (111) substrates in a cold-wall, horizontal-geometry, RF induction-heated, MOCVD reactor where the propane flow rate is variable. A 15 µm SiC layer was grown on the Si (111) substrate.

In the final stages of the project this summer, reactive ion etch (RIE) rates were calibrated. With proper calibration and one final wet etch to release the probes, the probes would be complete and ready for testing.

Acknowledgments:

My sincere thanks go to the NSF and the NNUN for allowing me to participate in the REU program, as well as to the wonderful staff at the MSRCE, especially Dr. Gary Harris, Mr. Crawford Taylor, Mr. James Griffin, and Ms. Yvette Williams, for their assistance in this project. I would also like to thank Ms. Melanie-Claire Mallison for her efforts in putting together this year's REU program.

References:

[1] Russel, P., et al. SEM and AFM: Complementary Techniques for High Resolution Surface Investigations. North Carolina State University, 2001.

[2] Choyke and Devaty. SiC-The Power Semiconductor for the 21st Century: A Materials Perspective. University of Pittsburgh, 1999.

[3] nanoScience Instruments education website. http://www.nanoscience.com/education/index.html

[4] Veeco Research Library. http://www.veeco.com/html/product_bymarket_research.asp

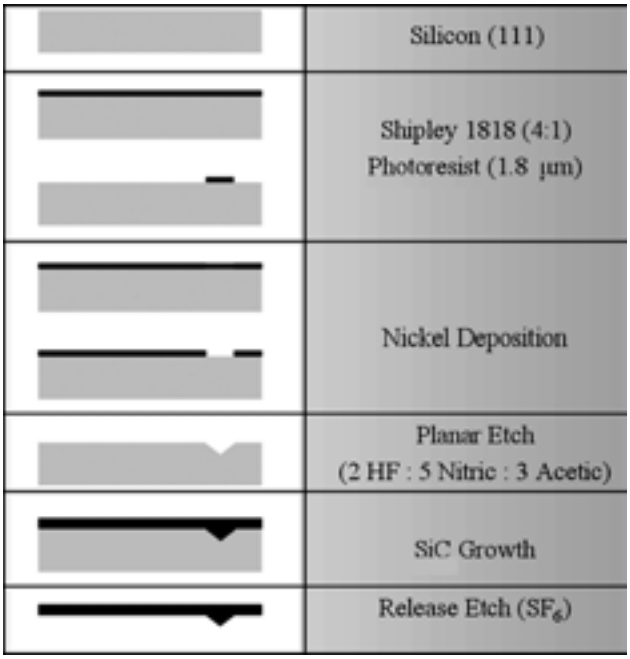

Figure 4: Steps in the fabrication process.

Developing IR (8-14 μm) Detectors (External Photoemission)

Moussa Souare, Electrical Engineering, the University of Akron, Ohio

Dr. Clayton Bates Jr., Dr. Gary Harris, Dr. Juan White, MSRCE, Howard University

ms46@uakron.edu, bates@negril.msrce.howard.edu,
gharris@msrce.howard.edu, juan@msrce.howard.edu

Abstract:

A composite film of Ag-Si was sputtered on a substrate of Si (111) to study the electrical properties using the Hall Effect. The composite is designed to be used to make a detector in the wavelength range of 8-14 μm. A volume fraction of 20% and 80% Ag and Si were used respectively. The sample of 2.0 μm thickness was subjected to chemical etching until complete removal of the segregated layer, a thin conductive layer caused by the aggregation of Ag atoms on the film's surface. The step after etching was the evaporation of 200Å chromium (Cr) and 2000Å gold (Au) in an atmosphere of 10^{-7} Torr onto the composite film. To reduce the resistance between the evaporated metals and composite, the sample was annealed at 700°C in a rapid thermal annealing system for 30 seconds. An I-V measurement was taken to ensure that the contacts were ohmic, i.e. linear. The final step before measuring the Hall Effect was to sandblast a cloverleaf pattern onto the composite with the contact on the periphery of each leaf. Finally, Hall measurement showed average carrier concentration of 2.94×10^{20} (cm^3) and the average mobility of 86.4 (cm^2/ volt-second).

Introduction:

For this work, our focus was on the investigation of the electrical properties of the Ag-Si composite for use as an infrared detector. To do so, Hall measurements techniques will be used in order to study the density and the mobility of the carrier. Since the human body radiates at an average of 9.4 μm, detectors designed to be sensitive on this range can be used to detect humans in military applications. To design a functioning detector, a material that is sensitive to this wavelength and possesses excellent transport properties is needed.

Procedure:

Samples were prepared using a UHV sputtering system. Sputtering is a process that takes place in a vacuum, which is similar to an evaporation process. Contrary to evaporation, which is a thermal process, sputtering is a physical one.

In the vacuum chamber of the sputterer, the source of the material sputtered onto the samples may come from an individual target of a particular element or compound. The targets used in this work were Ag or Si. To create the plasma, argon gas is introduced into the chamber and ionized to create the positive charges. These positive charges are attracted and accelerated toward the target to be sputtered. During acceleration, the charges gain momentum and then strike the target. By striking the target, the argon ions transfer part of their momentum to the atoms on the target causing them to scatter into the chamber. Some of those atoms will then be deposited on the wafer. See Figure 1.

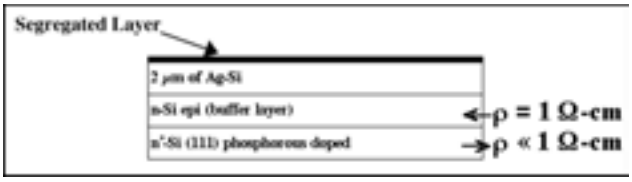

Figure 1: The sample before etching.

Preparation:

The composite of Ag-Si was etched with 4 ml of H_2O, 1 ml of HCl, and 3 ml of HNO_3. The mixed solution was heated for five minutes. Then to remove any oxide, another mixed solution of 10 ml of H_2O and 1 ml of HF was used for one minute. After rinsing in DI water, the sample was blown dry using Nitrogen gas. This process was repeated until complete removal of the segregated layer. The segregated layer is the thin conductive layer caused by the aggregation of silver atoms on the surface where they reach their lowest energy configuration states. See the sample before etching in Figure 2. The following step was the evaporation of 200Å of chromium and 800Å of gold onto the sample. To insure ohmic contacts, the samples were heat treated at 600°C with a rapid thermal annealer. The heat treatment lowers the resistance of the interface between the sample and contact.

Another important step was the test of the ohmic contact. The contacts have to be ohmic with as small a resistance as possible so that the current flowing through the semiconductor and contacts leads to the smallest voltage drop possible. Any voltage drop across the contacts must be proportional to the current so that the contacts do not allow unexpected nonlinear characteristics into the circuits.

To do so, the measurements of I/V were made, verifying the relation R = V/I. See Figure 3. The final step was to etch the cloverleaf mask pattern over the four contacts. To ensure that the metal cloverleaf mask adhered during the sand blasting, a crystal bonder would be used to bond the mask to the samples. The mask was removed by soaking the samples in acetone.

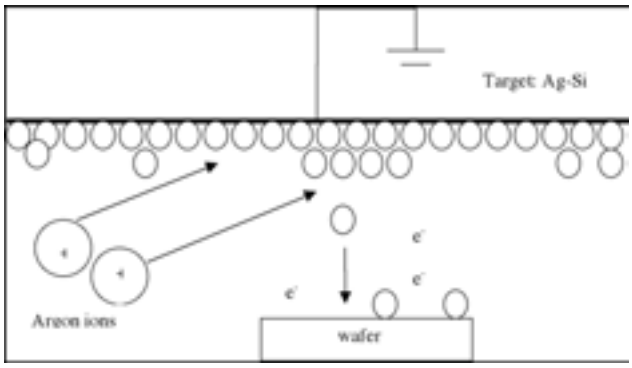

Figure 2: Principle of sputtering.

Hall Measurements:

The Hall effect is used to determine the contributions to the conductivity from the density and the mobility of the carrier. $\sigma = nq\mu$, where σ is the conductivity, n is the electron concentration in the conduction band, q is the electron charge and μ is the conductivity mobility (see Figure 4).

Results:

Thickness	**2.0 μm**
Magnetic Field	**1500 Gauss = 0.15T**
Temperature	**297.4 K**
Mobility 1	**100.3**
Mobility 2	**83.4**
Mobility 3	**75.6**
Average Mobility (cm2/V-S)	**86.4**
Carrier 1	**2.50E20**
Carrier 2	**3.00E20**
Carrier 3	**3.33E20**
Average Carrier ($1/cm^3$)	**2.94E20**

Conclusion:

The results show the electrical properties of the composite Ag-Si film. The carrier density was determined to be in the range of~ 10^{20} carriers/cm^3. The mobility was found to be greater than 50 cm^2/V-S with the average of 86.4 cm^2/V-S.

Acknowledgments:

I would like to acknowledge the assistance and guidance of my mentor, Dr. Juan White. I wish to highlight a special acknowledgement to Dr. Bates for breaking down some of the mysteries about detectors; Dr. Gary Harris for his courtesy and his lectures on Nanotechnology; MSRCE & staff; NNUN and NSF; and Dr. Pan Ernian for his support.

References:

[1] Abdul R., C. W. Bates, A. F. Marshall, S. B.Qadri, T. Bari, Mater. Lett. 39 (1999).
[2] Michael Shur, Intro. to Electronic Dev.
[3] Peter Van Zant, Micro. Fab. Fourth ed.
[4] www.nist.gov

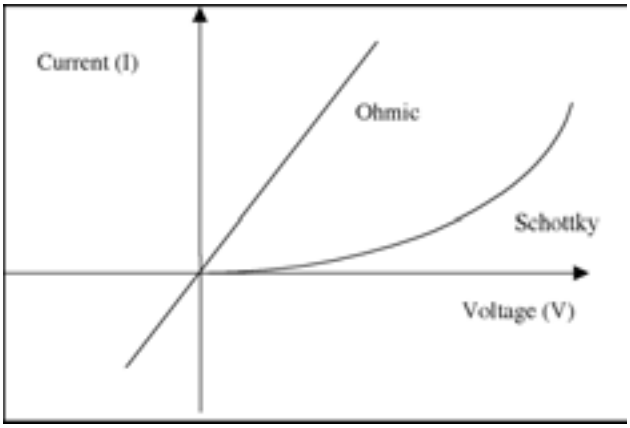

Figure 3, above: Ohmic vs. Schottky.

Figure 4, below: The Hall Effect and the Lorentz Force.

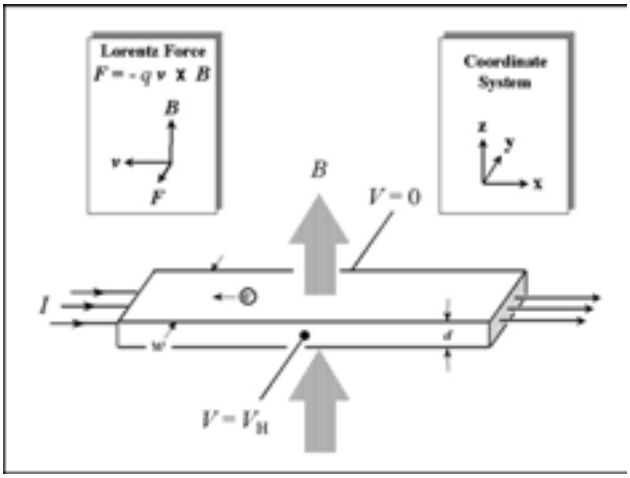

2003 NNUN REU Program at

Penn State Nanofabrication Facility

The Pennsylvania State University

http://www.nanofab.psu.edu/

PSNF/NNUN REU Intern ..... Major & School Affiliation ..... Principal Investigator

First Row:

Mr. Jason Lurie ..... Chemistry, Harvard University ..... Paul Weiss
Mr. Peter Waldrab ..... Electrical Engineering, The Pennsylvania State University ..... Jeff Catchmark

Second Row:

Mr. Rylund Lewis ..... Chemical Engineering, Colorado State University ..... Stephen Fonash
Mr. Daniel Gift ..... Elect. Engr./Physics, The Pennsylvania State University ..... David Allara
Ms. Heather Levin ..... Electrical Engineering, UC Santa Cruz ..... Peter Eklund
Mr. Greg McCarty ..... PSNF, The Pennsylvania State University ..... NNUN REU Coordinator & PI

Third Row:

Mr. Christopher Pontius ..... Biotechnology, Rochester Institute of Technology ..... Carlo Pantano
Mr. Nicholas Strandwitz ..... Engineering Science, The Pennsylvania State University ..... Stephen Fonash
Ms. Lisa Daub ..... PSNF, The Pennsylvania State University ..... NNUN REU Coordinator

Not Pictured:

Ms. Megan Maness ..... Biomedical Engineering, Case Western Reserve University ..... Greg McCarty

Electrical Characteristics of Organic Molecules on GaAs for Micro-Computing Purposes

Daniel Gift, Electrical Engineering and Physics, Pennsylvania State University

David Allara, Chemistry, Pennsylvania State University

Christine McGuiness, Chemistry, Pennsylvania State University

djg238@psu.edu, dla3@psu.edu

Abstract:

Organic molecules were assembled on GaAs to determine if these molecules had electrical characteristics that would make them suitable for use in computer circuitry. Self assembled monolayers (SAM)s of the molecules were formed on GaAs, and a gold contact was deposited on top of the SAM in order to obtain electrical measurements from this modified Schottky diode. The current/voltage (I/V) curves of the devise were then taken to find the I/V properties of the SAM.

Introduction:

The field of molecular electronics has seen much research in the past decade. In recent experiments by Loo, Lang, Rogers, and Hsu [2], reproducible results are moving this chaotic field towards a better understanding of the mechanisms involved. This experiment used a Shottky diode setup with one major variation: a self assembled monolayer (SAM) of an organic molecule was placed between a top contact of gold and the bottom semiconductor, GaAs. Any difference in the I/V curve from the usual one of a Schottky diode can be correlated to the inclusion of molecules. The goal of this project is to reproduce the results of Loo, Lang, Rogers, and Hsu, and if this was successful, to then extend this setup and procedure to find the current/voltage (I/V) curves of other molecules.

Procedure:

In order to conduct this experiment, there are two main parts that must be successfully accomplished. First, a well-ordered SAM must be formed onto a piece of GaAs wafer. To assemble the monolayer, GaAs pieces were cleaned by first exposing the sample to ozone to remove organic contamination on the surface. The native oxide layer was then removed by submersing the sample in concentrated ammonium hydroxide for 2 minutes. The sample was subsequently rinsed with ethanol and dried with N_2. The sample was submerged into 3 mM solutions of the SAM molecule of interest. The solutions were maintained at 52ºC in a water bath for greater than 12 hours [1].

The second part involves forming a top contact to the SAM. Two methods of contacting the SAM were attempted. The first used a PDMS stamp. The advantages of this method are that it is easy and will not destroy the SAM. The disadvantages are that there are many points in the process where contamination can occur. To make a PDMS stamp, a master wafer is made with the pattern of interest using photo-lithography. Next, the wafer is dry etched so that a feature depth of around 5 μm is produced. The pattern is then transferred into a stamp using the PDMS gel and curing agent which, when mixed at a 10:1 ratio and baked overnight at 60ºC, cures and forms the PDMS stamp. Gold is then evaporated on the stamp. By pressing the stamp onto the sample, a top contact is made [2].

The second method for making a top metal contact uses a shadow mask through which the metal is directly evaporated. This method is harder to carry out and has a good chance of destroying a well-ordered SAM, but is a much cleaner process. In order to make the shadow mask, a silicon-nitride wafer was designed using photolithography. After dry etching through the exposed nitride and then the resist, a wet etch was used to etch through the silicon. The etch consists of 71/2% tetra-methyl-ammonium-hydroxide at 80°C for around 6 hours. However, every 1 to 2 hours, the solution was changed to keep the etch rate constant. After the shadow mask was made, gold could be evaporated onto the sample through the mask to make the appropriate contacts.

Results:

SAMs of two different molecules were made: an NO_2 (substituted phenylene-ethynylene dithiol oligomer (NOPE) and a dithiol oligomer consisting of a viologen. These molecules were chosen because the former has already shown non-differential resistance while the viologen is proposed to make a resonant tunneling diode due to its two redox potentials [3]. The OPE SAM was successfully made and confirmed with IR spectroscopy. Making the viologen SAM proved much more difficult. It was found in the IR spectra that the SAM of this molecule was not well ordered which could cause unknown consequences to the results.

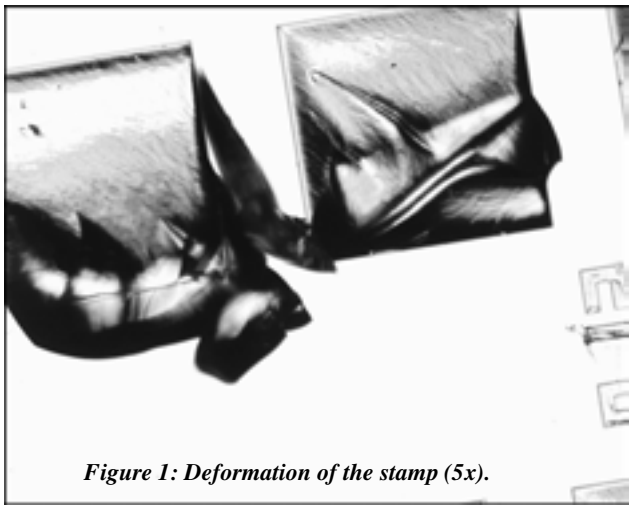

Figure 1: Deformation of the stamp (5x).

There were troubles making the PDMS stamp: deformation of the pattern occurred when the stamp was removed from the master wafer (Figure 1). However, by diminishing the feature depth, a stamp was successfully made and used to make the gold contacts (Figure 2). When measurements were taken, different sections of contacts would produce results that were magnitudes different than previous ones. It is suspected that the differences in magnitude were due to contamination. It was decided that using micro-contact printing introduced too many contaminants to the system. This encouraged a move towards using evaporation to make the gold contacts. A shadow mask was successfully made without any troubles (Figure 3). The next step in this project, work currently in progress, is to evaporate gold through the shadow mask and take measurements of the device.

Acknowledgements:

I would like to thank NNUN and NSF for funding this project. Thanks need to be given to the Penn State Nanofab and its staff for their help. Thank you to Dr. Allara for giving me the opportunity to work on this project. Finally, a special thanks to Christine McGuiness, Yoram Selzer, and Greg McCarty for all of their support and help during the troubles and tribulations experienced.

References:

[1] Christine McGuiness, Carole Mars, and David Allara - unpublished results.

[2] Loo, Yueh-Lin; Lang, David V.; Rogers, John A.; Hsu, Julia W. P. Electrical Contacts to Molecular Layers by Nanotransfer Printing. Nano Letters (2003), 3(7), 913-917.

[3] Gittins, D.I.;Bethell, D.; Schiffrin, D.J.;Nichols, R.J. Nature, 2000, 408, 67-69.

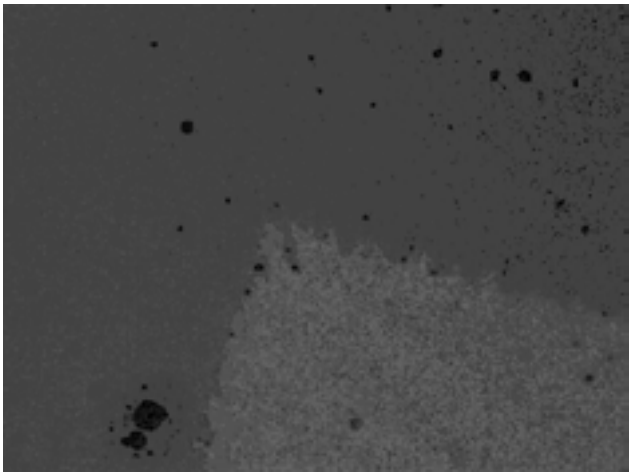

Figure 2, above: Gold deposited by micro contact printing (50x).

Figure 3, below: Shadow mask (5x).

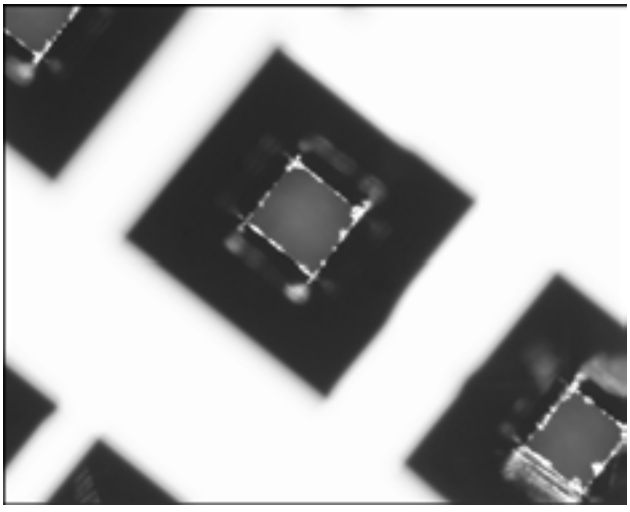

Fabrication and Measurement of Semiconductor Nanowire Devices

Heather Marie Levin, Electrical Engineering, University of California, Santa Cruz

Professor Peter Eklund, Physics, The Pennsylvania State University

Qihua Xiong, Physics, The Pennsylvania State University

heathermarielevin@yahoo.com, pce3@psu.edu

Introduction:

It is important to understand the physical characteristics of semiconducting nanowires because they can be used to fabricate nanometer scale diodes, as well as field-effect and bipolar transistors. Our project begins with making electrical contact with semiconducting nanowires and then investigating their electrical transport characteristics. The wires are grown, dispersed in solution, characterized, filtered and then spun onto a wafer that has been previously patterned via photolithography and liftoff. The substrate is then examined under the Atomic Force Microscope (AFM) to obtain the coordinates of suitable nanowires, which are then used to program the electron beam (e-beam) lithography writer. The e-beam writer exposes two to four contact lines connecting the semiconductor nanowire to the pattern on the substrate, which are then coated with metal during the procedures known as evaporation and liftoff. The pattern on the substrate is then connected to a Dual Inline Package (DIP) so that photoconductivity, temperature-dependent resistivity and gate-dependant current and voltage (I-V) characteristics of the nanowire can be measured.

Our study will eventually cover various II-VI and III-V semiconductor combinations but currently only investigates silicon nanowires.

Procedure:

First the semiconductor nanowires are grown with pulsed laser vaporization (PLV). In this process, silicon and iron powder are mixed, centered in a furnace, and then vaporized by a laser. The iron has a high melting point and provides a molten starting point for the vaporized silicon to grow the wire in the growth process known as vapor-liquid-solid (VLS). Once the sample is grown, it is dispersed in solution and characterized to ensure the proper morphology, structure and chemistry of the nanowires.

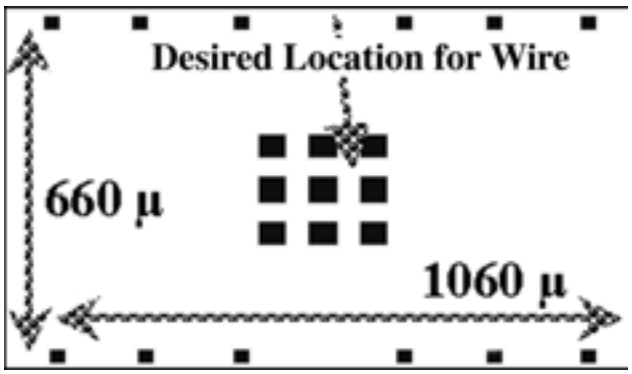

Figure 1: Single die in our photolithography mask.

Our research requires the nanowires to possess cylindrical geometry, a diameter of 20 nm or less and a crystalline structure with as few defects and impurities as possible. The various tools of analysis are the Scanning Electron Microscope (SEM), Field Emission Scanning Electron Microscope (FESEM), Atomic Force Microscope (AFM), and Transmission Electron Microscope (TEM). The methods employed beyond standard microscopy are Selective Area Diffraction (SAED), which ensures a crystalline structure and Energy Dispersive X-ray (EDX) and Electron Energy Loss Spectroscopy (EELS), which indicate the level and content of impurity. SAED, EDX and EELS were performed before the start of the REU Program and it was assumed that wires grown the same way during the Program would be virtually identical.

The next step was to pattern the silicon substrate used to connect the nanowires to the DIP. To do this, we first designed a photolithography mask with Coventerwave software consisting of a 4 x 4 matrix of the structure (die) shown in Figure 1. The 3 x 3 matrix of gold covering 100 x 100 µm squares (pads) interface the semiconductor to the DIP and the four sets of 1 x 3 matrices of gold covered 20 x 20 µm squares (alignment markers) aid in position location during e-beam lithography.

The Penn State Electrical Engineering Dept used a pattern generator to create our mask from our Coventerwave

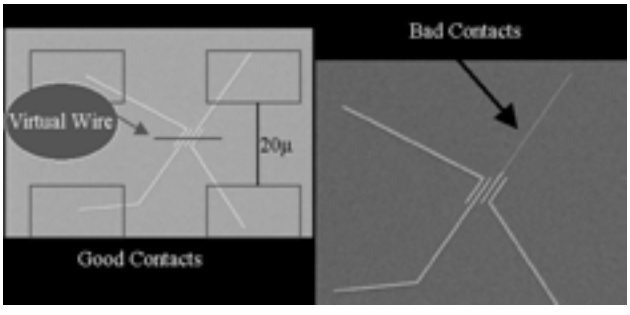

Figure 2. E-beam lithography practice writing (without real nanowires).

design. Once we had the mask, we performed photolithography, evaporation and liftoff to transfer our pattern to our substrate as a 20 nm bottom layer of chromium and a 60 nm top layer of gold. We chose chromium because it is a good adhesive between silicon and gold, and it is not easily eaten away during liftoff. The gold was chosen due to its high conductivity and its ease of visibility for alignment purposes in the E-beam lithography stage.

The wire solution was then spin-coated onto the substrate and observed under the AFM to find suitable nanowires positioned according to Figure 1. Once a wire was found, the AFM picture was then imported into Scion's measuring software to obtain the coordinates of the wire which were then used to draw out two to four contacts per wire in the e-beam lithography design software, L-edit. After the e-beam writer exposed our lines, we developed, cleaned with oxygen plasma, evaporated, and lifted off excess metal to obtain two to four 80 nm wide lines with a bottom layer of 30 nm of aluminum and top layer of 50 nm of gold. The aluminum was chosen so that we can make ohmic contacts between the semiconductor nanowires and conductor, Al, after annealing. The optimal conditions for each stage of fabrication are given in Appendix 1.

Once the substrate is ready for e-beam lithography, it has well over 20 hours of processing time associated with it. It was therefore important to make sure that all of the subtleties of e-beam lithography were understood and prepared for before writing to our substrate. We did this by drawing patterns in L-edit that assumed a virtual wire and writing to a substrate that was prepared the same as those having real wires. We were able to observe the proximity effect of the e-beam writer, determine the degree of alignment accuracy and practice the post e-beam lithography development stage with our practice run.

Our first e-beam write is shown in Figure 2. The three possible explanations for the missing top layer of gold are: (1) the substrate was not completely cleaned with oxygen plasma before liftoff, (2) the aluminum had oxidized before gold was deposited on top, (3) damage from ultrasonification during liftoff. The process was adjusted accordingly and our first attempt at contact with a real nanowire was successful as shown in Figure 3.

Results and Conclusions:

Unfortunately, the e-beam writer was "down" over half of the summer so I was unable to participate in the measurement aspect of the project. I was, however, introduced to the endless struggle of fabrication and research. In addition, I was extremely lucky to have worked with Qihua Xiong, Professor Peter Eklund and the Penn State Nanofab staff whose kindness, patience and intelligence meant this summer was one of the best learning experiences of my life.

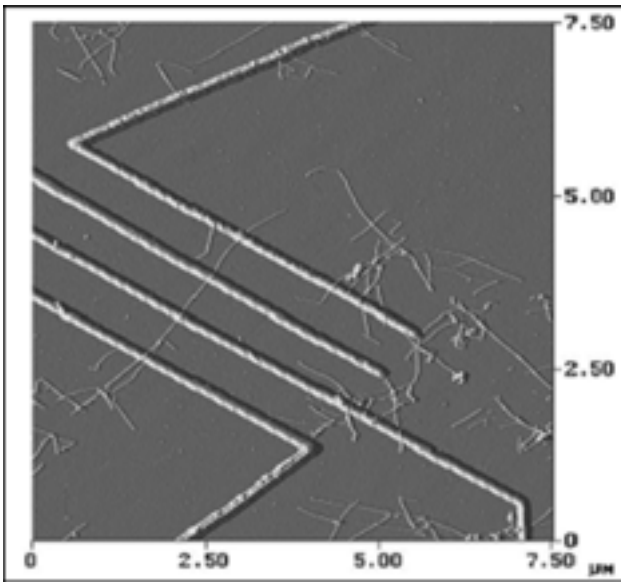

Figure 3. Electrical contact made to 3.5 µm long silicon nanowire with 20 nm diameter.

Appendix 1: Variables used in fabrication of silicon nanowires

Condition Variables for "Silicon Nanowire Electrical Contact Project 8/03"				
Centrifuge Speed (Post PLV Filter)	Photolithography	Evaporation & Liftoff (Substrate)	E-Beam Lithography	Evaporation & Liftoff (Contacts)
1000 RPM	Dehydration Bake	Chromium	Dehydration Bake	Aluminum
	Time: 5 minutes	Evaporation Rate: 1Å/sec	Time: 5 minutes	Evaporation Rate: 1Å/sec
	Temp: 250°C	Height: 20 nm	Temp: 200°C	Height: 30 nm
	First Level of Resist (LorA)	Evaporation Distance: 80 cm	First Level of Resist (MMA/MAA)	Evaporation Distance: 80 cm
	Speed: 2000 RPM	Gold	Speed: 3500 RPM	Gold
	Thickness: 150 nm	Evaporation Rate: 1Å/sec	Thickness: 180 nm	Evaporation Rate: 1Å/sec
	Post Bake	Height: 60 nm	Soft Bake	Height: 50 nm
	Time: 5 minutes	Evaporation Distance: 80 cm	Time: 2 minutes	Evaporation Distance: 80 cm
	Temp: 170°C	Lift Off (Nanoremover PG)		Lift Off (1165 Resist Stripper)
	Second Level of Resist (LorA)	Temp: 60°C	Second Level of Resist (PMMA)	Temp: 50°C
	Speed 4000 RPM	Time: 30 minutes	Speed: 4000 RPM	Time: 1 hour
	Thickness: 1200 nm	Rinse: Acetone & Isopropanol	Thickness: 150 nm	Rinse: IPA
	Post Bake		Soft Bake	
	Time: 1 minute		Time: 3 minutes	
	Temp: 100°C		Temp: 180°C	
	Development (Shipley MF326)		Development (1:1 of IPA to MBIK)	
	Time: 60-70 sec		Time: 60 sec	
			Temp: 20°C	
			Reative Ion Etch	
			Power: 25W	
			Pressure: 100 mT	
			Time: 12 sec	
			Lost PMMA: 400Å sec	
			Etch Rate: 40 sccm	

Nanoparticle Based Detection of Biological Systems

Rylund Lewis, Chemical Engineering, Colorado State University

Stephen Fonash, Penn State Nanofabrication Facility, Pennsylvania State University

Ali Kaan Kalkan, Penn State Nanofabrication Facility, Pennsylvania State University

Rylewis@engr.colostate.edu, sfonash@psu.edu, akk105@psu.edu

Abstract:

The focus of this study is to detect biological molecules and their interactions using a novel surface-enhanced Raman scattering (SERS) substrate material.

This novel SERS substrate, being a Ag/Si nanocomposite, enables high-throughput detection of analyte molecule arrays spotted on it. Furthermore, due to the SERS enhancement, the Raman signal can be obtained in the non-resonant regime rendering minimum laser-induced damage to the molecules.

Project Summary:

Surface-enhanced Raman scattering (SERS) is one of the most sensitive spectroscopic methods for detection of molecules. Raman Spectroscopy probes vibrationally excitable levels of a molecule. Once a vibrational level is excited by a photon, the energy of the photon shifts by an amount equal to that of the level (Raman scattering). Therefore, by analyzing the scattered light, one can monitor the vibrational modes of the molecule being its fingerprint (Raman spectroscopy). Raman scattering however is a very low probability event. In SERS, analyte molecules are adsorbed on noble metal nanoparticles. These nanoparticles, once excited by light, set up plasmon modes, which, in turn, create near fields around each particle. These fields can couple to analyte molecules in the near field regions. As a result, concentration of the incident light occurs at close vicinity of the nanoparticles enhancing the Raman scattering from the analyte molecules. This method can enhance the detection of biological systems by as much as a factor of 10^{14}.

Standard Raman Spectroscopy of bio-molecular systems today utilizes ultraviolet excitation. This is because the majority of molecular systems have electronic transitions in the UV range (resonant Raman scattering). On the other hand, it is likely that with SERS enhancements, one may also get a detectable Raman signal in the non-resonant regime. This would be very beneficial as bio-molecules are subject to serious damage in the resonant regime. Accordingly, we decided to investigate the usage of nonresonant SERS for the detection of biological systems.

The first step in making our novel SERS substrate is to deposit nanostructured void-column Si films onto glass substrates using an Electron Cyclotron Resonance Plasma-Enhanced Chemical Vapor Deposition machine (ECR-PECVD). In the presence of highly active plasma and low substrate temperature, the extremely low surface mobility of the deposition species yields nanostructured void-column morphology. The nanostructure of the Si films consists of 20-30 nm wide nanocolumns with an average separation of 20 nm. These Si films serve two purposes; they limit the growth of the nanoparticles upon impregnation of the glass substrates, and they limit aggregation of the particles while excited by the Raman laser.

Next, the glass substrates are impregnated with Ag nanoparticles, which have plasmon resonance in the visible spectrum of light. The resulting SERS substrates are synthesized simply by immersion of the nanostructured void-column Si films into a 2 millimolar $AgNO_3$ solution for about 110 seconds. Free Ag ions in the solution are reduced by the Si nanocolumns to form nanoparticles as seen in Figure 1. The analyte molecules were spotted on our SERS substrates in solution form using a micro-pipet. Raman signal was obtained after focusing the 514.5 nm laser beam at the substrate/analyte interface.

After initial testing of our SERS substrates, improvements were made to help further reduce the aggregation of the Ag nanoparticles. As the Raman laser excites the sample and the substrate, Ag nanoparticles begin to aggregate. When the Ag aggregates enough (on the order of the wavelength of

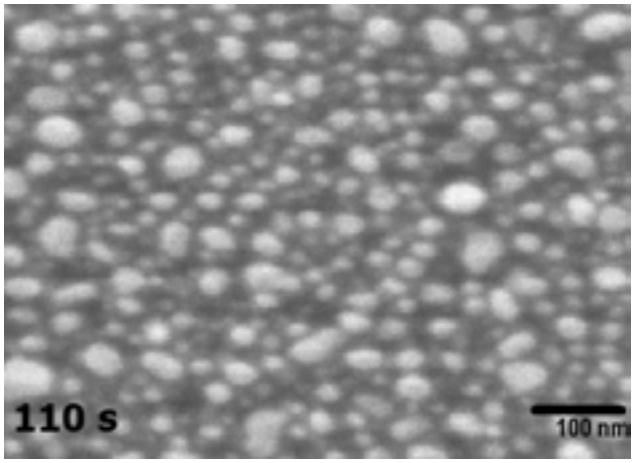

Figure 1: Ag nanoparticles dispersed on a nano-structured void-column Si film to form a SERS substrate.

laser), the plasmon modes weaken, and the Raman signal is greatly reduced to less than that which can be detected.

Two methods investigated involved the height of the Si nanocolumns, and the concentration of the Ag nanoparticles in and on the SERS substrates. The concentration of the Ag nanoparticles can be reduced by either reducing the concentration of the $AgNO_3$ solution, or by reducing the amount of time the Si films are immersed in the $AgNO_3$ solution. Through experimentation, it was concluded that shorter Si nanocolumns can help reduce aggregation because there is less Ag nanoparticle buildup between the columns, and therefore less particles to aggregate. Also concluded was that both methods to reduce the concentration of the Ag nanoparticles successfully helped to reduce the aggregation.

Using our novel Si deposited SERS substrates, we successfully obtained spectra for many different types of biological systems. We obtained spectra of a protein, streptavidin, and its interaction with a drug molecule, Biotin (Figure 2). Also acquired was the spectrum of Adenine (Figure 3). Both of these spectra show that our SERS substrates can enhance the detection of bio-molecules and bio-molecular interactions within non-resonant Raman regime to the detectable level.

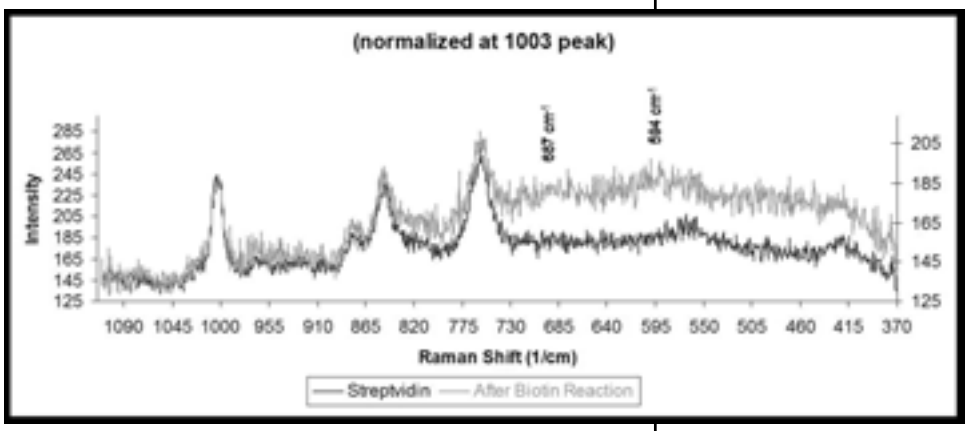

Figure 2, left: The protein (Streptavidin) and its reaction to the drug (Biotin).

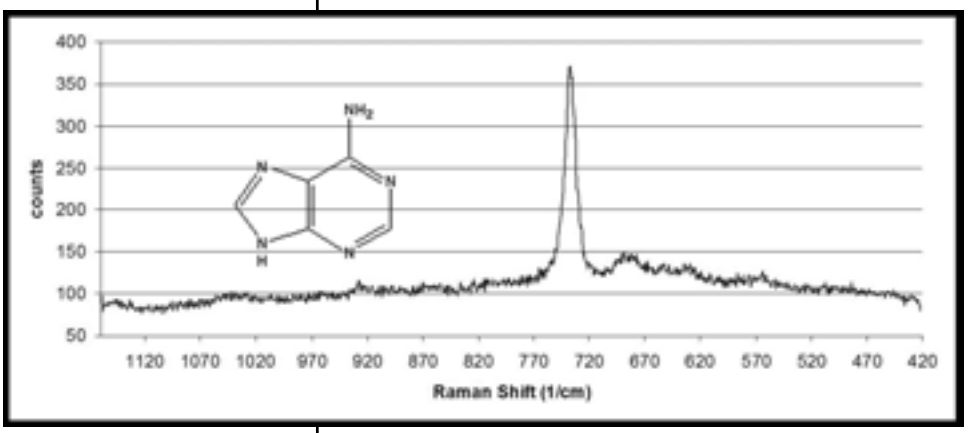

Figure 3, right: Adenine - A molecule of one of the base pairs of DNA.

Combining Conventional Nanolithography with Self- and Directed-Assembly to Create Ultrahigh Resolution Structures with Precision

Jason Lurie, Chemistry, Harvard University

Paul S. Weiss, Chemistry and Physics, The Pennsylvania State University

Mary E. Anderson, Chemistry, The Pennsylvania State University

lurie@fas.harvard.edu, stm@psu.edu

Abstract:

"Molecular rulers" are self-assembled multilayers of a controlled thickness that allow lithographic techniques to be used to create nanometer-scale features. Selective deposition of self-assembled multilayers on initial metal structures form a "molecular ruler resist" for metal deposition, creating secondary structures whose spacing from the initial structure is dependent on resist thickness. In the work described, molecular rulers combine the ease and cost-effectiveness of conventional photolithography with feature sizes approaching and even surpassing those of electron beam lithography. Molecular rulers thus hold promise as a tool to miniaturize electronic devices further.

One area in which the process could use improvement is the chemical lift-off of the molecular ruler resist. Utilizing a different multilayer system is one solution to this problem. Another approach to removing the multilayers is to utilize alternative lift-off conditions, such as different solvents, amounts of agitation and temperatures. Both of these methodologies were researched to improve the lift-off of molecular rulers.

Attempts were made to utilize a multilayer system with 1,10-decanediylbisphosphonic acid as the organic component, instead of the previously used mercaptoalkanoic acids, and different metal ions, namely Zr_4^+ and Zn_2^+. This multilayer framework has different stability conditions than the multilayer system initially utilized. Attempts were also made to lift-off the 16-mercaptohexadecanoic acid / copper multilayer system with an assortment of different solvents and environmental conditions.

Introduction:

The fabrication of sub-100 nm structures is very important for continued progress in the design of advanced electronic devices [1]. Conventional lithographic techniques fail to meet the needs of the scientific community in this regard; electron beam lithography is costly and suffers from proximity effects that reduce resolution at the desired scale [1] and even the best photolithography cannot produce the desired resolutions. "Molecular rulers", self-assembled multilayers of controlled thickness, allow lithographic techniques to be used to create nanometer-scale features. The process is illustrated in Figure 1 [1].

Initial metal structures (A) are subjected to selective deposition of self-assembled multilayers (B) to form a "molecular ruler resist" for metal deposition (C) and then lift-off creating secondary structures whose spacing from the initial structure is dependent on resist thickness (D). Current lift-off procedures utilize the harsh commercially-available organic stripper ACT-935 which attacks not only organics but also aluminum and thus restricts the utility of the molecular ruler technique in the fabrication of devices. We took two approaches to this problem: (1) use a different multilayer system than the currently used mercaptoalkanoic acid / copper system, and (2) perform lift-off of the mercaptoalkanoic acid / copper system using alternative solvents and conditions. Part 1 utilized an established multilayer scheme [2, 3] but we had some difficulty in reproducing the results.

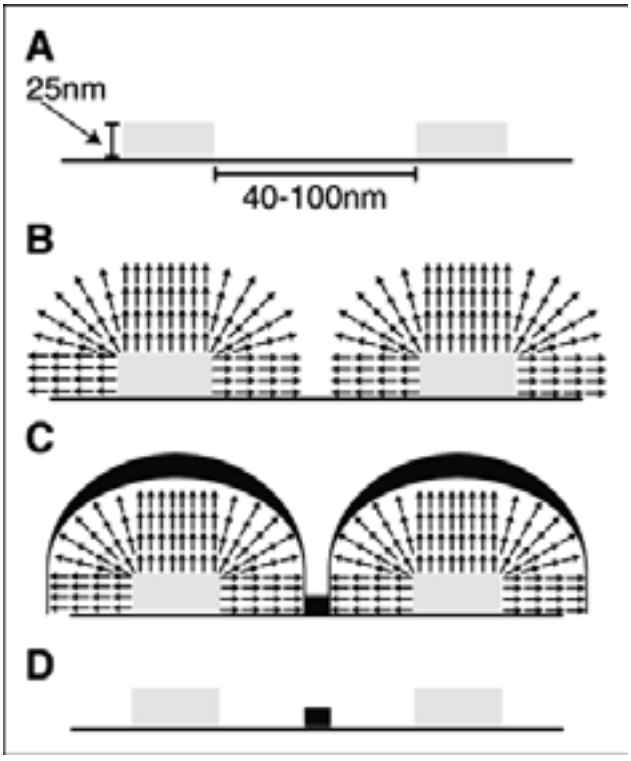

Figure 1: Schematic of molecular ruler process.

Procedure:

800Å Au was evaporated onto SiO_2 wafers, with 100Å Cr used as an adhesion layer. The wafers were cleaned in ACT-935 at 60ºC for 60 minutes. They were then rinsed in ethanol and nanopure H_2O and dried with compressed Ar.

Part 1: The wafers were placed in 5 mM 1,11-mercaptoundecanol for 12 hours and a self-assembled monolayer (SAM) formed. The free hydroxyl groups were phosphonated by immersion in 0.2 M phosphorous oxychloride in 0.2 M 2,4,6-collidine and acetonitrile for 1 hour. The wafers were rinsed in ethanol and H_2O, and dried. The wafers were then put through a sequential dipping procedure alternating between 5 mM metal ion (either Zn_2^+ or Zr_4^+) and 5 mM 1,10-decanediylbisphosphonic acid (DBPA), with rinsing in ethanol and drying with compressed Ar between each step. Length of dip varied between the "normal" 60 minute dip and the "quick" 10 minute dip. Solvents used were 100% ethanol and 95% ethanol, and zinc acetate and zinc perchlorate were used as Zn_2^+ sources. Film thicknesses were measured after varying numbers of layers by ellipsometry as shown in Figure 2.

Part 2: Seven layer thick multilayers of 1,16-mercaptohexadecanoic acid (MHDA) and Cu_2^+ were grown on other wafers by alternating immersion of the wafers in 5 mM MHDA for 1 hr followed by a 10 min rinse with constant agitation in ethanol and a 10 min air dry, and 5 mM $Cu(II)Cl_2$ followed by the same rinsing and drying process. Film thicknesses were measured by ellipsometry. The wafers were then immersed in various solvents at different temperatures for varying lengths of time, and the reduction in film thickness was measured as shown in Figure 3.

Results and Conclusions:

Part 1: As shown in Figure 2, there was no linear growth using Zn_2^+ as the metal ion. Although there does appear to have been linear growth using Zr_4^+ as the metal, later experiments [4] show that this growth was on both the silicon wafer and the gold evaporated onto it. Therefore, both Zn_2^+ and Zr_4^+ are unsuitable as metal ions for the molecular ruler process. Future work could be done using La_3^+ to determine if an intermediately charged metal ion would function as desired.

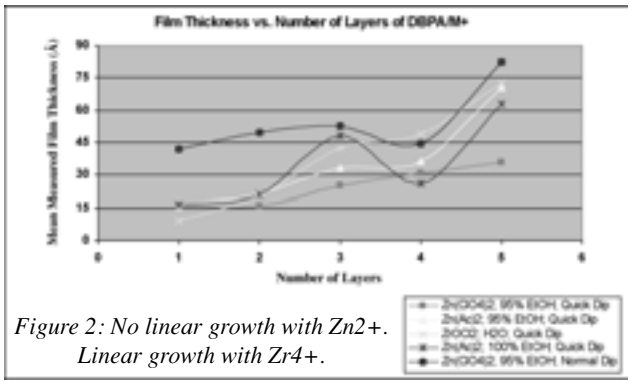

Figure 2: No linear growth with Zn2+. Linear growth with Zr4+.

Part 2: As we can see in Figure 3, most of the reagents tested had little effect on the film thickness. However, tetrahydrofuran (THF) and chloroform functioned effectively identically to the currently used ACT-935 under similar conditions to those ACT-935 is used (ie, 1 hour at 55ºC). Later experiments [4] using THF as the lift-off reagent showed incomplete or "spotty" lift-off of the molecular ruler resist. Future work to incorporate THF as the lift-off solvent is being pursued.

Acknowledgements:

I would like to thank M.E. Anderson and the rest of the Weiss group at Penn State for their assistance with my work. I would also like to recognize the staff of the Penn State Nanofabrication facility. Funding was generously provided by the National Nanofabrication Users Network, the Defense Advanced Research Programs Agency and the National Science Foundation.

References:

[1] Hatzor, A., Weiss, P. S. Science 2001 291: 1019.

[2] Lee, H., Kepley, L.J., Hong, H.G., Akhter, S., Mallouk, T.E., Journal of Physical Chemistry 1988 92: 2597.

[3] Yang, H.C., Aoki, K., Hong, H.G., Sackett, D.D., Arendt, M.F., Yau, S.L., Bell, C.M., Mallouk, T.E., Journal of the American Chemical Society 1993 115: 11855.

[4] Anderson, M.E., unpublished results, 2003.

Chemical	Time (Hr)	Temp (°C)	Reduction in Thickness (%)
Triethylamine	12	20	26
Hexanes	12	20	9
Benzene	12	20	15
Toluene	12	20	11
Dicholormethane	12	20	13
Ether	72	20	32
Chloroform	72	20	67
Chloroform	12	20	73
Chloroform	1	55	67
THF	72	20	87
THF	12	20	79
THF	1	55	84
1:1 THF:Chloroform	1	55	84
ACT-935*	1	55	85

*Figure 3: * indicates currently used method.*

Cell Adhesion for Applications in Intracellular Communication Research

Megan Maness, Biomedical Engineering, Case Western Reserve University

Gregory S. McCarty, Penn State Nanofabrication Facility, The Pennsylvania State University

mam67@cwru.edu, gsm107@psu.edu

Abstract:

The development of a device that enables directed neuronal growth, multiplexed stimulation solutions, and detection of exocytosis is of fundamental importance to research into intracellular communications, drug discovery, and disease diagnosis and treatment. The creation of such devices will provide the opportunity to study and characterize cell-to-cell communication and to monitor neurotransmitter release patterns. Here, attachment of PC-12 cells onto the surface of a substrate was guided by a protein-patterned surface. After successful cell adhesion, efforts were begun on monitoring intracellular communication, which involved the implementation of the calcium indicator dye, fluo-4, to monitor exocytosis using fluorescence microscopy.

Introduction:

Determining a method in which to pattern cells to a surface was the first objective of this research. Though the end goal of this project will be to monitor communication between neurons, PC-12 cells were used at this point in the research because they are an immortalized cell line and they have larger vesicles than neurons. The second objective was to determine the best method to monitor cell activation.

Research has shown that an action potential in a cell leads to calcium entry into the presynaptic terminal, which, in turn, drives neurotransmitter release [1]. In this case, the activation, or neurotransmitter release, is known as exocytosis, and is one of the basic steps of intracellular communication. Therefore, since an elevation of intercellular calcium drives exocytosis, the detection of calcium entry into a cell allows one to monitor cell activation [2]. In order to monitor this calcium influx, a type of fluorescence microscopy, entitled calcium imaging, was employed.

Experimental Procedure:

Preliminary research demonstrated that the most effective way to pattern cells on a substrate was to use a protein-patterned surface to guide cell adhesion. In order to do this, microcontact printing with a polydimethylsiloxane (PDMS) stamp was used to pattern proteins onto the surface. After using photolithography (photoresist 1827, developer CD-26) to create a master wafer, a 10:1 solution of PDMS and curing agent was poured on top of the master wafer, cured for 8-12 hours at 60°C, and then peeled away from the wafer. In order to pattern the proteins, the PDMS stamp was swabbed with the protein solution, placed face down on the silicon wafer, and then removed after 60 seconds.

With proteins now patterned on the surface, the next step was to attach the cells. After culturing the cells, protein-patterned glass substrates were placed in Petri dishes and plated with PC-12 cells. They were then incubated for 2-4 days at 37°C, in order to provide time for defined cell adhesion.

Successful cell adhesion led to the next step of the research, imaging with fluorescence microscopy in order to monitor activation of the cells. Since calcium

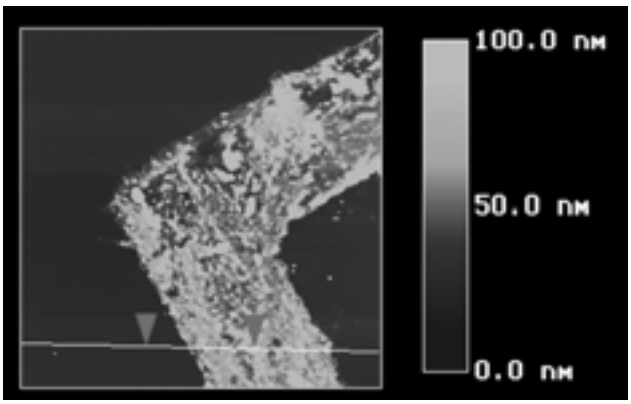

Figure 1: AFM image of a laminin patterned surface.

does not auto-fluoresce, secondary fluorescence was performed with the use of the fluorochrome stain, fluo-4 (Molecular Probes). Preparation of the fluo-4 dye involved incubating a dish of cells in a solution of fluo-4, dimethylsulfoxide, and a calcium buffer for 45 minutes at 37°C, rinsing them with the buffer solution, and then re-incubating the cells in the buffer solution for another 15 minutes. Imaging of the cells began after this second incubation.

In order to image, a single cell was located and a series of 30 images, each taken 1 second apart, was taken. After allowing a few images in order for the cell to reach equilibrium, the cell was stimulated with a potassium rich solution. In this case, potassium depolarized the cell and opened its calcium channels, allowing calcium to enter the cell. The fluorescence images of the cell immediately following the stimulation therefore appeared brighter due to the increased intercellular calcium concentration.

Results:

Initial attempts to pattern the proteins laminin, poly-L-lysine, and collagen IV were promising, but did not show the complete patterning needed for accurate cell attachment. Therefore, a silanization reaction was performed on the substrates with either aminopropyl-triethoxysilane or Bioconext in order to promote greater protein adhesion. Attempts to pattern proteins on the newly silanized surfaces were successful with both poly-L-lysine and laminin. Collagen IV, however, showed only minimal patterning, and so was dropped from the experiment.

In order to prove the patterns that formed were proteins, and not other substances, images of substrates stamped with a variety of substances were taken using an Atomic Force Microscope. The resulting AFM images showed that the laminin-coated stamping resulted in a 40-60 nm thick pattern (Figure 1), while the poly-L-lysine coated stamping produce a pattern ~20 nm thick, and the control stamps (bare or coated with a Trizma/NaCl solution similar to the solution in which the proteins were stored) only showed patterns of 2-5 nm thick. These results demonstrated that the surface patterns were indeed proteins.

After the initial plating of cells onto previously patterned surfaces, images such as Figure 2 were taken. These results were promising, because, as the image demonstrates, cells have been patterned on the surface. Initial attempts to plate PC-12 cells on laminin were very successful, while those with poly-L-lysine showed little or no cell attachment. This difference in cell adhesion was most likely because the thicker coating of laminin, as referenced earlier, was more conducive to cell attachment or a difference in the protein structure between laminin and poly-L-lysine.

Though more research is needed in order to perfect the calcium imaging process, the initial results look promising, as demonstrated in Figure 3.

With the main beginning objectives completed, the next step in this research will involve integrating these initial steps together.

Acknowledgements:

Special thanks to NSF, the NNUN, Leslie Sombers, Angelique Blackburn, and my mentor, Greg McCarty.

References:

[1] R. Levi et al. Neuroscience 118 (2003) 283-296.

[2] Clark R. A. and Ewing A. G. Molecular Neurobiology 15 (1997) 1-16.

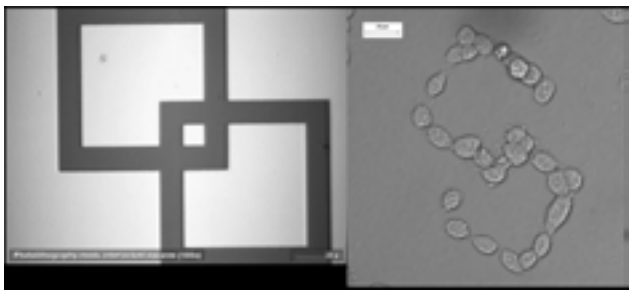

Figure 2: Cell attachment - initial mask pattern (left), actual cell patterning (right).

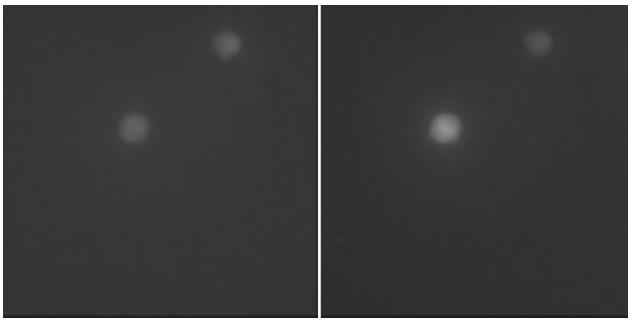

Figure 3: Fluorescent microscopy images - the image on the right, taken after potassium stimulation, is much brighter due to an increase in intercellular calcium.

Sol/Gel Derived Functionalizaed Coatings for DNA Immobilization

Christopher J. Pontius, Biotechnology, Rochester Institute of Technology

Dr. Carlo G. Pantano, Materials Research Institute, The Pennsylvania State University

Caner Durucan, Physics, The Pennsylvania State University

rabid_canuck@hotmail.com, pantano@ems.psu.edu

Abstract:

The immobilization of biomolecules on solid surfaces is a common strategy used in bioassays. One technological application is the array-type platform known as the DNA microarray. This relies on chemical activation of the glass surface to attract and immobilize DNA strands in an orderly fashion. The objective of this project is to explore the physical interaction of DNA solutions with functionalized coatings developed on glass surfaces. A comparative study for an amino-functionalized monolayer coating and a sol/gel derived microporous coating has been performed. The physical interaction between the DNA solutions and coatings was studied through contact angle measurements as functions of time, buffer type, and DNA concentration. These observations were related to the morphological and micro-structural properties of the coatings characterized by AFM. The potential of XPS to study DNA retention/penetration on hybrid microporous coatings was explored.

Introduction:

A DNA microarray is composed of selected DNA primers immobilized on a glass surface through ionic interactions between DNA strands and chemical functionalities on the glass surface. Functionalization is performed by silanization using 3-aminopropyl triethoxysilane (APS). Through a series of condensation reactions, APS bonds to the glass surface forming a monolayer. The aminopropyl tails confer upon the surface the ability to immobilize DNA through ionic interaction with the negatively charged phosphate groups found in the backbone of DNA. They also cause ionic solutions to "ball up" due to hydrophobic interactions with the organic chains. When DNA primers are applied in small volumes in an ordered pattern, it is simple to test sample DNA against numerous different primers at the same time. This is used in the pharmaceutical industry to test various forms of inheritable cancers, birth defects, and other genetic disorders.

This project aims to develop and characterize a sol/gel derived coating that will generate a microporous layer atop the glass substrate. The hybrid sol/gel contains APS and will therefore confer the same properties to the glass substrate as the standard APS monolayer would with one additional aspect—a higher surface area due to their microporous nature.

Methods:

The physical interaction between the DNA solutions and coatings was studied through contact angle measurements as functions of time, buffer type, and DNA concentration. Contact angles were determined by sessile drop technique. In a typical measurement, 3 μL of a 1 mg/mL DNA (Herring Sperm DNA-Sigma) in Tris-EDTA buffer was deposited to an amino-silanized or to a hybrid sol/gel coated glass.

These results were compared with those collected from inquiries performed with 3 μL of 5 mg/mL DNA in Tris-EDTA buffer solution and also 3 μL of 1 mg/mL DNA in SSC (saline sodium citrate) buffer solution. All spots were observed for 30-40 minutes after initial deposition and measurements were taken at regular intervals, usually every 5 minutes.

These observations were related to the morphological and micro-structural properties of the coatings

Figure 1: Amino-silanized surface on the left and hybrid sol/gel on the right. The smaller diameter of the spot on sol/gel represents more hydrophobic interaction.

characterized by atomic force microscopy (AFM) using a Digital Instrument Dimension 3100 Nanoscope IIIa in Tapping Mode. Preparation of these samples involved spin-coating 3 mL of the hybrid sol/gel solution or dip coating in 1 wt % aqueous APS solution for 15 minutes followed by drying in a 120°C oven for one hour. Samples for X-ray Photoelectron Spectroscopy (XPS) were soaked in 1 wt % DNA in Tris-EDTA buffer solution for 10 or 30 minutes. One from each time period was UV irradiated to further cross-link the DNA strands to the chemical functionalities.

Results:

The comparison of spot morphology on a hybrid sol/gel coating versus an APS coating was intriguing. In Figure 1, there are images of 3 μL droplets of 1 mg/mL DNA in Tris-EDTA buffer solutions as deposited on each surface. The droplet on the hybrid sol/gel coating is narrower with a greater contact angle. This resulted from a more hydrophobic interaction with the surface, presumably due to a greater density of carbon tails on the surface of the hybrid coating. When observed for 30-40 minutes, there is a noticable discrepancy between the rate of evaporation on the amino-silanized surface versus on the hybrid sol/gel. The droplet shrinks much faster on the hybrid than on the silanized surface. This can be attributed to the solution seeping into the hybrid coating rather than just evaporating.

The AFM images in Figure 2 show that the hybrid coating developes a microporous layer rather than a smooth monolayer as with a silanized surface. The surface of the hybrid sol/gel coating is much rougher than the silanized surface. This is attributed to pore openings on the surface.

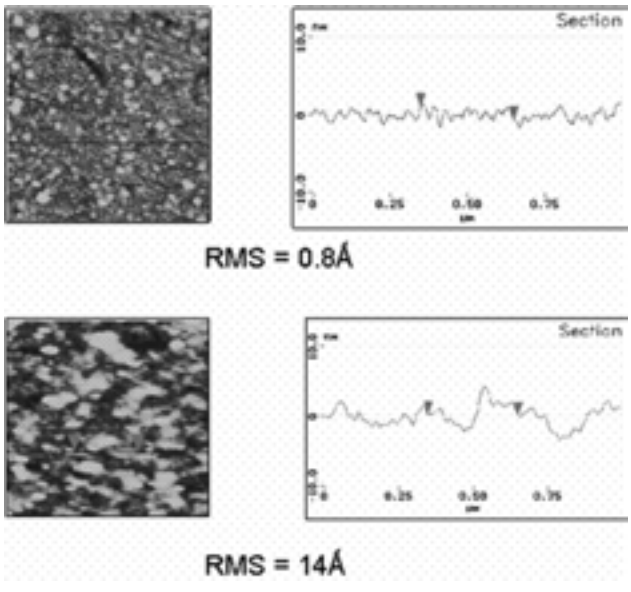

Figure 2: Sectional view demonstrates roughness.

Figure 3 is a graph of XPS data from a sample that was soaked in 1 wt % DNA solution in Tris-EDTA buffer for 30 minutes and left unwashed. This sample had the most DNA on the surface because physically attached DNA had not been washed off. The small line in the bottom left corner represents the phosphorous content (in atomic %) as a function of distance from the surface, indicating that it is indeed possible to detect the presence of DNA on the surface. However, XPS could not detect DNA at depths beyond the surface.

Conclusions:

A sol-gel derived coating provided an alternative surface for DNA immobilization, providing higher surface area and greater functional $(NH_3)^+$ group density than the amino-silanized surface. AFM studies indicated that hybrid sol/gel coatings exhibit a more rough and open surface morphology compared to amino-silanized surfaces. Contact angle measurements demonstrated that DNA solutions infiltrate the sol/gel coatings with time. XPS did not give a quantitative result about DNA penetration, but seemed to be a useful tool and can still provide useful information about the efficiency of DNA attachment on the surface.

Acknowledgements:

Dr. Carlo G. Pantano, Dr. Caner Durucan, and I wish to acknowledge the Center for Nanoscale Science, an NSF Materials Research and Engineering Center (MRSEC) at PSU for their support.

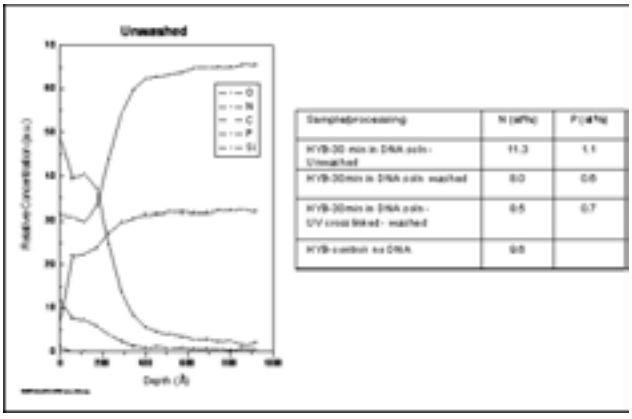

Figure 3: The unwashed sample retained the most DNA.

Nano-Scale Gas/Vapor Sensor

Nicholas Strandwitz, Engineering Science, Pennsylvania State University
Stephen Fonash, Engineering Science and Mechanics, Pennsylvania State University
Handong Li, Engineering Science and Mechanics, Pennsylvania State University
strandwitz@psu.edu, sfonash@psu.edu, handing@psu.edu

Abstract:

A gas/vapor nano-sensor has been created using a deposited nano-structured silicon thin film. This film is an arrayed void-column network deposited by ECR-PECVD and has a large surface-area-to-volume ratio, making it an ideal material for gas/vapor sensing.

The sensor's process flow begins with oxidation of a silicon oxide layer on a silicon substrate to produce electrical isolation. Next gold electrical contacts with separations ranging from 500 nm to 1 μm were formed by a lift-off process with e-beam lithography and thermal evaporation. Finally, another lift-off process was used to define the sensing area into which the porous film was then deposited. The fabricated sensor was then used to monitor changes in electrical conductivity in the film between the Au contacts caused by the gas/vapor adsorption. Sensing responses were explored in the presence of water vapor.

Introduction:

Nano-structured silicon thin films are of useful study due to their very large surface-to-volume ratio. The higher surface-to-volume ratio allows for more reactivity and sensitivity to the surrounding environment. In this example, the electrical conductivity of a deposited porous Si thin film was monitored. This has been done before in a similar manner to this for sensing of humidity [1] and other gasses [2, 3]. It is believed that deposited porous Si thin films will have a faster response time than electrochemically etched porous Si due to a more open surface morphology of the former. This sensor utilizes thinner (500 nm - 1 μm) electrical wires and smaller wire separation in the sensing region in hopes of greater sensitivity. Potential applications of this device include gas/vapor sensing at chemical plants or other facilities that house such materials, to low cost CO sensors in everyday homes and buildings. As hundreds of sensors could be produced on a single Si substrate, individual sensors could potentially be very inexpensive.

Procedure:

The process flow for device creation began with oxidation of a silicon substrate surface for electrical isolation. Next e-beam lithography was used to define wires, leads, and pads for electrical testing. Chrome and gold were then evaporated onto the surface and lifted off. An optical lithography process was then used to define a window into which the porous film would be deposited. This window defines the active testing area for the sensor. The porous film was then deposited by ECR-PECVD in a PlasmaTherm SLR 7700. The porous film consists of a void-column network of amorphous silicon with the presence of various silicon crystallites. The precursor gasses for deposition were silane and hydrogen. Other parameters were set to for conditions in which the porous film would develop on the surface to a thickness of approximately 3000 Å. Lifting off the porous film from all but the testing area concludes the device fabrication. A completed sensor is shown in Figure 1.

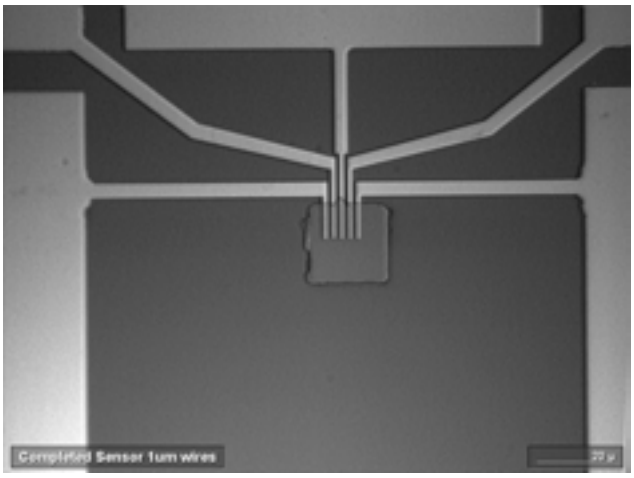

Figure 1: Sensing region of completed sensor.

The testing of the device was done with a computer controlled HP4140B inside an ESPEC Temperature and Humidity Chamber. As electrical resistance was the method of sensing in this case, I-V curves were found for the device at different amounts of relative humidity at constant temperature. The most response, or the largest change in current, was found by testing the device at 8 Volts (see Figure 2). Therefore this was the voltage used for the actual humidity sensing test.

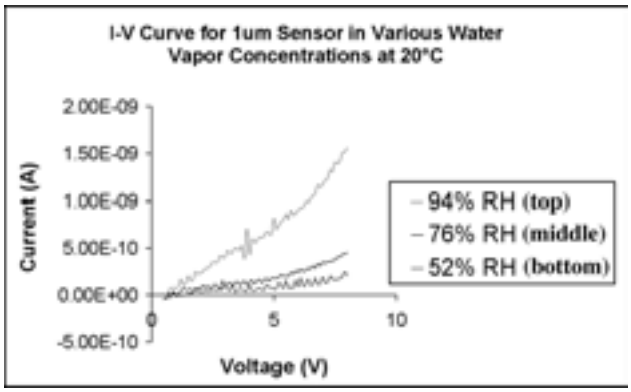

Figure 2: IV curve at various humidities.

The actual humidity sensing was conducted by varying the relative humidity from 55% to 95% at 20°C in the ESPEC chamber. At constant voltage, current was monitored at the various relative humilities and recorded. This was done on sensors with 500 nm and 1 μm wires.

Results:

A general trend of increasing current with increasing relative humidity was found for both the 500 nm and 1 μm wire sensors. Typically the increase in current was one order of magnitude and in the nano-amp range, and is shown in Figure 3. Response was almost identical for the 500 nm and 1 μm sensors. This response was generally exponential in nature.

Conclusions:

A successful nano-scale device has been fabricated and preliminary tests show sensitivity to water vapor. Previous tests done show a 6 order of magnitude change [1]. These tests had a greater separation between the wires in the testing area, making a larger sensing area. Greater sensitivity was not found in this case, most likely due to the smaller sensing area.

The method of conductivity in the case of water vapor presence is believed to be due to the ionization of the water molecules by the porous film. As a voltage is present across the film, an electric field is created. This field, along with incomplete bonding of surface molecules, causes the ionization of the water molecules and a means of conductivity. This is limited by the surface area of the porous film.

The non-linearity of the curve in Figure 3 is due to the non-linear increase in charge carriers as the relative humidity is increased linearly. For example, as the relative humidity approaches 85%, the rate of charge carrier formation increases, which can be interpreted as the slope of the graph. Although the device shows only a one order of magnitude increase in current, greater increases may be found by increasing wire spacing as in [1] and increasing wire length. Also, placing thin (100 nm) wires on top of the porous film may also greatly increase sensitivity, because conductivity will be influenced by gas/vapor particles that congregate under the wire.

Note that in this case, the porous film was on top of the wires. Also, placing the wires on top of the film could allow for a through-wafer conductivity measurement by placing an electrode on the back of the substrate in future work.

References:

[1] A. Kaan Kalkan, Sanghoon Bae, Handong Li, Daniel J. Hayes, and Stephen J. Fonash, J. Appl. Phys. 88, 555 (2001).

[2] James L. Gole, Lenward Seals, et.al., J. Appl. Phys. 91, 2519 (2002).

[3] Schechter, I., Ben-Chorin, M., Kux, A., Analytical Chemistry. (67) 20, 3727-3732 (1995).

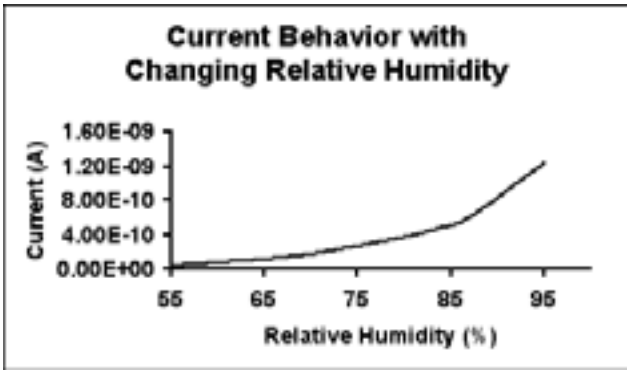

Figure 3: Current vs. relative humidity curve.

Deposition of Molecular Rulers on a Patterned Sacrificial Layer

Peter Waldrab, Electrical Engineering, The Pennsylvania State University

Dr. Jeffrey Catchmark, Materials Research Institute, The Pennsylvania State University

Shyamala Subramanian, Materials Research Institute, The Pennsylvania State University

pww112@psu.edu, jcatchmark@engr.psu.edu

Abstract:

In 2001, Dr. Weiss's Group at the Penn State Nanofabrication Facility developed a process for scaling down the gap between two host structures using an organic resist; allowing wires less than 15 nm to be created. This research seeks to make that scaling process commercially feasible by patterning the parent structures on a sacrificial resist. This sacrificial resist would allow simple lift-off of the parent structure in a chemical developer but would leave the daughter structure intact.

Introduction:

During the NNUN REU Program, I worked with Dr. Jeffrey Catchmark and Shyamala Subramanian to develop the science of molecular ruler nanolithography into practical nanolithography processes that can be utilized by industry. Our goal was to implement a bi-layer host structure consisting of a metallic host layer on a sacrificial resist using materials and techniques that are compatible with standard semiconductor device manufacturing processes.

In 2001 Dr. Paul Weiss, post-graduate student Anat Hatzor and their team at the Penn State Nanofabrication Facility developed a process for creating wires 15-70 nm wide spaced 10-40 nm apart, as is depicted in Figure 1. These wires were created using "molecular rulers" to incrementally scale down the gap between two electron-beam patterned host structures. Metal is then deposited into the gap to form the desired wire. Weiss's results can be seen in Figure 2.

The organic scaling resist is a mercaptoalkonic acid called mercaptohexadecanoic acid [$HS(CH_2)_{15}COOH$]. This particular molecule was chosen for its selective attachment to metals and for its precise molecular length—2 nm. This precise length allows the user to select the gap width to within 4 nm.

With these molecules, Weiss's group was able to prove that organic resists could be used to incrementally scale a feature to a desired size. Unfortunately, in order to demonstrate this, his group used a monolayer Au host structure. This design made it virtually impossible to strip the parent structure without removing the daughter structure, making the process unsuitable for commercial applications.

Summary:

Our group explored a bi-layer host structure in which the Au parent structure is formed on a patterned sacrificial layer. Employing this concept, simple lift-off could then be performed to remove the parent structure, leaving the daughter structure intact and rendering the process compatible with standard semiconductor device manufacturing processes.

After considerable trial and error, our group was able to develop a process that combined the ruler technology of Dr. Weiss's group with a traditional nanolithography lift-off process. The result is a streamlined nine-step process.

The wafers are first spin-coated with the lift-off resist. Thin layers of chrome and gold are then evaporated onto the surface for adhesion and ruler growth. To this, a layer of imaging resist is spin-coated. Using either the optical stepper or electron-beam lithography, the imaging resist is then exposed. A chemical developer removes the exposed resist. A combination of wet and dry etches is used to etch

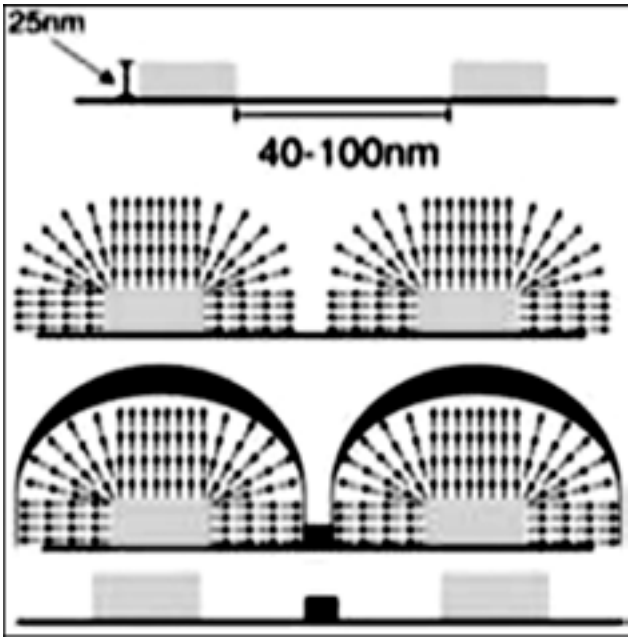

Figure 1: Process for creating wires 15-70 nm wide spaced 10-40 nm apart.

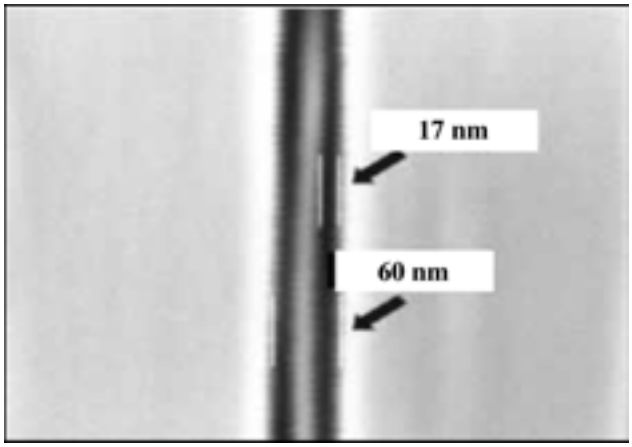

Figure 2: Incrementally scaled down gap between two electron-beam patterned host structures.

through the remaining lift-off resist and metal layers. Once cleaned of all organic contaminants, the wafer undergoes molecular ruler self-assembly. The platinum and chrome are then evaporated onto the surface to form the desired wire. Finally the wafer is immersed in a chemical developer to remove the lift-off resist and with it, the host structure.

By far the most time-consuming developmental stage was creating the etch procedure for the lift-off resist. The molecular ruler self-assembly requires a slight undercut of the lift-resist on which the Au host layer sits. Our group encountered numerous failures in the etch process from excessive etches which destabilized the host structure and insufficient etches which left lift-off resist in the patterned region.

We finally settled on a process that combined dry etching with a Reactive Ion Etcher (RIE) and wet etching in a chemical developer to achieve the necessary undercut.

Our initial attempt at a complete run failed when the molecular ruler self-assembly became contaminated. Each ruler layer consists of a film of mercaptohexadecanoic acid molecules "capped" at both ends by metal atoms. The initial layer is capped at one end by the Au host layer. Each additional layer is capped with Cu_2^+ $[CuClO_4]$ ions. Because of the selective attachment of the mercapto molecules to metal atoms, the rulers should not grow on the bare silicon substrate. Figure 3 indicates that the rulers attached indiscriminately. Large bumps on the order of 200 nm can be seen in the image. The self-assembly should not have achieved more than 60 nm of growth. X-ray Photoelectron Spectroscopy (XPS), Figure 4, of the wafer surface indicated that during the growth process, the mercapto and Cu_2^+ solutions became cross-contaminated, creating pre-capped free-floating globs that randomly attached to the surface.

In our follow-up attempt, problems arose in the ruler growth step once again. This time, a thin layer of metal was redeposited on the Si surface during RIE of the resist layer. The redeposited metal layer allowed ruler growth on the silicon substrate for a second time.

Future Research:

Dr. Jeff Catchmark and Shyamala Subramanian's continued research in this area should prove this process to be feasible and an accurate bridge between the technology pioneered by Weiss' group and the common manufacturing techniques that are currently practiced. Once completed, this research will open the door to creating nanoscale sensors, and smaller, faster, more efficient semiconductor devices.

Acknowledgements:

1. National Science Foundation
2. National Nanofabrication Users Network
3. The Pennsylvania State University
4. PSU Nanofabrication Facility

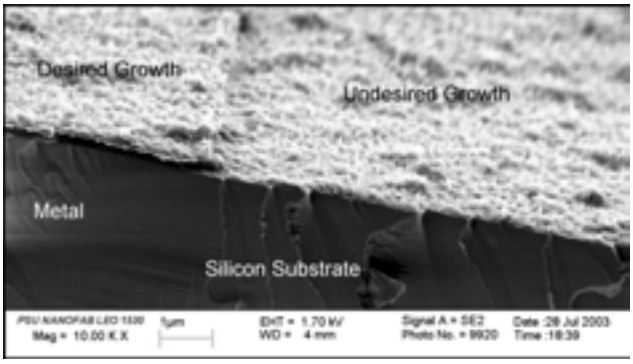

Figure 3: The rulers attached indiscriminately. Large bumps on the order of 200 nm can be seen in the image.

Figure 4: XPS of the wafer surface indicated the mercapto and Cu_2^+ solutions became cross-contaminated.

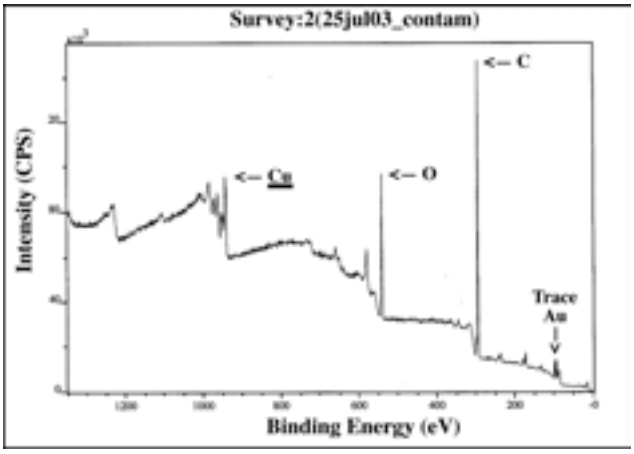

2003 NNUN REU Program at

Stanford Nanofabrication Facility

Stanford University

http://snf.stanford.edu/

SNF/NNUN REU Intern ..... Major & School Affiliation ..... Principal Investigator

First Row:

Mr. Keith Craig ..... Bioengineering & Business, University of Washington ..... Richard N. Zare
Ms. Jennifer Yu Zhao ..... Materials Science & Engineering, Cornell University ..... Bruce M. Clemens
Ms. Sarah Rickman ..... Chemical Engineering, Lehigh University ..... Paul C. McIntyre
Ms. Grace Hsin-Yi Lee ..... Computer Engineering, UC Santa Barbara ..... Reinhold Dauskardt
Ms. Karen Havenstrite ..... Chemical Engineering, University of Nevada Reno ..... Hongjie Dai
Ms. Mariam Aghajan ..... Molecular & Cell Biology, UC Berkeley ..... Peter Griffin
Mr. Siavash Dejgosha ..... Applied & Engineering Physics, Cornell University ..... Fabian Pease

Second Row:

Mr. Steven Floyd ..... Mechanical Engineering, Washington University St. Louis ..... Hongjie Dai
Mr. Nicholas Fichtenbaum ..... Electrical Engineering, Washington University ..... James Harris
Mr. Douglas Jorgesen ..... Electrical Engineering, University of Illinois ..... James Harris
Mr. Ashley Evans ..... Electrical Engineering, CSU Fresno ..... Shan Wang
Mr. Robert Gagler ..... Stanford University ..... NNUN REU Alum and Resident Advisor
Dr. Michael Deal ..... Stanford Nanofabrication Facility, Stanford University ..... NNUN REU Coordinator

Pyrosequencing in a Microchannel

Mariam Aghajan, Molecular & Cell Biology, University of California at Berkeley

Peter Griffin, Electrical Engineering, Stanford University

Ali Agah, Electrical Engineering, Stanford University

mariam_113@hotmail.com, griffin@plumb.stanford.edu

Abstract:

Pyrosequencing is a novel technique used to perform real-time DNA sequencing. Currently, however, DNA sequencing is time consuming and expensive. To accomplish multiplex DNA sequencing that is faster and cheaper, we aim to execute pyrosequencing in microchannels on a chip using DNA immobilized on glass beads. In this project, we performed various pyrosequencing experiments so as to better understand the enzyme kinetics involved. This was necessary to refine our simulation program (Virtual Cell) so that the simulation results would match that of the experimental, which was mostly accomplished. The simulation program will be used to optimize the concentrations of reagents for pyrosequencing in a microchannel since the micro-scale makes manual optimization unpractical. Also, we began fabricating the chip using KOH to etch the microchannels, but this was not completely successful as over-etching was a problem we failed to curtail. In the future, once these obstacles are overcome, rapid genetic analysis on-demand and for diagnosis in the health sciences will soon be able to follow.

Introduction:

Pyrosequencing is a quick and versatile real-time DNA sequencing technique used for genome sequencing, expression analysis, and ecogenomic studies. Utilizing the enzyme Luciferase, pyrophosphate released from base incorporation is converted into light (Figure 1) [1]. Thus, each base incorporated can be detected by a CCD camera and recorded as a pyrogram peak.

Currently 96 free DNA samples of 50 µL each can be run simultaneously. With these numbers, however, genetic studies are very costly and time consuming, resulting in the lack of commonality of genetic analyses within the public realm. To alter this, we aim to maximum the number of samples and decrease the cost by demonstrating pyrosequencing on DNA immobilized glass beads in a microchannel. Since the glass beads have at least a diameter of 30 µm, many beads can be analyzed concurrently; also, the small size allows for less chemical consumption, resulting in a lower cost for DNA sequencing.

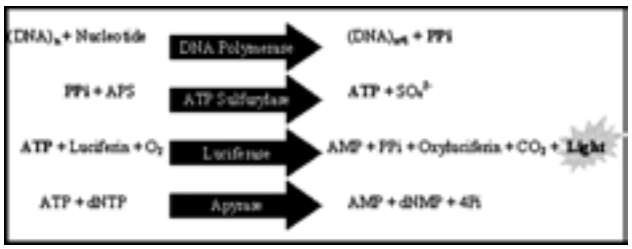

Figure 1: Details of the pyrosequencing reactions.

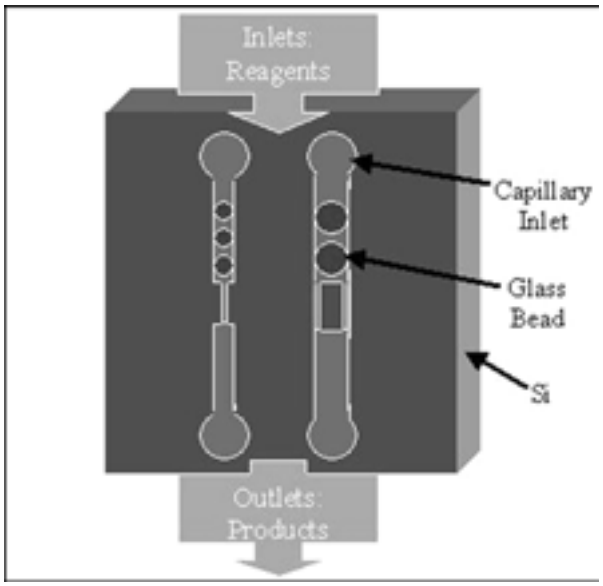

Figure 2: Bird's eye view of the two channel designs tested.

To meet these goals, pyrosequencing must be optimized under these new conditions. Due to the impracticality of optimizing the micro-scale reaction manually, we used a computer simulation program (Virtual Cell) [2]. Initially, however, the computer model did not match the experimental model, with the time-to-peaks of the two pyrograms having a discrepancy of 1 second (Figure 4). Thus, we performed a variety of pyrosequencing experiments aimed at isolating the incongruity between the simulation pyrogram peak and the experimental. Next, we began fabricating the chip using lithography.

Procedures:

Multiple experiments were done using Pyrosequencing's PSQ' 96 machine and related protocol. Various enzymes

and/or substrates, such as DNA Polymerase, Sulfurylase, Luciferase, Apyrase, ATP, and PPi were either omitted or had their concentrations varied. Normal experimental enzyme concentrations are: 10 units DNA Polymerase (2 pmol DNA), 1000 ng Luciferase, 65 mu Sulfurylase and 50 mu Apyrase. Results of experiments were used to refine simulation model.

For chip fabrication, a nitride layer was deposited on the chip. Both high-stress and low-stress nitrides were tested. Next, using standard lithography, two channel designs, 6 channels of varying width per design (67.66 μm, 77.33 μm, 87 μm, 106.33 μm, 145 μm and 203 μm), were developed on the chip. Figure 2 shows a bird's eye view of our chip design with the two channel designs illustrated. The different channel widths pertain to the different bead diameter sizes: 30 μm, 35 μm, 40 μm, 50 μm, 70 μm and 100 μm, respectively. The exposed nitride was removed followed by removal of the photoresist. This allowed for 30 % KOH etching of the channels without etching the nitride layer on the chip. Etching was done at 80°C (constant temperature bath) for ~ 3-4 hours (reported etch rate of 1.4 μm/min), viewing the chips under the microscope to determine when etching was complete. In Figure 3, we see a cross section of our chip design in Figure 2, illustrating the v-groove channel KOH etches at a known angle of 54.7°.

Results and Conclusions:

Due to time constraints, the chip fabrication was not completed, and therefore, pyrosequencing in a microchannel was not tested.

The reason why the initial simulation pyrogram did not match that of the experimental was because either the reaction rates were unknown or, for those enzymes with relevant literature available, the reaction rates were inaccurate. Thus, the experimental results obtained from the various pyrosequencing reactions allowed for more information to be gathered about the reaction rates involved, and therefore, a more accurate computer simulation model. This resulted in the time-to-peak of the simulation pyrogram matching that of the experimental pyrogram (Figure 4). A few more experiments will be done in the future so that the slopes of the simulation and experimental pyrograms may match perfectly.

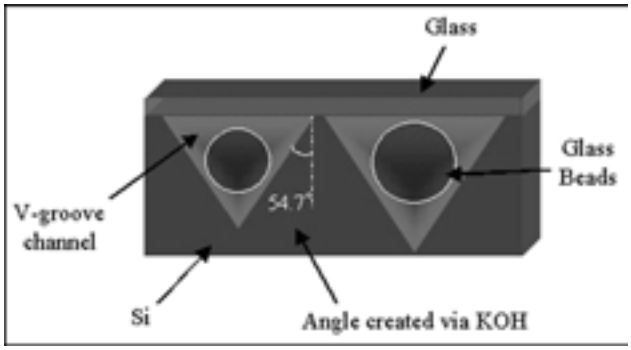

Figure 3: Cross section of chip design in Figure 2.

For chip fabrication, all steps proceeded smoothly except for KOH etching. Initial trials resulted in complete etching of the bottleneck region of the channels, leaving fully rectangular channels that were clearly over-etched. Similarly, our cross-shaped alignment marks were etched to what appeared to be a square. Further analysis using the SEM revealed that etching resulted in the nitride to peel away or fold inwards, which was due to high-stress and over-etching, respectively. For later trials, low-stress nitride deposition was done to avoid peeling of the nitride layer. This proved to be successful to an extent. After approximately 3 1/2 hours of KOH etching, the channels appeared to be etched completely and crisply without over-etching or nitride peeling. The widest channel, however, failed to be etched completely. Yet, after we put the chip back into the KOH bath for further etching of 1 hour, all channels, including the widest, were over-etched. Further experiments to be done include locating the time when etching of all channels is complete and lacking over-etching, separating the narrower and wider channels onto different chips, or simply leaving out the widest channel.

After channel etching is complete, capillaries inlets and outlets may be added prior to annealing a glass cover onto the chip. Then, pyrosequencing may be tested on DNA immobilized glass beads within the microchannels.

Acknowledgements:

I would like to thank Dr. Peter Griffin, Ali Agah, Dr. Mostafa Ronaghi, and all others involved in this research group for their guidance and assistance. I would also like to thank Dr. Michael Deal, Jane Edwards, the SNF staff, CIS, and the NSF.

References:

[1] M.Ronaghi, M.Uhlen & P. Nyren, A sequencing method based on the real-time pyrophosphate. Science 281(5375), 363, (1998).

[2] Griffin, P., Agah, A., Plummer, J.D., Eltoukhy, P.H., Salama, K., El Gamal, A., Ronaghi, M. and Davis, R.W. (2002) Miniaturized DNA Analysis Devices. First International Forum on Post-Genome Technology April(17), 19-20.

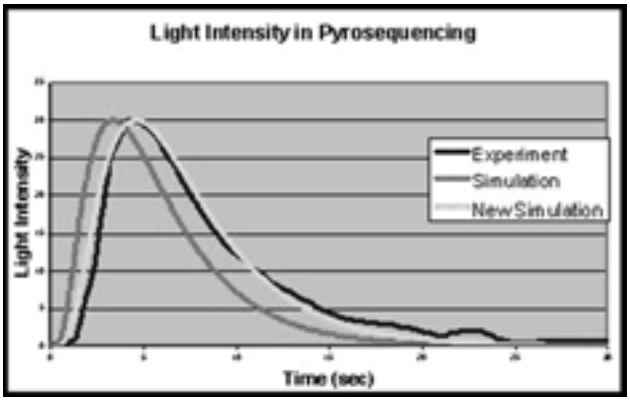

Figure 4: Comparison between the time-to-peaks of the three pyrograms.

Polymer-Bound Electrophoresis Chips

Keith Craig, Bioengineering, University of Washington
Richard Zare, Department of Chemistry, Stanford University
Hongkai Wu, Department of Chemistry, Stanford University
kacraig@u.washington.edu, zare@stanford.edu

Abstract:

Widely used in microfluidic systems, capillary electrophoresis (CE) separates biological samples with high-efficiency, short separation time, and low consumption. The best material for CE separation is glass; however, fabrication of fluidic channels in glass is quite laborious and time-consuming mainly because of the high temperatures and exacting skills required for bonding glass. This project explores a simple method for producing glass chips in ambient temperature with a fast turnaround time. After fluidic channels are etched in a glass wafer, it is pressed against another glass wafer coated with a thin layer of UV-curable resin. Heating the resin slightly bonds these two pieces of glass together. After protecting the resin area in the channel with a dark liquid, any area surrounding the channel is crosslinked under UV light. The remaining resin in the channel is dissolved by a developer to expose the underlying glass surface. Because the thickness (~2 μm) of the crosslinked layer is much smaller than the periphery (usually > 100 μm) of the channel, it is expected that the glass chip, when fabricated using this simple technique, will have similar efficiency in CE as the conventional one.

Introduction:

Scientists have used capillary electrophoresis (CE) for several decades to separate amino acids, proteins, and DNA. CE provides several advantages over traditional gel electrophoresis including faster separations, low sample consumption, and easy preparation. Furthermore, CE does not denature proteins, a common problem with chromatography techniques.

CE separates samples with the use of an electric field. The sample resides within a basic buffer, which flows toward the cathode at the electro osmatic flow (EOF). Meanwhile, the different particles within the buffer move according to their corresponding charges at the electrophoretic flow. As the sample moves down the capillary channel, it separates, allowing measurement by a fluorescent detection system.

Fabrication of CE microfluidic chips is a difficult and time-consuming process. It requires a heating step of up to 900°C in order to bond the glass. Often times the glass cracks, requiring the fabrication of a new glass wafer with the necessary features. This experiment tests a method for constructing these chips by placing a bonding agent between the two glass layers to simplify the bonding procedure. Placement of a polymer between the two layers of a CE chip would decrease the time and effort to fabricate a CE chip. It would also allow for the subsequent separation of the two sides if a step in the bonding procedure fails.

Experimental Procedures:

Using standard photolithography methods, 10 μm of SPR220-7 is applied to a 4-inch Borofloat wafer. Figure 1 shows the pattern for exposure. After development, the wafer is etched in hydrofluoric acid with a channel depth of 20 μm. Holes are drilled to access the reservoir channel using a diamond 1030FD drill bit.

A thin layer of UV-curable bonding agent, XP SU-8 2, is applied to a new Borofloat wafer. The wafer is spun at 2000 rpm for 15 seconds and placed in contact with the etched wafer. The wafers are heated at 96°C for 15 minutes, until the bonding agent is in complete contact with both layers of glass.

Figure 1: Mask used for CE chips (1 cm x 8 cm).

Black ink is injected into the channel with a micropipet bulb. After flushing any remaining air through the channel, the chip is exposed for 5 seconds to crosslink the polymer resting between the glass layers. The bonding agent that lines the channel wall is then developed (by flushing with 1-methoxy-2-propanol acetate) to expose the underlying glass surface.

Results and Discussion:

Figure 2 shows the results of one of the completed chips with three fluorescent-labeled amino acids. The data should have three sharp peaks indicating the location of each of the amino acids. However, the inconsistent layer of bond lining the channel wall prevented uniform flow through the channel. This caused the fluorescent sections to disperse, resulting in a single flattened peak.

There are two complications that prevent successful fabrication of this chip. The first difficulty was in establishing a clean contact between the top and bottom layers of glass. The bonding agent had patches where the two wafers were not in complete contact. Solving this problem with higher temperature and more weight usually led to the channels filling with bond, which prevented any flow. The second problem occurred with development of the channels. The layer of bonding agent in the channel did not completely dissolve when flushed with developer. To solve this problem, the chip was exposed for less time, which lead to over-development of the channels and an unevenly eroded channel wall.

This method could be improved with the use of a vacuum to suck the developer through the channels. It could potentially create a smoother channel surface by providing a timely and uniform flow through the channels. The equipment was not available in the clean room facility to test this.

Conclusion:

Unfortunately, the complications associated with this experiment forced the addition of several new steps for successful fabrication. The purpose of this study was to find a simple method for fabrication, and even though an altered method could potentially work, the time and effort required don't add any benefits over traditional fabrication.

Acknowledgements:

I would like to thank to my mentor, Hongkai Wu, for his guidance and support in this project. I would also like to thank the National Science Foundation and the Center for Integrated Systems at Stanford University for the opportunity to conduct this research.

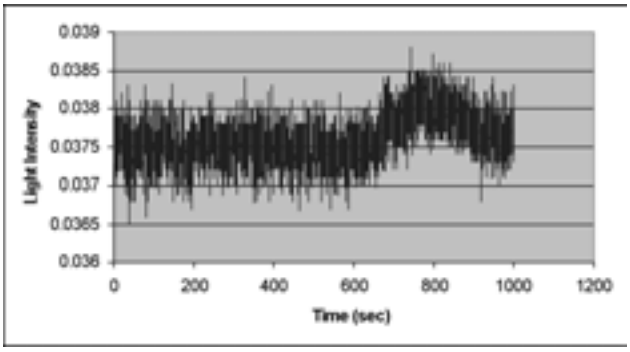

Figure 2: Fluorescence detection results for capillary electrophoresis chip.

SuperGhost: A Novel Software-Based Optical Proximity Correction Algorithm

Siavash Dejgosha, Applied and Engineering Physics, Cornell University

Prof. R. Fabian W. Pease, Electrical Engineering, Stanford University

Jun Ye, Consulting Professor, Rafael Aldana, Electrical Engineering, Stanford University

sd82@cornell.edu, pease@cis.stanford.edu

Abstract:

Electron beam lithography suffers from proximity effects when exposing dense patterns. For every exposed element, forward-scattered and back-scattered electrons cause undesirable exposure in surrounding elements. Processing and development also introduce other biases. A previously published method, Ghost [1], corrects exposure bias with a second exposure that applies the inverse pattern with a low-dose defocused beam. The second exposure and the original back-scattering combine to add a constant dosage offset. We investigated modifying the Ghost exposure to account for these other process biases. With a known process bias, SuperGhost precompensates by using the second exposure to modify the bias and the iso-dense bias.

We investigated several algorithms for SuperGhost including writing on the inverted pattern, writing on every pixel, and on some combination of the two. A computer simulation of wafer exposure with the SuperGhost method shows our results. More work is needed to characterize the process bias and refine the simulation.

Introduction:

Electron beam lithography (EBL) offers extremely high resolution fabrication of layouts. For this reason, the majority of masks used in optical lithography are created by EBL. Other applications include high resolution research patterns and microelectronics. EBL is similar to optical lithography in that a specified pattern is exposed onto a sensitive resist. Unlike optical lithography, source limitations dictate exposing the pattern pixel by pixel. This rasterization and the need to avoid Coulomb interactions within the resist and the electron beam make EBL very slow. Pattern fidelity by the reduction of proximity effects is a more pressing concern for research and low-throughput applications.

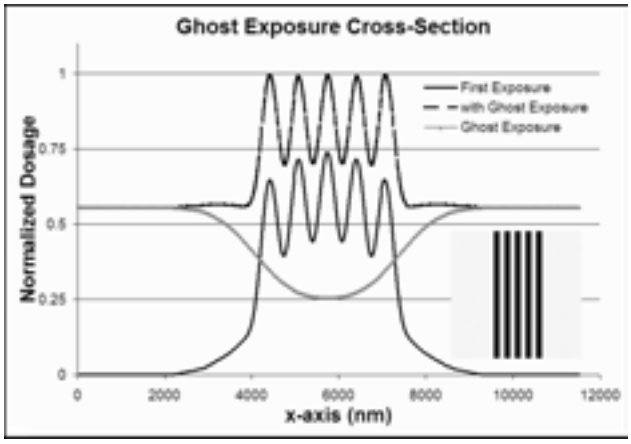

Figure 1: Ghost on equal lines and spaces.

These proximity effects are modeled through Gaussians [2]. The source energy distribution may be modeled as a Gaussian (FWHM ~ 10 nm). On passing through the resist, the beam forward-scatters to ~20 nm. Finally, at the resist-substrate interface, a wide (several μm) yet low energy scattering occurs. The sum of these scattering events on nearby pixels is called the proximity effect and it is dependent on factors such as resist, beam energy, and substrate.

Ghost attempts to correct for backscattering. The pattern is exposed normally. Then, a second pass with a beam profile similar to the original backscattering is applied on the inverted pattern. The backscattering of the second pass is neglible compared to the original dosage. The two passes are combined to set the offset of the entire exposure by a certain amount but to neutralize the backscattering by equalizing it everywhere on the pattern (Figure 1).

Other than scattering, the development and

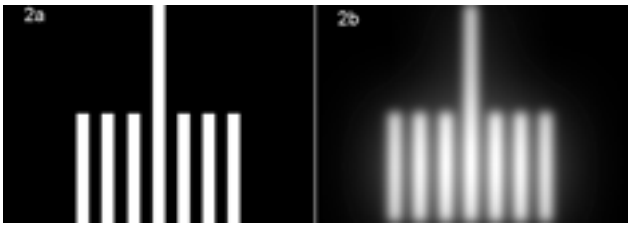

Figure 2: A. Ideal test pattern. B. Exposure.

processing may introduce other errors in the pattern. We can model these errors as an unknown and incorporate extra dosage in the exposure. Once this process bias is known, we can precompensate the pattern with a modified Ghost pass that integrates the process- and exposure-induced biases.

Procedure:

Design layouts are specified in a vector-based format called GDSII. GDSII files contain elements like polygons, lines, and other shapes. We first converted GDSII files into bitmaps. A program, written in C++, accomplishes this task.

Next, MATLAB scripts simulate the e-beam lithography process. We assumed the resist and beam were such that the energy deposition rate through the thickness of the resist was constant and only a function of the radial distance from the center of an exposure. The scripts convolve the circuit layout with a double-gaussian point-spread-function (PSF), which models scattering. We calculate the PSF parameters so that the total energy deposited in forward scattering matches the total energy deposited in backscattering.

To quantify our results, a binary dosage threshold was applied. Holding this threshold constant allows the linewidth of different exposure parameters to be measured consistently.

Simulations involved modifying the parameters of the PSF's and the design pattern.

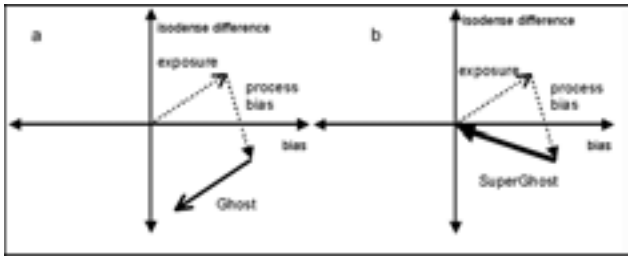

Figure 3: Iso-dense difference/Bias plane.

Results and Discussion:

Consider an ideal pattern (Figure 2a) and its exposure (Figure 2b). The critical dimension (CD) is defined as the desired line width. Bias is defined as the difference between the CD and the line width for the isolated top line after exposure. The line width of the bottom center line, in the dense region, is larger than in the top. The difference between the top and bottom line widths is defined as the iso-dense difference. The bias/iso-dense difference plane illustrates the difference between Ghost (Figure 3a) and SuperGhost (Figure 3b). Ghost counteracts the exposure process bringing it back to the origin but ignores process bias. SuperGhost corrects the exposure and process bias returning the layout to the origin. The vectors may not simply add together since the exposing process may not be linear. Empirical results are needed to verify linearity.

Simulations varying the Ghost amplitude and width showed a nonlinear dependence on both. Figure 4 summarizes the effect of varying the inverted and noninverted pattern dosages. The regular exposure bias was defined as zero and all values are calculated from that base. A large iso-dense difference exists without correction. Ghost significantly reduces this at the cost of higher bias. Generally, the more pattern exposure, the larger the bias, and the more inverse exposure, the lower the iso-dense difference. However, from the small number of simulations, it's not possible to find an exact relationship. Further studies varying different parameters are needed.

Future Work:

Image processing is a well-developed field whose techniques may be applied on the patterns to achieve specific biases. Dilation and erosion filter, when properly applied might achieve a good level of control. An investigation of previous dose adjustment algorithms might yield fruitful results. A more pressing issue is obtaining realistic parameters and checking them against an empirical e-beam fabrication.

Acknowledgments:

I would like to thank Profs. Fabian Pease, Jun Ye, my mentor Rafael Aldana, and the rest of the Pease Group. Work was done at Stanford Nanofabrication Facility and was funded by the National Science Foundation.

References:

[1] G. Owen and P. Rissman, J. Appl. Phys. 54 (6), 3573-3581 (1983).

[2] Handbook of Microlithography, Micromachining, and Microfabrication. P. Rai-Choudhury (Ed.) Vol. 1 Section 2.3 www.cnf.cornell.edu/SPIEBook/spie3.htm (1997).

Comments	Pattern (%)	Inverse (%)	Bias (nm)	Iso-dense diff. (nm)
no 2nd pass	0	0	0	400
Ghost	0	100	400	100
	20	80	500	175
	30	70	500	150
	80	20	450	200

Figure 4: Simulation results.

Study of the Effect of Domains on Thin Stripes of Magnetic Material

Ashley Evans, Electrical Engineering, California State University Fresno

Shan X. Wang, Materials Science and Engr, and Electrical Engr, Stanford University

Ankur Mohan Crawford, Materials Science and Engineering, Stanford University

ashleye@csufresno.edu, sxwang@ee.stanford.edu

Abstract:

The performance of planar spiral inductors can be greatly enhanced by the use of one or two magnetic ground planes. However, the magnetic properties of a ground plane are significantly affected by the physical construction. It has already been shown that leaving gaps within the magnetic ground plane reduces eddy current loss [1]. In this project, the effect of varying the width of the stripes of magnetic material on the magnetic properties was explored.

Layers of 0.2 μm and 0.4 μm thick CoTaZrTb were constructed, in different patterns varying from 2 μm to 15 μm wide and 140 μm long, using standard photolithography processes and ion etching. The magnetic domains were observed with a microscope that utilizes the Kerr effect, and furthermore, the magnetization of the material was measured with respect to the variation of the magnetic field. These characteristics were observed with respect to the width of the stripes so the performance of the magnetic ground plane could be understood with respect to its construction. It was found that favorable magnetic properties were reduced as the stripe width was decreased.

Introduction:

In the interest of saving time, space and costs, the demand for on-chip inductive components has increased as an alternative to integration with a printed circuit board. CMOS compatible planar spiral inductors have been developed [1], and it was shown that the inclusion of a magnetic ground plane significantly increased the inductance. It was also shown that patterning the material increased the cut-off frequency with a trade-off of decreasing the inductance [1, 2]. The purpose of this experiment was to explore how variations of this patterning affected the magnetic properties of the material. Particularly, the magnetic domain patterns were observed as the width of the stripes of material was decreased.

Procedure:

Single layers of CoTaZrTb, 0.2 μm and 0.4 μm thick, were deposited on 4-inch silicon wafers. During deposition, a magnetic field was applied in order to orient the easy axis of magnetization of the material in a particular direction. Standard photolithography processes were used to create the desired pattern in photoresist on the wafers. This pattern consisted of areas that each contained rectangles that were 140 μm long with widths of 2 μm, 4 μm, 6 μm, 10 μm, 12 μm, or 15 μm. The pattern was created with the easy axis of magnetization perpendicular to the length of the rectangles. The wafers were then dry ion etched to create the final pattern of magnetic material.

A microscope that utilizes the Kerr effect was used to take images of the magnetic domains within the stripes of material. An illustration of the expected magnetic domain pattern is shown in Figure 1, where closure domains aligned perpendicular to the easy axis of magnetization are present. Vibrating Sample Magnetometry was used to obtain the hysteresis loops for each sample. From these measurements, the magnetic anisotropy was estimated. The relative permeability of the patterned material was also measured in the 10 kHz range with respect to stripe width.

Results and Discussions:

Images of the magnetic domains were successfully

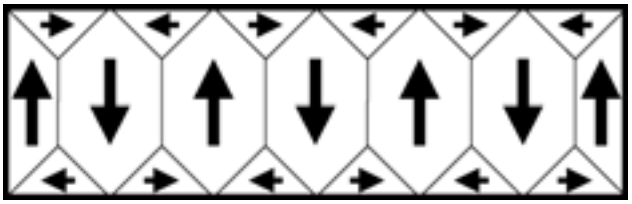

Figure 1: Expected domain pattern.

taken, with special attention focused on the size of the closure domains. Figure 2 shows an image taken of the 0.2 μm thick, 15 μm wide stripes. The closure domains on the edges of the rectangle can be seen as taking up significant area of the magnetic material, but as the stripe width is decreased the closure domains occupy an increasing percent of the area. Figure 3 shows an image taken of the 0.4 μm thick, 12 μm wide stripes, and Figure 4 shows an image of the 0.4 μm thick, 10 μm wide stripes. At this point, the closure domains can be seen reaching into the middle of the stripes, thus decreasing the useful magnetic properties of the patterned material. The resolution of the Kerr microscope was about 2 μm, so successful images of the 2 μm and 4 μm wide stripes were not obtained.

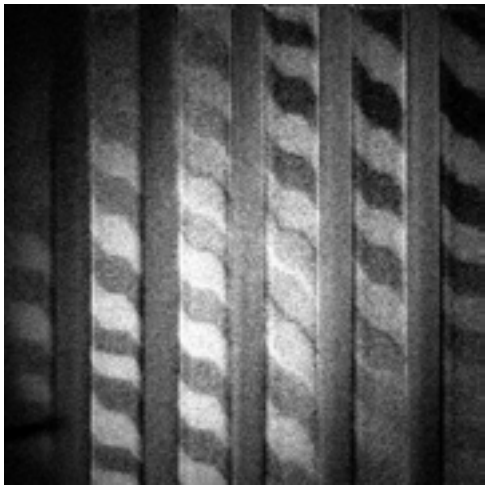

Figure 2: 0.2 μm thick, 15 μm wide stripes domain image.

The magnetization measurements were expected to reveal a decrease in anisotropy as stripe width was increased, which would agree with the idea that the closure domains would increase magnetic anisotropy in thinner stripes. This result was verified down to the 10 μm wide stripes, but for stripes thinner than that unexpected results were obtained. The same anomaly occurred with the relative permeability measurements. For wider stripes the relative permeability increased, but for the 2 μm and 4 μm wide stripes, higher values than expected were obtained.

Summary:

Successful imaging of the magnetic domains showed that thinner stripes experienced an increase in the area occupied by closure domains and a resulting increase in magnetic anisotropy. Thus the ability of the magnetic material to contribute inductive enhancement to passive components is affected by the size of the patterning. Some patterning, though it reduces the effective permeability, is required to increase cut-off frequency and reduce eddy current loss. These results indicate that careful attention must be paid to the width of stripes of patterned magnetic material.

Acknowledgements:

I would like to thank my principal investigator Dr. Wang, my mentor Ankur Mohan Crawford, as well as the rest of the Wang Research Group, and Scott Andrews, for their assistance and guidance. I would also like to thank Mike Deal, Jane Edwards, the SNF staff, the NNUN, and the National Science Foundation.

References:

[1] A. M. Crawford, D. Gardner, S. X. Wang, "High-Frequency Microinductors with Amorphous Magnetic Ground Planes," IEEE Trans. Magn., vol. 38, no. 5, pp. 3168-3170, Sept. 2002.

[2] A. M. Crawford, D. Gardner, S. X. Wang, "Fabrication and Comparison of Broad-band Inductors with One and Two Co-based Amorphous Ground Planes," Trans. Magn. Soc. Japan., vol. 2, no. 5, pp. 357-360, 2002.

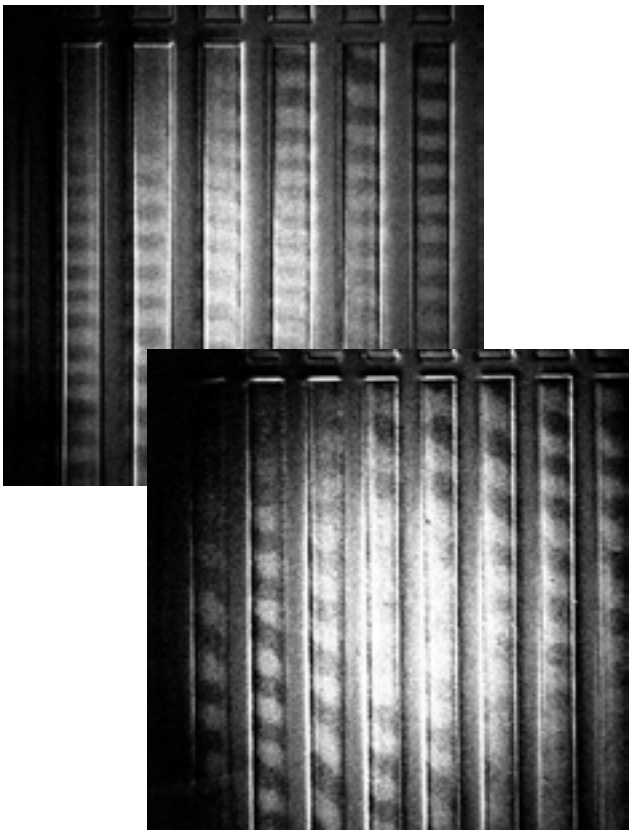

Figure 3, left: 0.4 μm thick, 12 μm wide stripes domain image.

Figure 4, right: 0.4 μm thick, 10 μm wide stripes domain image.

In Situ Optical Monitoring of Selective Wet Oxidation of AlGaAs Alloys

Nicholas Fichtenbaum, Electrical Engineering, Washington University in St. Louis

James S. Harris, Electrical Engineering, Stanford University

Evan Thrush, Electrical Engineering, Stanford University

NF1@cec.wustl.edu, harris@snowmass.stanford.edu

Abstract:

Recent work in the field of optoelectronics, particularly vertical-cavity surface-emitting lasers (VCSEL), has shown that wet oxidation of selected AlGaAs layers significantly improves the optical and electrical properties of the devices. One essential component to VCSEL performance is the creation of highly reflective mirrors called distributed Bragg reflectors (DBR), which are formed by creating alternating layers of GaAs and AlGaAs. Oxidizing the AlGaAs layers changes the refractive index of the material, such that it has a greater contrast with its coinciding GaAs layer. This in turn makes the DBR much more reflective. In addition, it will provide more defined current apertures, which will improve the VCSEL efficiency by eliminating surface recombination.

Present oxidation systems for AlGaAs are in place, but there is minimal control over the present procedure. A new method for wet oxidation has been developed. It is the goal of our research to get this system working consistently and accurately, and develop suitable calibration and control techniques. A particular challenge for this system is achieving strict control through in situ optical monitoring. This system will greatly expand the efficiency and performance of VCSEL technology.

Experimental Setup:

The premise of our experimental setup is similar to that of previous GaAs oxidation furnaces, except that it possesses in situ optical monitoring capabilities. As shown in Figure 1, N_2 is run through a bubbler with H_2O in order to provide a mechanism for delivering O^{-2} to the AlGaAs system. The furnace chamber is put under a small vacuum in order to provide quick and easy evacuation of the chamber in order to stop the oxidation reaction. Since heating the substrate and other procedures take considerable time in which it is not necessary for O^{-2} to be in the system, pure N_2 can also be run into the chamber. In addition, the vacuum will prevent condensation from forming on the underside of the viewport, which would obscure the image. Also, the presence of O_2 molecules has been shown to actually retard the oxidation reaction, so the vacuum and pure N_2 allow for the evacuation of these molecules prior to beginning the oxidation process. Imaging is achieved using a 20x long working distance objective, which is then connected to CCD camera and fed into a TV monitor.

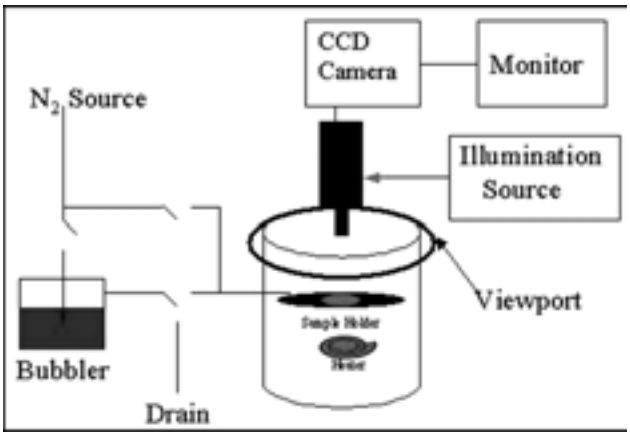

Figure 1: Schematic of the oxidation system.

Experimental Procedure:

The first part of our experimental procedure was to develop a protocol for running the oxidation furnace. It was determined that it was first necessary to allow the N_2 to bubble through the heated H_2O for 1.5 hours in order to remove any O_2 molecules that might be present in the H_2O. We then placed our sample in a 10:1 water, ammonium hydroxide bath for approximately 1 min. to remove any previous oxidation that was formed due to contact with the air. The sample was then placed in the furnace, and the heater was

ramped to the desired oxidation temperature, which is typically around 400°C. Upon achieving oxidation temperature, the H_2O saturated N_2 was then allowed into the chamber and the pure N_2 sample switched off. By observing test samples in the monitor, it was determined that the oxidation reaction takes place almost immediately after the H_2O is allowed into the furnace. After a suitable oxidation time, the furnace is switched back to pure N_2 and allowed to cool before removing the sample.

Results:

Successful oxidations were performed on over 30 simple test structures. Figure 2 is typical of what would be observed on the monitor during oxidation. The oxidation front is the lighter part of the mesa that is oxidizing laterally inward towards the center of the mesa. Several of our test runs were spent determining a suitable flow rate for the N_2 source, which was eventually determined to be about 4 scfh. This flow rate allows oxidation to take place in the saturation region of the oxidation rate vs. carrier gas flow curve which ensures that the reaction is not reactant limited [1]. Figure 3 shows another image on an oxidation front captured in the TV monitor. The ringing effect observed in this image, as opposed to the consistent oxidation front in Figure 2, is due to interference effects that are brought about by the triangular oxidation front that can be observed in Figure 4.

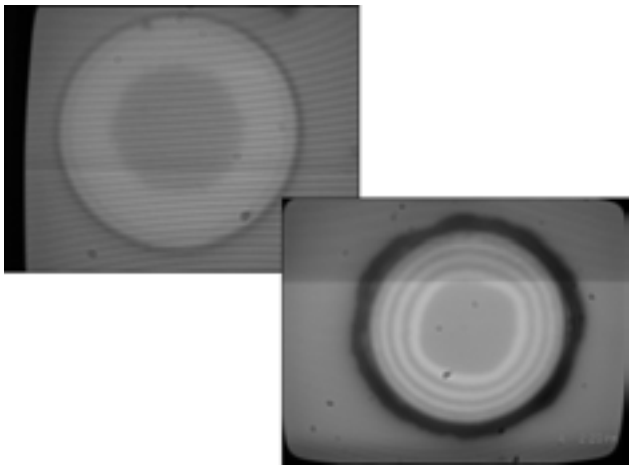

Figure 2, above left: Partially oxidized mesa captured using an 800 nm long pass filter.

Figure 3, above right: Partially oxidized mesa captured using an 800 nm long pass filter.

Future Work and Conclusions:

Future work on this system will be to explore imaging real devices. In order to make this a more feasible goal, it has been hypothesized that bandpass filters instead of longpass filters will be ideal. Both are necessary because oxidizing the AlGaAs reduces the index of refraction of the layer which will cause a change in reflectivity. This change in reflectivity is what is hoped will provide significant enough contrast to image VCSELs. I believe that the work done this summer has demonstrated that in situ monitoring is possible to achieve with a GaAs oxidation furnace.

Acknowledgements:

I would like to thank my mentor Evan Thrush, Jung-Yong Lee, Mark Wistey, and Professor James S. Harris for all of their support and guidance. Also, I would like to thank NSF, NNUN, and SNF.

References:

[1] Choquette, K. D., et al. "Advances in Selective Wet Oxidation of AlGaAs Alloys". IEEE Journal of Selected Topics in Quantum Electronics, Vol. 3, No. 3, June 1997.

[2] Feld, S.A., et al. "In Situ Optical Monitoring of AlAs Wet Oxidation Using a Novel Low-Temperature Low-Pressure Steam Furnace Design". IEEE Photonics Technology Letters, Vol. 10, No. 2, Feb. 1998.

[3] Wilmsen, C., Temkin, H., and Coldren, L. "Vertical-Cavity Surface-Emitting Lasers" Caimbridge University Press, 1999.

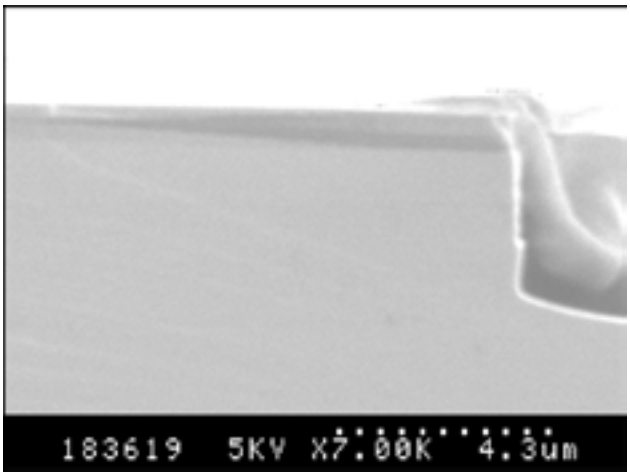

Figure 4: SEM image of the oxidation front in Figure 3.

Carbon Nanotube Transistor Optimization

Steven Floyd, Mechanical Engineering, Washington University in St. Louis

Hongjie Dai, Department of Chemistry, Stanford University

Ali Javey, Department of Chemistry, Stanford University

David Mann, Department of Applied Physics, Stanford University

srf2@cec.wustl.edu, hdai1@stanford.edu

Abstract:

The electrical properties of carbon nanotube field-effect transistors (CNFETs) can be drastically altered by adjusting a number of device parameters. These parameters include contact (gate, source, drain, etc.) material and annealing temperature. In order to properly utilize these advanced properties, devices must be designed to take advantage of all device parameters and still be conducive to the consistent formation of carbon nanotubes. Electron beam lithography, in conjunction with metal evaporation and conventional lithography methods, is used as a means of creating new devices with necessary feature sizes.

We fabricated and characterized devices with different contact materials to optimize both n-type and p-type CNFETs. Materials included palladium (Pd), platinum (Pt), titanium (Ti), and nickel (Ni). Annealing was done at temperatures ranging from 150°C to 250°C. Results indicate the superiority of Pd as a contact material. The effects of annealing seem to be a shift in threshold voltage as a function of annealing temperature.

Introduction:

The world of integrated circuits relies on the interactions of millions of transistors. Each generation of new computer chip has smaller transistors that are more numerous, and more densely packed. The press to make computers faster leads producers to continuously seek new ways to reduce the size of individual transistors and arrays of transistors. Enter the carbon nanotube: a molecular semiconductor that has a diameter as small as 1 nanometer (nm) and can be made as short as tens of nm. For reliable nanotube-based transistors, the scaling length is basically limited by the size of the metal contacts on either end of the tube [1].

When designing transistors, a few key properties are used to determine performance. First, high on-state, and low off-state conductances are needed. Conductance is proportional to current at a given voltage bias. Also, a large change in conductance (several orders of magnitude) accomplished in a small change in gate voltage (V_g) is required. Work done by others on carbon nanotube transistors has shown that the work function of the contact and gate material can affect both of these properties [2].

In this project, transistor devices were fabricated on a mat of carbon nanotubes grown by either chemical vapor deposition (CVD) or plasma enhanced chemical vapor deposition (PECVD). The devices were made with one or two metallic layers so that clean contact with the tube and wafer could be ensured, and the work function of the contact as a whole would be high. It has been shown [2] that a high work function for the contact material leads to a high on-state conductance for the transistor. After initial probing, samples were annealed and then reprobed to determine what effect, if any, the annealing had. It is hoped annealing leads to a cleaner contact between tube and metal, and a corresponding increase in on-state conductance.

Procedure:

Random ferritin (a protein containing iron) deposition is done on a silicon wafer with a 67 nm SiO_2 oxide layer. The sample is then heated to 900°C while a mixture of CH_3 and C_2H_4 is flowed. Carbon nanotubes grow from the ferritin catalyst particles and eventually stick to the SiO_2 substrate in a random fashion.

Electron beam resist is spun onto the sample and then etched away in a standard electron beam lithography process. This produces devices with a source/drain (S/D) separation of ~300 nm that may have a nanotube crossing the two electrodes. Metal is then evaporated onto the sample, and the excess

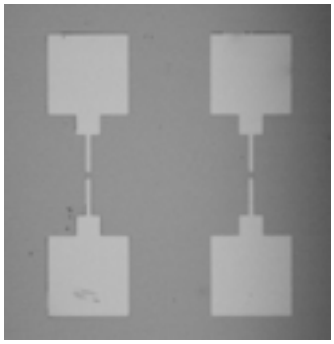

Figure 1: Typical device with opposing fingers spaced ~ 300 nm apart.

removed. If one metal was used, thickness was nominally ~20 nm. In the case of two metals, the first is ~5 nm and the second ~15 nm (unless otherwise noted). The result is a pair of contact pads with opposing "fingers" that point to an ~300 nm gap which may be spanned by one or more carbon nanotubes. (Figure 1.)

After production, the on-state conductance and transistor characteristics were recorded for several different S/D metal combinations. A S/D voltage bias of 10 mV was applied while the gate voltage was swept from $^{-}5$ to $^{+}5$ V. Devices that had off-state currents two or more orders of magnitude lower than their on-state current were classified "depletable." All devices with smaller change, or metallic properties (no change in current as V_g was varied) were classified "non-depletable." Samples were then annealed at 300°C and the same data was collected again.

Results/Conclusion:

Results can be interpreted in a straightforward manner from Figures 2 and 3. Mats of tubes grown by CVD had higher—or at least comparable—yields than those grown by PECVD (prior to annealing). After annealing, the CVD samples for Pd/Pt, Ti/Pt, and Ni/Pd had currents in the hundreds of nanoamps, which implies resistances in the tens of kilo-ohms, thus approaching the theoretical limit of 6.45 kilo-ohms [2]. Overall, Pd/Pt seems the best candidate for a bilayer material combination.

Annealing effects were most obvious on low conductance tubes with some nanotube devices that appeared to be noise clarified into transistors after annealing. Because of the high yields, almost all devices had multiple tubes bridging the gap. This, in combination with the presence of some metallic tubes, led to a large number of non-depletable transistors being reported. Further study on low yield samples may shed some light on the true distribution of the performance of nanotube transistors. Annealing did not seem to increase the on-state conductance for low resistance tubes significantly, and only resulted in a shift in the threshold voltage. Further study into this phenomenon may follow.

References:

[1] Ultrahigh-Density Nanotransistors By Using Selectively Grown Vertical Carbon Nanotubes. Choi, WB; Chu, JU; Jeong, KS; Bae, EJ; Lee, JW; Kim, JJ; Lee, JO. Applied Physics Letters; NOV 26 2001; v.79, no.22, p.3696-3698.

[2] Ballistic Carbon Nanotube Field-Effect Transistors. Javey, A; Guo, J; Wang, Q; Lundstrom, M; Dai, HJ. Nature; AUG 7 2003; v.424, no.6949, p.654-657.

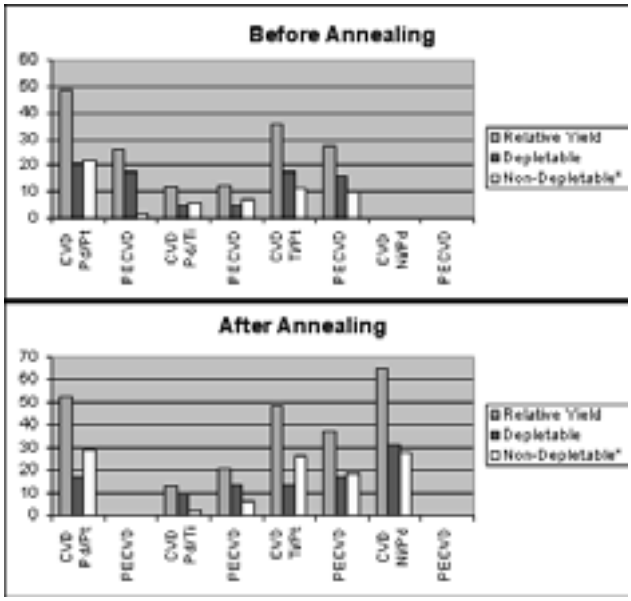

Figure 2, above: Chart of material combination yields before and after annealing.

Figure 3, below: Chart of average depletable on-state current in nA.

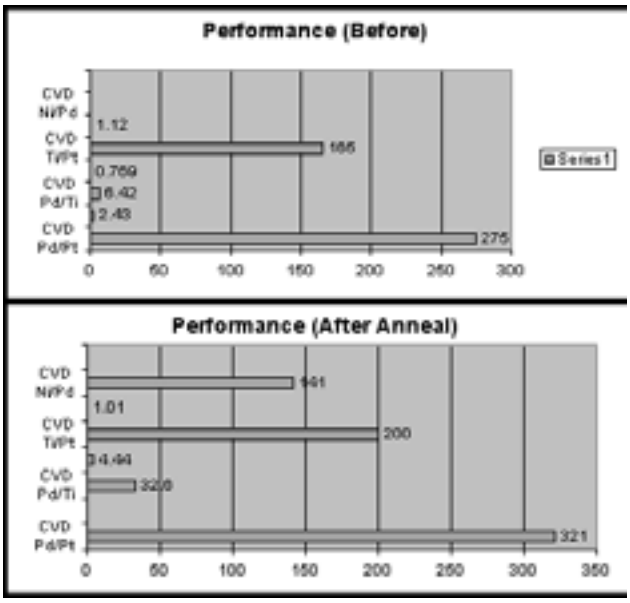

Optimization of Carbon Nanotube Based Sensors for Biosensing Applications

Karen Havenstrite, Chemical Engineering, University of Nevada, Reno

Hongjie Dai, Department of Chemistry, Stanford University

Robert Chen, Qian Wang, Department of Chemistry, Stanford University

klh53@cornell.edu, hdai1@stanford.edu

Abstract:

Carbon nanotube based field effect transistors with varying architectures have been fabricated with standard microfabrication techniques enabling the investigation of protein binding on nanotubes in solution. Working off of previous designs, we tested a device with a thin oxide layer in order to optimize the signal due to nonspecific binding of proteins in the solution phase. With the thin oxide variation of the architecture, we found that the sensitivity was similar to that of the original thicker oxide device.

Introduction:

Micro and nanofabrication in combination with methane chemical vapor deposition has enabled the fabrication of novel carbon nanotube based field effect transistor devices. These transistors have led to a new generation of carbon nanotube based devices, including new electronic materials and gas phase sensors. The quality and sensitivity of these sensors is largely dependent on the nanoscale structure of the device. It has been proposed that the binding of proteins to the nanotube surface causes a change in the conductance of the device through charge doping or a change in the metal contact work function. In this paper, we take advantage of this property to investigate the effectiveness of various device geometries. We will use our observations to create a new architecture which maximizes sensitivity and quality for solution phase biosensing.

Experimental Procedure:

Materials. Human chorionic gonadotropin (HCG) and anti-HCG were purchased from BiosPacific. Human serum albumin (HSA) was purchased from Aldrich.

Methods. The devices were fabricated according to the schematic shown in Figure 1. The first devices were fabricated with an oxide thickness of 67 nm underneath the nanotubes; this is very thin in comparison with the 500 nm oxide found in the original devices. Devices are currently being fabricated with a gap size of 100 μm between the electrodes as opposed to the 5 μm gap found in the original design. No results have been obtained for these large gap devices as their fabrication is not yet complete.

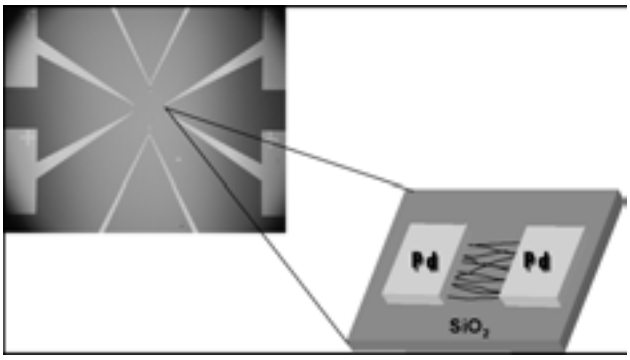

Figure 1: Architecture of the existing biosensing devices.

Alumina-supported catalyst islands were deposited and carbon nanotubes grown between the islands using chemical vapor deposition. Metal was then evaporated onto the device and liftoff was done to form the electrodes. Sensing was carried out by sealing the device against a liquid cell which exposed the active center region of the device to the protein solution and prevented solution contact outside the active region. Concentrated protein aliquots were added to the cell and allowed to diffuse through the solution. Conductance was monitored real time with a semiconductor parameter analyzer. The source drain bias was set at 10 mV and the gate potential was set to equal 0.

Results and Discussion:

Human chorionic gonadotropin (HCG) is an antigen

that is found in pregnant women and therefore the detection of this protein is utilized as an accurate pregnancy test. Anti-HCG is an antibody that is made synthetically and binds exclusively to HCG. This biospecificity is utilized to functionalize the surface of the nanotube in order to carry out selective sensing. Our approach is to bind HCG onto the surface of the nanotubes and use this first layer as both a biospecific layer and a blocking layer which will prevent any further non-specific bonding. This approach allows for the selective sensing of anti-HCG.

The typical sensing procedure was used to test the selectivity and sensitivity of the thin oxide devices. First, a concentrated solution of HCG was added to functionalize the surface of the nanotubes and allow for the exclusive detection of HCG. Next HSA was added to determine the selectivity of the device. Finally anti-HCG was added in increasing concentrations in order to test the sensitivity of the device.

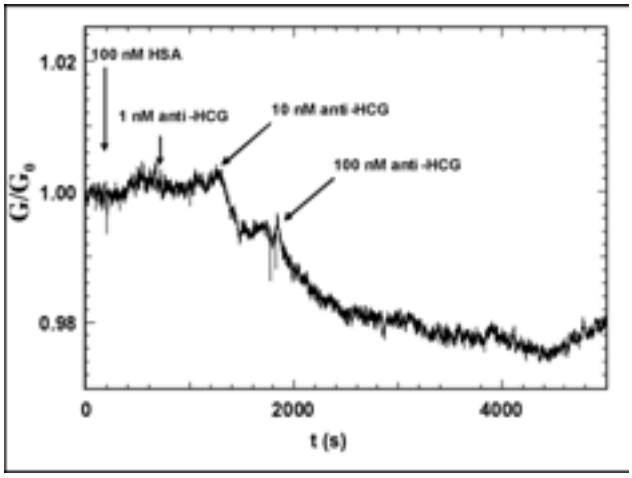

Figure 2: Normalized conductance plotted versus time for a device fabricated with a thin oxide layer.

The graph in Figure 2 shows the results from the device with a 67 nm oxide layer. From these results, it appears that the device exhibited selectivity because there was no significant conductance change observed after the addition of HSA. There is also sensitivity as can be seen by the conductance change observed after the addition of the 10 nM anti-HCG. For comparison, the results from the original device design are shown in Figure 3. The data for the original device shows larger more clearly defined conductance changes when anti-HCG is added. These preliminary results indicate that while the thin oxide device does show both sensitivity and selectivity, it is unclear if the device will perform better with this design modification.

Conclusion:

We have manufactured carbon nanotube field effect transistors which are capable of selectively sensing anti-HCG using HCG as a selective biolayer. In the future, the thin oxide seems to be promising but more studies must be done and the oxide layer may need to be thinner.

Acknowledgements:

I would like to thank the National Science Foundation and the Center for Integrated Systems at Stanford University for providing the funding for this program. I would also like to thank Robert Chen, Qian Wang, Hongjie Dai and the Dai Research Group for their assistance with this project.

References:

[1] R. J. Chen, S. Bangsaruntip, K. A. Drouvalakis, N. W. S. Kam, M. Shim, Y. Li, W. Kim, P. J. Utz and H. Dai. Noncovalent functionalization of carbon nanotubes for highly specific electronic biosensors, Proceedings of the National Academy of Sciences 2003, 100(9), 4984-4989.

[2] Dai, Hongjie. 2002. Accounts of Chemical Research. 35: 1035-1044.

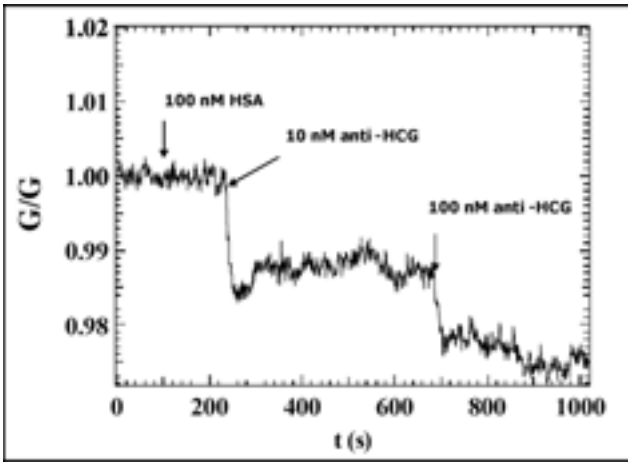

Figure 3: Normalized conductance plotted versus time for the original device with a thick oxide layer.

Substrate Temperature Measurement During Molecular Beam Epitaxy Growth of GaInNAsSb Quantum Wells

Douglas Jorgesen, Electrical Engr, University of Illinois at Urbana-Champaign

James Harris, Seth Bank, Electrical Engineering, Stanford University

djorgese@uiuc.edu, harris@snow.stanford.edu

Introduction:

Molecular Beam Epitaxy is used to create quantum well lasers by heating a substrate and depositing layers of semiconductor material. Though rough temperature estimation methods have historically been sufficient, the recent fabrication of temperature-sensitive GaInNAsSb lasers requires more precise measurement techniques. Varying substrate temperatures changes growth kinetics resulting in varying bandgaps of GaInNAsSb.

In this project, we attempt to create a reflectance spectroscopy system to accurately monitor the substrate temperature. In this technique, a broadband light source is reflected from the surface of the substrate into a spectrometer. Because the bandgap, and thus absorbed light, of the material is dependent on its temperature, the reflected spectrum provides an indication of the substrate temperature. A system is proposed for real time reflectance spectroscopy during epitaxy growth, allowing better control of the quantum well bandgap and thus better lasers.

Background and Theory:

Recently, tremendous advances have been made in semiconductor laser technology by growing lasers from GaInNAsSb using molecular beam epitaxy. Currently edge-emitting lasers have been fabricated using this material [1]. In order to fabricate vertical cavity surface emitting lasers, which have several desirable qualities, better control of the substrate temperature is required. Substrate temperature is very important for the growth kinetics of the material, and changes the percentages of the compositions deposited. We are creating a reflectance spectroscopy system to control the temperature.

Reflectance spectroscopy is a method of determining the temperature of a material by shining light onto it and then monitoring the spectrum of the reflected light [2-4]. In our situation, the material that we would like to observe is the GaAs substrate upon which the lasers are being grown. Because this is a semiconductor material, the reflected spectrum is dependent upon the bandgap of the material. The bandgap of a semiconductor material is dependent on the temperature of the material according to Varshni's equation: $\Delta E = \alpha T^2/(\beta+T)$, where ΔE is the bandgap of the material, T is the temperature, and α and β are constants dependent upon the semiconductor material.

When a photon is incident on the material, it will be absorbed if its energy is sufficient to excite an electron from the valence band to the conduction band. As the material is heated, the bands move closer together because of extra thermal energy, and the required energy becomes less. Less energy corresponds to a longer wavelength. As a result of this, the reflected spectrum will have a well-defined increase at the point where the wavelength becomes long enough that the photon is not energetic enough to be absorbed. This creates a spectrum like Figure 1.

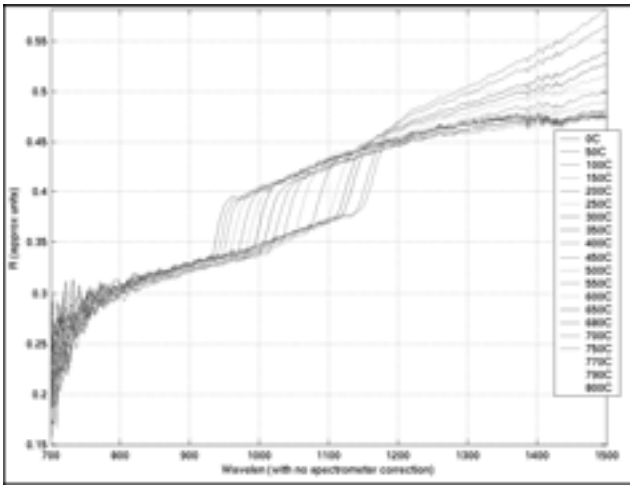

Figure 1: Spectral response of wafer at varying temperatures showing red shift with increasing temperature.

With heavily doped material, the absorbed energy point is smeared out due to doping effects as the light passes through the material. As a solution to this, it is possible to use polarized light that will only affect the surface of the wafer. TM light is reflected off of the surface at an angle where TE light is almost completely absorbed. This allows almost complete extinction of light that passes through the surface, leaving only the spectrum of the surface of the wafer.

System Design:

While reflectance spectrometry has been around for a while, it has not been demonstrated to work for real time temperature measurement and control. This is the novel aspect of our project. In the original system we worked with, a broadband halogen light source is focused onto the substrate. It is reflected off of the substrate, and the image is focused onto a fiber optic bundle. The bundle carries the light to the input of a spectrometer. Inside the spectrometer is a diffraction grating with an adjustable angle. The grating breaks the light into components and the variable angle allows different wavelengths to be shone upon the output slit. In the standard setup, one nanometer of light is shone upon an intensity meter, and the spectrum is scanned. In order to monitor in real time, we are replacing the intensity meter with a CCD camera with responsivity in the IR range.

A CCD instead of an intensity meter allows the system to scan light 10 nm at a time instead of 1 nm at a time. The cost, however, is resolution. More noise is introduced into the spectrum readings when the CCD is used instead of the intensity meter. In order to overcome this, aggressive averaging and noise reduction techniques were used.

As an indication of the temperature, the inflection point in the spectrum where longer wavelength light is reflected is used. As can be inferred from Figure 2, the inflection point increases linearly with increasing temperature; hence temperature can be calculated from this inflection point directly. In order to track the temperature as fast as possible, the system only scans over a small wavelength range (~ 100 nm) around the previous inflection point with each temperature scan. Software then divides out a reference spectrum (taken with a uniformly broadband reflector wafer like aluminum or gold), takes the derivative of the spectrum, and finds the maximum value in the range. This allows for continuous, non-intrusive temperature measurement.

Conclusion:

We propose a real time reflectance spectroscopy system for the control of temperature during molecular beam epitaxy. This system will allow for better control of the bandgap during laser growth, allowing for better lasers. Work on this system has begun. Continuing work includes implementing all the elements of the system, as well as calibrating and optimizing the system.

Acknowledgements:

I would like to thank Seth Bank and Mark Wistey for their patience and assistance with this project. I would also like to thank my collaborator, Chris Fesenmaier, for all of his hard work, as well as the National Science Foundation and Center for Integrated Systems for funding this research.

References:

[1] Harris, J S, 2002 Semicond. Sci. Technol 17 880-891.

[2] Johnson S R, Lavoie C, Tiedje T, and Mackenzie J A 1992 J. Vac. Sci. Technol. B 11 3 1007-1010.

[3] Hellman E S, and Harris J S 1987 J. Crystal Growth 81 38-42.

[4] Herman I P 1995 J. Quantum Electronics 1 4 1047-1053.

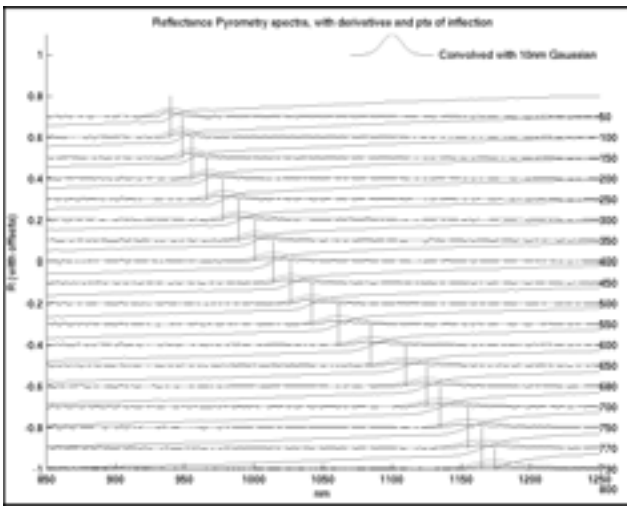

Figure 2: Reflectance spectra from wafer showing inflection point location increasing linearly with increasing temperature.

Adhesion of Lithographically Patterned Thin Film Structures

Grace H. Lee, Electrical Engineering, University of California Santa Barbara

Professor Reinhold H. Dauskardt, Materials Science and Engineering, Stanford University

Christopher S. Litteken, Materials Science and Engineering, Stanford University

glee@engr.ucsb.edu, dauskardt@stanford.edu, litteken@stanford.edu

Abstract:

The dimensions of materials utilized in emerging device technologies play an important role in determining their mechanical behavior, particularly when confined to the micron length scale. The intent of the present study is to investigate the role of feature size on the interfacial adhesion of a patterned thin-film structure. Fabrication of lithographically patterned Cu thin film structures using two different liftoff processes is reported. Arrays of Cu lines are manufactured such that the feature width varied between 2-12 μm. Fabrication of this patterned structure will serve as a basis for future studies on the interfacial adhesion of thin patterned Cu films.

Project Summary:

The intent of the present study is to fabricate and investigate the adhesion of lithographical patterned arrays of Cu films. As microelectronic device length scales decrease, the mechanical properties of their thin films deviate from bulk values. The use of Cu as the metallization within the interconnect structures of advanced microelectronic devices has become widespread due to its lower electrical resistance compared to Al. Recent studies of the adhesion of blanket thin-film interconnect structures have established that plastic energy dissipation can dominate the interfacial adhesive characteristic of thin-film structures containing thin metal and polymer films [1, 2]. Figure 1 illustrates that a dramatic increase in interfacial adhesion was measured with increasing Cu film thickness.

The increase in adhesion was attributed to an increase in plastic energy dissipation ahead of the crack tip. Currently, there is little understanding of how the size of lithographically patterned features utilized in technologically relevant structures will influence plasticity and hence the fracture resistance of such patterned structures.

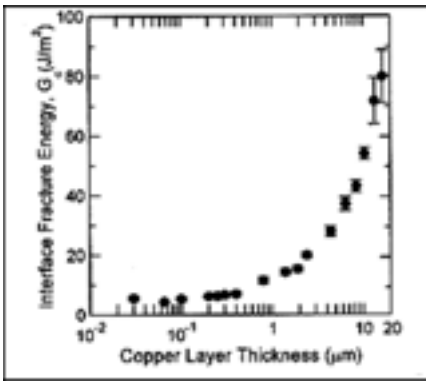

Figure 1: TaN/SiO_2 interface adhesion as a function of Cu layer thickness [1].

Procedures:

To investigate the effect of feature size on interfacial adhesion, arrays of Cu lines were fabricated using two liftoff processes. The structures consisted of five different arrays of Cu lines processed on the same 4" Si (100) wafer, shown in Figure 2. Each array was 25 x 35 mm in size and contained lines with an identical width. Lines widths (w) of 12 μm, 6 μm, 4 μm, 3 μm, and 2 μm were fabricated with each patterned line isolated by a 1.5 μm gap (Figure 3). In order to produce a large range of aspect ratios (width/height) the height of the Cu lines (h) was either 1.0 μm or 0.3 μm.

Two similar liftoff techniques, standard and dual layer processes, were used to pattern the Cu arrays. Using standard processing, the Si substrate was first primed with hexamethyldisalizane (HMDS). HMDS is a chemical primer used to remove surface moisture and improve photoresist adhesion. A 1.6 μm layer of photoresist (Shipley AZ3612) was deposited on the Si substrate. The resist was then exposed using a chrome mask containing the desired patterns for 1.6 seconds using a vacuum contact chuck. The pattern was developed by removing the exposed portion of the resist with LDD26W developer. In order to remove any residual photoresist from the Si surface, the developed patterns were etched in HF for ~ 15 seconds. A 25 nm layer Ti was deposited to enhance adhesion

Figure 2: 1.5 μm lines of photoresist separated by a 12 μm gap

between the Si and the subsequent Cu film. A 300 nm Cu film was then deposited over the patterned photoresist and Ti film. Using standard processing, the thickness of the Cu layer was limited to be less than half of the thickness of the original photoresist to ensure a discontinuous Cu film. Removing the remaining photoresist, a procedure known as "liftoff", produced the patterned arrays of Cu lines. Liftoff was accomplished by immersion in acetone or photoresist remover (Microposit 1165) at 50˚C for two 10-minute intervals. To ensure the photoresist and overlaying metal was completely removed, the patterned films were then soaked in fresh remover for 12 hours. The use of an ultrasonic bath was observed to effectively accelerate the liftoff process.

In order to fabricate Cu lines 1.0 μm in height, a dual layer photoresist process was employed. The double layer resist controls the resist edge profile, giving it a negative slope, or undercut, where bottom layer geometry gets a positive bias compared to the top imaging layer either by higher sensitivity to exposure doses, or higher dissolution rate in the developer. This process achieves good liftoff thus obtaining cleaner surfaces and taller structures [3], and is equivalent to the standard process with the addition of the LOL2000 layer, deposited by spin coating on the Si substrate. LOL2000 is an inert, non-UV-sensitive polymer, which can be etched with most standard developers [4]. The LOL2000 ensures a clean undercut that varies between 0.3 - 0.5 μm in width. To obtain less undercut, LOL2000 baking temperature was increased (130 - 180˚C) and development time is altered accordingly.

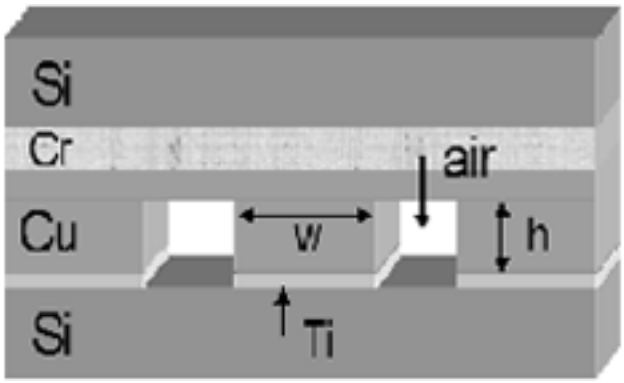

Figure 3: Sandwich structure for mechanical testing.

Conclusions:

The standard process can be used to fabricate structures ~ 300 nm in height. With the addition of a LOL2000 layer, the height can be increased to ~ 1.0 μm due to controlled undercutting. Baking temperature and development time are crucial to the dimensions of the pattern. Figure 3 shows the sandwich structure for mechanical testing. Although time did not permit mechanical testing, interfacial adhesion and the associated fracture surface characterization related to these patterned structures will be studied to determine prevailing plastic deformation mechanisms.

Acknowledgments:

The author wishes to thank Professor Reinhold Dauskardt, and Christopher Litteken of Stanford University for their guidance; Professor Evelyn Hu, Professor Kenneth Millett, Professor Robert Geller, and James Champlain of UCSB for their inspirations.

References:

[1] M. Lane, R.H. Dauskardt, A. Vainchtein, and G. Huajian, Plasticity contributions to interface adhesion in thin-film interconnect structures. Journal of Materials Research, 2000. 15(12): p. 2758-2769.
[2] Litteken, Adhesion of Polymer Thin-Films and Patterned Lines. International Journal of Fracture, 2003.
[3] http://fy/chalmers.se/assp/snl/public/wproc/LOL2000_Liftoff.html
[4] http://snf.stanford.edu/Process/Lithography/liftoff.html

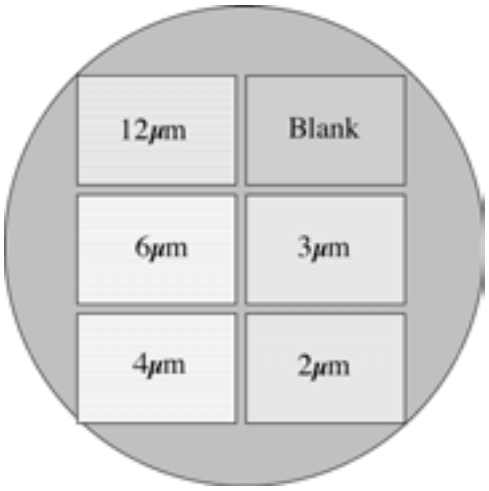

Figure 4: Plan view of patterned 4" Si wafer.

Ferroelectric Thin Films for Nonvolatile Memory Applications

Sarah Beth Rickman, Chemical Engineering, Lehigh University

Professor Paul McIntyre, Materials Science and Engineering, Stanford University

Dr. Lawrence Schloss, Department of Materials Science and Engineering, Stanford University

sbr3@lehigh.edu, pcm1@stanford.edu

Abstract:

Ferroelectric random access memory (FeRAM) has shown much potential in replacing volatile dynamic random access memory (DRAM), the current choice for computer technology. FeRAM is nonvolatile, meaning that the charge stored upon the bit capacitor is stable, negating the need for an energy-intensive data refresh. Thus, for portable applications where energy is limited, FeRAM is attracting significant interest.

One reliability issue encountered with FeRAM is fatigue, which is defined as a loss of switchable polarization, or signal strength, with repeated switching. In this work, this phenomenon will be studied by measuring the energy levels and populations of defect levels in a capacitor with deep level transient spectroscopy (DLTS). The capacitors consist of lead zirconate titanate [Pb(Zr, Ti)O_3 or PZT] sandwiched between rectifying and ohmic metal contacts. Electron beam deposition will be used to deposit several different metals onto the PZT to find a suitable ohmic contact as one has not yet been found. The significance of this project is to shed some light on an issue that if overcome, could integrate FeRAM even further into today's state of the art technology.

Introduction:

Dynamic random access memory (DRAM) is commonly used in most of today's computer technology. However, it is volatile, meaning that it must have access to a power source at all times, and any data stored upon it must constantly be refreshed in order to maintain it. As ferroelectric random access memory (FeRAM) is nonvolatile, it does not need constant access to a power source, giving it an advantage over DRAM in terms of power conservation.

Fatigue, which is one of the reliability issues encountered with FeRAM will be studied in the ferroelectric lead zirconate titanate [Pb(Zr, Ti)O_3] or PZT thin films in this work. Fatigue is defined as the loss of switchable polarization with repeated switching. The switchable polarization is derived from the electric field-driven movement within each unit cell of the body-centered cation either up or down relative to the oxygen anions. The polarization charge translates to a one or zero stored on a computer memory's capacitor, which is made of a ferroelectric material sandwiched between two metal electrodes.

The loss of switchable polarization could be due to impurities within the PZT that trap electronic charge, thereby changing the ferroelectric's internal electric fields. A deep level transient spectroscopy (DLTS) system will be used to identify carrier traps within the materials through quantification of trap energies and densities. To use the DLTS system, a Schottky contact and an ohmic contact, are needed as shown in Figure 1. Since an ohmic contact to PZT is not currently known, we have set out to find one.

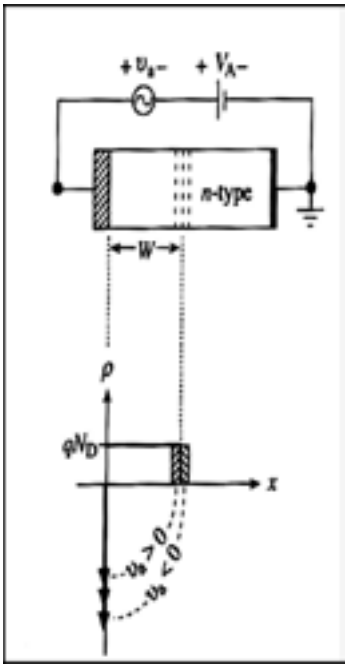

Figure 1: Schematic of metal-semiconductor-metal capacitor displaying both Schottky and ohmic contacts.

Experimental Procedure:

It was suggested in the literature that low work function metals would act as ohmic contacts [1, 2]. Therefore, aluminum, chromium, and zirconium were chosen for the bottom electrodes on the Si/Ir/PZT samples. Platinum was also deposited as a bottom electrode as a reference metal exhibiting Schottky behavior. Figure 2 shows the respective amounts of each material. The wafers were preannealed at 650ºC for thirty minutes in flowing nitrogen gas. 500 Å of each metal was deposited first at 25ºC through a shadow mask using electron beam deposition followed by 500 Å of iridium deposited at 300ºC to prevent oxidation of the underlying metal.

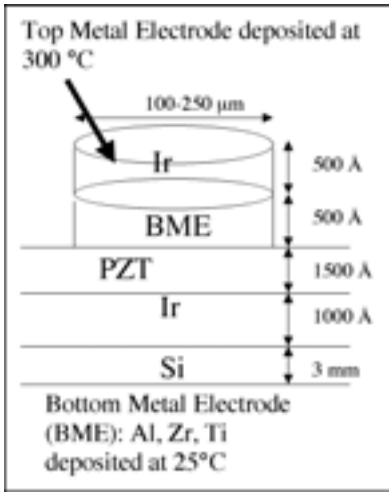

Figure 2: Structure of electrodes and PZT used in the experiment.

Next, to gain access to the buried iridium bottom electrode, a small section of the PZT was etched through using a mixture of hydrofluoric acid, hydrogen peroxide, and hydrochloric acid. Using a probe station, each electrode type was tested by performing current and voltage (I-V) measurements. We were looking for a linear relationship, which is indicative of an ohmic contact.

Results:

Figure 3 displays a plot of current density versus electric field of three electrodes from each sample. One can see that the platinum electrodes' results are all within the same order of magnitude, while the curves from the other top electrodes are not as reproducible. The samples with zirconium electrodes all shorted out which suggests that a chemical reaction occurred between the PZT, which is oxygen rich, and the metal electrodes, which are all highly reactive with oxygen, when the iridium was deposited at 300ºC. This might

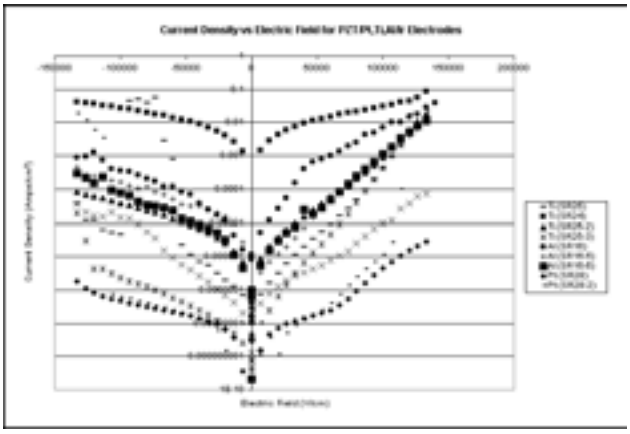

Figure 3: Chart displaying resulting J vs E curves from three different electrodes chosen from each sample.

result in variations of electrode electrical properties depending on the extent of the reaction and the stability of the electrodes. Regardless, none of the curves suggest the discovery of an ohmic contact, so further study of these materials is needed.

Future Work:

The next step in this project would be to make another set of samples, replacing the iridium capping layers with platinum because, unlike iridium, platinum displays excellent electrical and structural properties when deposited at room temperature. This reduces the chances of significant metal oxidation during the top electrode deposition process. Once an ohmic contact is found, then the DLTS system may be used to determine the energies and locations of the carrier traps. If the samples are not ohmic, more research will need to be done to determine the next step.

Acknowledgements:

I would like to thank Professor Paul McIntyre, Dr. Lawrence Schloss, Dr. David Taylor, Ms. Melanie-Claire Mallison, Dr. Michael Deal, Ms. Jane Edwards, and the McIntyre Group for all of their help and support. I would also like to acknowledge the National Nanofabrication Users Network, the National Science Foundation, and the Stanford Nanofabrication Facility for the use of their equipment.

References:

[1] Lee, J.J. and S.B. Desu, Ferroelectrics Letter Section, 20, 27(1995).

[2] Cann, D.P.; Maria J.-P. and Randall, C.A. Journal of Materials Sciences, 36, 4969(2001).

Optimizing Platinum Surfaces for Spin Magnetic Injection

Yu Zhao, Material Science and Engineering, Cornell University

Bruce Clemens, Material Science and Engineering, Stanford University

Scott Andrews, Material Science and Engineering, Stanford University

yz69@cornell.edu, clemens@soe.stanford.edu

Abstract:

Spin magnetic injection involves injecting electrons through one nano-scale ferromagnet of a fixed state to alter the state of another ferromagnet. Thus the state of the second magnet can be induced to become spin up or spin down. This mechanism can be used for high density information storage such as memory for a computer. A layer of platinum is used as the conducting lead for electron conduction in this design. Since the magnetic injection structures are on the nano-scale, the roughness of the platinum coat may cause undesirable variation in the induced magnetic field. The atomic force microscope (AFM) has been used to characterize the surface of sputtered platinum for roughness analysis. Neel's formula was used to approximate coupling energy which was too insignificant to affect spin injection.

Introduction:

Standard methods of magnetization involve placing an object in a magnetic field. It has been shown that on the nanometer scale charge density can become extremely high; magnetization direction can be changed by passing a current of a uniform spin through the material. The magnetic structure consists of two cobalt layers: a polarizing layer (15 nm) and a switching layer (2 nm) separated by a thick layer of copper as seen in Figure 1. The polarizing layer is given a uniform polarization direction. Since this layer is relatively thick, electrons of random spin directions will be polarized to one magnetization direction as they pass through. As these polarized electrons pass through the switching layer, the thin layer of cobalt will switch magnetization direction to conform to the direction of the polarized electrons.

Since the magnetic structure is on such a small scale, an electrical contact of a convenient size must be made to conduct a current. Platinum is used as a bottom conducting layer. However, the surface of the deposited platinum is not atomically smooth. In fact, the roughness of the platinum surface can cause roughness in the subsequent layers. Roughness in the magnetic layers can cause Neel's coupling also known as orange peel coupling. When magnetic layers are perfectly smooth, the magnetization of each layer is independent of the other layer and is completely in plane as in Figure 2a. In Figure 2b, the magnetization in two rough surfaces come in close contact and is no longer independent. To switch such a layer, extra energy would be needed and non-uniform magnetization may result as well.

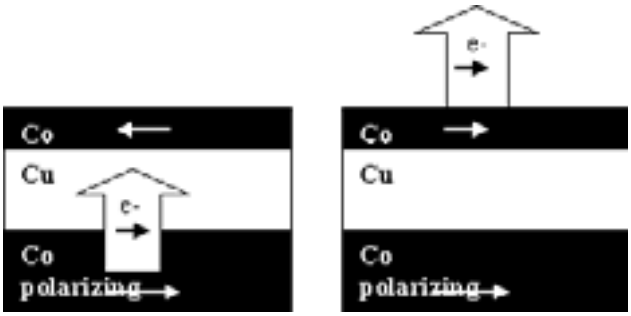

Figure 1: Magnetic structure. The polarizing layer and switching layer with polarized electrons.

Spin injection can be used for memory storage. For example, one direction of the switching layer is the "1" state and the other direction is the "0" state. Data can be written by selectively passing current through structures. In order to optimize the performance of spin injection devices, the roughness of the platinum layer must be reduced.

Methods:

Using UHV sputtering deposition, samples of varying platinum thickness and composition were produced. Sample A is the control template which had 10 nm Pt on 90 nm of Cu. Sample B had 2 nm Cr as a seed layer, 5 nm Cu, and 2 nm Pt from bottom up on

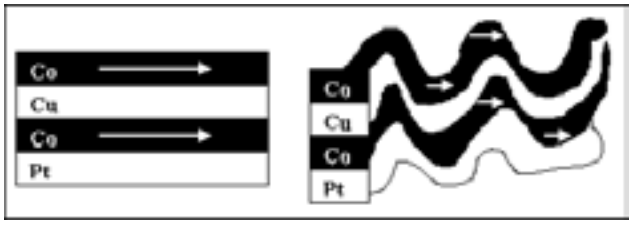

Figure 2: Neel's coupling. A schematic diagram of smooth and rough layers.

the control template. In sample C, the Cu layer was adjusted to 10 nm. In Sample D, the Cr layer was excluded from the structure.

AFM was used to characterize platinum surfaces. Scanning an area of 1 μm^2 using contact mode, several pictures were produced and analyzed.

Results and Discussion:

The rms roughness values for each sample were calculated using NanoScope software. The rms of the control template was 0.740 nm, and Sample B and C were close to 0.700 nm. However, Sample D, without the seed layer chromium, had an rms of 1.362 nm. Figure 3 shows AFMs of sample C and D.

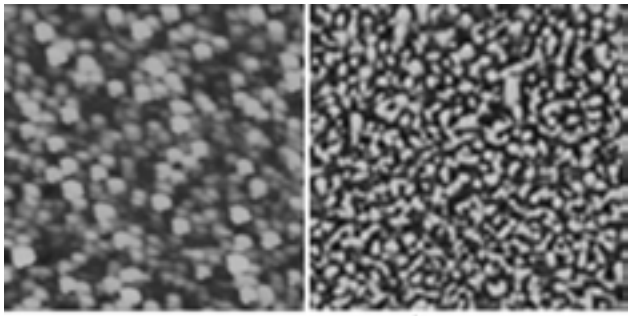

Figure 3: AFMs of sample C and D on a scale of 1 to 10 nm.

Neel's formula was used to approximate the coupling energy using the rms values as the amplitude and 50 nm as the wavelength of the surface modeled a sine curve. All rms values produced about 6.2 x 10^{-5} j/ m^2 of coupling energy. This number is on the order of one percent of the energy needed to form a domain wall in a ferromagnet. This energy from Neel's coupling should have minimal effect on switching of the cobalt layer.

Conclusions:

Clearly, the presence of a chromium seed has a significant effect on the roughness of platinum surface. For this reason, chromium was always used to ensure film smoothness in our devices. However, since the energy from Neel's coupling was not significant enough to affect spin injection, current film depositing techniques as sufficient for our devices. Also, as seen in samples B and C, varying the thickness of the interstitial layer of copper has no effect on the smoothness of the platinum surface.

Acknowledgements:

I would like to thank Professor Bruce Clemens and Professor Joachim Stöhr for their advice and encouragement, Scott Andrews for his guidance, and a team of amazing researchers: Yves Acremann, Venkatesh Chembrolu, Bill Schlotter, John Paul Strachan, and Gloria Wong. This project was funded by the National Science Foundation, National Nanofabrication Users Network, and Stanford Nanofabrication Facility.

References:

[1] L. Berger, Phys. Rev. B 54 (1996) 9353.
[2] J.C. Slonczewski, J. Magn. Mag. Mater. 159 (1996) L1.
[3] http://www-ssrl.slac.stanford.edu/stohr/spin.pdf

$$E = \frac{\pi^2}{\sqrt{2}} \frac{h^2}{\lambda} \frac{M_s M_s'}{\mu_0} e^{(-2\pi\sqrt{2}\, t/\lambda)}$$

Figure 4: Neel's Formula approximated coupling energy h = amplitude, π = wavelength, M_s = magnetic constant, t = thickness.

2003 NNUN REU Program at
Nanotech, Nanofabrication Facility at UCSB
University of California, Santa Barbara
http://www.nanotech.ucsb.edu/

UCSB/NNUN REU Intern ..... Major & School Affiliation ..... Principal Investigator

First Row:

Mr. Tony Lin ..... Mechanical Engineering, University of Texas Austin ..... Kimberly Turner
Ms. Kristina Schmit ..... Chemical Engineering, UC Santa Barbara ..... Gui Bazan
Mr. Lucas Fornace ..... Mechanical Engineering, UC San Diego ..... Vojislav Srdanov

Second Row:

Mr. Tristan Cossio ..... Electrical Engineering, University of Florida ..... Steve DenBaars
Mr. Rey Honrada ..... BioChemistry, Allan Hancock College ..... Ram Seshadri
Ms. Adele Tamboli ..... Physics, Harvey Mudd College ..... Frank Brown
Ms. Tiffany Coleman ..... Biology & Chemistry, University of Missouri at Kansas City ..... Samir Mitragotri
Ms. Liu-Yen Kramer ..... CNSI, University of California, Santa Barbara ..... NNUN REU Coordinator
Ms. Krista Ehrenclou ..... University of California, Santa Barbara ..... NNUN REU Coordinator

Third Row:

Mr. Matthew Jacob-Mitos ..... Elect. Engr. & App. Physics, Rensselaer Polytechnic Institute ..... Evelyn Hu
Mr. Eric Hoffmann ..... Physics & Mathematics, University of Puget Sound ..... James Allen
Mr. Michael Reichman ..... Chemical Engineering, University of Texas Austin ..... Eray Aydil
Dr. Brian Thibeault ..... ECE, University of California, Santa Barbara ..... NNUN REU Group Mentor

High Throughput Screening of Transdermal Chemical Penetration Enhancers

Tiffany Coleman, Biology, University of Missouri at Kansas City

Samir Mitragotri, Chemical Engineering, University of California, Santa Barbara

Pankaj Karande, Chemical Engineering, University of California, Santa Barbara

kcfootball@usa.com, pkarande@yahoo.com

Introduction:

It is well known that some chemicals cause the skin to become more permeable by upsetting the lipids in skin membranes. In the past, Franz Diffusion Cells (FDC) were used to find out more specific information about the permeability of the skin when exposed to a Chemical Penetration Enhancer (CPE). This process took three days and many man hours to complete. Using the patented High Throughput Screening (HTS) assembly (Figure 1), we can cut this time down to one day and decrease man hours by increasing overall yield from experiments. This allows us to form a database of information on the CPE without spending all the time FDC needs to conduct thorough experiments.

There are around 300 to 350 known CPEs at this time. All of those CPEs are known to increase permeability while adding a distinct amount of irritation to the skin. The hypothesis is that if you combine smaller percentages of one known CPE with another small percentage of a known CPE, the result will be more penetration and less irritation from the combination. Using HTS allows one to conduct between 400-800 experiments per day, therein creating a database of information about the combinations of CPE. This allows one to "screen out" the potentially good candidates from the rest of the bunch. When doing only four different combination percentages in solution, with eleven set ratios of CPE A and CPE B you would have more than five million experiments to conduct. This process of screening out the good candidates shortens the overall experiment time tremendously.

After a database of CPE combinations is completed the good candidates can be screened out and then used in FDC. This allows for industry standard results to be generated and a comparison of data can ensue. It is important that we have this data so that the overall goal of achieving simpler ways to get drugs into the body can be achieved. It is important to remember that taking medicine by the mouth is less effective than injection, but that injection is a painful process that many patients do not adhere to when at home.

We hope that the the information gathered using HTS will allow us to know which CPE are effective and then use them to help move large molecules, such as insulin, across the skin.

Project Summary:

This summer, twelve combinations were tested. Using 1:1 Ethanol:PBS as the base solution, CPEs were added to make 2% stock solutions (CPE A and CPE B). Each combination was created from zero to three milliliters (i.e. 300 microliters CPE A to 2.7 milliliters CPE B). The combinations were then added in percentage to the base solution from 0.5% to 2%. These combinations were then added to the porcine skin and checked for resistance using a multimeter, with a waveform generator set to 100 hertz and 143 milliamps. The skin was checked for resistance at zero hours and twenty-four hours.

After the experiments, the combinations were screened out. Enhancement ratio (ER) was determined

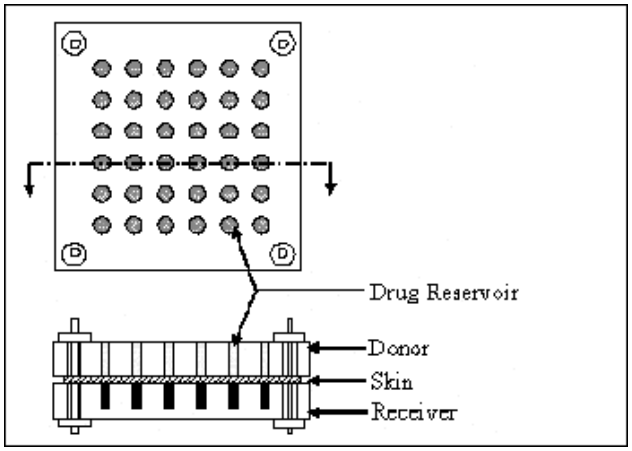

Figure 1: Patented high throughput screening assembly.

using ending resistance at twenty-four hours and dividing by starting resistance at zero hours. Standard deviations of ER greater than 70 and total enhancement ratios equal to or less than 3.0 were removed from the screening pool. A Tec Plot was then used to create color contour maps of the CPE in combination with each other. Figure 2 shows NLS-Cineole as a color contour map in greyscale. This allowed a visual representation of ER.

Of the twelve combinations used, NLS-Cineole was screened out as the best and will be used in FDC to get industry standard results. NLS-Cineole is not the best ever seen but only the best done over this short summer period. NLS-Cineole came out with an average ER of 45. ER of 45 is low compared to other combinations done previously which had an average ER of 65 or more.

Future Work:

It is important to remember that HTS is used to screen out potentially good candidates for FDC. Creating this database of CPEs in combination allows us to develop a theory on how CPEs affect the skin. Once this is known, more precise combinations can be created and we are hopeful we will reach the goal of enhancing permeability with little or no irritation to the skin.

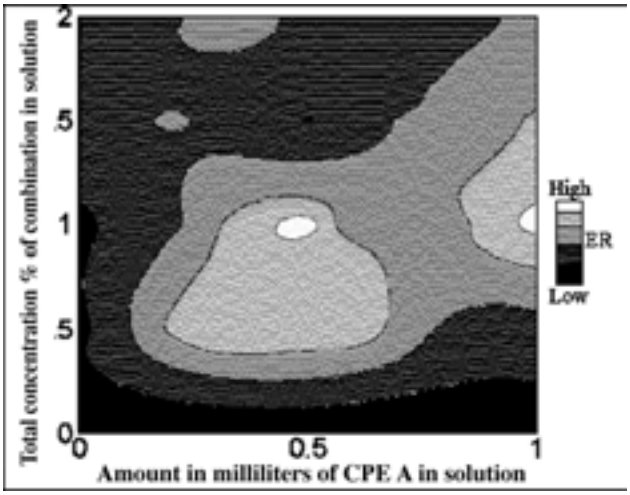

Figure 2: CPE A-NLS in combination with CPE B-Cineole.

Investigation of Heating's Effect on the Performance of Ultra-Violet Light-Emitting Diodes

Tristan Cossio, Electrical Engineering, University of Florida

Steve DenBaars, Materials Science; Electrical & Computer Engr, UC Santa Barbara

Tom Katona, Electrical and Computer Engineering, University of California, Santa Barbara

lordfunk@ufl.edu, denbaars@engineering.ucsb.edu

Abstract:

The purpose of this research was to investigate the effects of self-heating in the electrical performance of ultraviolet light emitting diodes (UV LEDs). Previous studies show that the relative external quantum efficiency of these devices decreased as the input DC current was increased. In this study, we investigated the extent that heating causes the reduction in quantum efficiency, by operating the device under DC compared to pulsed current injection. Light output vs. current input was used as the metric for comparison.

Introduction:

UV LEDs have applications in the detection of biological and chemical weapons, and in solid-state white lighting. Current crowding is a major concern with these devices because they have topside n-type and p-type contacts, requiring lateral current flow in addition to vertical current flow at the diode junction. Current crowding results in non-uniform current injection and artificially high current densities in areas adjacent to the n-contacts. This effect causes premature localized heating.

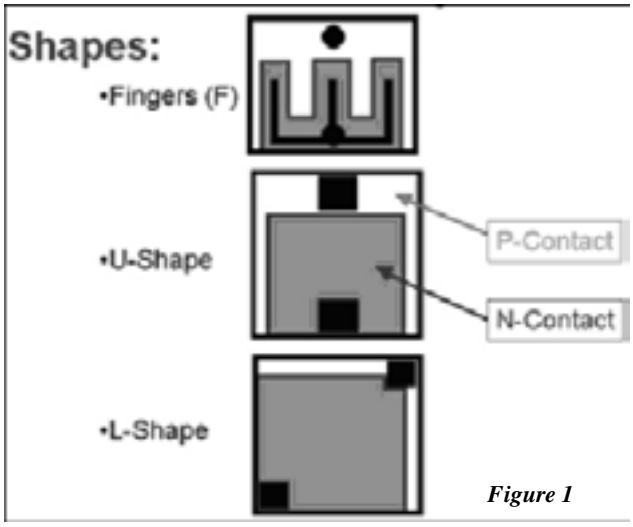

Figure 1

Gallium nitride LEDs with peak wavelengths of 340 nm were prepared using Metal Organic Chemical Vapor Deposition (MOCVD). Devices were processed with three distinct n-contact geometries as shown in Figure 1: interdigitated finger n-contacts, with the metal contact spread throughout the mesa like "fingers"; U-shape, with the n-contact surrounding three sides of the square geometry diode; and L-shape, with the n-contact on two sides of the device. Different geometry diodes were processed in order to investigate the effect of device geometry, and corresponding current crowding, on device heating.

Procedure:

To examine the effects of device self-heating on electrical performance, a pulsed testing setup was designed and Labview software was written to interface the equipment using a standard PC. A HP8114A pulse generator was used as the voltage source, a Hamamatsu 2281 broad area (100 mm^2) silicon photodetector located ~ 6 mm above the LED wafer was used for measuring output power, and a Hamamatsu C2719 photosensor amplifier was used to amplify the photodetector signal by 10^5. A HP54542C 500 MHz digital oscilloscope was used to monitor voltage across the LED, the input current into the LED, and the output voltage of the photosensor amplifier.

By knowing the responsivity of the photodetector at the peak wavelength of the LED, the Labview program converted the output voltage from the photosensor amplifier into the output power from the LED. We estimate that this technique captures 21% of the emitted light, assuming uniform emission at all angles.

Pulsed measurements were taken using a 10 Hz pulse with 1% duty cycle and compared to DC measurements.

Results:

Figure 2 shows DC measurements on a 500 μm by 500 μm UV LED. The output power of this particular L-shaped device was found to be 114 μW at 100 mA. As can be seen from Figure 2, the experimental light-current relationship was nonlinear. Initial testing of interdigitated finger shaped diodes showed a smaller differential between predicted and experimental behavior, as expected. This is possibly explained by the idea that heating has a smaller effect on performance due to decreased current crowding throughout the device.

The output power of a 300 μm by 300 μm UV LED under both DC and pulsed current injection is shown in Figure 3. Under DC current injection, the output power reached 114 μW at 100 mA. Relative external quantum efficiency decreased from 0.027% to .016% as DC current increased from 25 mA to 100 mA respectively. The pulsed testing results, shown in Figure 3, are almost identical to the DC measurements. The relative external quantum efficiency under pulsed conditions showed the same diminishing performance as under DC conditions, decreasing from 0.031% to 0.016% as input current increased from 25 mA to 100 mA respectively. The small difference between pulsed and DC performance observed thus far can be explained by a variety of factors.

One possible explanation is that the LEDs are heating too quickly. Because the pulsed data was taken using a relatively long pulse (pulse width of 1 ms), heating could be causing the same deterioration in performance in both tests. By decreasing the pulse width, we would expect device performance to improve and more closely resemble ideal behavior.

Another possibility is that at low currents, heating is not the main cause of decreased device performance. The ultraviolet LEDs could be saturating at much higher currents than those tested, so we would expect there to be a greater difference in pulsed performance and DC performance at higher currents. By testing the devices at a greater range of currents, we would be able to determine whether this is a factor. Further testing is needed to verify these effects.

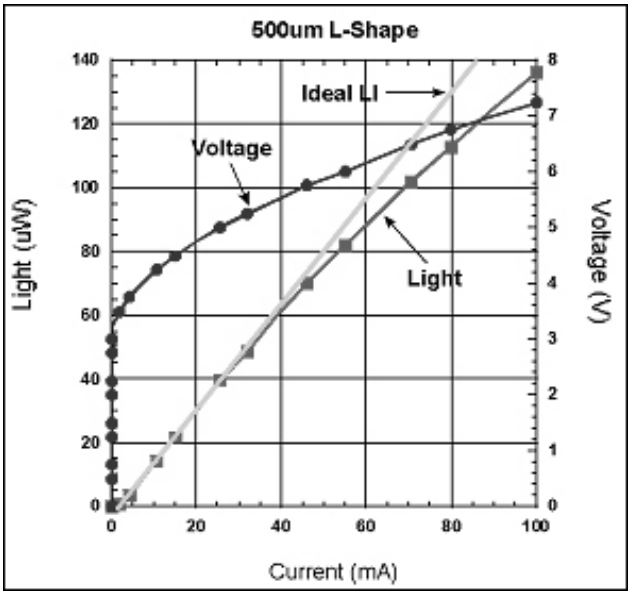

Figure 2: DC measurements made on a 500 μm² UV LED.

Conclusions:

We investigated the effects of self-heating on UV LEDs by comparing pulsed and DC light vs. current measurements. DC and pulsed measurements showed little difference for 10 Hz pulse frequency with a 1% duty cycle. This is likely due to the relatively long pulse width, 1 ms, or low current operation, < 100 mA. DC measurements yielded 114 μW of output power at 100 mA injection current for a relative external quantum efficiency of 0.016%.

Acknowledgements:

The authors wish to thank Morgan Pattison, Tal Margalith, the MOCVD group, and Dan Cohen for all their technical assistance. The authors also wish to express gratitude to NNUN and John Carrano for funding support.

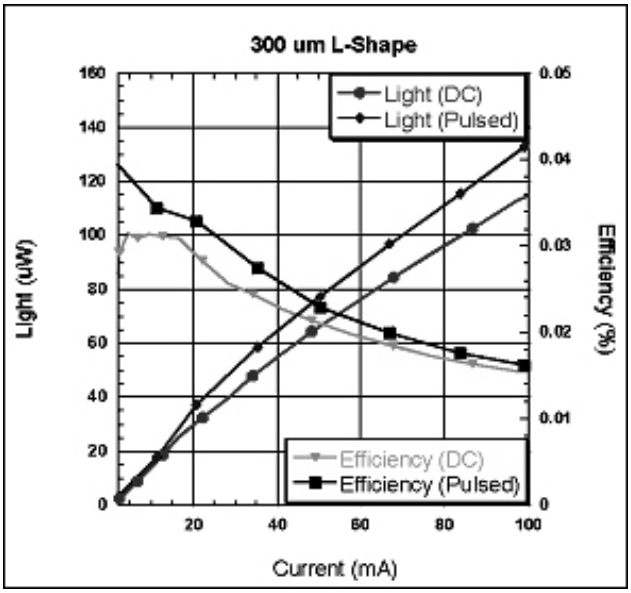

Figure 3: Output power of a 300 μm² UV LED under both DC and pulsed current injection.

Organic Light Emitting Devices by Molecular Beam Epitaxy

Lucas Fornace, Mechanical Engineering, University of California San Diego

Dr. Vojislav Srdanov, Institute for Polymers and Organic Solids, UC Santa Barbara

lfornace@hotmail.com, srdanov@chem.ucsb.edu

Abstract:

The dream of using organic materials in high performance optoelectronic devices is rapidly becoming a reality, including organic light emitting devices (OLEDs). Such organic devices have reached performance levels comparable to, or in some cases, even better than their inorganic counterparts. There is still much room for improvement; namely in further understanding the energy transfer phenomena that can occur between two molecules. It is the goal of our research to understand these processes and contribute our findings to science such that the end result is an improvement in the efficiency of OLEDs.

Introduction:

My project focused on the growth of mixed organic thin films consisting of two molecules that form an energy-transfer donor-acceptor pair. Our goal was to see the influence of molecule stoichiometry on the energy transfer processes via photoluminescence (PL) and electroluminescence (EL). A recently developed method in our laboratory (patent pending) allows for a continuous change of thin film stoichiometry along a rectangular substrate, starting from nearly pure compound A at one end and finishing with nearly pure compound B at the other. In this way, one saves a great deal of time as compared to producing many individual samples to cover the entire range of possible stoichiometries. From correlated absorption and the PL measurements at different points of the film, we were able to determine the best molecular ratio for optimal energy transfer. We then set out to determine if the same stoichiometry would result in optimal OLED operation. This required that we design and fabricate working and reproducible devices.

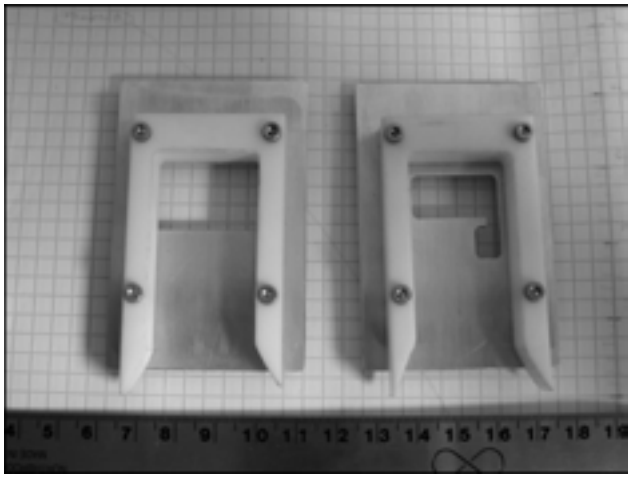

Figure 1: Masks used for the fabrication of simple OLEDs.

Figure 2: Digital photograph of a photo-excited CBP/Ir(PIN)$_3$ thin film.

Procedure:

To this end we put together a high-vacuum chamber for thermal evaporation of organic compounds, which was optically coupled to a remote diode-array spectrophotometer. This allowed for acquisition of absorption spectra during thin film deposition and thus provided immediate feedback regarding the film thickness. Thickness is directly related to absorbance as represented by Beer's Law: A = kd, where A is absorbance, d is thickness, and k is a factor related to materials light-absorption ability (i.e. the absorption coefficient). Research was conducted last summer at UCSB to accurately determine these coefficients for the individual materials that would be used in our OLED fabrication.

The co-deposited thin films of donor-acceptor mixture were excited by an Hg lamp resulting in a bright luminescence which we captured with a digital

camera. The PL measurements were then made using an argon-ion laser to excite the donor molecule, which transfers its energy to the acceptor—the latter of which emits a green photon resulting in the PL spectrum that was measured by a spectrometer.

Typical OLED geometry consists of a transparent, yet conductive, indium-tin-oxide (ITO) substrate on which we deposit the mixed organic layer, sandwiched between a hole-transport and an electron-transport layer. On top of this, we deposit an aluminum thin film that serves as the cathode. For these controlled depositions, we had to make a series of shadow masks designed for either 1" x 1" or 1" x 3" OLEDs, the former of which would be used solely to test the basic performance of our devices. These masks can be seen in Figure 1 along with their Teflon docking bays which locate the substrate.

For the longer substrate type, masks were developed so that there are numerous small OLEDs effectively produced along the substrate length. Utilizing these masks in conjunction with our variable stoichiometry technique for the emissive layer, we have created a device that tests the aforementioned energy transfer processes by means of electroluminescence.

Results:

For this project, we decided to study energy transfer from 4, 4' - N, N'-dicarbazol-biphenyl (CBP) to an Iridium organometalic complex ($Ir(PIN)_3$). A digital photograph of the mixed CBP/$Ir(PIN)_3$ thin film in Figure 2 reveals an efficient energy transfer between the photo-excited CBP donor (blue emitter) to the $Ir(PIN)_3$ acceptor (green emitter). At the $Ir(PIN)_3$ end, the luminescence is weak because of the concentration quenching effects. As $Ir(PIN)_3$ molecules become diluted in CBP, the luminescence intensity increases to a maximum at 10% of $Ir(PIN)_3$ in CBP (denoted by the arrow). The actual spectrum at this point is shown in Figure 3. When the $Ir(PIN)_3$ concentration drops below 2%, the energy transfer is no longer complete so some of the CBP luminescence becomes visible.

The basic 1" x 1" OLEDs were first constructed using a fixed CBP/$Ir(PIN)_3$ stoichiometry. There we encountered shorting problems which we later attributed to ITO of dubious quality. The problem was eliminated with the arrival of new ITO substrates but the remaining time was insufficient to build working 1" x 3" devices of varying stoichiometry.

Conclusion:

We demonstrated that the new method for producing thin films with varying stoichiometry allows for an efficient way of studying energy transfer processes. The correlated of absorption and PL measurements of a single CBP/$Ir(PIN)_3$ thin film revealed immediately the optimum stoichiometry (10:1) for the most efficient energy transfer. The electroluminescence measurements of such films are in progress.

Acknowledgments:

I would like to thank my advisor Dr. Vojislav Srdanov for his expertise and friendship, as well as Dr. Edin Suljovrujic, Aleksandar Ignjatovic, and Kevin Herlihy for their much appreciated help in the laboratory. I must also thank Liu-Yen Kramer, Krista Ehrenclou, Claudia Guitierrez, and everyone else at the UCSB campus that made this summer go smoothly. At Cornell I must thank Melanie-Claire Mallison and others who contributed their time to the NNUN REU program, as well as the National Science Foundation for providing the funding that makes these programs possible. Finally I will thank all of the interns—especially the UCSB team—for their summer friendship and for honing my Frisbee skills.

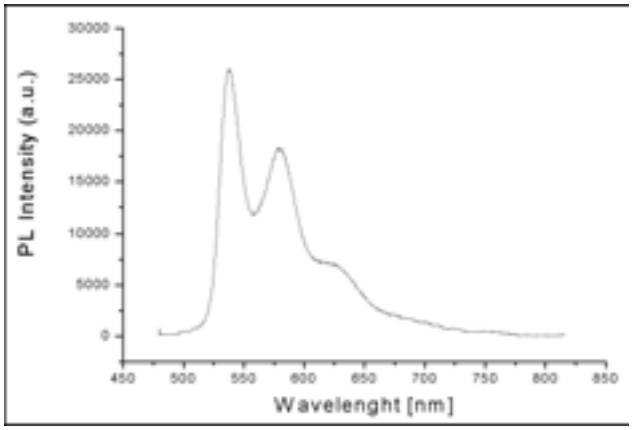

Figure 3: PL Spectra of a mixed CBP/$Ir(PIN)_3$ film at the best stoichiometry.

Terahertz Circular Dichroism Spectroscopy

Eric Hoffmann, Physics and Mathematics, University of Puget Sound

S. James Allen, Physics, University of California, Santa Barbara

Jing Xu, Physics, University of California, Santa Barbara

ehoffmann@ups.edu, allen@qi.ucsb.edu

Abstract:

Biological molecules are composed of chiral polymers of amino acids or nucleic acids that absorb right circularly polarized light differently than its left-handed counterpart. This differential absorption is commonly called circular dichroism (CD). CD in the visible and infrared frequencies has already been investigated. In fact, optical CD is used to study real-time conformational changes of polymers undergoing environmental and structural perturbations.

CD in the terahertz range has not been explored, and may provide a different set of information on biological molecules. Creating perfect circularly polarized light in the terahertz range is one challenge of terahertz CD spectroscopy. This research involves creating circularly polarized light by interfacing a computer to a stepper-motor-coupled translation stage that automates the phase shifter of an interferometer. Hence allowing reliable automated positioning of the interferometer's translation mirror in conjunction with automated CD measurements.

Introduction:

Objects that are chiral on the molecular level are unequally sensitive to circularly polarized light. That is, depending on the handedness of the object, it will absorb more right circularly polarized light than left circularly polarized light or vice versa. This difference in absorbance identifies chiral objects. Chiral objects are three-dimensional with no mirror plane of symmetry; therefore, these objects look different to incident light traveling in opposite directions. So oppositely handed circularly polarized light interacts differently with the dis-symmetric material. Any generic difference in absorbance is called differential absorption. Because circularly polarized light is being absorbed in this situation, we call the process circular dichroism (CD).

Optical CD is well understood and developed. But terahertz CD has never been researched before. Optical light ranges from 400-700 nm, while the terahertz-frequency source at UCSB ranges from 60 μm-1 mm. Optical light induces electronic transitions in biological macromolecules (molecules with more than 500 atoms), but terahertz light induces global vibrations in macromolecules because of its long wavelength. Therefore, terahertz CD allows us to analyze the fundamental global structure of macromolecules. Differential absorption is frequency-dependent, creating spectrums unique to specific structures (Figure 1). So terahertz CD spectrums could potentially be used to detect biological life, fingerprint biomolecules, and study biological processes in real-time.

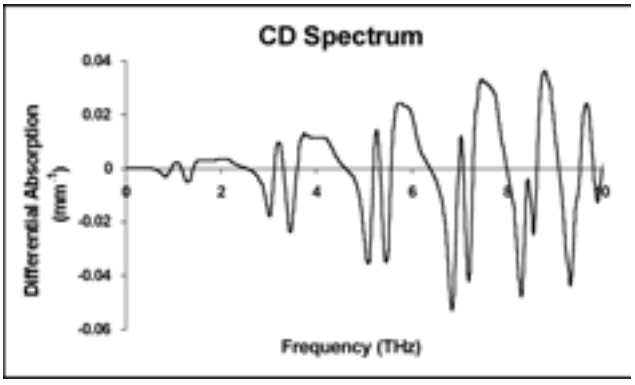

Figure 1: A theoretical CD spectrum for the protein bacteriorhodopsin.

Making an apparatus to alternate between perfect right and left circularly polarized light in the terahertz range is challenging. In addition, the apparatus must be able to operate over a range of frequencies in order to produce CD spectrums. The best approach to this problem is an interferometer. Interfering two equal-amplitude orthogonally polarized beams of light constructs a single beam with a unique polarization. The difference in phase between the two original beams

dictates the polarization of the constructed beam. If the original beams are 90° or -90° out of phase, the resulting beam is left or right circularly polarized, respectfully. The goal of the research project has been to interface a computer with a stepper motor to automate the position of the interferometer's translation mirror in order to control the phase difference.

Procedure:

Computerized control of the motor was achieved using Hewlett-Packard Visual Engineering Environment (HP VEE) version 5.01, the same program used for automated data acquisition. The program was designed to communicate with a Stanford Research System Model SR830 DSP Lock-In Amplifier via a GPIB connection. The Lock-In provided the necessary Transistor-Transistor Logic (TTL) pulse to the stepper motor driver. An Applied Motion Products PDO 5580 stepper motor driver was used to power an Applied Motion Products Model 5023-122 stepper motor. The stepper motor was coupled to the dial of a Newport AD-100 Electrostrictive Actuator used to move the translation mirror of the interferometer. Because the actuator dial travels horizontally when turned, the motor was mounted to a Newport Model 462 stage so the motor could travel with the mirror. This setup also had the tendency to damp vibrations created by the motor.

Positioning the mirror when using small wavelength light, wavelengths less than 200 μm, is done entirely with the Newport AD-100 Electrostrictive Actuator. At larger wavelengths, the stepper motor and the electrostrictive actuator work together to position the mirror. The stepper motor moves the mirror the majority of the distance with coarse precision, and then the electrostrictive actuator positions the mirror with the precision of about one micron.

Results and Conclusions:

To test the performance of the automated interferometer, several scans were made over the same interval to produce a single-period interference pattern.

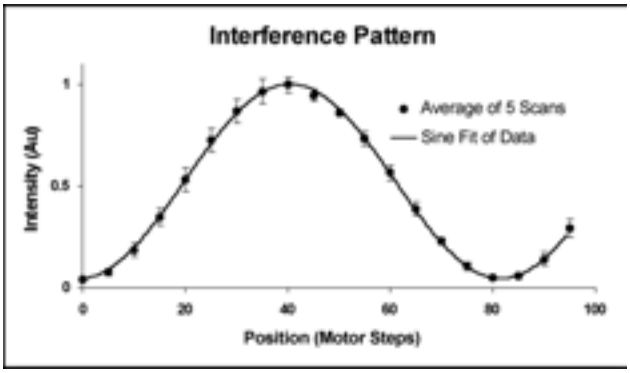

Figure 2: An experimental interference pattern and a sine fit of the data.

The data from each scan was averaged, and a sine wave was fit to this average (Figure 2). The standard deviation was used to place error bars on each data point. The sinusoid fits the interference pattern well, with a correlation coefficient of 99.8%. This proves the motor is moving the mirror linearly and the interferometer is producing strong constructive and destructive interference. The repeatability of the interference patterns proves that the stepper motor reliably positions the translation mirror. The inflection points of the interference pattern indicate the location to place the mirror to create left and right circularly polarized light. Future work involves implementing software to move back and forth between these inflection points to create left circularly polarized light then right circularly polarized light one after another.

Acknowledgments:

I would like to thank my Professor James Allen, Professor Pavlos Savvidis, Dr. Kevin Plaxco, and David Enyeart for their encouragement and advice. I would like to thank especially my mentor Jing Xu who has given me wisdom and support. I appreciate the coordinators who have made this internship possible: Ms. Melanie-Claire Mallison, Liu-Yen Kramer, Krista Ehrenclou, and Claudia Gutierrez. And thanks to all the boys and girls at camp Cachuma for a great summer.

Microwave Assisted Synthesis of Magnetic Oxide Nanoparticles

Rey Honrada, Biochemistry, Allan Hancock Community College
Ram Seshadri, Materials Research, University of California, Santa Barbara
Aditi Risbud, Materials Research, University of California, Santa Barbara
vagrantminded@yahoo.com, seshadri@mrl.ucsb.edu

Introduction:

The general research of magnetic oxide nanoparticles is not a new area. Magnetic oxide nanoparticles are naturally occurring crystals. According to Blakemore [1], certain bacteria found in swamps and marshes produce 100 nm crystals. Blakemore found that these magnetic particles aligned themselves in a chain creating a working compass [1]. There are a number of recorded studies concerning these nanoparticles. Due to the recent availability of fine-tuned scanning technologies, such as x-ray diffraction, neutron diffraction, and transmission electron microscopy, magnetic oxide nanoparticles can now be accurately studied. This is very exciting due to the fact that new applications for quality magnetic oxide nanoparticles are just now being found.

Magnetic oxide nanoparticles can be used within the medical, automotive, and computer media industries. Alongside a variety of applications comes a demand for the large-scale synthesis of these nanoparticles. The aim of this particular research is to answer this demand with a process that not only produces magnetic oxide nanoparticles in bulk, but also decreases material expenses and production time. The key to achieving this goal is in the use of low cost materials and placing great emphasis on the process of digestion.

The digestion of crystalline materials is a recent technique. During digestion, ions in poorly formed crystals become agitated and vibrate from the absorption of heat energy via an external source (i.e. hot-air oven). This results in ions being redistributed among crystals to achieve monodispersed particles. The traditional method of digestion involves hours of heating and stirring a solution on a hot plate [1].

This research proposes the replacement of the hot plate with a microwave as a means of digestion. To determine whether this is feasible, various metal oxide combinations and microwave digestion times were explored. In the final product, we concentrated on obtaining the proper crystalline structure: the spinel crystalline structure to be exact. It's important to understand that the spinel structure has a cubic unit cell which repeats infinitely in 3-dimensions [2]. This fact makes way for the use of x-ray diffraction to analyze all final samples for the desired nanoparticle spinel structure.

Procedure:

Three particular metal oxides were explored. These metal oxides were $ZnFe_2O_4$, $NiFe_2O_4$, and $CoFe_2O_4$. The following outlines the preparation and analysis of $ZnFe_2O_4$. This procedure can be applied to the other metal oxides with only the first metal being changed.

First, the number of grams for a 0.2M 100mL aqueous solution of zinc chloride and a 0.4M 100mL aqueous solution of iron chloride were calculated. Both solutions were combined into one beaker. Using deionized water as the solvent allowed the cost of production to be minimized. The grams needed for a 3M 100mL aqueous solution of NaOH were calculated and dissolved into a separate beaker.

A pH meter monitored the pH level as NaOH was slowly introduced into the beaker containing the zinc and iron chloride solutions. As the NaOH was added, precipitation was immediately visible. NaOH was constantly stirred in until a pH level of 12 was reached. A colloidal dispersion with a varied brown color (depending on which metals are used) was created. The liquid precipitate was then brought to a reaction temperature of 70°C and stirred for exactly one hour. The reaction was then halted and the precipitate cooled to room temperature. To isolate the precipitate from supernatant liquid, the beaker contents were separated into two centrifuge tubes. These were centrifuged for ten minutes at 3000 rpm. The supernatant liquid was

decanted, then centrifuged again until only a thick brown precipitate remained.

This remaining precipitate was then divided into three separate samples. The first sample was microwave digested for two minutes, the second sample for three minutes, and the third sample for ten minutes. The final product, post-microwave digestion, can be described as a dried black substance resembling fine gravel. The acquired substance is then ground into a fine powder. The $ZnFe_2O_4$ powder was then checked for magnetism by observing its reaction, or non-reaction, when placed next to a strong magnetic field.

Lastly, a Scintag 2 x-ray diffractometer is used to detect the underlying lattice structure. X-ray plots acquired from our samples were compared with that of a standard $ZnFe_2O_4$ in hopes of a near-perfect match.

Results and Conclusions:

Without the use of microwave digestion, dried samples exhibited no magnetic behavior. With the use of microwave digestion, the $ZnFe_2O_4$ exhibited magnetic behavior for two, three, and ten minute microwave digestion times.

The lattice-plane spacings for the microwave digested $ZnFe_2O_4$ created desirable constructive x-ray interference. On the x-ray diffraction plot, constructive interference is represented by a peak along the x-axis as seen in Figure 1. The presence of the spinel structure was indicated by these peaks. Combined with magnetic properties found in all three samples, the microwave digested $ZnFe_2O_4$ was a success.

Conversely, $NiFe_2O_4$ was proven to be a difficult combination. Even with more traditional synthesis methods, $NiFe_2O_4$ was difficult to stabilize due to nickel exhibiting a strong initial stability by itself. Nickel is reluctant to react and chemically combine with other elements. The $NiFe_2O_4$ exhibited a weak response to a strong magnetic field. The x-ray diffraction plots for all three $NiFe_2O_4$ samples were rather disappointing. We did not obtain an x-ray diffraction pattern showing a desirable spinel structure from any of the three samples.

The final metal oxide, $CoFe_2O_4$, was just as successful as the $ZnFe_2O_4$. $CoFe_2O_4$ showed a strong response to magnetism, even more so than $ZnFe_2O_4$. The x-ray diffraction patterns for $CoFe_2O_4$ showed the presence of the spinel structure. With $ZnFe_2O_4$ and $CoFe_2O_4$ yielding desirable test results, research can continue with these materials.

Next steps include analyzing the particle sizes, examining the magnetic properties in a quantitative manner, and introducing a surfactant into the solution as a capping agent. The introduction of a surfactant will allow for more control over size during particle formation. To check for the proper nanoparticle size, around 4 to 10 nm, transmission electron microscopy will be used. To analyze magnetism as a function of temperature, a superconducting quantum interference device (SQUID) magnetometer will be used.

References:

[1] R. Seshadri, Oxide Nanoparticles, edited by C.N.R. Rao, et al., Weley-VCH, Weinheim, Germany (to be published).

[2] H. Bennet, Concise Chemical & Technical Dictionary, Chemical Publishing Company, Inc. (c) 1986.

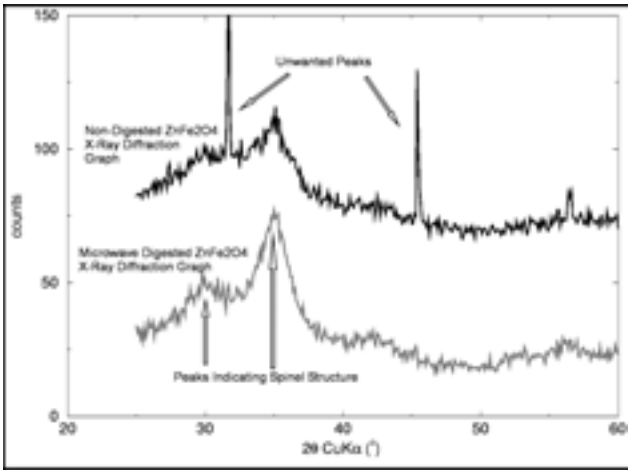

Figure 1: X-ray diffraction plot. Constructive interference is represented by a peak along the x-axis.

Atomic Force Microscope Lithography

Matthew Jacob-Mitos, Electrical Engineering & Applied Physics, Rensselaer Polytechnic Institute

Evelyn Hu, Electrical and Computer Engineering, University of California, Santa Barbara

Brian Thibeault, Electrical and Computer Engineering, University of California, Santa Barbara

jacobm2@rpi.edu, hu@ece.ucsb.edu, thibeault@ece.ucsb.edu

Abstract:

Researchers in science and engineering are now requiring sub-100 nm features which conventional optical lithography techniques cannot easily produce. In this paper, we attempt to develop a process to consistently reproduce these nanoscale features through lithography with an atomic-force microscope (AFM). AFM-based lithography uses electrically conductive tips to form a strong electric field which assists in hydroxide ion diffusion into the sample material. Due to the small size of the AFM tips, this results in nanoscale-sized features which can be used to transfer patterns directly into the material of interest.

This research explores the various parameters involved in oxidizing silicon surfaces as well as other materials, such as metals or GaAs. These parameters include tip bias, room humidity, tip height from surface, surface preparation and scan rate across the surface by the tip. We have found that all of these play equally important roles in the oxidation process on silicon.

By using a tip bias of -8 volts, < 40% humidity and a scanning rate of 6 µm/sec, we were able to produce oxide features 2 nm high and < 30 nm wide. These oxides withstood KOH wet etching and Reactive Ion Etching, resulting in efficient pattern transfer to silicon.

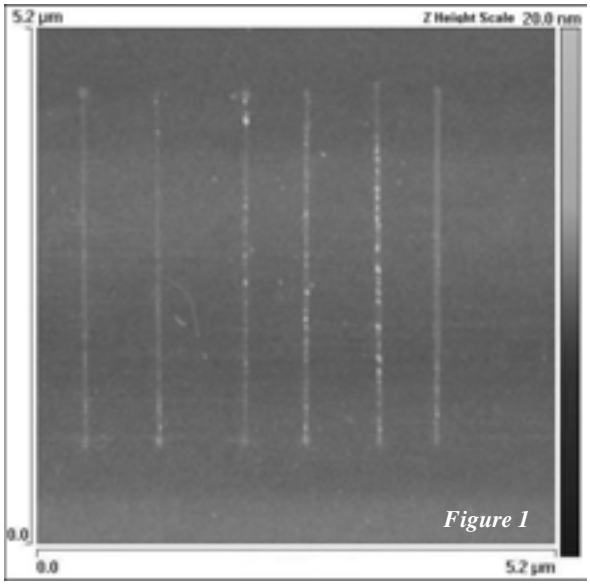

Figure 1

Introduction:

Current commercial lithography techniques involve the use of a light source or electron beam source to expose a desired pattern onto a material, usually photoresist. Optical lithography has limits on the ultimate minimum size which can be transferred due to diffraction limits. Electron beam lithography boasts higher resolution than optical techniques, however it significantly more expensive and time consuming. This provides the motivation to explore alternate lithography techniques, such as AFM lithography.

Our pattern was created through the formation of oxide on the surface of a silicon substrate. Silicon forms a natural oxide which is very stable and there are various etching techniques known for silicon and silicon-dioxide, allowing us to use the oxide as a mask for subsequent processing steps.

The oxidation process is a fairly simple. Due to the extremely small distance between the AFM tip and the surface being studied, a voltage applied to the tip on the order of -10 volts will result in an electric field which is approximately 10^9 V/m and is highly concentrated between the tip and the surface. This electric field will then ionize water molecules in the

Figure 2

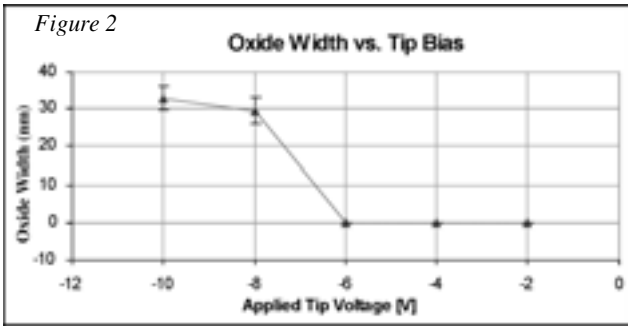

water meniscus around the tip, leaving hydroxide ions behind. These negatively charged ions will then diffuse into the surface with the help of the high electric field. The diffused ions react with the silicon atoms to form silicon-dioxide (SiO_2) which extends into and out of the surface. Due to the small size of the tip (10 nm diameter at the point), the oxide that results is confined to a very small area allowing the formation of nanoscale sized features.

Procedure:

AFM lithography results in the formation of extremely small features. For this reason it is important to begin with a clean surface to oxidize. Samples were new, prime grade substrates, cleaned in successive treatments of acetone, methanol and isopropyl alcohol, and dried under a nitrogen flux. Samples were stored in an evacuated chamber or in a cleanroom environment. This helped prevent particles from dirtying the surface, which would reduce the effectiveness of the oxidation process.

Following proper surface preparation, the sample was loaded into the AFM and normal AFM scanning engaged. Since the concentration of this project was on studying the effect of the parameters, we made a series of lines so that clear relationships could be extracted. An example of these lines is shown in the topographical image in Figure 1.

The software used allowed for easy manipulation of the parameters and the path for the tip to follow. Lines for the tip to follow were simply drawn on the screen over the previously scanned area. For each series of lines, all but one parameter was held constant. Each line was a successive variation of a single parameter. This allowed us to drawn relationships from the line width and height data.

Results and Conclusions:

The three parameters we primarily studied were; tip bias, tip height reduction and scan rate.

The tip bias was varied from -2 volts to -10 volts (lower values were not supported by our equipment). Figure 2 shows a plot of the average line width as a function of tip voltage. This shows that the oxidation process has a threshold voltage of -6 V. At values greater than -6 volts, no oxide was formed. The error bars are the standard deviation of the line width measurements, taken at various points along the line, and give an idea of how consistent the line widths are.

The tip height reduction study was a variation of the distance to which the tip was lowered from its imaging setpoint. In this experiment, we found that there was an ideal range for oxidation. For values less than this range, we found that no oxide would form on the surface. For values greater than the range, we found that the lines would consist of a number of blobs separated by a gap. This type of line had a very poor quality and would result in poor features after etching. This data is shown in Figure 3.

The scan rate variation study showed that as scan rates increased, the amount of oxide which formed would drop. However, for our experiments, it appeared that the range of values was not large enough to sufficiently show this trend (Figure 4).

The last main parameter was humidity of the ambient air. It proved to be very difficult to study this parameter as a change in humidity resulted in a change in setpoint values for imaging and tip height reduction values. Therefore all experiments were performed at a constant 37% humidity.

Acknowledgments:

I would like to thank Evelyn Hu, Brian Thibeault and Bill Mitchell for their help in this research project, and the NSF and NNUN.

References;

[1] J. Vac. Sci. Technol. B 20(3), May/June 2002.

[2] APL 71(2), 14 July 1997.

Figure 3

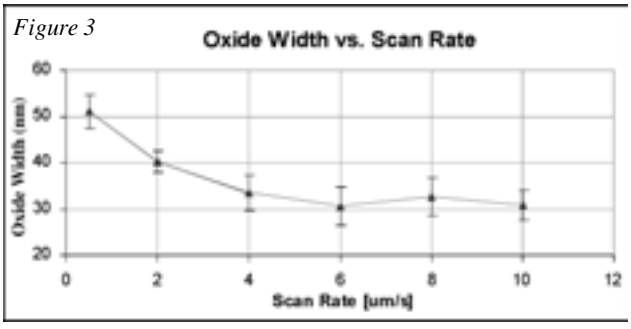

Figure 4

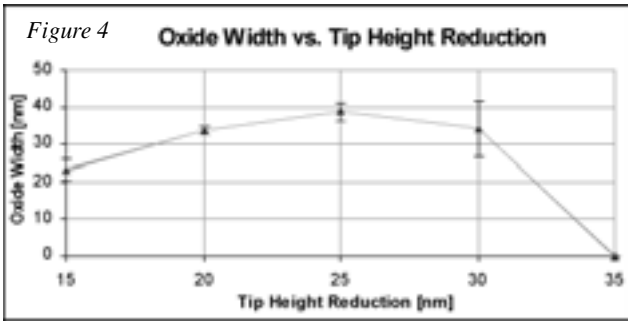

Characterization of the Mechanical Properties of Micro-Electro-Mechanical System (MEMS) Oscillators

Tony Lin, Mechanical Engineering, The University of Texas at Austin

Kimberly Turner, Mechanical and Environmental Engineering, UC, Santa Barbara

Wenhua Zhang, Mechanical and Environmental Engineering, UC, Santa Barbara

lin82@mail.utexas.edu, turner@engineering.ucsb.edu

Abstract:

MEMS oscillators, if used as ultra sensitive mass sensors, can provide a far more precise and compact method of mass detection than present-day mass sensors. With purported sensitivity of mass detection down to 10-12 grams, the potential to surpass today's most precise mass sensors can already be seen. Before MEMS sensors can be applied in real world applications such as biological and chemical sensing, issues of controllable dynamic and static response, sensitivity, reliability, and quality must be addressed.

The focus of this project is to characterize the mechanical properties of our MEMS devices including frequency response, spring constants, sensitivity of mass detection and motion behavior. Testing of these properties was carried out using computer generated 3-D models, a motion characterization setup, and a nanoindenter capable of physically pushing on the device to determine spring constants.

Introduction:

In the broadest sense, our research was to understand the mechanical properties of microscale silicon devices and the effects of fabrication on them. Specifically, our devices are MEMS oscillators with a future potential to be used as chemical or biological sensors. Most importantly, they possess higher sensitivity, smaller packaging and higher quality factors. The key to their use as sensors is their resonance behavior, illustrated in Figure 1. The property of resonance is the mechanical property that our research centered on. By using computer generated 3-D models and running tests on actual devices, we studied the relationships between resonance frequencies, spring constants and mass changes.

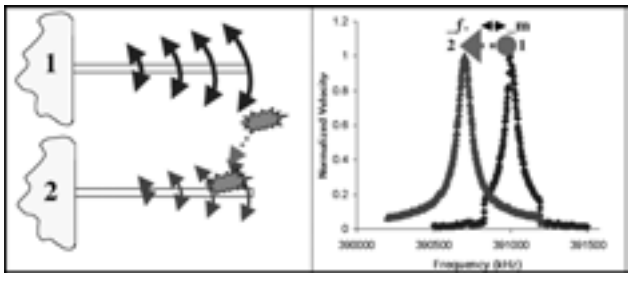

Figure 1: Illustration of resonance frequency shift resulting from a mass change.

Device:

Using two different design models, five working devices were fabricated and tested. The devices are electrostatically-driven single crystal silicon oscillators fixed at four points and otherwise freestanding. They were fabricated using a SCREAM technique allowing us to selectively release certain portions of our device while keeping others fixed. Covering an area of approximately 200 μm^2, the general layout of our design is that of two fixed-fixed beams spanned by a relatively rigid backbone. The electrostatic forces are applied to the teeth of the backbone causing 1st mode in-plane movement. The spring constant of the device is controlled by the properties of the fixed-fixed beams and most of the mass is contained in the backbone. Figure 2 is an SEM image of one of the devices.

Testing:

Using ANSYS software and finite element analysis, 3-D computer models of our MEMS oscillators were

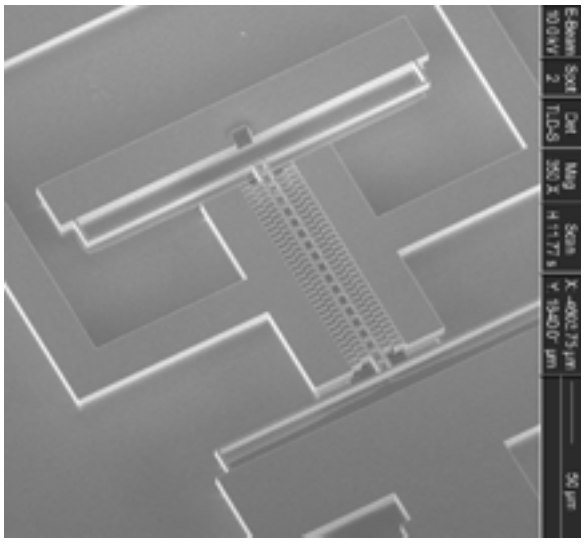

Figure 2: SEM image of Device 1. Image by Wenhua Zhang.

developed. Initially, model dimensions were based on the exact values of the mask design, and the Young's Modulus of the device material was assumed to be that of pure single crystal silicon. Eventually, dimensions and properties of our model were changed to more closely resemble the device after fabrication.

Using the laser vibrometer setup to measure real-time dynamic frequency response, we were able to find the frequency of greatest response, the resonance frequency. A schematic diagram of the setup is shown in Figure 3.

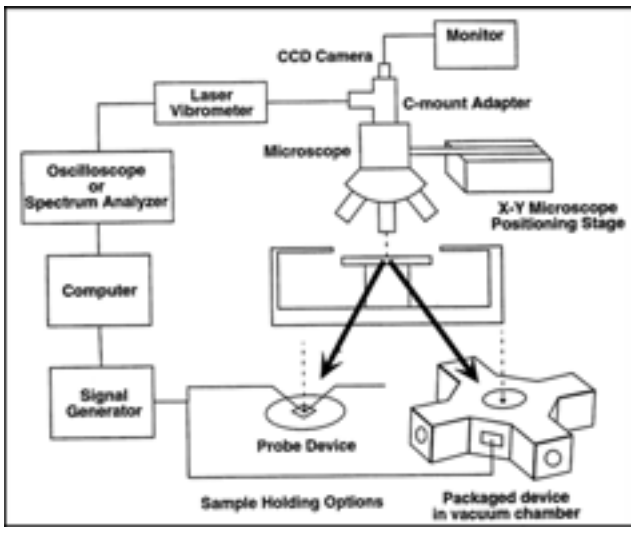

Figure 3: Schematic diagram of the laser vibrometer setup.

A Hysitron Triboindenter was used to test the static properties of our oscillators. A 5 μm tip was put into contact with the backbone of our oscillator and the force applied with nN accuracy. The resulting displacement was then measured with sub-nm accuracy, enabling us to determine the out-of-plane spring constant of our device.

The sensitivity of our devices was tested by removing different amounts of material from the backbone using a focused ion beam. The small amount removed was assumed to have little to no affect on the stiffness of the backbone while giving a measurable mass change.

Results and Conclusions:

Resonance frequency testing on the laser vibrometer setup produced very consistent results varying less than 0.1% between test runs (Figure 4) and showed high quality factors in the range of 8000 for our devices. While the actual resonance frequencies of the ANSYS model and the vibrometer testing did not match up very well, the shift in values from one model to the other was consistent between the two methods. This leads us to believe that ANSYS can be used to accurately model our microscale devices. With known issues of accurately defined material properties and device geometries, different sets of parameters are being tested to more accurately model the real life device.

The results of the spring constant testing have not been as consistent as we would have hoped. The first set of test resulted in differences of one order of magnitude between the ANSYS model and Triboindenter data. In addition to known issues with the model parameters, the Triboindenter was originally designed to perform nanoindentations for hardness testing and not tests on flexible MEMS devices. New software has been installed and initial test results are improved.

Preliminary testing of the sensitivity to mass change has produced some unexpected results. Of the five devices, the masses of two were reduced by removing approximately 5 μm^3. Resonance frequency shifts in the two altered devices were detected while the three unaltered devices remained consistent; however, the shift was to a lower resonance frequency, opposite of what was expected after removing mass. The cause of this unexpected behavior is not yet known, but the fact that there was a detectable change holds promise.

In conclusion, many of the properties of our MEMS oscillators were successfully characterized but did not remain consistent throughout the different types of tests. On the whole, the data collected has not been good enough to accurately describe the mechanical properties and behavior of our oscillators. More progress must be made before the mechanical properties of our devices can be fully understood and modeled.

References:

[1] K. L. Turner, Multi-dimensional MEMS motion characterization using laser vibrometry, Transducers'99, Digest of Technical Papers,, Sendai, Japan, 7-10 June 1999, p. 1144-1147.

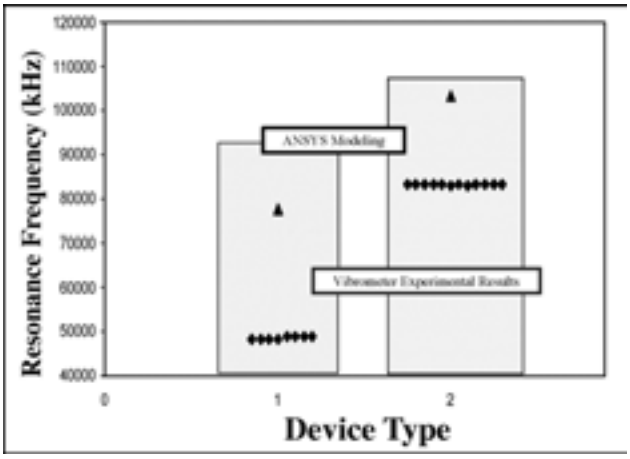

Figure 4: Resonance frequency data.

Growth of ZnO Nanowires and Their Application in Dye-Sensitized Solar Cells

Michael Reichman, Chemical Engineering, University of Texas at Austin

Eray Aydil, Chemical Engineering, University of California, Santa Barbara

Jason Baxter, Chemical Engineering, University of California, Santa Barbara

reichman@mail.utexas.edu, aydil@engineering.ucsb.edu

Abstract:

Growth of ZnO nanowires was achieved through Metal Organic Chemical Vapor Deposition (MOCVD) using the precursor, Zinc Acetylacetonate, and characterized by Scanning Electron Microscopy (SEM). Well-aligned ZnO nanowires with various lengths and diameters were grown on a-plane Al_2O_3 and a transparent conducting oxide. The important factors determining the morphology were; the pressure within the vacuum chamber, carrier gas flow, time duration of growth, and the heating ramp. The wires have many applications including use in photoelectrochemical cells due to their large surface areas and unique electron transport properties.

Introduction:

The purpose of this research is the construction of a novel photoelectrochemical cell based on the idea of separation of charge production and charge transportation [1]. First introduced by Michael Gratzel, this type of solar cell uses a photosensitive dye to eject an electron into a mesoporous semiconductor. The electron flow through the semiconductor has been identified to be a hopping mechanism which exhibits slow non-exponential current and charge recombination thus limiting efficient charge transfer [2]. In order to solve the problem of slow charge flow, we proposed using ZnO nanowires grown vertically from the electrode to replace the mesoporous semiconductor. The nanowires will have large surface areas and long conduction pathways that lead straight to the electrode for efficient and fast charge transfer. A photosensitive dye will be adsorbed onto the ZnO nanowires to absorb light and create an excited electron, and a transparent conducting oxide will encapsulate the cell, which is then filled with an electrolyte for hole conduction.

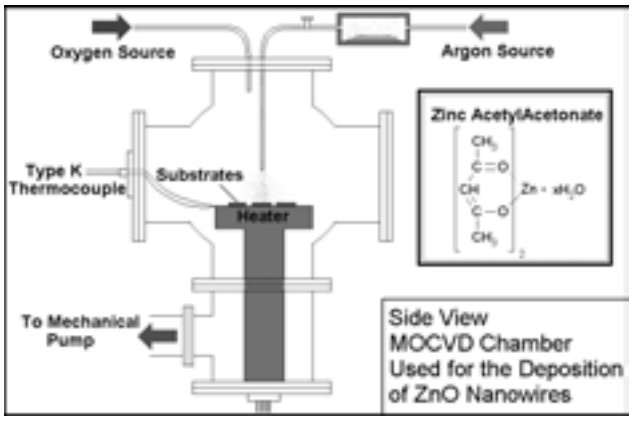

Figure 1: Metal organic chemical vapor deposition chamber.

Procedure:

Growth of the ZnO nanowires on a transparent conducting oxide substrate was the critical step in this research; therefore, most of the research was devoted to growing nanowires with repeatable geometric structures and directions. Metal Organic chemical vapor deposition (MOCVD) was used to synthesize nanowires using Zinc Acetylacetonate as the precursor in the process. Silicon, sapphire, and transparent conducting oxide substrates were placed on a heater at 550°C. The precursor was heated in another chamber from 75°C to 120°C depending on the desired morphology, while 20 sccm of the carrier gas, argon, was passed over the solid and directed onto the substrates. This process was performed in the presence of oxygen in order to increase the rate of decomposition of the precursor into ZnO. Several problems were encountered during the course of the research which required a study of the properties of the precursor: Zinc Acetylacetonate. This study was accomplished using infrared spectroscopy, thermogravimetric gas analysis, and residual gas analysis. Finally, construction and efficiency testing of the cell was completed using an apparatus designed to measure the current versus potential of the cell under a known light intensity.

Results and Conclusions:

Chemical Vapor Deposition of ZnO produced a wide variety of morphologies, because of the chemical structure of the precursor used. Initial growth experiments produced three characteristic types of wires with varying densities, diameters, and lengths (see Figure 2). The results of the initial experiments showed either one of these three morphologies even if the experiments were done under the same conditions. This made repeatable growth impossible and therefore it was not possible to construct a complete solar cell. These difficulties required an analysis of the most complex part of the experiment: the precursor.

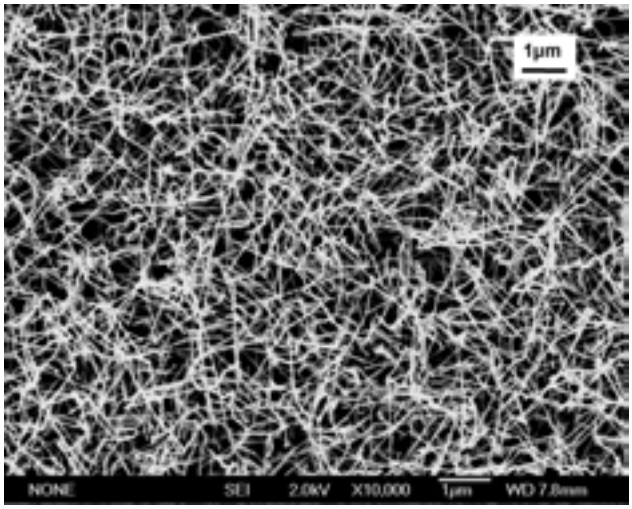

Figure 2: Irreproducible nanowires. 75°C, 2.2 torr, 90 minutes.

A study of Zinc Acetylacetonate hydrate produced interesting results about the effects of the heating rate on the precursor's bonding. Thermogravimetric and Residual Gas analysis of the Zinc Acetylacetonate hydrate showed that the rate of water loss increased with an increasing temperature ramp; therefore the ratio of water to Zinc Acetylacetonate in the carrier gas changed during different heating ramps. It is unclear how the presence of water affects the growth and morphologies of the nanowires; however, if left uncontrolled it does produce a wide variety of morphologies. Infrared Analysis of Zinc Acetylacetonate hydrate heated at different heating ramps show the unheated precursor with peaks indicating hydroxyl and carbonyl bonding as expected from the precursor's structure. As the temperature is increased, these peaks are reduced and a peak most likely associated with crystalline ZnO appears. The heating ramp determined the amount of precursor that decomposed into ZnO and therefore has an effect on the amount of precursor in the carrier gas stream.

Conclusion:

From these results, it was apparent that the heating ramp was a major concern during the growth experiments. Using this information, the heating ramp was controlled accurately and it was possible to grow nanowires reproducibly on sapphire and fluorine doped tin oxide. Nanowire morphology was controlled by varying the time the precursor was heated; small diameter and shorter length wires forming at lower time durations (see Figure 3).

Although the complete mechanism for ZnO nanowire growth using Zinc Acetylacetonate is still unknown; this research has provided insight into the properties of the precursor and information on the growth characteristics of the nanowires.

Acknowledgements:

I would like to thank Jason Baxter, Ron Bessems, and Eray Aydil for their guidance and support throughout the summer, and for providing me with the opportunity to learn about nanowire growth and dye-sensitized solar cells.

References:

[1] M. Gratzel, Nature 414, 228 (2001).
[2] J. Nelson, Phys. Rev. B. 59, 23 374 (1999).

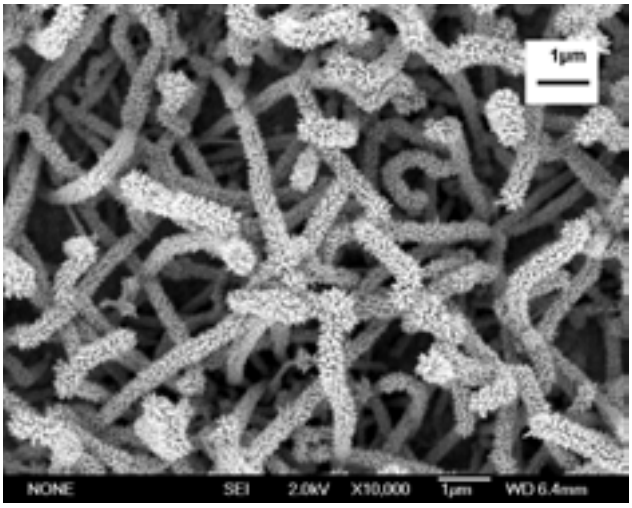

Figure 3: Reproducible nanowires. FTO, 2°C/min, 114°C, 1440 min.

Organometallic-Based Photovoltaic Cells

Kristy Schmit, Chemical Engineering, University of California, Santa Barbara

Guillermo Bazan, Chemistry, University of California, Santa Barbara

Jacek Ostrowski, Chemistry, University of California, Santa Barbara

kristils@umail.ucsb.edu, bazan@chem.ucsb.edu

Abstract:

Photovoltaic (PV) cells provide a source of energy that is renewable and clean. The goal of this project is to make more efficient and more affordable solid-state PV cells. A new approach was taken by making the hole transporting material of the PV cell out of an organometallic compound. Not only are organic materials inexpensive and readily available, they have many other desirable properties. Organic compounds can be spin-coated easily on a variety of substrates, as well their properties make them flexible.

Several organometallic iridium complexes were designed and synthesized for this use, as shown in Figure 1. After synthesis of the tris(2-thiophene-5-(pyridine-2'-yl) thiophene) iridium(III) compound (see Figure 1A), tests were run to determine the hole mobilities, lowest unoccupied molecular orbital levels (LUMO), and highest occupied molecular orbital levels (HOMO). If the characteristics were found to be favorable, the material could be integrated into a basic Grätzel PV cell.

The basic components of the Grätzel cell include the titanium layer, which acts as the cathode or electron transport; rubidium dye, used to absorb the incoming photons; and our iridium compound, the hole transporting material. These components are layered on an indium tin oxide (ITO) glass substrate. The cells would then be tested for conductivity and other properties.

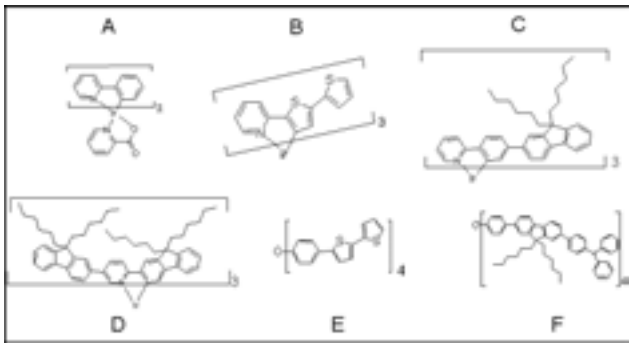

Figure 1: (A) The compound synthesized: tris(2-thiophene-5-(pyridine-2′-yl) thiophene), (B)-(D) other iridium complexes, (E)-(F) purely organic species.

Introduction:

A PV cell operates by absorbing light and using the discrete energy from the photons to move electrons to their excited state, as depicted in Figure 2. The excited state is migrated through the layers of materials to produce an electrical current. The ruthenium dye absorbs the light and the excited electrons then hop to the TiO_2 layer. The electrons are then transferred as an electrical current, through materials such as carbon nanotubes. A current is generated by this process and can be used as a reliable, renewable source of electricity.

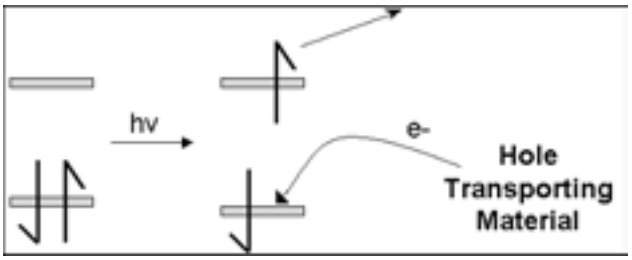

Figure 2: Schematic for photon absorption.

The goal of this project was to synthesize a new hole transporting material to substitute the carbon nanotubes. This material would replace the missing electron in the ground state so there would be less of a chance of the excited electron hopping back down. This should significantly increase the efficiency of PV cells because a greater percentage of the photons absorbed will be converted to electrical current.

The objectives of this research included the following: synthesize an organometallic iridium compound; test its redox potentials (Highest Occupied Molecular Orbital and Lowest Unoccupied Molecular Orbital levels), optical spectra, and hole and electron mobilities.

Since the organometallic iridium compound properties were found suitable, a Grätzel PV Cell will be created. Further research will test the cell for efficiency as well as testing the properties and interactions of the films.

Procedure:

The first task was the synthesis of the compound tris(2-thiophene-5-(pyridine-2'-yl) thiophene) iridium(III). Once synthesis was complete, an electrochemical cell was assembled for cyclic voltammetry measurements. Within the solution of the cell (containing the iridium compound, solvent, and electrolyte), the electron potential was controlled and the resulting current measured. This provided data to calculate the HOMO level of the compound.

A sample of the compound dissolved in solvent was then run through the UV-Vis spectrometer to measure the absorbance at different wavelengths. This data gave the size of the band gap, which is the distance between HOMO and LUMO levels. In order for a Grätzel PV cell to operate properly, the HOMO and LUMO levels must be in the appropriate positions in comparison to those levels of the titanium oxide layer and the ruthenium dye (see Figure 3). The HOMO level of the hole transporting material must be below that of the Ru dye, and the LUMO level of the material must be higher than the level for the TiO_2. These spacings provide the best pathway to encourage the appropriate flow of electrons.

We measured the band gaps for all of the four iridium compounds, along with two purely organic compounds, used for comparison. The hole and electron mobilities were the next properties to be tested. A simple transistor was made by spin coating the material on standard substrates. Tests were run with a three-probe device; with one probe each placed on the gate, the drain, and the source. This data produced graphs of source current versus the square root of the gate voltage. The slope of that curve was taken and the mobilities were calculated.

Results:

The redox potentials for all four of the iridium compounds tested were determined appropriate for integration into a Grätzel PV cell. As shown in Figure 4, the HOMO levels were all greater than -3.0 eV and the LUMO were all less than -4.5 eV. Mobilities (also shown in Figure 4) for each compound were very low in comparison to most conventional non-organic devices, but were suitable enough for this specific use. The compound that produced the most promising results was the synthesized tris(2-thiophene-5-(pyridine-2'-yl)thiophene) iridium(III) compound. Its hole mobility was two orders of magnitude higher than the other compounds examined (see table in Figure 4B).

Conclusions:

Integration of an organometallic hole transporting material, such as the iridium complexes tested, seems like it will produce promising results. The compound has a good mobility that would be satisfactory in eliminating the hopping down of electrons to their ground state. The efficiency of a Grätzel PV cell should be sufficiently increased with the addition of a hole transporting material. In further research, the integration of the material will be made, and we hope to verify this statement.

Acknowledgements:

Jacek Ostrowski, Hadjar Benmansour, Glenn Bartholomew, James Swensen, Guillermo Bazan, The Bazan group, DOE, NNUN, UCSB.

References:

[1] Hagfeldt, Andres; Grätzel, Michael. Molecular Photovoltaics. Accounts of Chemical Research 2000, 33, 269-277.

[2] Brabec, C.J.; Sariciftci, N.S.; Hummelen, J.C. Plastic Solar Cells. Advanced Functional Materials. V11, No. 1, Feb, 2001.

[3] Nelson, J. Organic Photovoltaic Films. Current Opinion in Solid State & Materials Science 2001. 6, 87-95.

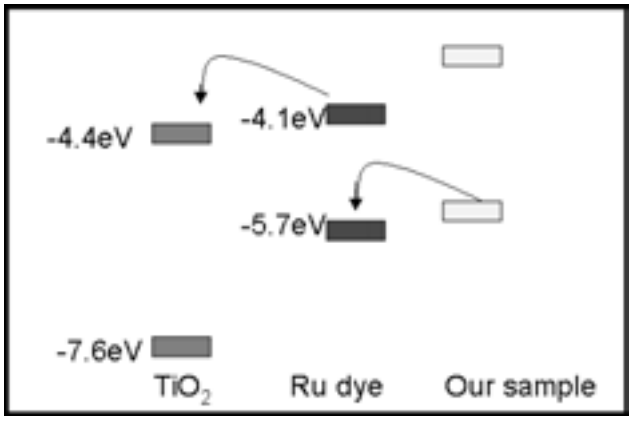

Figure 3: Example of appropriate positioning of energy levels for electron flow.

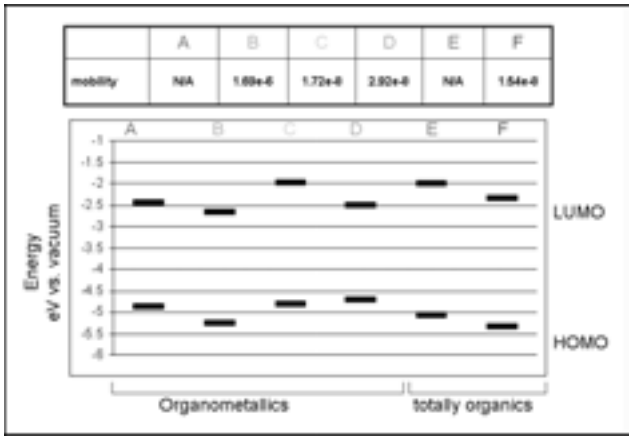

Figure 4: Mobilities [$cm^2/V/s$] and band gaps of the samples.

Amphiphile Aspect Ratio and Membrane Bending Rigidity in a Solvent-Free Cell Membrane Model

Adele Tamboli, Physics, Harvey Mudd College

Frank Brown, Chemistry, University of California, Santa Barbara

Grace Brannigan, Physics, University of California, Santa Barbara

atamboli@hmc.edu, flbrown@chem.ucsb.edu, gbrannig@physics.ucsb.edu

Abstract:

Cell membranes can be simulated efficiently using a solvent-free model. Monte Carlo techniques, which minimize the free energy of a system, were used with a model that treats lipids as rigid rods which interact according to three potential energy parameters that simulate amphiphilic interactions with a solvent. The region of parameter space for which the membrane is fluid was found. This fluid region narrows in size as the length of the amphiphiles decreases, becoming negligibly small for an aspect ratio of 1.5 or less. The effect of aspect ratio on flexibility was also examined. Membrane bending rigidity, or flexibility, decreases with aspect ratio.

Introduction:

Simulations in chemistry provide information about a system when an experiment is difficult or impossible to perform. Biological systems, however, are often too complex to be exactly modeled by a computer program. Cell membranes, for example, are composed of amphiphilic lipids which form a bilayer in solvent, but contain a variety of other components such as proteins and cholesterol that affect the dynamics of the membrane as a whole. Cell membrane models range in complexity from uniform sheet models, used to simulate large systems or long times, to atomistic models, which can only simulate very small systems, but do so very precisely.

The model used in this project treats each lipid as a rigid rod with a hydrophilic head and hydrophobic tail to simulate interaction with a solvent. They interact according to three potential energy terms: alignment (c_{aln}), so that the rods tend to point in the same direction; tail attraction (c_{tail}), which minimizes contact between tail ends and the surrounding solvent; and excluded volume (c_{core}), which enforces shape and limits overlap.

Because of its relative simplicity, this model should be able to include simplified proteins so that their interactions can be studied. Membrane-bound proteins interactions and aggregation have been implicated in many aging-related diseases such as Alzheimer's disease and macular degeneration. With this model, the motion of membrane-bound proteins could be investigated in a way that is not possible with real experiments. Perhaps this simulation could suggest new theories about how protein aggregation occurs.

To match this membrane model to experimental data, two characteristics of the membrane were considered: bending rigidity and compression modulus. Bending rigidity (k_c), a measure of the flexibility of the membrane, is defined by how much energy is required to bend the membrane. Membranes without cholesterol generally have a bending rigidity of about 10-20 ε [1], where $\varepsilon = 4*10^{-21}$ J. The compression modulus, k_a, which ranges from 100-200 mN/m [2], represents the amount of energy needed to stretch or compress a membrane.

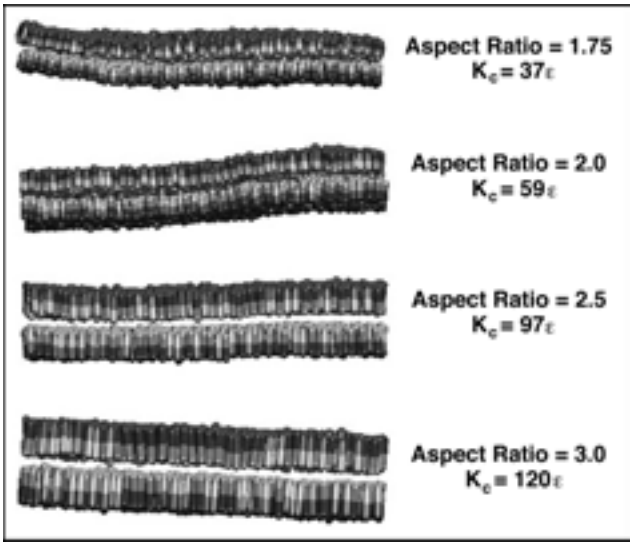

Figure 1: Fluid bilayers become more flexible as aspect ratio decreases.

Procedure:

Initially, the rods used in this model had an aspect ratio of 3. This number was chosen to simplify comparison to other models, since it is a common choice in similar simulations. At this value, the compression modulus was in the correct range, but the bending rigidity was too high. Theory developed for uniform sheet membranes suggests that

$$k_c \sim k_a * d^2$$

bending rigidity scales with aspect ratio squared [3]. Since k_a should not change with thickness in this model, k_c should decrease with decreasing lipid aspect ratio (see Figure 1).

Because cell membranes are fluid, the potential energy parameters need to be set correctly to find the fluid phase of the simulated membrane. For these systems, five phases were found:

1. micelles: spherical clumps of lipids
2. isotropic fluids: lipids dispersed evenly throughout the box
3. monolayers: two noninteracting layers
4. defective bilayers: systems with pores or channels
5. fluid bilayers

A parameter space search over the alignment and tail attraction terms was performed at an aspect ratio of 2 to find the fluid phase. Since the phase diagram had already been measured for an aspect ratio of 3, the two were compared to show that the fluid phase did not shift in phase space, but simply narrowed. At aspect ratios of 1.5 or less, the fluid phase disappeared completely (see Figure 2).

The Fourier modes of fluid membranes with aspect ratios in the range of 1.75 to 3 were fit to give a measurement of the bending rigidity. Some systems were run at constant pressure instead of constant volume to measure the dependence of surface tension on area per molecule, which yields a value for compression modulus.

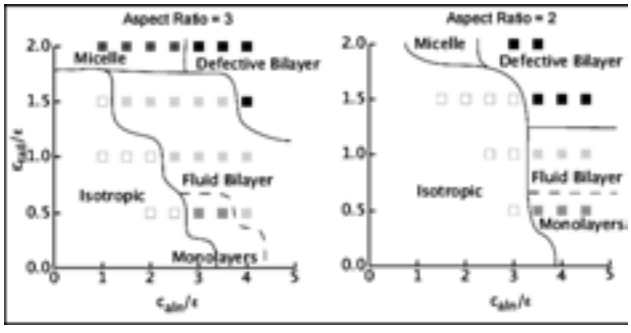

Figure 2: Parameter space phase diagrams.

Results:

The bending rigidity did increase with increasing aspect ratio, but with a power of 0.584 dependence (see Figure 3). The data could be fit with a power of 2.17 dependence if bending rigidity was constrained to go to 0 at 0 aspect ratio, corresponding to spherical lipids. While this constraint may seem sensible, the other fit has the bending rigidity going to 0 at an aspect ratio of 1.57, meaning that membranes fall apart for an aspect ratio of less than about 1.57. The fluid phase did disappear for aspect ratios less than about 1.5, so the 0.584 dependence seems consistent with phase diagram data. Theory describing membrane bending rigidity was developed for uniform sheet models, not fluid membranes, so minor deviation was expected.

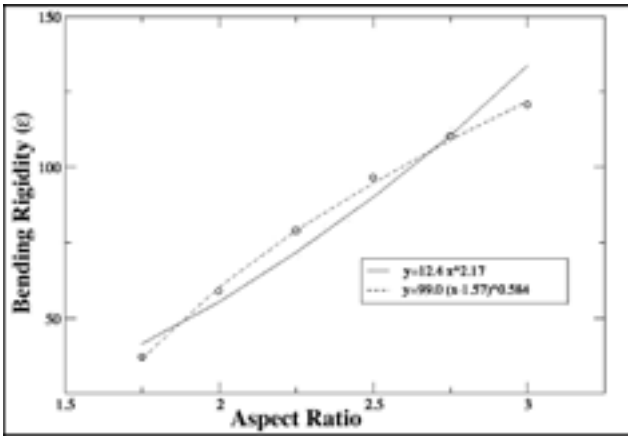

Figure 3: Bending rigidity dependence on aspect ratio.

The initial compression modulus data suggests that k_a may also vary with aspect ratio, contrary to theory. If this is the case, it may partially account for the deviation of bending rigidity data from theory. Additional constant pressure data should determine this dependence more conclusively.

Acknowledgements:

Grace Brannigan, Frank Brown, Liu-Yen Kramer, Krista Ehrenclou, NSF.

References:

[1] U. Seifert and R. Lipowsky, Structure and Dynamics of Membranes, ed. R. Lipowsky and E. Sackmann (Elsevier Science, 1995), vol. 1.

[2] E. Sackmann, Structure and Dynamics of Membranes, ed. R. Lipowsky and E. Sackmann (Elsevier Science, 1995), vol. 1.

[3] G. Brannigan and F. L. H. Brown, "Solvent-free simulation of fluid membrane bilayers," Journal Of Chemical Physics, In Press, 2003.

THANK YOU
to everyone
for a
great summer!

Keep In Touch!

The 2003 National Nanofabrication Users Network Research Experience for Undergraduates Program

Index

(2003 NNUN REUs are in Bold)